Star formation and quenching in galaxy formation models

Rachel Asquith

Thesis submitted to the University of Nottingham
for the degree of Doctor of Philosophy

August 2019

"Stop thinking of what you intend to do. Stop thinking of what you have just done. Then, stop thinking that you have stopped thinking of those things. Then you will find the Now, the time that stretches eternal, and is really the only time there is."

- Robin Hobb, Royal Assassin

Supervisors:	Prof. Frazer Pearce
	Prof. Omar Almaini
Examiners:	Dr. Rita Tojeiro *(University of St Andrews)*
	Prof. Alfonso Aragón-Salamanca *(University of Nottingham)*
Submitted:	8 April 2019
Examined:	23 May 2019
Final version:	15 August 2019

Contents

List of Figures

Abstract

Galaxies locally have been observed to have a bimodal distribution for many properties, such as colour, star formation rate and morphology. These properties can be used to separate galaxies into two classes - the 'blue cloud' and the 'red sequence'. Galaxies move from the blue cloud to the red sequence in a process called 'quenching'. Learning exactly how and why galaxies are quenched is vital to understanding galaxy evolution. In this thesis, we use galaxy formation models to investigate the processes governing star formation and quenching, with the aim of understanding exactly which mechanisms are needed to produce a realistic population of galaxies.

Firstly, we compare nine different galaxy formation models with recent observational results in Chapter 2, focusing on the evolution of the stellar mass function (SMF) in the redshift range $0.5 < z < 3.0$. Although most of the models are able to match the SMF at low redshift, they tend to overproduce the number density of low-mass star-forming galaxies at high redshift. We then look at the haloes these galaxies are in, and find that the average stellar mass in low-mass haloes at high redshift in the models is larger than observations suggest. This means that the star formation is more efficient in these haloes in the models than the real Universe. Together, this suggests that the models struggle to decouple the growth of a galaxy from the growth of its dark matter halo.

We then chose one of these nine models to investigate a rare class of galaxies called post-starbursts (PSBs), which have been rapidly quenched, sometimes following a burst of star formation. Using the Lgalaxies semi-analytic model, we construct a mock lightcone survey in Chapter 3, which is designed to mimic the UKIDSS Ultra Deep Survey (UDS). With this mock, we explain in Chapter 4 how the Principal Component Analysis method is used to classify PSBs based on photometry alone. We then compare PSBs from our mock with PSBs identified in the UDS, and find differences in their stellar mass and redshift distribution. In the UDS, PSBs can be broadly split into two populations - high-mass at high redshift and low-mass at low redshift. However, in the mock, although the shape of the SMF is broadly similar to observations, the number of PSBs increases with cosmic time more in the models.

Building on the work from the previous chapters, we investigate the evolution of our population of simulated PSBs in Chapter 5. By tracking their properties

in time, we can try and figure out what mechanisms are responsible for quenching these galaxies. PSBs that are satellites or orphans appear to be quenched due to their environment. Their hot gas is stripped so after they have used up their cold gas supply they can no longer form stars. For centrals, it appears that they have a merger which initiates a starburst in the galaxy. However, this also funnels hot gas into the central black hole, switching on radio mode feedback from an active galactic nuclei (AGN). This heats the gas in the galaxy and quenches star formation. Relating this back to the UDS, most of the high-mass PSBs at high redshift in the mock are centrals, so we would expect AGN signatures in their spectra. Most of the low-mass low redshift PSBs are centrals or orphans, the latter of which we would expect to be environmentally quenched. However, the quenching pathway for the low-mass, low redshift centrals in the UDS is less clear. One option may be winds from supernovae heating the gas in a similar way to AGN feedback.

Acknowledgements

Firstly, I would like to thank my supervisors, Frazer and Omar, for your guidance throughout my entire PhD. You've both always had your doors open to me at any time, given me encouragement when I needed it most and pushed me to do the best I can do. I really appreciate all the time you've invested in me, it's been a great experience working with you both. I'd also like to thank my collaborators for all your help, as you've all been instrumental in helping this work make it into this thesis. To everyone from the UDS group, thank you for looking at my plots so many times and helping me work out what they mean!

The CAPT building has been a great place to work for the last three and a half years, due to all the wonderful people there. Charutha, Mehdi and Finlay deserve a special mention for being amazing friends from the 2015 crew, distracting me with so many weird conversations. Thanks to my office mates in B105, for the great atmosphere and nice chats. Lizzie and Lizzie, for making sure it's never too quiet! The tea and coffee crew, for keeping me topped up with caffeine. All the Inflativerse managers, for laughs lying in the dark, trying to spot holes in the dome. Mike, for all the undergraduate tutorials. Meghan, for helping me gain self confidence.

I'm grateful to all my friends for the support you've given me these last few years. Carissa, Naomi, Alicia, Louise, and Emma, for keeping me grounded and distracting me with chats and DnD. Kirstin, for the bestie weirdness we share and feeling like it's been no time since we last saw each other. Chris, for our lunches at Portland. Kate, for always being there for a chat and a rant, your friendship means so much to me and I'll always be glad that you came up to me in 2nd year labs. Steph and Ed, for the hilarious board games and Dominos nights.

I also want to thank my family for all their help. Gill and Paul, for being interested (or at least pretending to be interested) in what I do. My sister Claire, for being one of my best friends and for making weird noises at me down the phone! My mum and dad, for believing in me and always encouraging me to do what I loved, no matter what anyone else thought.

Finally, I'd like to thank my partner, Jake. You've always made me feel like I can do anything I set my mind to, and supported me whilst I then went and did it. I wouldn't have been able to finish this PhD without you.

Published work

Much of the work in Chapter 2 has been previously presented in paper I listed below. The work in Chapters 3, 4 and 5 will feature in paper II, in preparation.

I **Rachel Asquith**, Frazer R. Pearce, Omar Almaini, Alexander Knebe, Violeta Gonzalez-Perez, Andrew Benson, Jeremy Blaizot, Jorge Carretero, Francisco J. Castander, Andrea Cattaneo, Sofía A. Cora, Darren J. Croton, Julien E. Devriendt, Fabio Fontanot, Ignacio D. Gargiulo, William G. Hartley, Bruno Henriques, Jaehyun Lee, Gary A. Mamon, Julian Onions, Nelson D. Padilla, Chris Power, Chaichalit Srisawat, Adam R. H. Stevens, Peter A. Thomas, Cristian A. Vega-Martínez, Sukyoung K. Yi, *"Cosmic CARNage II: the evolution of the galaxy stellar mass function in observations and galaxy formation models"*, 2018, MNRAS, 480, 1197.

II **Rachel Asquith**, Omar Almaini, Frazer R. Pearce, Aaron Wilkinson, Stefan Hilbert, Vivienne Wild, *"The evolution of post-starburst galaxies in the* LGALAXIES *semi-analytic model"*, in preparation.

III Alexander Knebe, Frazer R. Pearce, Violeta Gonzalez-Perez, Peter A. Thomas, Andrew Benson, **Rachel Asquith**, Jeremy Blaizot, Richard Bower, Jorge Carretero, Francisco J. Castander, Andrea Cattaneo, Sofía A. Cora, Darren J. Croton., Weiguang Cui, Daniel Cunnama, Julien E. Devriendt, Pascal J. Elahi, Andreea Font, Fabio Fontanot, Ignacio D. Gargiulo, John Helly, Bruno Henriques, Jaehyun Lee, Gary A. Mamon, Julian Onions, Nelson D. Padilla, Chris Power, Arnau Pujol, Andrés N. Ruiz, Chaichalit Srisawat, Adam R. H. Stevens, Edouard Tollet, Cristian A. Vega-Martínez, Sukyoung K. Yi, *"Cosmic CARNage I: on the calibration of galaxy formation models"*, 2018, MNRAS, 475, 2936.

The vast majority of the work presented in this thesis was performed by the author, with advice from the paper coauthors listed above. Where the material presented is the result of more collaborative work, this is mentioned at the beginning of the relevant chapter.

Chapter 1

Introduction

One of the greatest challenges in astronomy is understanding the physical processes that shape the wide variety of galaxies that we observe locally. Multi-wavelength surveys at high redshift have enabled us to start to understand the history of galaxy formation, but we can only view each galaxy at one point in its life. In order to understand the full evolutionary path of galaxies, we need to connect populations of galaxies through time to their progenitors and descendants. One way to gain insight into this problem is to use galaxy formation models, which allow us to track the properties of individual galaxies through time and understand the processes which have shaped their evolution. By comparing the output from these models with observations, we can both inform the models about what physical processes might be missing, and learn about how certain populations of galaxies evolve.

1.1 Cosmology and the formation of structure

1.1.1 The ΛCDM cosmological model

The ΛCDM cosmological model is the current paradigm for structure formation, describing a universe dominated by a cosmological constant (Λ), which is associated with dark energy, and cold dark matter (CDM). One of the best pieces of evidence that we have for the ΛCDM model is from the Cosmic Microwave Background (CMB). This is the oldest light in the Universe, seen today as black-body radiation with a temperature of 2.73K across the whole sky. It was accidentally discovered in 1964 by Arno Penzias and Robert Wilson (Penzias & Wilson 1965), who were using a radio telescope and measured an 'excess antenna temperature' isotropically in all directions which was consistent with a black body spectrum. This was interpreted as evidence for the Big Bang model, where the Universe starts out in a hot, dense state and subsequently expands and cools. The background cosmic radiation that Penzias and Wilson measured was left over from this hot initial phase and matched what was expected from the Big Bang.

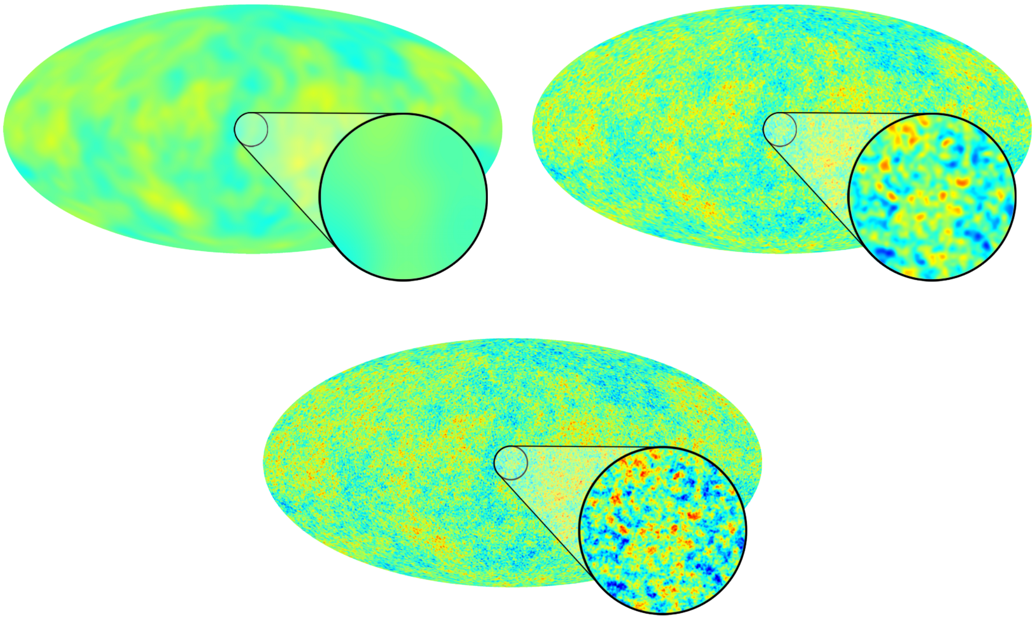

Figure 1.1. Comparison of the CMB maps from COBE (top left), WMAP (top right) and Planck (bottom). The colour shows the temperature, with red and blue areas hotter and colder than average respectively. The resolution increases from COBE to Planck, with clear fluctuations observable in the map from Planck. Image credit: Chris North, Cardiff University.

Later observations by the COsmic Background Explorer satellite (COBE, Smoot et al. 1990), Wilkinson Microwave Anisotropy Probe (WMAP, Bennett et al. 2003) and the Planck satellite (Planck Collaboration et al. 2011) have improved our observations of the CMB, as shown in Figure 1.1. Anisotropies have now been measured in the temperature of the CMB, which are believed to be due to primordial density fluctuations in the early Universe, consistent with some models of inflation (Starobinskii 1979). By fitting the power spectrum of the CMB, which characterises the size of fluctuations as a function of angular scale, the value of the six parameters describing the best fitting ΛCDM model can be found.

Current observations suggest that the Universe is spatially flat, consistent with the theory of inflation. This means that the density parameter, Ω, is very close to 1. Today's density parameter, Ω_0, can be described by:

$$\Omega_0 = \Omega_{m,0} + \Omega_{\gamma,0} + \Omega_{\Lambda,0}, \tag{1.1}$$

where $\Omega_{m,0}$ is the matter density today, $\Omega_{\gamma,0}$ is the radiation density today and $\Omega_{\Lambda,0}$ is the dark energy density today. The best fitting ΛCDM model gives the values for these parameters as $\Omega_{m,0} \simeq 0.31$, $\Omega_{\gamma,0} \simeq 0$ and $\Omega_{\Lambda,0} \simeq 0.69$ (Planck Collaboration et al. 2018). This means that today about 69% of our Universe is dark energy and the other 31% is matter, which can be split into 26% cold dark matter and 5% baryonic matter.

We currently have not yet observed dark matter directly, but instead have indirect evidence for its existence. For example, dark matter is used to explain the rotation curves of galaxies. The rotational velocity of material as a function of galaxy radius should reduce towards the outskirts. However, instead a constant rotation velocity is measured (Rubin, Ford & Thonnard 1978), meaning that there must be more mass within the galaxy than observed. This non-luminous matter is thought to be dark matter. Similar evidence for dark matter comes from galaxy clusters, where the velocity dispersion of galaxies is higher than expected from the virial theorem (Zwicky 1933). Taking dark matter into account then solves this discrepancy. Other evidence comes from gravitational lensing, where the masses of lenses derived from this effect lead to mass-to-light ratios that match with expected dark matter densities (Refregier 2003). Despite this, we have yet to observe dark matter directly and we do not know what it consists of.

Even less is known about dark energy. Its existence is motivated by observations of the CMB, which suggest that the Universe is close to flat and therefore the dark energy density is non-zero. Other evidence for dark energy comes from the relationship between redshift and distance of Type Ia supernovae, which are standard candles. In the late 1990s, the supernovae data from two teams suggested that the expansion of the Universe is accelerating (Riess et al. 1998; Perlmutter et al. 1999), which can be explained by invoking a dark energy term. Baryon acoustic oscillations have been used as standard rulers to get accurate measurements of the distance and redshift of galaxies independent of supernovae data, confirming that a dark energy term is needed to explain the apparent accelerated expansion of the Universe (Eisenstein et al. 2005). These three measurements together suggest that dark energy makes up nearly 70% of our Universe today.

1.1.2 Structure formation

Structure formation is also governed by the ΛCDM model. The primordial density fluctuations observed in the CMB are amplified by inflation and then grow in a highly non-linear way via gravitational instabilities (Frenk, White & Davis 1983). The largest perturbations are the first to collapse under their own gravity, accreting more dark matter until they form dark matter haloes. Dark matter is thought to be cold and non-relativistic, allowing structures to grow hierarchically. The smallest structures form first, which then merge to form larger structures as the Universe ages (see Figure 1.2). 'Top-down' models of structure formation have also been tested, but these require hot dark matter (HDM) and underpredict the number of the smallest structures (White, Frenk & Davis 1983).

Dark matter haloes also accrete baryons, with the amount depending on the

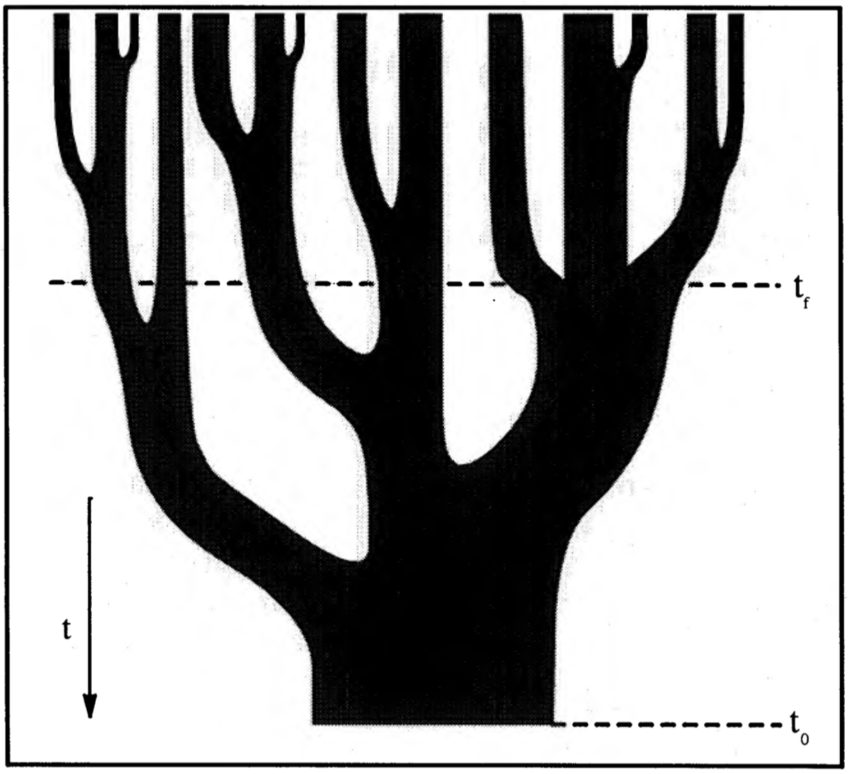

Figure 1.2. Schematic of a halo merger tree from Lacey & Cole (1993), showing how a halo grows in mass through a series of mergers with other haloes. Time increases from top to bottom and the width of each 'branch' indicates the mass of each halo at that time.

depth of their potential well. The low metallicity gas falling into a halo is shock heated to temperatures above 10^4K and is ionised. This hot gas can support itself via radiation pressure, so must cool before it is able to collapse. This can occur via bremsstrahlung radiation, recombination and collisional excitation. Once the gas is cool, it is able to collapse into a rotating disk. As this disk is unstable, star formation can take place within it (Eggen, Lynden-Bell & Sandage 1962).

Galaxies then form in the centre of dark matter haloes, with groups and clusters of galaxies forming as haloes merge to form larger structures. On a large-scale this forms the 'cosmic web', with galaxies connected by filaments and sheets. The distribution of galaxies can be used as a highly biased tracer of the underlying dark matter distribution. Figure 1.3 from Springel, Frenk & White (2006) compares the galaxy distribution obtained from spectroscopic surveys and from mock catalogues based on dark matter simulations. We can see the cosmic web structure observed in both the Universe and in simulations based on ΛCDM. The model also reproduces the clustering of galaxies seen in observations and its dependence on colour and magnitude (Springel 2005).

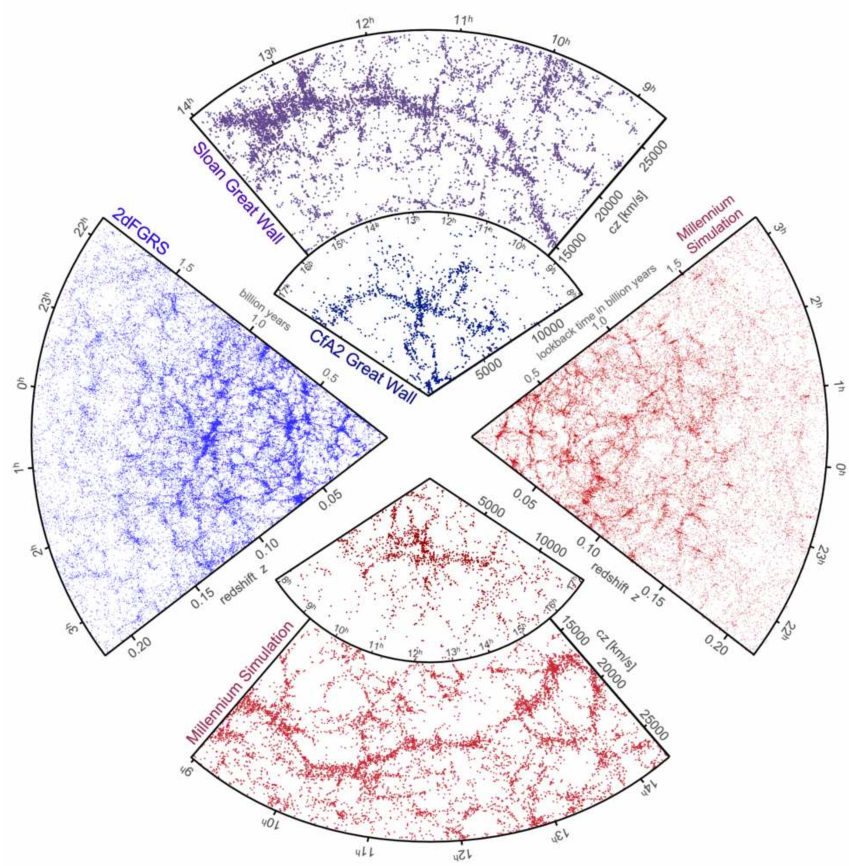

Figure 1.3. Comparison of the galaxy distribution obtained from spectroscopic surveys and from cosmological simulations, from Springel, Frenk & White (2006). The top and left wedges are from SDSS and 2dFGRS respectively and show the observed galaxy distribution on different scales. The right and bottom wedges show the galaxy distribution from mock catalogues. These are based on the Millennium simulation and show the same large-scale structure as observations.

1.2 Galaxy evolution

1.2.1 Mass assembly

Dark matter haloes accrete gas from the cosmic web, which fuels the star formation of the galaxies they contain. The growth of a galaxy could then be expected to follow the growth of its dark matter halo, as this is the main driver of gas accretion rate in galaxies, which then in turn drives the star formation rate. The star formation history of the galaxy then traces the dark matter mass accretion history, which, in the favoured ΛCDM structure formation scenario, is approximately self-similar for haloes of different masses. However, the shape of the halo mass function does not match the shape of the galaxy stellar mass function, as seen in Figure 1.4. If the number density of galaxies scaled with that of dark matter haloes, we would expect to observe both more low-mass and high-mass galaxies.

Observational evidence also points towards a seemingly ‘anti-hierarchical’ forma-

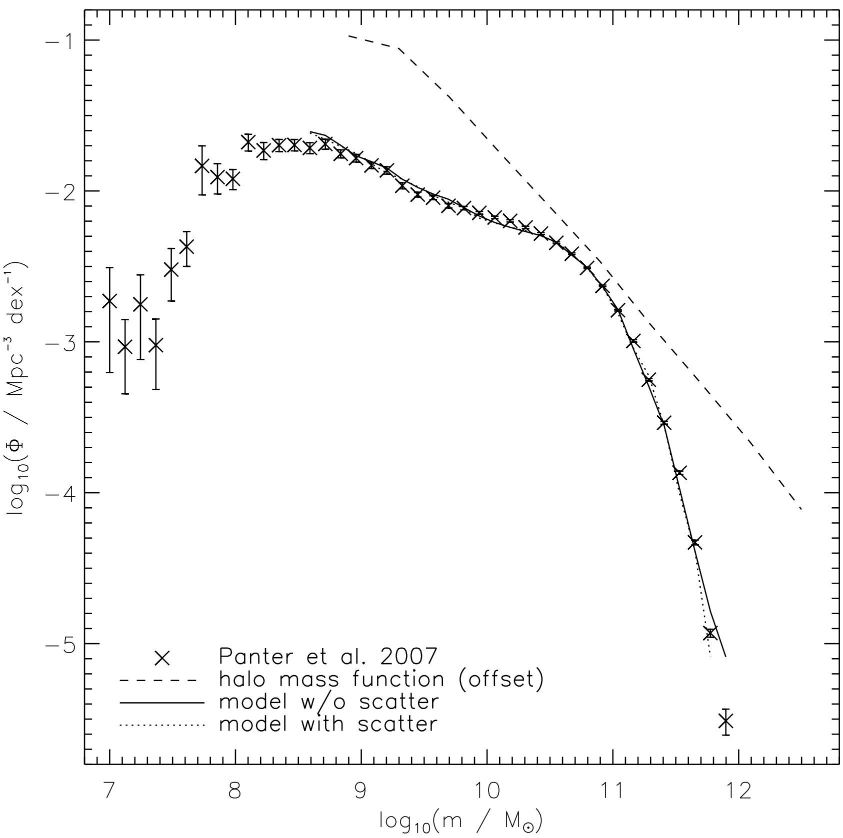

Figure 1.4. Comparison between the halo mass function (dashed line) and the observed galaxy stellar mass function (cross symbols) from Moster et al. (2010). The halo mass function is offset by a factor of 0.05 to match the knee of the stellar mass function. There is a deficit of both low-mass and high-mass galaxies.

tion scenario where high-mass galaxies form earlier with their abundance changing little from $z \sim 1$ to the present day, whereas there is a rapid evolution in the number of low-mass galaxies at late times (e.g. Fontana et al. 2004, 2006; Faber et al. 2007; Pozzetti et al. 2007; Marchesini et al. 2009, 2010; Pozzetti et al. 2010; Ilbert et al. 2010, 2013; Muzzin et al. 2013). This is sometimes referred to as 'mass assembly downsizing' (Cowie et al. 1996; Cimatti, Daddi & Renzini 2006; Lee & Yi 2013).

Feedback processes are used to reconcile the hierarchical assembly of dark matter with observations of galaxies and disconnect the growth of galaxies from that of their dark matter haloes. In order to decrease the efficiency of star formation in low-mass galaxies, supernova feedback and winds from star formation are thought to remove gas from the galaxy (Larson 1974; White & Frenk 1991). In high-mass galaxies the feedback mechanism is associated with active galactic nuclei (AGN), which can heat up the gas in galaxies to prevent star formation (Bower et al. 2006; Croton et al. 2006). Feedback also acts to reduce star formation in low-mass haloes at high redshift, allowing for the seemingly anti-hierarchical growth of galaxies.

Although the distribution of galaxies follows the underlying dark matter distribution, the evolution of the galaxy itself is also dictated by various baryonic processes, such as feedback, star formation, gas cooling, stellar evolution and mergers. It can often be difficult to disentangle the processes that have occurred during a galaxy's lifetime: for instance, did a high-mass galaxy grow in size through in situ star formation or by mergers? All of these processes act together to produce the wide variety of galaxies that we observe today.

1.2.2 Galaxy bimodality

Many galaxy properties at low redshift have been observed to have a bimodal distribution, which can be used to separate galaxies into two classes - the 'blue cloud' and the 'red sequence' (e.g. Bell et al. 2004). The larger of these two groups is the blue cloud, where galaxies tend to be star-forming, low-mass, disk-dominated and have high star formation rates (SFRs). They also tend to be blue in the optical, which gives this population its name. On the other hand, galaxies in the red sequence are much redder in colour and tend to be passive, high-mass, with low SFRs and elliptical or lenticular morphologies. These two populations have been well studied at low redshift, but it is less clear whether the bimodality in galaxy properties extends to higher redshifts. Some studies up to $z \sim 2$ have observed bimodality in galaxy properties (Cirasuolo et al. 2007; Muzzin et al. 2012; Foltz et al. 2015; Balogh et al. 2016), but at redshifts beyond this there is less evidence.

We also do not know how all of these galaxies properties are linked. For example, when transitioning to the red sequence, do galaxies decrease in SFR or change their morphology first? There has been evidence from Galaxy Zoo of both red galaxies with late-type morphologies (Bamford et al. 2009; Skibba et al. 2009) and blue galaxies with early-type morphologies (Schawinski et al. 2009), suggesting that different galaxies may take different evolutionary pathways. We will now review our current understanding of the bimodality in various galaxy properties.

Morphology

Galaxies can be broadly split into being either disk-dominated or elliptical. More massive galaxies tend to be spheroidal whilst low-mass galaxies tend to have disks (Strateva et al. 2001; Hogg et al. 2002) or have irregular morphologies. A common way to classify galaxies based on their visual morphology is to use Hubble's Tuning Fork (Hubble 1936, see Figure 1.5). Here galaxies are split into early-type (ellipticals and lenticulars) and late-type (barred and unbarred spirals). The term early-type and late-type do not refer to an evolutionary sequence, but rather the complexity of their morphology. Early-type galaxies are smooth and featureless, with no structures like spiral arms or bars. They are dominated by old stars, which for ellipticals are in random orbits around the centre of the galaxy, whilst lenticulars have rotation-

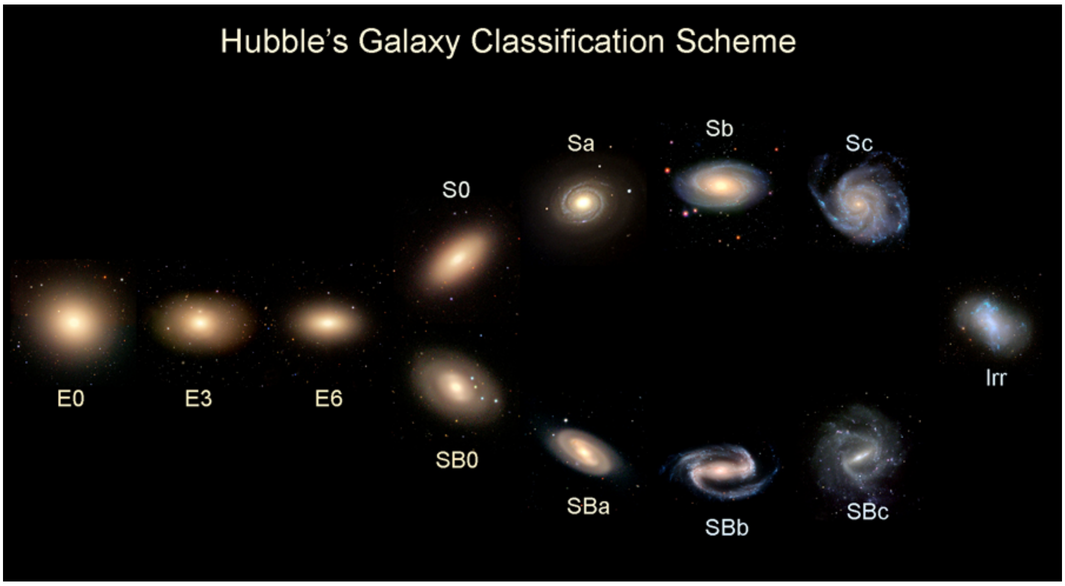

Figure 1.5. Hubble's Tuning Fork diagram used to classify galaxies based on their visual morphology. Galaxies can be broadly separated into either early-type or late-type morphologies. Image credit: Galaxy Zoo, Lintott et al. (2008).

dominated kinematics. Late-type galaxies have a rotating disk of stars, with spiral arms, a central bulge and sometimes a bar.

One way to quantify the morphology of a galaxy is with structural parameters. The most common way is to fit a Sérsic function to the surface brightness profile of the galaxy (Sérsic 1968) and get a value for the Sérsic index, n. This parameter describes how centrally concentrated the light from a galaxy is, with high n values representing a profile that is centrally peaked. Disks tend to have a value of $n = 1$, whilst elliptical galaxies tend to have a de Vaucouleurs profile with $n = 4$. Studies have found that galaxies with $n < 2.5$ tend to be disk-dominated, whilst galaxies with $n > 2.5$ are often ellipticals (Bell et al. 2004; Nair & Abraham 2010; Mortlock et al. 2013). This bimodality in Sérsic index has been observed up to $z \sim 2$.

Star formation rate

The SFR of galaxies is another property that has been observed to be bimodal. The logarithm of the SFR is approximately proportional to the logarithm of the stellar mass for most galaxies (Brinchmann et al. 2004; Salim et al. 2007; Daddi et al. 2007; Elbaz et al. 2007; Whitaker et al. 2012b), placing them on the star-forming 'main sequence'. However, some galaxies have SFRs that are lower than expected for their stellar mass (Bluck et al. 2016; Cano-Díaz et al. 2016). These are passive galaxies that have little to no star formation ongoing. This bimodal population has been observed up to $z \sim 1$ (Ilbert et al. 2013).

As we can see from Figure 1.6, galaxies can also be found in the 'green valley' between the main sequence and the passive population. The galaxies here are believed

Figure 1.6. Cartoon of SFR against stellar mass, showing where the main sequence, the green valley, red galaxies and starbursts lie. Most galaxies are on the main sequence, but some are forming stars at higher or lower rates than expected for their stellar mass. Image credit: CANDELS collaboration.

to be in the process of evolving from the red sequence to the blue cloud (Bell et al. 2004; Faber et al. 2007; Mendez et al. 2011; Zehavi et al. 2011; Gonçalves et al. 2012; Trayford et al. 2016), although some may just be scatter from both populations. Galaxies can also be found above the main sequence as starbursts if they are undergoing a period of heightened star formation (Hernquist 1989; Barnes & Hernquist 1991; Hopkins et al. 2006).

Colours and spectra

The colour of a galaxy is defined as the difference in magnitude between two wavelength bands. There is a bimodality in galaxy colours (Strateva et al. 2001; Blanton et al. 2003; Kauffmann et al. 2003; Baldry et al. 2004), with optically blue galaxies tending to be lower mass and disk-dominated, whereas optically red galaxies are typically high-mass and elliptical. On a plot of rest-frame colour against stellar mass (see Figure 1.7), these two populations form the red sequence and the blue cloud, where red galaxies have a tight correlation between stellar mass and colour but there is more scatter for blue galaxies. Between these two populations is the green valley.

The bimodality in galaxy colour can be understood by considering stellar evolution. The light that we receive from galaxies is the sum of the light that we receive from their stellar populations. Stars are sorted in types based on their temperature, with the sequence O B A F G K M. The hottest and bluest are O type stars, with M type stars being the coolest and reddest of these. Figure 1.8 shows the spectrum

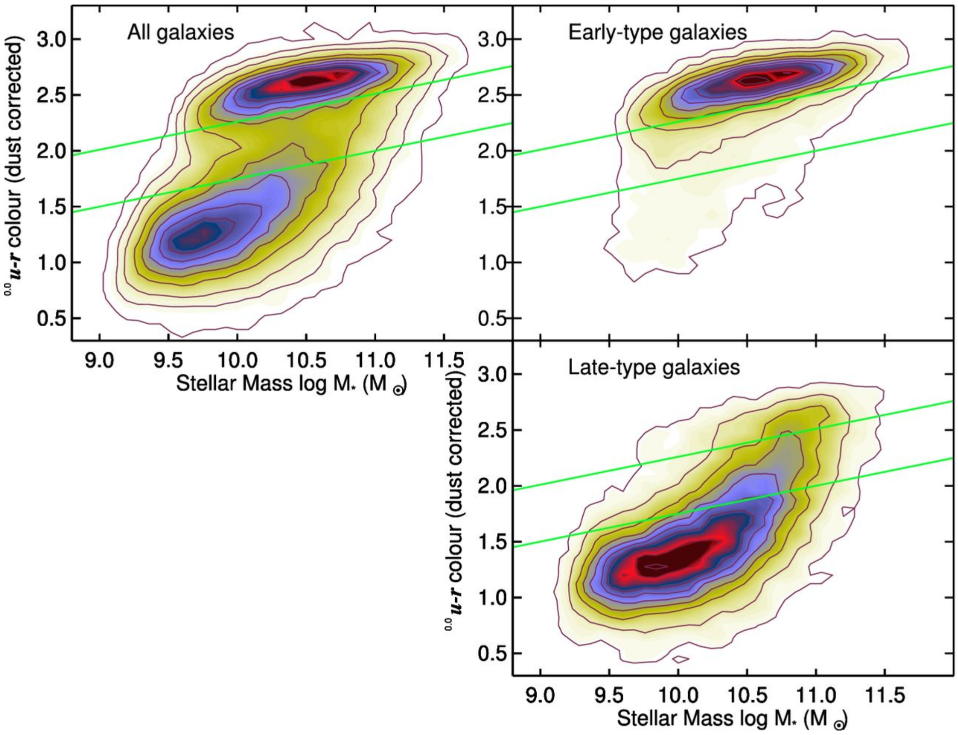

Figure 1.7. $u-r$ colour-mass diagram for SDSS at $z \sim 0$ from Schawinski et al. (2014). The top left panel shows all galaxies and has two peaks in the distribution, one for the blue cloud and one for the red sequence. Galaxies between these two are in the green valley. The top right and bottom right panels show the correlation of morphology with colour bimodality.

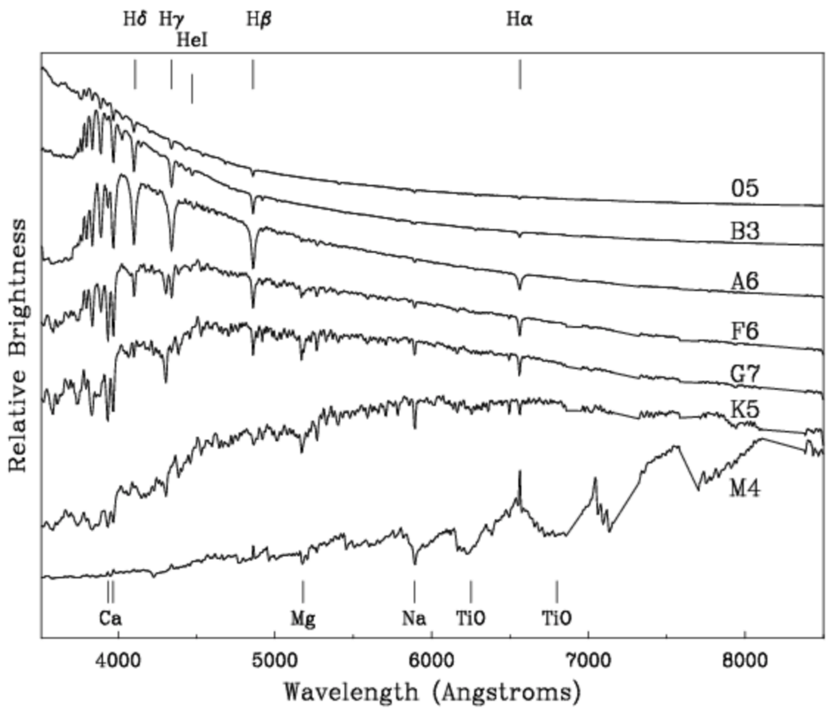

Figure 1.8. Stellar spectra of O B A F G K M type stars. The hottest and bluest are O type stars, with M type being the reddest and coolest of these. Image credit: Jules Halpern.

of each of these types of star. O and B type stars are bright at the blue end as they are hotter and younger, whereas K and M type stars have a higher continuum in the red part of the spectrum as they are older and cooler. The absorption lines occur due to atoms in the chromosphere and are different strengths for different types of star.

Figure 1.9 shows the spectrum of a typical passive galaxy (top panel) compared to a typical star-forming galaxy (bottom panel). Red galaxies tend to be more massive and are dominated by old, G and K type stars that are metal-rich. The spectra of red galaxies have lots of absorption features such as Mg and Na lines, with little to no [OII] emission. They also have strong 4000Å breaks due to the lack of blue stars and the accumulation of absorption lines below 4000Å, so the red end of the spectrum dominates the light emitted from the galaxy.

Blue galaxies tend to contain younger, more massive stars such as O and B type stars. These stars are short lived, but very bright, and emit at the blue end of the spectrum, causing star-forming galaxies to look blue in colour. Like red galaxies, blue galaxies have some absorption lines, but also contain emission lines due to ionised gas in the galaxy re-radiating at specific wavelengths. They usually have strong [OII] emission and several other narrow emission lines such as Hα, Hβ and [OIII]. However, dust obscuration can make star-forming galaxies appear redder and dimmer than they actually are. If a galaxy is enshrouded by dust, the light emitted by stars can be absorbed and re-emitted at longer wavelengths. Dust also scatters light from the galaxy, and as the light from young, bright stars is preferentially scattered, this has a reddening effect on the galaxy.

1.2.3 Possible quenching mechanisms

The existence of the blue cloud and the red sequence is well documented, but we do not know how galaxies transition between these two populations. Galaxies are thought to form in the blue cloud before evolving onto the red sequence, but this must be a quick transition to explain the lack of galaxies observed between these two populations. The process of a galaxy moving to the red sequence is known as 'quenching' and is linked to the feedback mechanisms discussed in Section 1.2.1. However, exactly which physical processes quench galaxies and what effect they have on various galaxy properties is still unclear.

One way that a galaxy is thought to be quenched is via environmental processes. Observations have found that in dense environments such as clusters, galaxies with early-type morphologies dominate, whereas in low-density regions galaxies have predominantly late-type morphologies (Hubble & Humason 1931; Abell 1965). Dressler (1980) found that there is a steady increase in the fraction of elliptical and lenticular galaxies towards cluster centres, whilst the fraction of spirals and irregulars

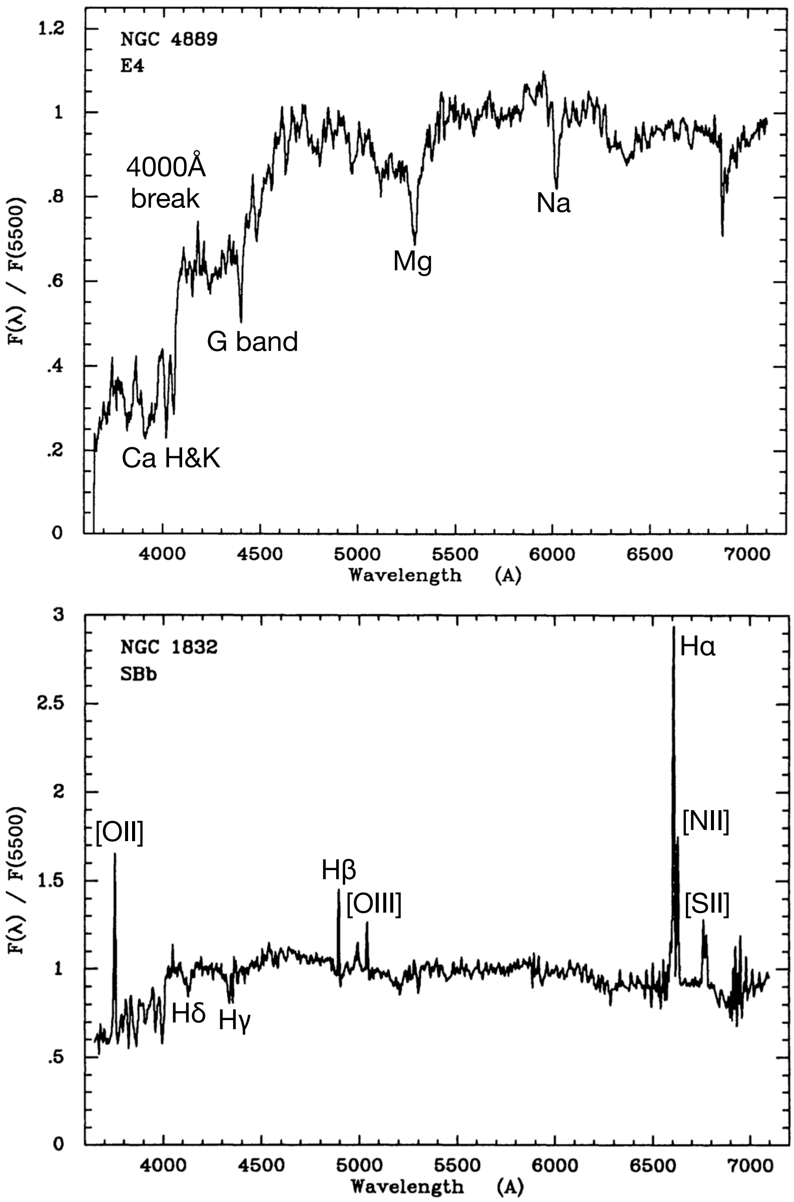

Figure 1.9. Spectrum of a typical passive galaxy (top panel) and a typical star-forming galaxy (bottom panel), adapted from Kennicutt (1992) and labelled with common spectral lines. The passive galaxy has a strong 4000Å break, absorption lines but little emission, whereas the star-forming galaxy has several narrow emission lines.

decreases. The colour and SFR of galaxies is also strongly correlated with environment, with galaxies in dense environments appearing to be redder on average than in field environments (Blanton et al. 2005; Baldry et al. 2006) and tending to have lower SFRs (Lewis et al. 2002; Gómez et al. 2003). The fraction of AGN in the local Universe is also found to be lower in cluster environments than in the field (Dressler, Thompson & Shectman 1985; Kauffmann et al. 2004). Together, this points towards the fact that as galaxies enter cluster environments, they begin to move onto the red sequence, changing morphology, colour and SFR.

However, some studies suggest that environmental processes are not the main mechanisms responsible for galaxy quenching (e.g. van den Bosch et al. 2008; Tanaka et al. 2004). Cluster galaxies are typically older than field galaxies with a similar mass. As galaxy properties are strongly correlated with internal properties of the galaxy (Roberts & Haynes 1994; Kauffmann et al. 2003) they are therefore more likely to be spheroidal, red and have little ongoing star formation. Some studies (e.g. Kauffmann et al. 2003) have found evidence of a critical mass beyond which galaxies change their properties, suggesting that some quenching mechanisms may be independent of the environment a galaxy is in, but depend only on some intrinsic galaxy property, such as stellar mass.

Peng et al. (2010) investigated quenching mechanisms by examining the relationship between stellar mass, environment and SFR. They found that up to $z \sim 1$, high-mass galaxies are more likely to be quenched, irrespective of environment, and that galaxies in overdense regions were also more likely to be quenched, regardless of stellar mass. This can be seen in Figure 1.10, where the passive fraction of galaxies is shown as a function of both stellar mass and overdensity. Peng et al. (2010) suggest that there are two separate quenching mechanisms - 'mass quenching' and 'environmental quenching'. We will now review the possible quenching mechanisms for both mass and environmental quenching.

Mass quenching mechanisms

It was suggested by Peng et al. (2010) that the more massive a galaxy is, the more likely it is to be quenched. Some of the processes that could be responsible for quenching a galaxy of high stellar mass are:

- *AGN feedback* - Accretion onto a supermassive black hole at the centre of a galaxy fuels AGN activity and is a potential cause for galaxies being quenched at high masses. AGN feedback is thought to occur in two modes - 'quasar mode' and 'radio mode' (Fabian 2012). Quasar mode feedback occurs when the black hole is accreting at close to the Eddington limit and can generate high velocity outflows and radiative feedback, which can lead to the heating or even ejection of some of the interstellar medium (ISM). On the other hand, radio

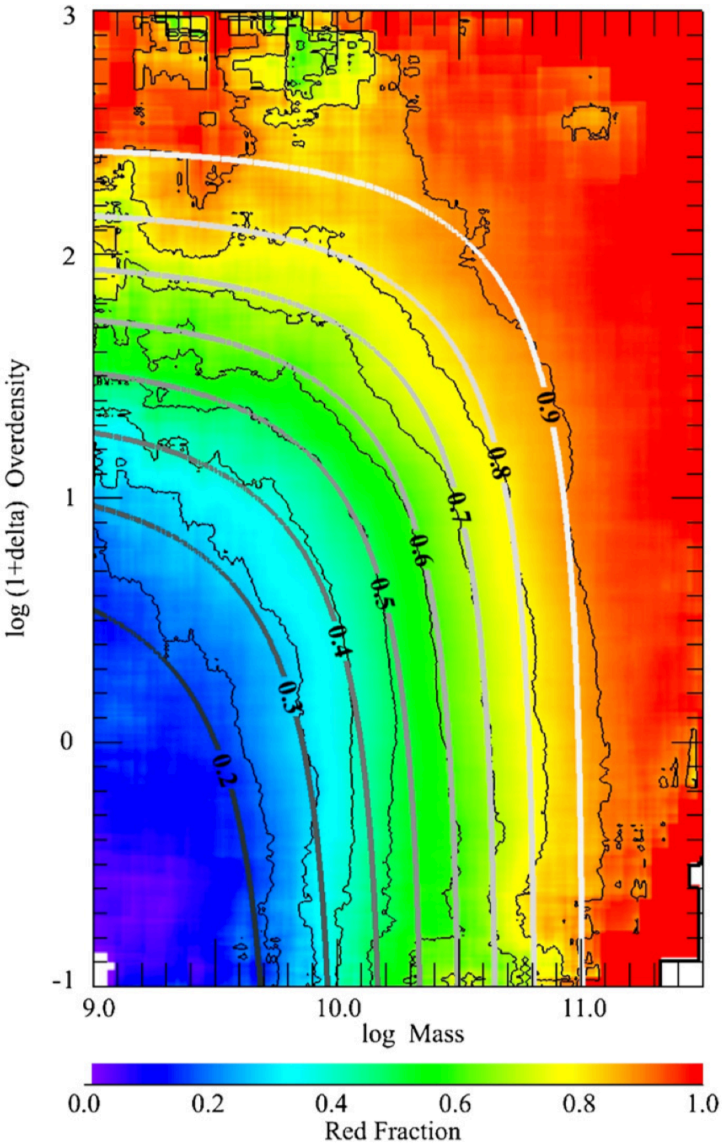

Figure 1.10. Passive fraction of galaxies as a function of stellar mass and overdensity, taken from Peng et al. (2010). Galaxies with high stellar mass, independent of density, and galaxies in overdense region, regardless of stellar mass, are more likely to be passive.

mode feedback occurs when accretion rates are low, and results in powerful relativistic jets being created by the black hole, which can heat the gas in the galaxy's halo. Simulations have shown that quasar mode feedback can quench star formation by heating and dispersing cold gas (Di Matteo, Springel & Hernquist 2005; Springel et al. 2005; Bower et al. 2006), whereas radio mode feedback is used to regulate star formation by balancing heating and cooling (Croton et al. 2006).

- *Stellar feedback* - In galaxies undergoing a starburst, the energy generated by supernovae and stellar winds can drive outflows from the galaxy (Chevalier & Clegg 1985; Leitherer, Robert & Drissen 1992). This can have a similar effect to AGN feedback, heating and ejecting gas from the galaxy and quenching star formation. Stellar feedback has been used since the earliest simulations to reduce the efficiency of star formation in low-mass galaxies and therefore reduce the number of low-mass galaxies (White & Frenk 1991; White & Rees 1978). It has also been suggested that stellar feedback may play a role in quenching compact high-mass galaxies at high-redshift, due to the high surface density of star formation (Diamond-Stanic et al. 2012).

- *Morphological quenching* - A requirement for efficient star formation is gravitational instabilities in the gas disk, allowing for gas clouds to form through fragmentation (Kawata, Cen & Ho 2007). However, the transition from a stellar disk to a spheroid can act to stabilise the gas disk, stopping star formation even if a cold gas reservoir is still present in the galaxy (Martig et al. 2009).

- *Shock-heating* - When gas falls into a dark matter halo and loses potential energy it is heated up. In haloes more massive than $\sim 10^{12}\mathrm{M}_{\odot}$, this gas cools slowly and forms a halo of hot gas in the centre of the dark matter halo (Birnboim & Dekel 2003; Kereš et al. 2005). Any new gas that then enters the halo is shock-heated when it encounters this gas. This prevents gas in the galaxy cooling onto a disk and forming stars. However, on long enough timescales (~ 2 Gyr) this gas should cool and begin forming stars, so this is not likely to be the sole way that galaxies are quenched.

Environmental quenching mechanisms

As galaxies fall into the potential well of a larger host object, there are many environmental effects that can act to change the SFR, morphology, gas content and even stellar content of a galaxy. These can be split into two main types - gravitational interactions or hydrodynamical processes due to the interaction of a galaxy with external gas, such as the intracluster medium (ICM) (see Boselli & Gavazzi (2006) for a review). Some of the mechanisms that could be responsible for environmentally affecting a galaxy are:

- *Mergers* - Galaxies can merge with one another in group or cluster environments, resulting in the merging of their stellar populations which significantly affects the resulting morphology (Bekki 1998). Mergers are commonly separated into 'major' and 'minor' depending on the mass ratios of the galaxies involved, with minor mergers typically having ratios of 4:1 or larger. Another way to separate mergers is into 'wet' and 'dry' mergers. In a wet merger, the galaxies merging are gas-rich. The gas is compressed and funnelled into the centre, leading to a starburst and compact remnant (Mihos & Hernquist 1996; Barton, Geller & Kenyon 2000). Along with stellar feedback, an AGN can also be triggered by the merger (Hopkins et al. 2005). Both of these processes can heat and remove gas from the galaxy, quenching it. In a dry merger there is little gas, so no associated starburst event occurs (van Dokkum 2005; Bell et al. 2006).

- *Harassment* - The culmination of repeated encounters with other galaxies in dense environments can have significant effects on a galaxy, as in cluster cores galaxies have high relative velocities (Moore et al. 1996). This harassment effect is enough to tidally strip both hot and cold gas from a galaxy, in addition to altering its morphology.

- *Interactions with the host potential* - Galaxies can also be affected by tidal forces due to the potential well of the host. In clusters, this effect can truncate the dark matter halo of an infalling object (Merritt 1983), leading to the hot gas reservoir being removed. Interactions with the host potential can also cause tidal compression of gas in the galaxy, actually temporarily enhancing star formation (Byrd & Valtonen 1990).

- *Ram pressure stripping* - Infalling galaxies can have their cold gas removed due to the ram pressure exerted on the galaxy by the ICM (Gunn & Gott 1972). As ram pressure stripping can remove even the cold gas from the disk of a galaxy, it can lead to a very rapid shut off of star formation on the timescale of hundreds of Myr (Steinhauser, Schindler & Springel 2016). However, early on in this process gas can be compressed and star formation temporarily enhanced (Dressler & Gunn 1983; Evrard & Henry 1991). Evidence of ram pressure stripping comes from star formation being observed in the HI tails of 'jellyfish' galaxies (Fumagalli et al. 2014) and from the role ram pressure plays in simulations (Abadi, Moore & Bower 1999; Arthur et al. 2019; Yun et al. 2019).

- *Strangulation* - Sometimes the ram pressure and tidal forces detailed above cannot overcome the gravitational binding energy of the cold gas, but are still able to remove the hot gas from the galaxy. This is referred to as strangulation; the exclusive removal of the hot gas reservoir. In instances such as these, cold gas is still available for star formation, so the quenching process is slower than if both gas components were fully depleted, stopping star formation on the timescale of > 1 Gyr. However, once the cold gas is used in star formation it will not be replenished and no further star formation can occur (Larson, Tinsley & Caldwell 1980).

1.2.4 Post-starburst galaxies

One way to investigate various quenching methods is to look at galaxies that are between the blue cloud and the red sequence. Known as green valley galaxies, they are thought to be in the process of having their star formation shut down and could still retain signatures of the process that quenched them. However, it is still unclear whether these galaxies are truly transition objects, or just scatter from the blue cloud and the red sequence. Another approach is to look at galaxies which have been recently quenched, but still have evidence of recent star formation in their spectra. These galaxies are known as 'post-starburst' (PSB) galaxies, as they have been recently and rapidly quenched, sometimes following a burst of star formation.

The spectra of PSBs, also known as 'k + a' galaxies, resemble that of a red galaxy, overlaid with a population of A type stars (see Figure 1.11). They are characterised by the presence of strong Balmer absorption lines produced by the A type stars, but have little [OII] emission (Dressler & Gunn 1983; Yang et al. 2004; Wild et al. 2009). The lack of O and B type stars show that these galaxies are no longer actively forming stars, but the presence of A type stars indicates that the galaxy has formed a significant fraction of its stellar mass ($\gtrsim 10\%$) during the last Gyr through star formation (Norton et al. 2001; Yang et al. 2004; Kaviraj et al. 2007). This, added to the fact that the lifespan of A stars is short so their signatures will be short lived, suggests that PSBs must have been recently and rapidly quenched. Due to this, PSBs are rare at all redshifts and account for fewer than 5% of the galaxy population (Goto et al. 2003; Wild et al. 2016). However, although they can be difficult to identify, they are an ideal population to study the quenching of galaxies.

Although all PSBs have the same spectral features, they exhibit different characteristics in different redshift ranges. At $z < 0.5$ PSBs are very rare and have been observed to be generally massive and in low density environments. (Zabludoff et al. 1996; Quintero et al. 2004). They tend to have disturbed morphologies, suggesting that they could have had a gas-rich merger, which triggered an episode of heightened star formation followed by rapid quenching (Goto 2004; Wild et al. 2009; Cales et al. 2011; Cales & Brotherton 2015). Between $0.5 < z < 1.0$, PSBs tend to have lower stellar masses and have been found in clusters (Wild et al. 2016; Maltby et al. 2016;

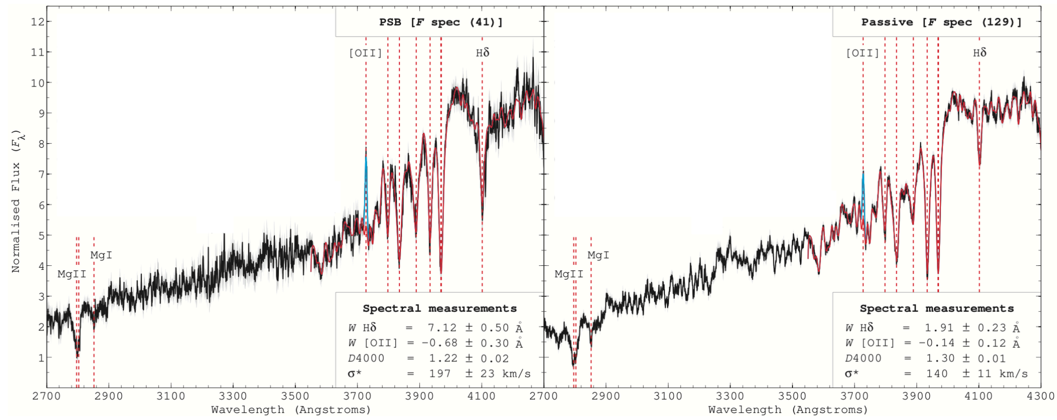

Figure 1.11. Stacked spectra for PSBs (left panel) and passive galaxies (right panel) at $z > 1$, taken from Maltby et al. (submitted). Compared to passive galaxies, PSBs have stronger Balmer absorption lines, which when paired with a general lack of emission lines, are the spectral signatures of PSBs. They also have a slightly different shape SED.

Socolovsky et al. 2018). At redshifts $z > 1$ PSBs have been observed to be extremely compact and spheroidal, suggesting they have been through a major morphological disruption (Almaini et al. 2017). By comparing the passive and PSB stellar mass functions at $0.5 < z < 2.0$, Wild et al. (2016) found that if the spectral features of PSBs are only visible for ~ 250 Myr, then it is possible for 100% of passive galaxies to have been through a PSB phase.

There is observational evidence to suggest that outflows are present in PSBs in the range $0.2 < z < 0.8$ (Coil et al. 2011), which can be particularly strong in the case of the most luminous PSBs (Tremonti, Moustakas & Diamond-Stanic 2007). Maltby et al. (submitted) have also found evidence of high-velocity outflows in PSBs in the redshift range $1.0 < z < 1.4$ and suggest that a compaction event triggered either a starburst event or AGN activity. However, they find no evidence of AGN signatures in the spectra of the PSBs. This agrees with other studies that have found no evidence of AGN activity in PSBs (e.g. Fabello et al. 2011; French et al. 2015; Rowlands et al. 2015), but conflicting studies have found low redshift PSBs hosting AGN (e.g. Schawinski et al. 2009; Alatalo et al. 2011; Cicone et al. 2014). It is still not clear what quenching mechanisms are acting on PSBs and if they differ with redshift.

The most robust way to identify PSBs is with good quality spectra covering the 4000Å break region. This is possible at low redshift but beyond $z = 1$ very few PSBs have been spectroscopically confirmed (Vergani et al. 2010; Maltby et al. 2016). In order to increase the number of PSBs, two techniques have been developed to identify them based on photometric data alone. Whitaker et al. (2012a) used a cut on the rest-frame UVJ diagram to separate PSBs and passive galaxies, but this is less reliable at high redshift. Wild et al. (2014) more recently established a technique that uses Principal Component Analysis (PCA) and selects PSBs based on the shape of their spectral energy distributions (SEDs). We will discuss the PCA method in more detail in Chapter 4 as this is the technique used in this thesis.

1.2.5 Deep surveys

One way to study galaxy quenching is to directly observe galaxies forming and evolving in the distant Universe. At high redshift ($z > 1$), deep near-infrared observations are vital to select galaxies by rest-frame optical light. Selecting high redshift galaxies using optical imaging will introduce strong biases against dusty galaxies or those with evolved (i.e. passive) stellar populations (e.g. Cowie et al. 1996). It is only recently that deep near-infrared surveys have been conducted with the required depth and area to produce large galaxy samples at high redshift, sufficient to allow accurate determinations of the galaxy stellar mass function while minimising the influence of cosmic variance. In particular, the UKIDSS Ultra Deep Survey (UDS) (Lawrence et al. 2007, Almaini et al. in preparation) and UltraVISTA (McCracken et al. 2012) are now deep enough to detect typical (i.e. M^*) galaxies to $z \sim 3$, over large volumes of the distant Universe ($\sim 100 \times 100$ projected comoving Mpc at $z = 3$). Using these surveys, we can directly test model predictions for the build-up of the galaxy populations, rather than inferring their evolution by extrapolating back in time. However, each galaxy is only being seen at one point in its life and we cannot infer the full evolutionary history.

In order to get a cohesive picture of what happens to galaxies throughout their lives, one approach is to link a population of galaxies at high redshift to a population at low redshift that could be their descendants. This can be done by selecting galaxies at a constant comoving number density when ranked by stellar mass or luminosity, with a correction to account for galaxy mergers (Mundy, Conselice & Ownsworth 2015). This method was partly motivated by the need to overcome 'progenitor bias', where new young star-forming galaxies enter the sample at low redshift that are not present at high redshift (Shankar et al. 2015). Not accounting for this bias correctly can lead to a poor selection of the set of galaxies being connected as progenitor and descendant and therefore incorrect conclusions being drawn about their evolution.

1.3 Galaxy formation models

A powerful method to trace galaxies through redshift is to use semi-analytic models (SAMs, see Kauffmann, White & Guiderdoni 1993; Cole et al. 1994; Baugh 2006; Benson 2010; Somerville & Davé 2015). SAMs are a type of galaxy formation model in which simple analytic prescriptions (in connection with merger trees from either cosmological simulations or extended Press-Schechter formalisms, Press & Schechter

1974) are used to model the physical processes occurring during galaxy formation and evolution. These models are able to evolve the same population of galaxies through redshift and connect them without the limitations of observational methods. These models are also computationally inexpensive, so can be used to simulate large volumes and produce large catalogues of galaxies with which to compare observational data. We will now review the physical processes generally involved in these models.

1.3.1 Dark matter

As discussed in Section 1.1.1, current observations suggest that roughly 26% of our Universe is comprised of dark matter (Planck Collaboration et al. 2018). The early fluctuations in the density of dark matter grow under gravity to form the cosmic web structure that galaxies trace. In order to recover the large-scale structure of galaxies, most SAMs use dark matter merger trees from dark-matter-only (DMO) simulations as an input. Here we will briefly discuss the development of DMO simulations and how merger trees are constructed from them.

Dark-matter-only simulations

The first simulations of how structure grows over time in a ΛCDM Universe were carried out by Davis et al. (1985), in order to improve our understanding of cosmology. In DMO simulations, boxes are populated with dark matter particles with initial density fluctuations, the amplitude of which are dictated by the power spectrum inferred from cosmology and the CMB. The system is then evolved over time under Newtonian gravity. One of the earliest DMO simulations, run by Davis et al. (1985), was $32.5h^{-2}$Mpc on each side and used 32,768 particles, with each dark matter particle having a mass of $\sim 6 \times 10^9 \mathrm{M}_{\odot}$. Since then, both computing power and the algorithms used have advanced rapidly, allowing N-body simulations with larger volumes and higher mass resolution to be run. The latest simulations, such as the Euclid Flagship simulation, are now of boxes $4h^{-1}$Gpc on each side, using over 4×10^{12} particles, each with a mass of $10^9 h^{-1}\mathrm{M}_{\odot}$. These increasingly large volumes allow more realistic mock observations to be made without any repetitions and lessen the effect of cosmic variance.

Figure 1.12 shows an example of a recent DMO simulation, MultiDark, that uses over 8 billion particles, each with a mass of $\sim 10^9 h^{-1}\mathrm{M}_{\odot}$, to simulate a box of side length $1h^{-1}$Gpc (Prada et al. 2012). The dark matter distribution follows the cosmic web structure, as we saw earlier in Figure 1.3. DMO simulations have also allowed us to learn about the density profiles of dark matter haloes (Navarro, Frenk & White 1996) and the abundance of dark matter haloes as a function of mass (Jenkins et al. 2001). The evolution of dark matter is now well understood and works as the basis for most SAMs.

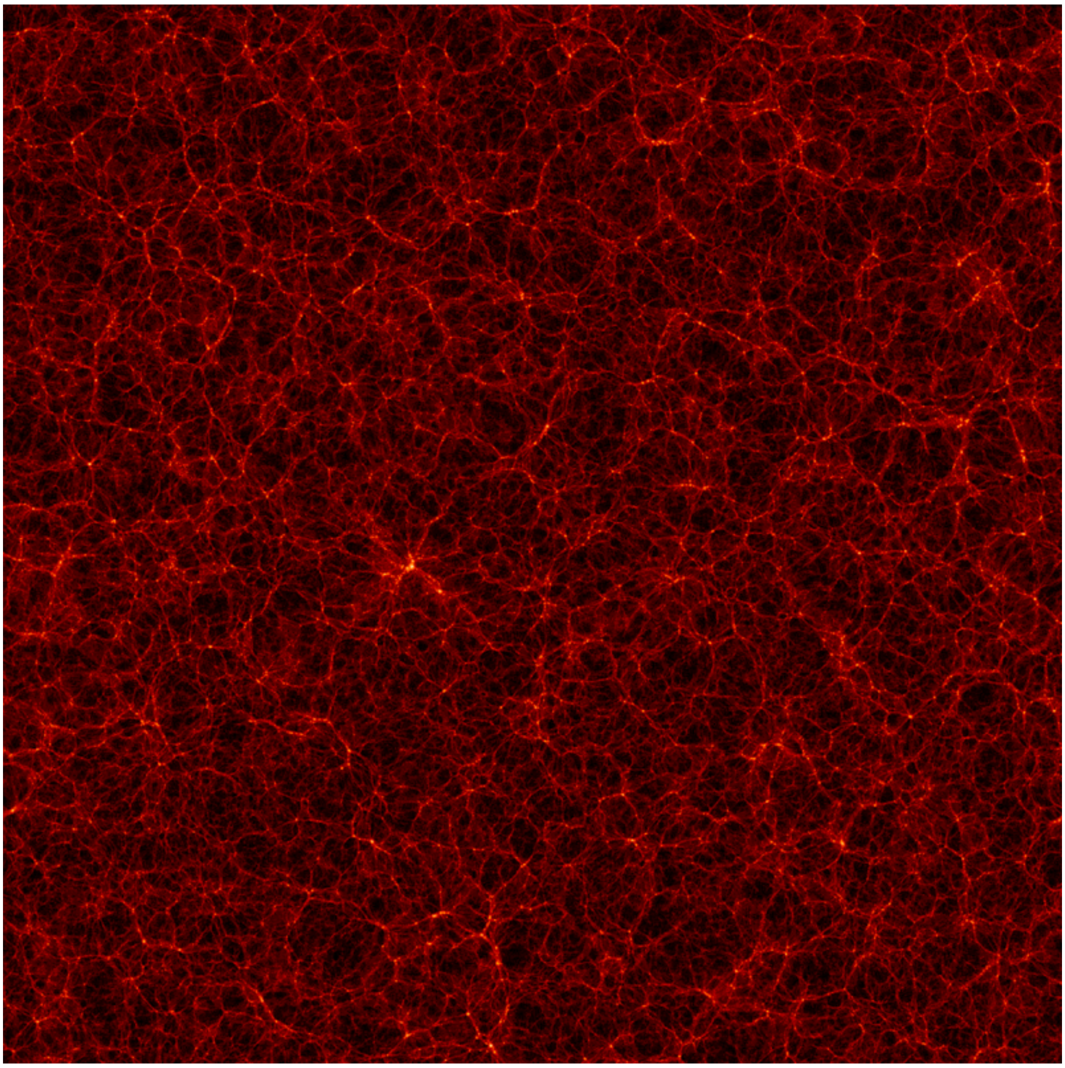

Figure 1.12. Slice through the MultiDark simulation at $z = 0$. The size of the box is $1h^{-1}$Gpc and this shows a slice $5h^{-1}$Mpc thick. The structure of the cosmic web is clearly visible. Image credit: Stefan Gottlöber, IDL, Prada et al. (2012).

Finding dark matter haloes

Once the DMO simulation has been run, the first step in post-processing is to use a 'halo finder', which identifies dark matter haloes and outputs a halo catalogue. Until the 90s, two main techniques were used. The first was developed by Press & Schechter (1974), who used a spherical overdensity (SO) method, whilst Davis et al. (1985) introduced a friends-of-friends (FOF) algorithm to identify haloes. These remained the standard methods until substructure was identified within dark matter haloes (Tormen, Bouchet & White 1997). Finding subhaloes within haloes presented a much more complex problem, which led to a surge in the number of new halo finder codes being introduced, helped by the rapid pace of technology development at the time.

Halo finders can be split into two main categories - 'density peak locators', such as SO, and 'direct particle collectors', such as FOF (Knebe et al. 2013). The first of these two types works by finding peaks in the density field of dark matter. Around these peaks, spherical shells are increased in size until the density drops below a specific value (usually derived from a spherical top-hat collapse). The haloes found using this method are spherical by definition. An example of a more recent code using this method is Amiga Halo Finder (AHF, Knollmann & Knebe 2009).

The particle collector method finds haloes by grouping particles that are close together based on their 3D (or 6D) coordinates. The haloes that are found are then not necessarily spherical in shape. Rockstar (Behroozi, Wechsler & Wu 2013) is a recent example of a particle collector code that uses the 6D coordinates of dark matter particles to find haloes, maximising consistency across timesteps. Some codes also use a hybrid technique. For example, SUBFIND (Springel et al. 2001) identifies dark matter haloes first using a FOF technique and then identifies local overdensities within each FOF group to find subhaloes.

Although they use different techniques, halo finders share the same main steps when finding dark matter haloes. Firstly, candidate identification takes place to create a list of potential halo centres. Particle collection then occurs to ensure that each dark matter particle is associated with only one halo. The next step is to find the centre of the halo, either from the peak in the density field or from the centre of mass of all particles in the halo. Next any gravitationally unbound particles are removed, before the mass and size of the halo is computed from its member particles. Some halo finders also add in a final step to ensure that no haloes are lost or added between snapshots. Comparisons of various halo finders has found that whilst there are still discrepancies between different methods when identifying subhaloes (Onions et al. 2012), there is good agreement for finding dark mater haloes (Knebe et al. 2011).

Building dark matter merger trees

One type of galaxy formation model, called halo occupation distribution modelling, assigns galaxies to haloes independently within each snapshot, without connecting them to their progenitors and descendants. However, SAMs have the advantage of being able to track a galaxy through time, allowing the evolution of various galaxy properties to be investigated. In order to do this, the connection of haloes to their progenitors and descendants also needs to be known. 'Tree builders' are used to connect halo catalogues from different snapshots, constructing a halo merger tree (as seen in Figure 1.2). In these merger trees, each halo has a main progenitor branch, with several other branches merging together to form the final halo. Each halo can only have one descendant, but can have many progenitors.

Most tree codes use a merit function to identify the progenitors and descendant of a halo (Srisawat et al. 2013). This works by looking at each dark matter particle in a halo and seeing how many are in common with another halo in a different snapshot. By maximising the number of particles in common, the codes can identify the main progenitor or descendant and begin to build up a merger tree. Often a halo will have more than one progenitor, as it will have considerable particle overlap with two separately identified haloes in the previous snapshot.

Some more sophisticated tree builders, such as ConsistentTrees (Behroozi et al. 2013), will also ensure that no haloes are lost between snapshots. One example where this could happen would be where a subhalo's orbit passes close to the centre of the larger halo it is in. In the initial snapshot the subhalo is identified, but could be missed in the next snapshot when the centres of the two haloes are close together. Here some tree builders will assume the two have merged. However, if the subhalo passes by without merging it will then reappear in the next snapshot with no progenitors and will not be connected to the subhalo that was there before. These issues are dealt with by constructing the 'missing halo' and inserting it into the halo catalogue. The satellite galaxy which would be within the subhalo in this example would then not be lost at any time.

Another technique used by some halo finders is to use the full 6D information from the halo, along with its mass and radius, to ensure that there are no spurious results. In a similar example to above, if one halo passes too close to the centre of another halo, its mass can suddenly increase due to particles from the other halo being misassigned to it, before decreasing again the next snapshot. The ConsistentTrees code smooths over these changes and instead inserts predicted halo properties. These merger trees are then used as the input for most SAMs.

1.3.2 Baryonic physics

Now that the backbone of the SAM has been provided in the form of a dark matter merger tree, the baryonic physics can be added. Generally the processes that govern how galaxies form and evolve are very complex. For example, we cannot just assume that the mass of a galaxy scales linearly with the mass of its halo, as the shape of the halo mass function and observed stellar mass function are different (see Section 1.2.1). Therefore, baryonic physics is added to SAMs in the form of analytic prescriptions, that include free parameters that can be calibrated to observations. From these parameter fits, we can then learn about the physics of galaxy formation. Figure 1.13 is a flow diagram which shows the general steps of a SAM and what order they are performed in. We will now give an overview of the physical processes typically included in modern SAMs.

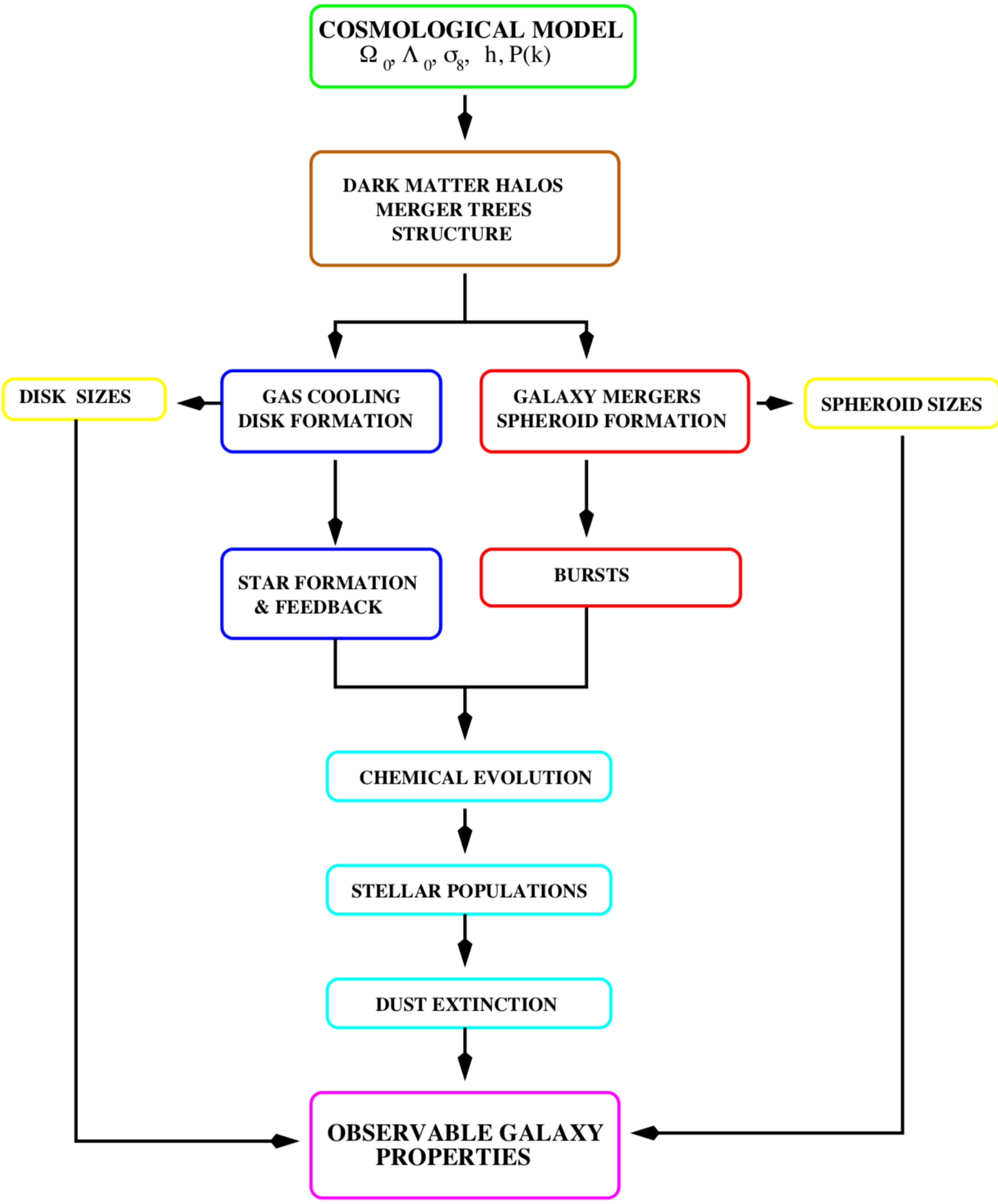

Figure 1.13. Overview of the processes involved in a galaxy formation model, taken from Baugh (2006). Along with cosmological parameters, a dark matter merger tree is used as an input. Baryonic processes such as star formation are included as analytic prescriptions.

Gas cooling

The gas is assumed to start with the same initial distribution as dark matter, with the ratio of dark matter to baryons being set by observed cosmological parameters. The dark matter begins to collapse under gravity, forming dark matter haloes, whose properties are then known from the merger trees which are given as an input. Gas falls into the potential well of a dark matter halo and is either shock heated to the virial temperature of the halo or cools almost immediately, depending on halo mass. The former produces a hot gas halo which is supported against continued collapse by radiation pressure from the gas itself.

This gas can then cool via a number of different mechanisms, such as: i) Inverse Compton scattering of CMB photons by electrons in the hot gas, ii) photon emission due to collisions causing transitions between energy levels, iii) Bremsstrahlung radiation from electrons being accelerated in the ionised gas. Which of these mechanisms dominate and therefore, the rate at which gas can cool, depends on the temperature of the gas and its chemical composition and density. The removal of pressure support once the gas is cool means that it then collapses into the centre of the halo, forming a cold gas disk to conserve angular momentum. The size of this disk is proportional to the angular momentum of the gas and inversely proportional to the mass of the cold gas and maximum circular velocity of the halo.

Star formation

SAMs generally use a top-down model for star formation, where cold gas clouds fragment and collapse to form stars (Krumholz, McKee & Klein 2005). The SFR is assumed to be proportional to the amount of cold gas available for star formation:

$$\mathrm{SFR} \propto \frac{M_{\mathrm{cold}}}{\tau}, \tag{1.2}$$

where M_{cold} is the mass of the cold gas disk and τ is the characteristic timescale for star formation. This timescale can be fixed or proportional to the dynamical time of the disk, R_*/V_{max}, where R_* is the disk radius and V_{max} is the maximum circular velocity of the halo. The disk radius is proportional to the angular momentum of the stars and inversely proportional to the stellar mass and V_{max}.

In some models, a fraction of the stars formed are assumed to be massive and short-lived, determined by the initial mass function (IMF). The mass associated with these stars is immediately returned to the gas disk. Some models also assume that when galaxies merge a burst of star formation can occur, details of which are given in the section on mergers below.

Feedback processes

Feedback processes are included in SAMs to regulate the cooling and make star formation less efficient in low-mass and high-mass haloes (see Sections 1.2.1 and 1.2.3). Generally, we can consider two forms of feedback - one where cold gas is heated and removed from the disk and one where the rate which gas cools onto the disk is reduced.

One of the main forms of feedback included in SAMs is from supernovae, which release energy into both the cold and hot gas components. Some of the cold gas is heated and removed from the disk, joining the hot gas halo, which is called 'retention' feedback. The hot gas is also heated and some of it is ejected from the halo in a wind into an external reservoir, which is called 'ejection' feedback. Some galaxy formation models also include a reincorporation timescale, which dictates the time taken for gas in the ejecta reservoir to be returned to the hot gas halo (e.g. Henriques et al. 2013).

Another form of feedback utilised in almost all SAMs is from AGN. Models usually have a 'quasar mode', where the mass of the black hole is increased during mergers and through cold gas accretion during starbursts. 'Radio mode' is also included, where the black hole accretes gas from the hot halo (Croton et al. 2006). Quasar mode is the primary way that black holes increase their mass, but in most models there is no associated feedback mechanism. However, in a few models galactic outflows can be driven by quasar mode feedback (e.g. Somerville et al. 2008). Radio mode feedback is included where energy is released into the hot halo, which can suppress cooling flows in more massive systems. This works by suppressing the cooling rate in proportion to the hot gas mass accreted onto the black hole.

Environmental effects

Galaxies can also be affected by their environment. Many models now incorporate environmental effects such as harassment, tidal stripping or ram pressure stripping. When a galaxy becomes a satellite after it falls into a larger halo, it is typically not allowed to accrete any new gas, and the dark matter halo and hot gas are tidally stripped away, which leads to strangulation of the galaxy. Some models include a delay in this stripping process in order to reduce the fraction of passive satellites (Font et al. 2008; Weinmann et al. 2010). Once the dark matter halo has been stripped from a galaxy, it can be classed as an orphan (e.g. Gonzalez-Perez et al. 2014; Henriques et al. 2015; Cora et al. 2018b). As orphans have no dark matter or hot gas, their potential well is not as deep and tidal forces then begin to disrupt the cold gas and stellar content of the galaxy, in some cases removing it completely. In this situation, the stars are added to the intracluster light and the cold gas is added to the hot gas halo of the central galaxy.

Ram pressure stripping of hot and cold gas can also occur in SAMs. If the ram pressure exerted on a satellite by the ICM exceeds the gravitational force binding the gas to the galaxy, it is removed and added to the hot gas reservoir of the central. Some SAMs incorporate ram pressure stripping of both hot and cold gas (e.g. Cora et al. 2018a), with the cold gas removal only occurring when the hot gas has been completely removed. However, most SAMs only consider ram pressure stripping of the hot gas component.

Mergers

Dark matter haloes grow hierarchically through mergers to form larger objects. Once a subhalo crosses the virial radius of a larger halo, it becomes a subhalo and the galaxy within it becomes a satellite. This satellite will then orbit within the dark matter halo of the central galaxy, losing energy through dynamical friction. The orbital energy of the satellite will decay and it will eventually merge with the central galaxy.

For a major merger, the disks of both the satellite and the central are usually destroyed and all of the stars in both galaxies, along with any formed during the merger, become the bulge of the descendant. In a minor merger, the disk of the central usually survives, accreting the cold gas from the satellite. All of the stars in the satellite are added to the bulge of the descendant and any stars formed during a minor merger stay in the disk of the descendant. For some models, the fraction of stars that are added to the bulge of the descendant depends on the merger mass ratio and gas fraction of the progenitors (e.g. Porter et al. 2014).

Stars are formed during the merger with a rate proportional to the combined mass of both cold gas disks. Another term is added in some models (e.g. Somerville, Primack & Faber 2001), where the SFR during the merger is scaled by the mass ratio of the merger. Another additional process that occurs during the merger is cold gas being accreted onto the black hole, which grows in quasar mode.

Chemical evolution

Stars forming and evolving changes the metal content of the ISM of galaxies. When stars form, cold gas and metals are removed from the ISM and when they die this material is returned with an enhanced metallicity. Some stars will experience a supernova explosion which can potentially remove material from the galaxy, so the amount of gas returned to the ISM compared to the mass of stars formed depends on the IMF.

The total mass of metals can be followed in SAMs, assuming that a set amount of metals are produced per solar mass of stars. This amount is determined by the yield for the IMF chosen. These metals are instantaneously produced and mixed with the cold gas, following this component if it is heated or ejected. More advanced methods of following metals (e.g. De Lucia et al. 2014) track the amount of individual metals as the stars age, considering both instantaneous recycling from type II supernovae and delayed enrichment from type Ia supernovae.

Spectral energy distribution

Many SAMs now compute galaxy SEDs in post-processing in order to compare predicted galaxy populations with observed ones. To do this, models couple the galaxy star formation histories (SFHs) with a stellar population synthesis (SPS) model. Each galaxy SFH includes information on how many stars were formed at each timestep, added for all the progenitors of the galaxy. The SPS model first constructs simple stellar populations (SSPs) of stars with the same age and a range of stellar masses, dictated by the IMF. The SEDs of different age SSPs are then added together, according to the dust content, SFH and metallicity evolution of each galaxy, to form composite stellar populations. This allows an SED to be computed for each galaxy.

Many early SAMs did not take into account the effects of dust on galaxy SEDs, but have since realised the importance of doing so. Dust in a galaxy absorbs energy and is heated, resulting in emission at longer wavelengths. This acts to make a galaxy SED looked redder than it actually is. Some early models simply rescaled the galaxy luminosity by a fixed factor to account for dust attenuation (e.g. Cole et al. 1994; Baugh et al. 1998), but the effect of dust isn't the same at all wavelengths. Most models now compute the dust extinction as a function of wavelength, with some separately considering dust in the ISM and molecular gas clouds (De Lucia & Blaizot 2007). Re-emission is presently only modelled in some SAMs as it is complex to model and very sensitive to the temperature of the dust (Kaviani, Haehnelt & Kauffmann 2003).

1.3.3 Model calibration

Changes to the precise processes implemented in SAMs are driven by observations, as models aim to match certain observables. In addition to providing motivation to incorporate new physics, observations are used to calibrate the free parameters included in the analytic prescriptions. This is done either using an automated method or by hand, until a good match to the observational data picked for calibration is obtained. The data input into the model as a calibration constraint cannot then be seen as a 'prediction' of the model, but is rather a 'prescription'. Depending on how the output catalogue is to be used, a model may choose to calibrate to a wider or narrower range of observational data.

Simultaneously matching several different observational data sets is difficult for models and can actually be impossible if the model does not include all the necessary physics. If an optimally calibrated model cannot match multiple observational results, it is either because the observations appear to disagree with each other or because the model is missing an important physical process. Model calibration is therefore an important step as it can tell us how certain physical processes scale with redshift, halo mass, etc., and help us assess exactly how various mechanisms need to be implemented in order to reproduce observational results.

1.4 Thesis outline

The aim of this thesis is to investigate the processes governing star formation and quenching in galaxy formation models. By comparing the results from these models to observations, we can learn about what physical processes are missing from the models and which of these mechanisms might be involved in quenching galaxies that we observe in the Universe.

In Chapter 2 we compare the results from nine different galaxy formation models, looking at the number density of galaxies as a function of stellar mass and redshift. By splitting these galaxies into star-forming and passive populations, we can learn more about whether the quenching processes included in each model produce galaxies that match what we observe. We then compare the halo masses of galaxies in the models with inferred halo masses from observations, allowing us to investigate the connection between galaxies and their dark matter haloes and how this impacts their star formation.

We then take one of the models from Chapter 2, Lgalaxies, and use it to construct a mock lightcone catalogue, designed to be as similar to the UDS survey as possible. In Chapter 3 we describe both the UDS survey and the Lgalaxies model, before detailing how we adapted the model to generate the output in a lightcone format. Further changes are then made to the output, adding synthetic scatter to the data to emulate the uncertainties when measuring galaxy properties observationally. We also test the mock lightcone survey to ensure that it matches observations to an acceptable degree and that the predictions from the model have not changed from the standard version of Lgalaxies more than we would expect.

With this mock lightcone survey, we want to investigate the properties of PSBs in order to investigate the physical processes that are quenching this rare population of galaxies in the models. However, we first need to classify the galaxies in the mock catalogue and find PSB candidates. We describe the PCA classification method in Chapter 4 and compare the number densities to galaxies classified in the same way in the UDS. To further test the PCA method, we compare the SFH of PSB galaxies with their classification, to see if they have undergone a period of heightened star formation before being rapidly quenched. We also discuss the resolution of the SFHs and how this may affect our results.

In Chapter 5, we investigate the evolution of the PSB galaxies identified in the mock from the previous two chapters. From the LGALAXIES model, we have information about how the properties of galaxies change with lookback time, enabling us to investigate how the PSBs in the mock may have been quenched. We can then compare these results with the two populations of PSBs found in observations and make predictions for the quenching mechanisms acting on each. By tracking the properties of galaxies into the future, we are also able to show the evolutionary paths PSBs take after being quenched, which may help observations to connect galaxies at different redshifts.

Finally, we summarise our results in Chapter 6, providing overall conclusions for this work. We also discuss the future outlook for observations and simulations, exploring the developments that may be made by future surveys and in modelling galaxy formation and evolution.

Chapter 2

The evolution of the galaxy stellar mass function in observations and galaxy formation models

In this chapter we present a comparison of the observed evolving galaxy stellar mass functions with the predictions of eight semi-analytic models and one halo occupation distribution model. While most models are able to fit the data at low redshift, some of them struggle to simultaneously fit observations at high redshift. We separate the galaxies into 'passive' and 'star-forming' classes and find that several of the models produce too many low-mass star-forming galaxies at high redshift compared to observations, in some cases by nearly a factor of 10 in the redshift range $2.5 < z < 3.0$. We also find important differences in the implied mass of the dark matter haloes that galaxies inhabit, by comparing with halo masses inferred from observations. Galaxies at high redshift in the models are in lower mass haloes than suggested by observations, and the star formation efficiency in low-mass haloes is higher than observed. We conclude that many of the models require a physical prescription that acts to dissociate the growth of low-mass galaxies from the growth of their dark matter haloes at high redshift.

The work presented in this chapter is published in Asquith et al. (2018).

2.1 Recent developments in galaxy formation modelling

Galaxy formation models, such as semi-analytic models (SAMs), are very useful tools to trace a population of galaxies through redshift and investigate their evolution. By comparing the models to key observables, e.g. the evolution of the stellar mass function (SMF), we can learn about the physics of galaxy formation. If models are not able to reproduce observational results it may mean that they are missing key physics which is important in galaxy formation and evolution. Model galaxies can also be separated into 'star-forming' and 'passive' types, to test for the quenching processes which transform galaxies from star-forming to passive.

Whilst it has been shown that SAMs are able to reproduce the SMF at $z = 0$, they struggle to simultaneously match observations at both low and high redshift (e.g. Fontanot et al. 2009; Weinmann et al. 2012; Guo et al. 2011; Knebe et al. 2015), due to the anti-hierarchical formation of galaxies which seemingly contradicts the hierarchical assembly of dark matter haloes. After much work understanding both active galactic nuclei (AGN) feedback and the mass assembly of high-mass galaxies (e.g. Benson et al. 2003; Di Matteo, Springel & Hernquist 2005; Bower et al. 2006; Croton et al. 2006), models are now able to reproduce the high-mass end of the galaxy SMF over a range of redshifts. However, models still typically overproduce the number of low-mass galaxies at high redshift. The main reason for this discrepancy appears to be that galaxies in the models follow the growth of their dark matter haloes too closely (Weinmann et al. 2012; Somerville & Davé 2015; Guo et al. 2016), whilst in the real Universe it appears that there is not such a tight correlation (White, Somerville & Ferguson 2015; Guo et al. 2016).

This excess of low-mass galaxies at high redshift was investigated by Fontanot et al. (2009), who found that in three different SAMs, galaxies in the stellar mass range $9 < \log(M_*/\mathrm{M}_\odot) < 11$ form too early and have little ongoing star formation at late times. They concluded that the physical processes operating on these mass scales, such as supernova feedback, needed a re-think. Weinmann et al. (2012) later used two SAMs and two cosmological hydrodynamical simulations and examined the evolution of the observed number density of galaxies. They found that although the models fit well at $z = 0$, the low-mass galaxies were formed at early times. They conclude that as the current form of feedback is mainly dependent on host halo mass and time, it is unlikely to be able to separate the growth of galaxies from the growth of their dark matter haloes.

Monte Carlo Markov Chain (MCMC) methods were used by Henriques et al. (2013) in an attempt to fit the SMF at all redshifts, but they could not find a single set of parameters that allowed this. They then changed the reincorporation timescale for ejected gas to be inversely proportional to halo mass and independent of redshift and found that they were able to fit observed numbers of low-mass galaxies from $0 < z < 3$. However, the passive fraction of low-mass galaxies was still too high. Their model was later updated further in Henriques et al. (2015) where they also reduced ram-pressure stripping in low-mass haloes, made radio mode AGN feedback more efficient at low redshift, and reduced the gas surface density threshold for star formation. They then found that their model reproduces the observed abundance and passive fraction of low-mass galaxies, both at high and low redshift.

Another attempt to solve this problem was by White, Somerville & Ferguson (2015), who tried three different methods to decouple the accretion rate in galaxies from their star formation rate (SFR). They found that changing the gas accretion to be less efficient in low-mass haloes at early times and increasing the dependence of stellar feedback on halo mass at high redshift were the most successful at qualitatively matching the evolution of the number density of low-mass galaxies. However, they allow these functions to scale with halo mass and redshift in an arbitrary way which may not be physically motivated. Hirschmann, De Lucia & Fontanot (2016) also investigated this problem with their model and found that they improved their agreement with observations by either reducing the gas ejection rate with cosmic time or varying the reincorporation timescale with halo mass, classed as 'ejective' and 'preventative' feedback schemes respectively. Although their results improve from their fiducial model, they still find too many low-mass, red, old galaxies between $0.5 < z < 2.0$.

However, the effect of adjusting certain physical prescriptions can be vastly different between models. White, Somerville & Ferguson (2015) investigated what effect replicating the changes in Henriques et al. (2013) had on their own model, but found that it did not make much difference to the observed number density of low-mass galaxies. They conclude that this is due to the sensitivity of the results to how the gas reservoirs are tracked and treated in the different codes. Croton et al. (2016) also had similar problems with this approach and found that it did not solve the problems with fitting the SMF. This presents difficulties to the modelling community, as it means that different models may require different changes to get them to match the observed evolution of galaxy properties.

It is also possible to try and match the galaxy SMF at all redshifts without changing the physics involved in the model. For example, Rodrigues, Vernon & Bower (2017) used Galform to identify a small region of parameter space where the model matched the observational data out to $z = 1.5$, without needing to adapt any of the physics involved. They found that the parameters controlling the feedback processes were most strongly constrained, suggesting that these processes are important when fitting the evolution of the galaxy SMF.

Halo occupation distribution (HOD) models, rather than modelling the physical processes that we think go into galaxy formation, use statistical methods to match galaxies to their corresponding dark matter haloes (e.g. Berlind & Weinberg 2002; Zheng et al. 2005). As these models are applied independently at each redshift, the evolution of each galaxy is not tracked, although they can be connected to their progenitors and descendants via dark matter merger trees. HOD models by design are able to reproduce the SMF at each redshift and are therefore able to reproduce the population of galaxies at any given time. This type of model is a very useful tool for learning about the relationship between galaxies and their host dark matter haloes and how this changes as a function of redshift. For example, Berlind et al. (2003) found that low-mass haloes are mainly populated by young galaxies and high-mass haloes by older galaxies.

Galaxy formation models such as HODs and SAMs must be calibrated using observational data sets. Varying the calibration data set, even for the same model, may produce significantly different catalogues. Essentially, the calibration data sets introduce tension, and it may not be possible for a single model to fit all the required observational data sets simultaneously. This could be because the model lacks some of the required physics or that the underlying observational data sets are incomplete or are physically incompatible with each other. For example, the evolution of the stellar mass density obtained by integrating the observed time evolution of the cosmic SFR density has been shown in some cases to be systematically different from other observations of the stellar mass density evolution (e.g. Borch et al. 2006; Hopkins et al. 2006).

The Cosmic CARNage mock galaxy comparison project (Knebe et al. 2018) sought to address some of these issues by requiring the participants to calibrate their models to the same set of observational data. This data included the galaxy SMF at $z = 0$ (Baldry et al. 2012; Li & White 2009; Baldry, Glazebrook & Driver 2008) and $z = 2$ (Tomczak et al. 2014; Muzzin et al. 2013; Ilbert et al. 2013; Domínguez Sánchez et al. 2011), the star formation rate function at $z = 0.15$ (Gruppioni et al. 2015), the black-hole bulge-mass relation at $z = 0$ (McConnell & Ma 2013; Kormendy & Ho 2013), and the cold gas mass fraction at $z = 0$ (Boselli et al. 2014). Participants were free to weight these five calibrations as they saw fit, and were asked to generate their 'best-fit' model that took all of them into account, i.e. calibration set '-c02' in Knebe et al. (2018).

We will build on previous work by investigating the evolution of the SMF for the eight SAMs and one HOD model that were used in Knebe et al. (2018). These models are all calibrated to the same observational data and are all run on the same background dark-matter-only (DMO) simulation, which means that we can discount the differences due to the underlying cosmological framework when considering the differences between the models. Our aim is then to see if the current physical prescriptions used in any of the galaxy formation models can produce a realistic population of galaxies at both low and high redshift. We will investigate the evolution of the SMF in the redshift range $0.5 < z < 3.0$ for all nine galaxy formation models and determine if models still struggle to simultaneously match observations both at low and high redshift.

2.2 Simulation data

The eight SAMs we will be using are DLB07 (De Lucia & Blaizot 2007), Galform (Gonzalez-Perez et al. 2014), GalICS-2.0 (Cattaneo et al. 2017, although the exact version used for this comparison is the one described in the appendix of Knebe et al. 2015), Lgalaxies (Henriques et al. 2013), Morgana (Monaco, Fontanot & Taffoni

2007), SAG (Cora et al. 2018b), SAGE (Croton et al. 2016) and YSAM (Lee & Yi 2013). The single HOD model is MICE (Carretero et al. 2015). A brief description of the physical prescriptions used in each model is given in the Appendix of Knebe et al. (2015). Any changes to any of the models since then are included in Section 2.2.1.

The underlying cosmological DMO simulation was run using the GADGET-3 N-body code (Springel 2005) with parameters given by the Planck cosmology (Planck Collaboration et al. 2014, $\Omega_\mathrm{m} = 0.307$, $\Omega_\Lambda = 0.693$, $\Omega_\mathrm{b} = 0.048$, $\sigma_8 = 0.829$, $h = 0.677$, $n_s = 0.96$). We use 512^3 particles of mass $1.24 \times 10^9 h^{-1}\mathrm{M}_\odot$ in a box of comoving width $125 h^{-1}$Mpc. The halo catalogues were extracted from 125 snapshots and identified using ROCKSTAR (Behroozi, Wechsler & Wu 2013). The halo merger trees were then generated using the CONSISTENTTREES code (Behroozi et al. 2013).

The models have all been run on this same underlying DMO simulation which may be different to the one used in the above reference papers. This can lead to changes in the predictions of each model, as can varying the initial mass function, yield, stellar population synthesis model and calibration data set used. A description of how the models were calibrated to the same observational data is given in Knebe et al. (2018).

We also need to account for the different stellar mass definition used in simulations and observations. In the models, the stellar mass is an intrinsic property of the galaxy which is tracked computationally, so does not have an associated measurement uncertainty. However, in observations the stellar mass of a galaxy is inferred from the amount of light received by a telescope. Both measuring the amount of light and using a mass-to-light ratio to convert to stellar mass have associated uncertainties, which lead to uncertainty in the stellar mass estimate. To account for this, the stellar masses from the models have been convolved with a $0.08(1+z)$ dex scatter during calibration. This value comes from Conroy, Gunn & White (2009), who estimate an uncertainty of ~ 0.2 dex at $z = 2$ when fixing the stellar population synthesis model. This is a very simple correction, as in reality the uncertainty on observational stellar masses is much more complex.

2.2.1 Galaxy formation models

A description of the physical prescriptions of each model is available in the Appendix of Knebe et al. (2015). Here we present a brief description of the changes to any of the models since then:

SAG

The changes implemented in SAG are described in detail in Cora et al. (2018b). We summarise them here:

Cooling Both central and satellite galaxies experience gas cooling processes. Satellite galaxies keep their hot gas haloes which are gradually removed by the action of ram pressure stripping, modelled according to McCarthy et al. (2008), and tidal stripping. When the mass of the hot gas halo becomes smaller than 10% of the total baryonic mass of the galaxy, it is assumed that it no longer shields the cold gas disk from the action of ram pressure stripping, which is modelled following the criterion from Gunn & Gott (1972); see Tecce et al. (2010) for more details. Values of ram pressure experienced by galaxies in haloes of different mass as a function of halo-centric distance and redshift are obtained from fitting formulae derived from the self-consistent information provided by the hydrodynamical simulations analysed by Tecce et al. (2010), as described in Vega-Martínez et al. (in preparation).

Supernova feedback and winds The mass reheated by supernova feedback involves an explicit redshift dependence and an additional modulation with virial velocity, according to a fit to results from FIRE (Feedback in Realistic Environments) hydrodynamical simulations (Muratov et al. 2015).

Gas ejection and reincorporation The energy input by massive stars eject some of the hot gas out of the halo, according to the energy conservation argument presented by Guo et al. (2011). The energy injected by massive stars is proportional to the mean kinetic energy of supernova ejecta per unit mass of stars formed, and includes the same explicit redshift dependence and the additional modulation with virial velocity as the reheated mass. The ejected gas mass is re-incorporated back onto the corresponding (sub)halo within a timescale that depends on the inverse of the (sub)halo mass (Henriques et al. 2013).

AGN feedback AGN are produced from the growth of central black holes. When this growth takes place from cold gas accretion during gas cooling, it depends on the mass of the hot gas atmosphere, following Henriques et al. (2015).

Orphans The positions and velocities of orphan galaxies are obtained from the integration of the orbits of subhaloes that will not longer be identified. The orbits are integrated numerically, considering the last known position, velocity and virial mass of subhaloes as initial conditions, and taking into account mass loss by tidal stripping and dynamical friction effects, following some aspects of the works by Gan et al. (2010) and Kimm, Yi & Khochfar (2011). A merger event occurs when the halo-centric distance becomes smaller that 10% of the virial radius of the host halo.

SAGE

The only change in SAGE is to the radio mode AGN feedback. It is explained in detail in Croton et al. (2016) and summarised here:

AGN feedback The radio mode AGN feedback has been modified in SAGE since Croton et al. (2006). There is now a heating radius, inside which gas is prevented from cooling. This heating radius increases with subsequent heating episodes and cannot decrease.

2.3 Evolution of the galaxy stellar mass function

We start by examining the evolution of the SMF in the models to different observational data than the combined data set used to calibrate the models. The data from Davidzon et al. (2017) is more recent than the calibration data set and also allows us to split our sample into passive and star-forming galaxies. We firstly compare Davidzon et al. (2017) to the SMF calibration data at $z = 0$ and $z = 2$ in Figure 2.1, where the blue shaded regions show the SMF from Davidzon et al. (2017) and the red shaded regions show the SMF calibration data. The two data sets largely agree, both at $z = 0$ and $z = 2$, although there is less uncertainty on the SMF from Davidzon et al. (2017). This is encouraging as it shows good agreement between different observations.

We compare the evolution of the SMF in the models to the data from Davidzon et al. (2017) in Figure 2.2, shown for the whole sample in the top row. The coloured lines are the SMF for each of the models, computed for each redshift bin using single snapshots at $z = 0.8, 2.0$ and 3.0 for each redshift bin respectively. We note that the precise choice of snapshot does not affect our conclusions. The observations from Davidzon et al. (2017) are based on the UltraVISTA near-infrared survey of the COSMOS field and are shown as a black line and dark shaded region. When finding the best-fit Schechter parameters to their SMF, they take into account the uncertainty in measuring stellar mass, known as Eddington bias. As they have applied this correction, when plotting the SMF we do not apply the $0.08(1 + z)$ dex scatter to the stellar mass values. In Section 2.5 we have included a version of Figure 2.2 where the model stellar masses do have this scatter applied, to show the differences to the SMF.

Inspecting the top panels, what is clear is that the observational number counts are evolving, with the high-mass end largely in place by $z = 3$, while the low-mass end rises at late times. Whilst the models match the observations well at low redshift, the strong evolution at the low-mass end is not seen for most of the galaxy formation models. The exceptions to this are MICE, LGALAXIES and SAG, which all show an

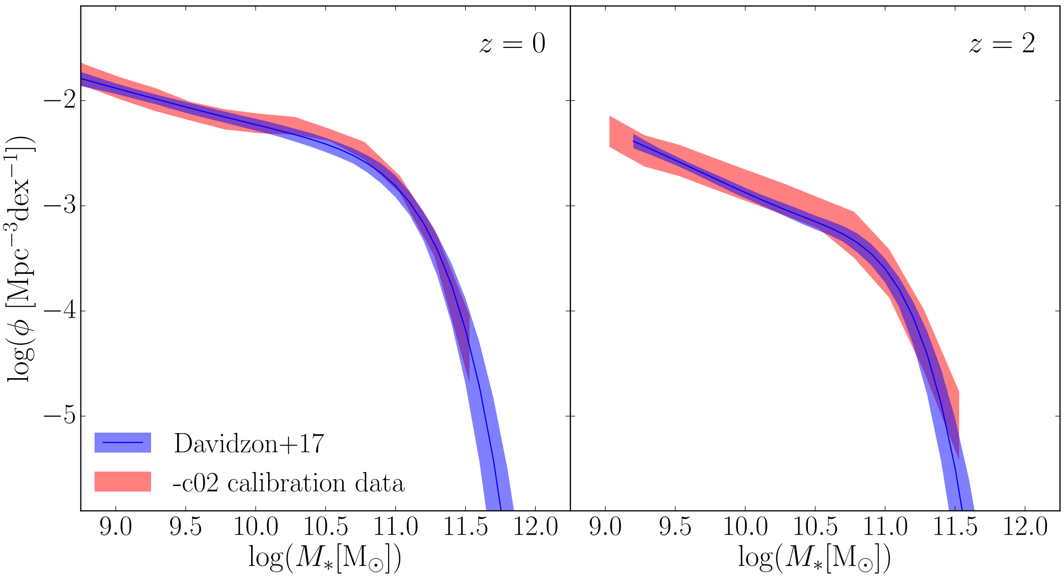

Figure 2.1. Comparison of the '-c02' SMF calibration data with the SMF from Davidzon et al. (2017), at $z = 0$ (left panel) and $z = 2$ (right panel). The red shaded regions show a combination of the calibration data, whilst the blue lines are the observational best-fit SMF from Davidzon et al. (2017) at the same redshifts, with the blue shaded regions showing the 1σ uncertainty. At $z = 0$ the sources of the SMF calibration data are Baldry et al. (2012), Li & White (2009) and Baldry, Glazebrook & Driver (2008). At $z = 2$ the calibration data are combined from Tomczak et al. (2014), Muzzin et al. (2013), Ilbert et al. (2013) and Domínguez Sánchez et al. (2011).

increasing number density of low-mass galaxies towards low redshift. As Mice is an HOD model it has been designed to match the evolution of the SMF. Lgalaxies and Sag likely do a better job of matching the SMF at high redshift due to the physics involved in the treatment of gas. Both follow the prescription suggested in Henriques et al. (2013) of scaling the reincorporation timescale of ejected gas with the inverse of the halo mass. This means the process of gas being reincorporated back into the halo takes longer for low-mass haloes, shifting the growth of galaxies in these haloes from early to late times. Sag also scales the reheated and ejected mass with redshift to make supernova feedback more efficient at high redshift.

At the high-mass end, the models underestimate the number density compared to observations, with Mice and GalICS-2.0 as the exceptions. One alternative reason for this tension at the high-mass end may be due to Davidzon et al. (2017) underestimating their uncertainties when accounting for Eddington bias, as it is very difficult to accurately measure all of the sources of uncertainty. Due to the steep slope of the SMF at high masses this would have a greater impact at the high-mass end of the SMF. The impact of Eddington bias on the SMF are discussed further in Section 2.5.

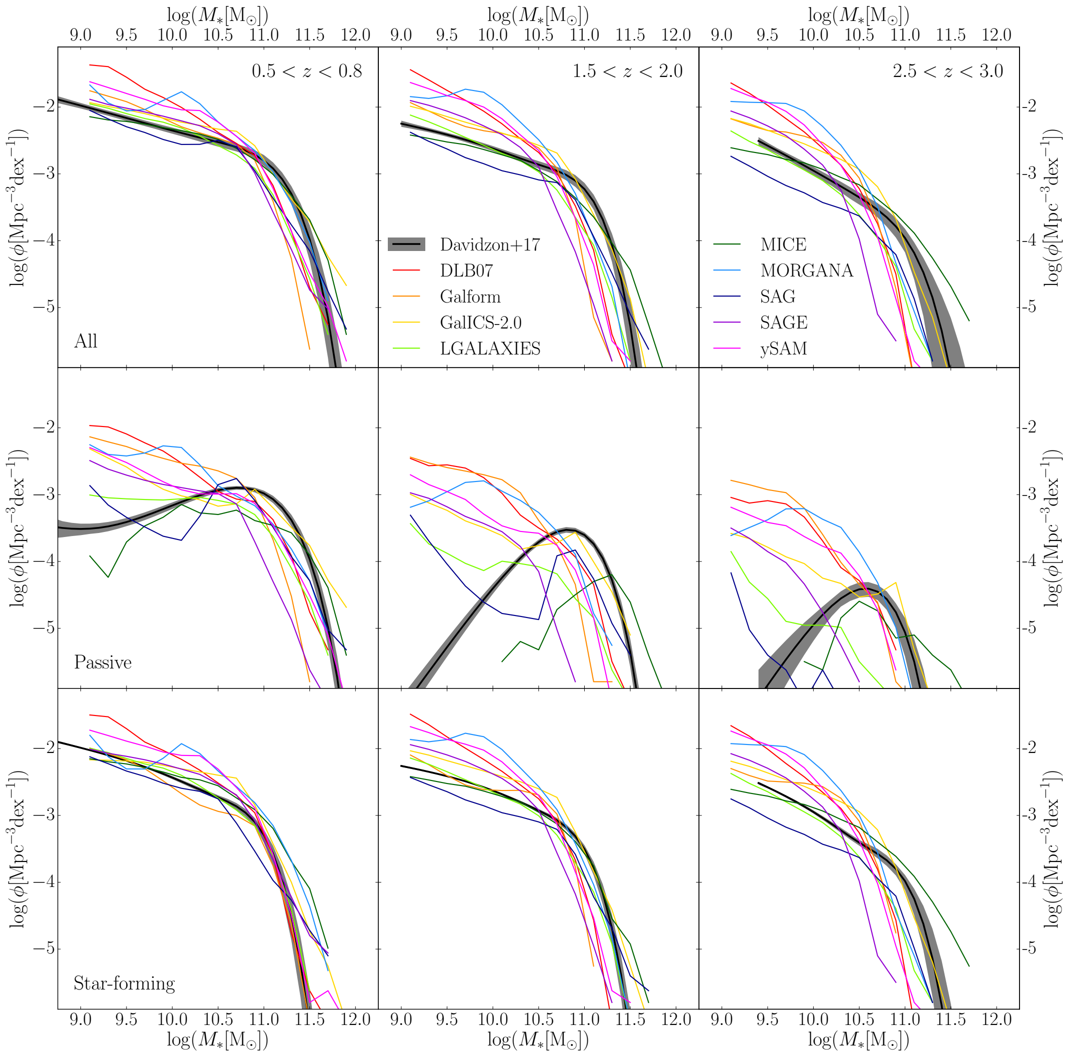

Figure 2.2. Evolution of the SMF for all the models over the range $0.5 < z < 3.0$. The SMF for the whole, passive and star-forming samples are shown in the top, middle and bottom panels, respectively, as coloured lines. The split between star-forming and passive galaxies in the models is done using a redshift-dependent specific star formation rate cut, whereas in the observations they are separated using the $(NUV - r)$ vs $(r - J)$ colour-colour diagram. The black lines are the observational best-fit SMF from Davidzon et al. (2017) at each redshift, with the dark grey shaded regions showing the 1σ uncertainty. For the models, each redshift bin contains one snapshot, at redshifts $z = 0.8, 2.0$ and 3.0 respectively. We can see that the models match well at low redshift (by construction), but deviate further from the observations at high redshift. The number density of the lowest mass objects is nearly constant in the models but changes by more than 0.5 dex in the observations. The models overproduce both low-mass star-forming and passive galaxies at high redshift.

2.4 Splitting into star-forming and passive galaxies

We now want to examine how the SMF differs for star-forming and passive galaxies. We separate these two classes using a redshift-dependent specific star formation rate (sSFR) cut of $\mathrm{sSFR}(z) = 1/(3t_{\mathrm{H}}(z))$ which gives a characteristic timescale for star formation, where $t_{\mathrm{H}}(z)$ is the Hubble time at that redshift (Lang et al. 2014). We test the robustness of this cut by examining the change in our results when using slightly different cuts of $\mathrm{sSFR}(z) = 1/(2t_{\mathrm{H}}(z))$ and $\mathrm{sSFR}(z) = 1/(4t_{\mathrm{H}}(z))$. We find that the shape of the SMF changes very little and makes no difference to any of the conclusions that we draw. In the observations the passive and star-forming galaxies are separated using the $(NUV - r)$ vs $(r - J)$ colour-colour diagram as described in Ilbert et al. (2013), which is best suited to differentiate fully quiescent galaxies from those with residual star formation. In practice, the exact location of the split makes little difference to the low-mass end of the star-forming SMF and the high-mass end of the passive SMF, as these galaxies will have very blue and red colours respectively.

2.4.1 Star-forming and passive galaxy stellar mass functions

We explore the stellar mass growth further in the bottom two rows of Figure 2.2, splitting the population into passive (middle row) and star-forming (bottom row) galaxies. Splitting the galaxy population in this way reveals that there is a large difference between the observations and the models for the star-forming population: low-mass star-forming galaxies appear to be far too common at high redshift in the models and the star-forming SMF evolves little from $z = 3$ to $z = 0.5$. The exceptions to this are Mice and Lgalaxies, which appear consistent with the observations at low masses up to $z = 3$. For the passive galaxies, the number density at low masses does evolve with redshift in the models, as seen in the observations. However, most of the SAMs show rising number density towards lower masses, in contrast with the observations which appear to show a turnover or flattening of the passive SMF towards lower masses. In order to solve these problems, models need to find a physically motivated way to reduce the star formation rates of low-mass galaxies at high redshift. The same galaxies at later times would then have lower stellar masses and star formation rates. This would then act to redistribute the passive SMF in the models to better match the observations.

2.4.2 Evolution of the passive fraction

Another way of looking at this result is to examine the passive fraction, which is shown in Figure 2.3. Again, the shaded regions indicate the observations taken from the same source as used for Figure 2.2. The passive fraction indicates the ratio of passive to star-forming galaxies. At low masses, some of the models, such

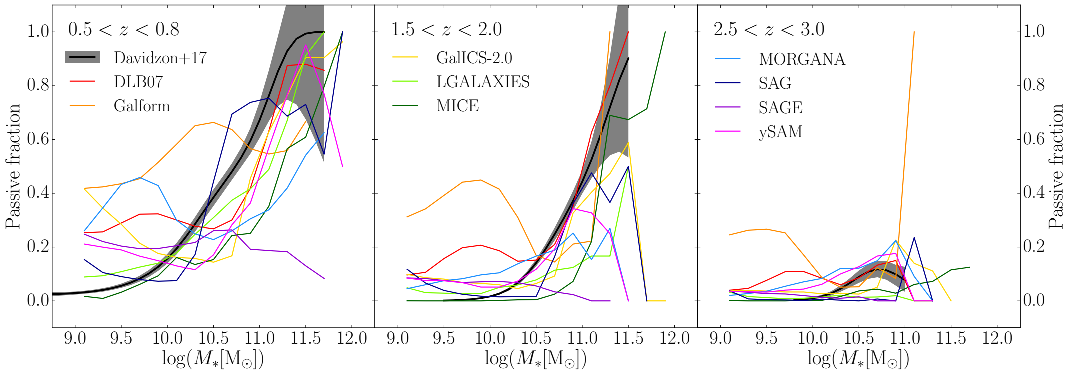

Figure 2.3. Evolution of the passive fraction over the range $0.5 < z < 3.0$. The coloured lines, black solid lines and grey shaded regions are the same as in Figure 2.2, as are the snapshots used in each redshift bin for the models. For a few models the passive fraction is too high at low masses, particularly at low redshift. The models match well at high masses at low redshift, but generally underpredict the passive fraction for high-mass galaxies at high redshift.

as DLB07, Galform and Morgana, tend to overestimate the passive fraction compared to observations. This has been seen previously and appears to be linked to how environmental processes are taken into account in the models (Lagos et al. 2014; Gonzalez-Perez et al. 2018). At low redshift the number of star-forming galaxies matches observations well, so this difference is due to the lack of a turnover or flattening of the passive SMF. At higher redshifts, the overproduction of low-mass star-forming galaxies would act to decrease the passive fractions. However, this is still too high in some models, again due to the rising number density towards low masses in the passive SMF.

At low redshift, the models tend to match the observations well at high masses, but one model, Sage, underpredicts the passive fraction. This is mainly due to an underprediction for the number of high-mass passive galaxies. As shown by Stevens & Brown (2017), detailing the structural evolution of galaxy disks with the Dark Sage variant of the model (Stevens, Croton & Mutch 2016) leads to more sensible passive fractions. In the redshift range $1.5 < z < 2.0$ the models tend to underpredict the fraction of high-mass galaxies, mainly due to the lack of high-mass passive galaxies above $z \sim 1$. The model which best matches the observed passive fraction for high-mass galaxies is DLB07, which slightly underpredicts the number density of both high-mass passive and star-forming galaxies in this redshift range.

2.5 Stellar mass function including Eddington bias

In Figure 2.2 we have compared the SMF from the models to observational data from Davidzon et al. (2017). We do not scatter the stellar masses in the models with the $0.08(1 + z)$ dex scatter used to mimic observational uncertainties, as Davidzon et al. (2017) have accounted for this when finding the best-fit Schechter parameters

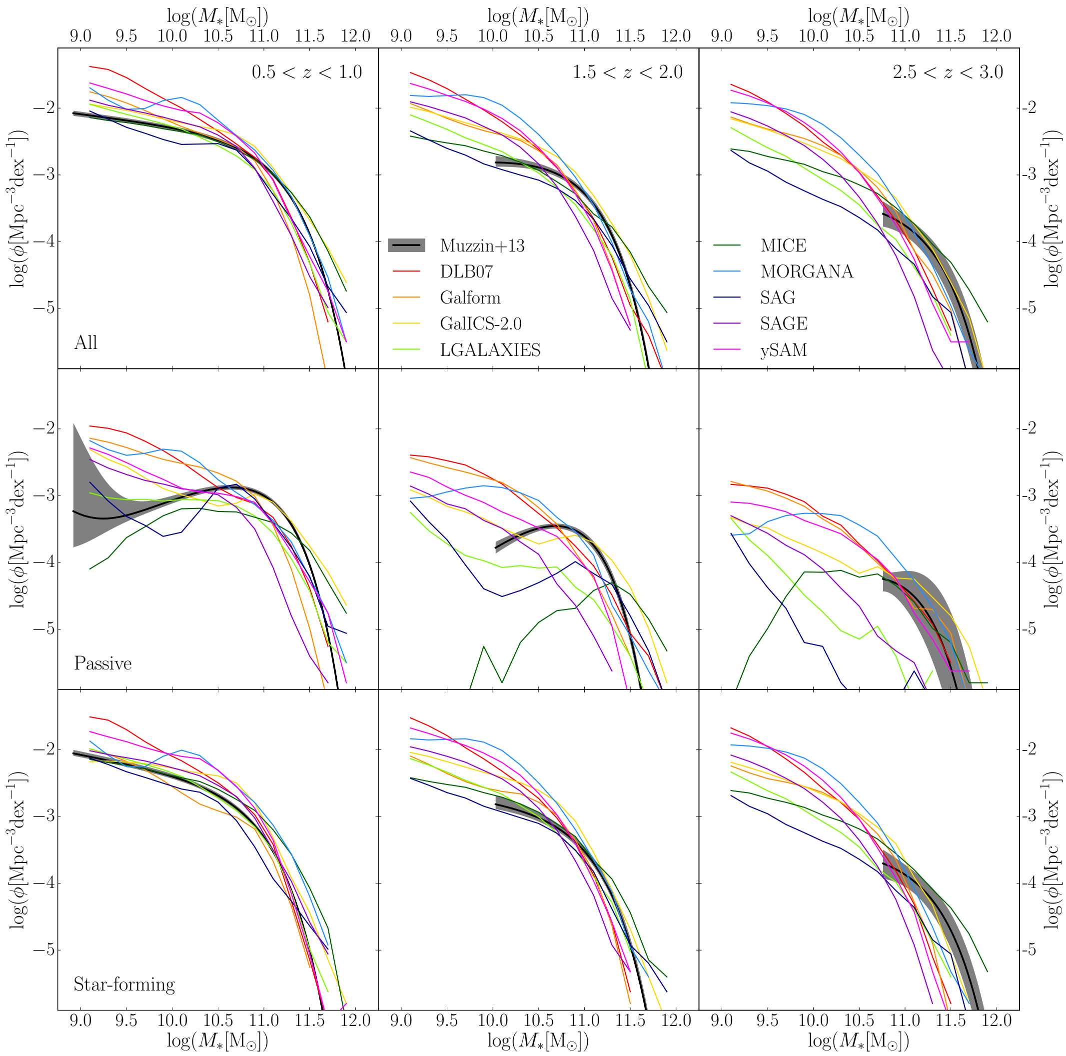

Figure 2.4. Alternative version of Figure 2.2, applying the $0.08(1 + z)$ dex scatter to the stellar mass values in the models. Here we compare to observational data from Muzzin et al. (2013), who do not take into account Eddington bias when finding the best-fit Schechter parameters. Here the models match the observations better at high masses and high redshift.

to their SMF.

Here we present an alternative version of Figure 2.2, shown in Figure 2.4, where we do apply the scatter to the stellar mass values in the models. We compare to observations from Muzzin et al. (2013), who do not correct their stellar masses prior to fitting the SMF. Instead, they use Monte Carlo methods to calculate the uncertainties on the SMF due to the uncertainty in the stellar mass values. Like Davidzon et al. (2017), the observations from Muzzin et al. (2013) are based on the UltraVISTA near-infrared survey of the COSMOS field.

Comparing Figure 2.4 to Figure 2.2, we can see that the main difference to the SMF from the models is at the high-mass end and that the low-mass end is largely unaffected. Due to the redshift dependence of the scatter we apply to the stellar masses, the differences are also larger at high redshift. As an example, the value of ϕ increases by over 0.5 dex at $10^{11}\mathrm{M}_{\odot}$ in the redshift bin $2.5 < z < 3.0$ in LGALAXIES when the scatter is applied.

In Figure 2.2, it appears that most of the models underpredict the number of high-mass galaxies at high redshift, with only MICE and GALICS-2.0 matching observations. However, in Figure 2.4 the models and observations agree better at high redshift for several other models, namely GALFORM and MORGANA. One important thing to note is that the data from Muzzin et al. (2013) form part of the combined data set used to calibrate the models, so it is natural that the models may match this data better.

2.6 Growth of the galaxy stellar mass function

In Figure 2.5 we examine the growth of the stellar mass function as a function of stellar mass and redshift. This is found by taking the value of the number density ϕ at fixed stellar mass for a certain redshift bin and normalising it by the value of ϕ in the lowest redshift bin $0.2 < z < 0.5$, which we call ϕ_0. This allows for easier comparison between the models and observations and will highlight when the number density of different populations increases. The dark grey region and black line with circular points shows data from Davidzon et al. (2017). The coloured lines then show the number density evolution for the nine models. The black dotted line shows where the number density is equal to the number density in the lowest redshift bin.

Looking at the passive galaxies, we can see that the models struggle to match the observed growth of the SMF at low masses, as the number density of low-mass galaxies increases in the models at higher redshift than the observations. The only exception is MICE, which has very few galaxies with stellar mass below $10^{10}\mathrm{M}_{\odot}$ above $z \sim 1$. At intermediate masses the models match the observations well, but at high masses the growth of the SMF occurs in observations before many of the models.

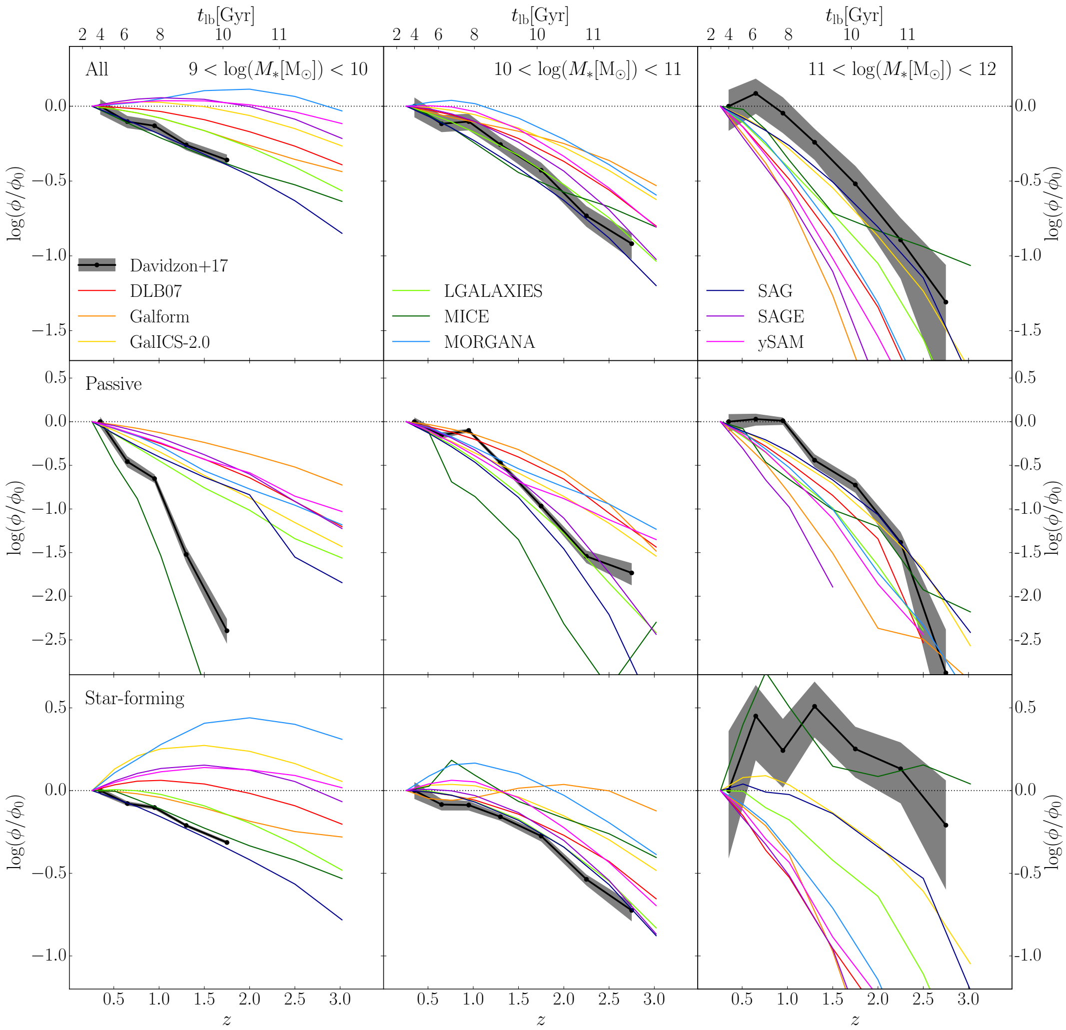

Figure 2.5. Evolution of the number density ϕ, in bins of stellar mass. This is normalised by the number density at $0.2 < z < 0.5$, which we call ϕ_0. We show three stellar mass bins as indicated (left to right panels) for all galaxies (top panels), passive galaxies (middle panels) and star-forming galaxies (bottom panels). The dark grey shaded regions and black lines with circular points show data from Davidzon et al. (2017). The coloured points and lines are for the nine models. In the lowest mass bin, most of the models assemble the galaxies before the observations. The models match the observations well at intermediate masses, but the observational number density increases before many of the models at high mass.

For the star-forming galaxies, at low masses there is a similar problem with several of the models; the SMF grows too much at high redshift. A third of the models have more low-mass star-forming objects in the highest redshift bin than the lowest redshift one. However, two of the models are more in line with the growth of the observed SMF, namely SAG and MICE. At intermediate masses, the number density of star-forming galaxies increases at higher redshift in the models than in the observations. The model that is most discrepant, MORGANA, has more intermediate mass star-forming galaxies between $1.0 < z < 1.5$ than in the lowest redshift bin. For high-mass galaxies, the observed number density evolution is noisier, but appears to change little since high redshift. MICE reproduces this trend well but in other models the number density increases at lower redshift. This may be in part due to the fact that there are low numbers of the highest mass galaxies which will naturally introduce more scatter in the proportional change in number density.

We can also see interesting differences between models when comparing the SMF to the growth of the SMF. Looking at the lower panel of Figure 2.2, we can see that DLB07 overpredicts the number of low-mass star-forming galaxies at both low and high redshift. SAGE agrees well with observations at low redshift but overproduces low-mass star-forming galaxies at high redshift. However, looking at the lower left panel of Figure 2.5, we can see that DLB07 matches observations of the growth of the SMF better than SAGE. These models therefore have slightly different problems; DLB07 has too many low-mass galaxies at all redshifts, but the number density increases at the correct rate. Conversely, SAGE has the correct number at low redshift, but the number density increases too early.

2.7 Relationship between stellar mass and specific star formation rate

In order to better compare star formation in the observations and the models, we also look at the sSFRs of the subset of star-forming galaxies. Figure 2.6 shows the average sSFR as a function of stellar mass at $z = 0.0$ for each of the models as a solid coloured line. The grey shaded region is taken from Elbaz et al. (2007), who used SDSS data to find a fit to the correlation between SFR and stellar mass at $z = 0$. Their sample is made up of 19590 galaxies with redshifts $z = 0.04 - 0.1$ and is complete to $M_B \leq -20$. Brinchmann et al. (2004) used Hα emission to derive the SFR of these galaxies and the stellar masses were derived by Kauffmann et al. (2003), who fit using a library of star formation histories to find the most likely stellar mass.

Most of the models match the observations well here, with LGALAXIES and SAG lying in the observational region at all masses. Some models appear to evolve less with stellar mass than the observations suggest, with some showing almost no trend,

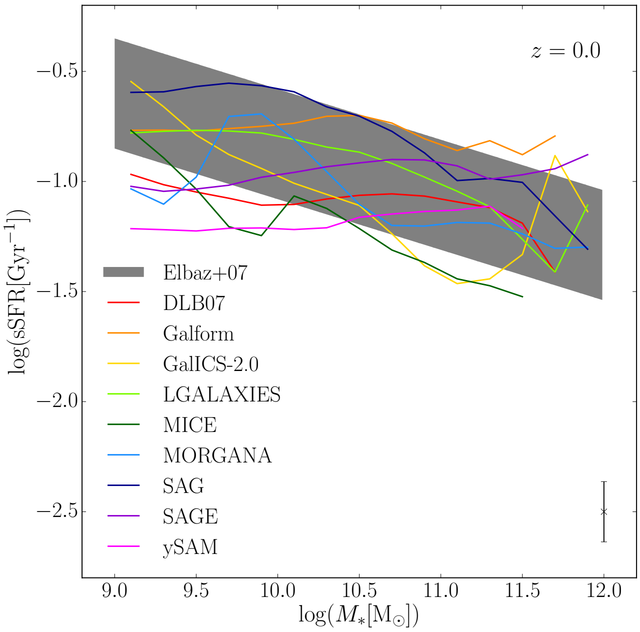

Figure 2.6. Relationship between stellar mass and sSFR at $z = 0.0$ for star-forming galaxies in the nine models. The model data is taken from one snapshot at $z = 0.0$ and the error bar in the bottom right shows the average 1σ scatter from the models. The grey shaded region is taken from Elbaz et al. (2007) and shows the observational best-fit to this relation. The sSFR of star-forming galaxies in the models matches observations well but there is less of a trend with mass in some models.

whereas the sSFR implied by the observations decreases by over 0.5 dex between $10^9\mathrm{M}_\odot$ and $10^{12}\mathrm{M}_\odot$. This means that some of the models, such as Galform, match at low masses but not high masses, and others such as DLB07 and ySAM match at high masses but not low masses. This was also discussed in Guo et al. (2016), who used data from two SAMs, Galform and Lgalaxies, and one hydrodynamical simulation, Eagle. They found that the median sSFR remained almost constant with stellar mass, in contrast with observations.

The relationship between sSFR and stellar mass at $z = 2.0$ is then shown in Figure 2.7. Here the observations are taken from Daddi et al. (2007), who use galaxies in the GOODS-S field to find the correlation between SFR and stellar mass at $z = 2$. They are complete to $K < 22$ and use only 24μm selected galaxies in order to exclude passive galaxies. The SFRs were estimated using the UV and the stellar masses were derived by Fontana et al. (2004) using SED fitting.

This comparison highlights large differences between the observations and models at this redshift, with the models almost completely outside the observational range. The sSFR of star-forming galaxies in the models is on average around 0.5 dex lower than measured in the observations. The models therefore predict a slower evolution of the sSFR with redshift than observations. This has been previously seen by Mitchell et al. (2014), who find that when they scale the reincorporation time of gas with redshift they are able to better match the evolution of the SMF, but still

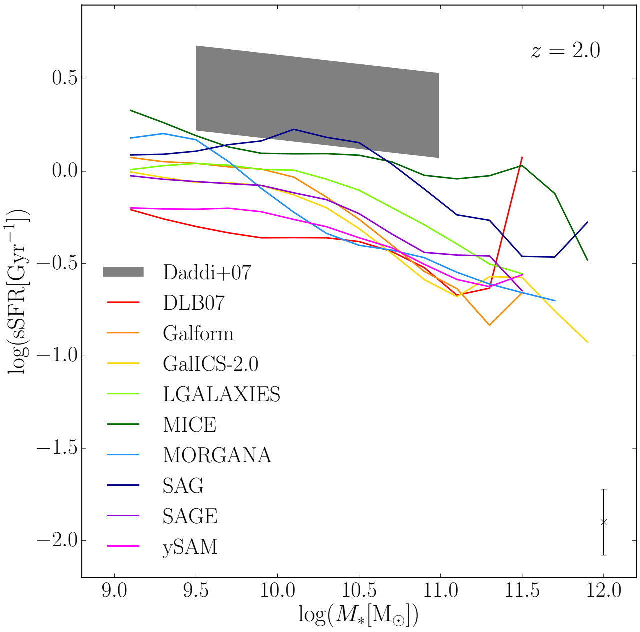

Figure 2.7. As for Figure 2.6, but for $z = 2.0$ and observations from Daddi et al. (2007). The model data is taken from one snapshot at $z = 2.0$. Here all of the models lie almost completely below the observational best-fit range.

underestimate the sSFR of high-mass galaxies at $z \sim 2$. Hirschmann, De Lucia & Fontanot (2016) also found that their ejective models predicted lower than observed sSFRs at high redshift, even when they could reproduce the growth of the SMF.

Reducing the star formation rates of galaxies above $z \sim 2$, as suggested in Section 2.4.1, may help to solve this problem. If galaxies have a lower star formation rate at higher redshift, their resulting stellar mass at lower redshift will be lower. A galaxy with the same star formation rate at $z = 2$ will then have a higher sSFR as it will have a lower stellar mass.

2.8 Relationship between galaxy stellar mass and halo mass

Another important property to investigate is the mass of the dark matter halo that each galaxy is situated in. Below we examine both the average halo mass as a function of stellar mass, and the average stellar mass within a given halo mass.

2.8.1 Average halo mass

In this section we study the average halo mass the galaxies reside within, shown in Figure 2.8. For the models we use single snapshots at $z = 1.0, 2.0$ and 3.5 for each redshift bin respectively. The dashed black line indicates the universal baryon fraction, i.e. where all the baryonic material within the halo has been converted

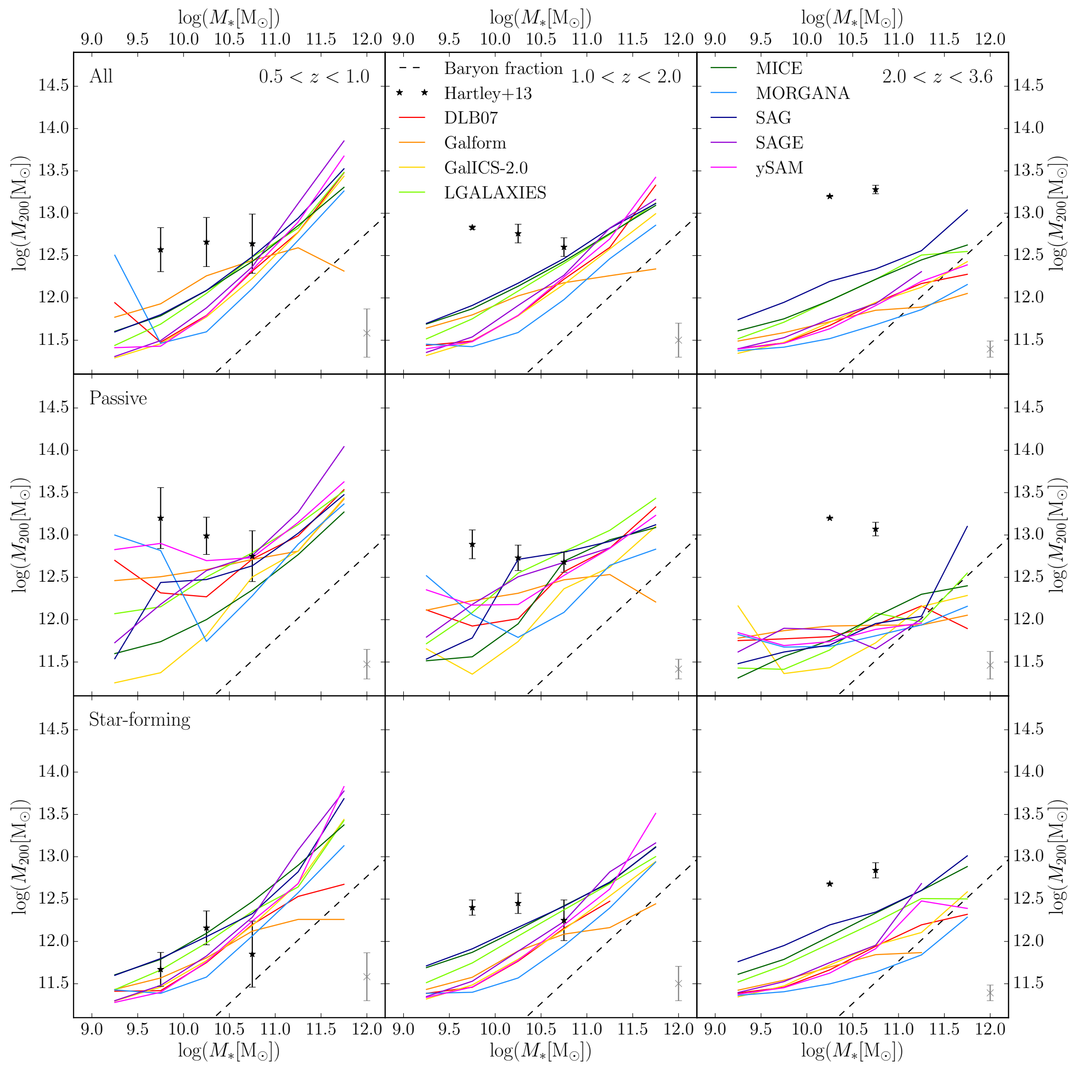

Figure 2.8. Average halo mass in the models compared to measurements from observations between $z = 0.5$ and $z = 3.6$. The black dashed line shows the baryon fraction. Observational measurements of the average halo mass from Hartley et al. (2013) are derived from clustering and are shown as stars. The values for each model are shown as coloured lines and the grey error bar in each panel shows the average 1σ scatter on the models. For the models, the mass of the main host halo was used rather than the subhalo, to better compare with observational halo mass measurements from clustering. The top panels cover the full galaxy sample, the middle panels are for passive galaxies and the bottom panels are for star-forming galaxies. The black dashed line shows the universal baryon fraction. For the models, we use snapshots at $z = 1.0, 2.0$ and 3.5 for each redshift bin respectively. For the passive sample, the halo masses from observations are approximately constant, but decrease by up to a factor of 10 in the models with increasing redshift. For the star-forming sample, the observations show halo mass increasing with increasing redshift, whereas in the models there is no real trend with redshift.

into stars. Each of the coloured lines indicates the average halo mass values for a different model, while the black points with error bars are average halo mass values taken from Hartley et al. (2013), who use the UDS Data Release 8 (DR8) data to estimate the halo masses from measurements of galaxy clustering. Galaxies are binned in stellar mass and redshift and then the 2-point auto-correlation function is calculated for each bin. By comparing this to the correlation function of the dark matter distribution over the same volume, a measurement of galaxy bias can be obtained, which can then be directly linked to a dark matter host halo mass (e.g. Mo & White 2002 and references therein).

For the models, here we use the mass of the main host halo for each galaxy rather than the mass of its subhalo. Host haloes do not reside within another halo, whereas subhaloes are contained within a host halo. Although using the host halo is not necessarily the usual choice when analysing simulation data, it allows us to compare to observational measurements of halo mass from galaxy clustering, which effectively measure the galaxy bias and use this to infer the mass of the main host haloes (Mo & White 2002). For this reason we also include both centrals and satellites, in order to best mimic the observational measurements. Assuming galaxy clustering measurements can correctly recover the host halo mass, we can then directly compare the observations and models.

Splitting the sample into passive and star-forming galaxies in Figure 2.8 we see that there are marked differences between the observations and the models. For passive galaxies, the average halo mass in observations stays constant over redshift, but rises towards low redshift in the models. For the star-forming population, while the observations indicate a general downsizing trend in halo mass of about an order of magnitude between high and low redshift, all the models show virtually no change. It is clear that the models start significantly below the observations at $2.0 < z < 3.5$ and only agree with the observations by $0.5 < z < 1.0$. Both passive and star-forming low-mass galaxies are therefore in lower mass haloes on average in the models than in the observations at high redshift.

One thing that can affect the average halo mass values in the models is the halo mass definition used, as this can lead to differences of up to 20% (Jiang et al. 2014). Although all of the models are based on the same DMO simulation, they can choose which halo mass definition to use, which may account for some of the scatter between the models. However, the differences between the observations and models cannot be explained by this alone. Another factor that could affect the observational measurements of halo mass from clustering is 'halo assembly bias', which refers to the fact that halo clustering can depend on other properties besides halo mass. For example, Gao, Springel & White (2005) found that at fixed halo mass, haloes that assembled earlier are more clustered than those that assembled later. Therefore, galaxies in older haloes will be more strongly clustered than they should be for

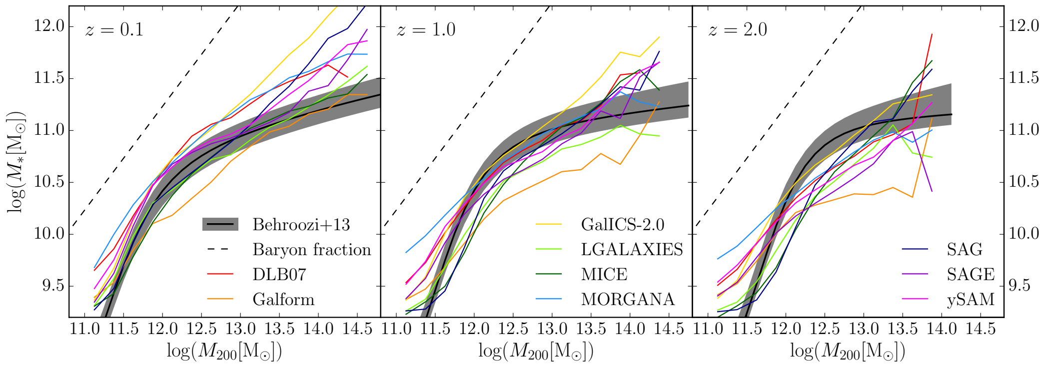

Figure 2.9. Comparison of the average stellar mass for each halo mass bin in the models to the abundance matching model of Behroozi, Wechsler & Conroy (2013), considering only central galaxies. The results from the models are shown as coloured lines and the stellar mass - halo mass relation is shown as a dark grey shaded region and black line. The black dashed line shows the universal baryon fraction. The panels are for each redshift, increasing from left to right, using snapshots at $z = 0.0, 1.0$ and 2.0 respectively. Looking at the data from Behroozi, Wechsler & Conroy (2013), we can see that the average stellar mass stays approximately constant with redshift, but increases in the models towards low redshift, particularly at high halo masses.

their halo mass, which means that their halo masses will be measured as higher than they actually are. This could alleviate some of the discrepancy between the observations and models. For example, if the passive galaxies observed at low redshift are associated to older haloes, then their halo masses could have been overestimated.

2.8.2 Stellar mass - halo mass relation

In Figure 2.9 we display measurements of the average stellar mass of central galaxies in bins of halo mass, comparing the models with the abundance matching model of Behroozi, Wechsler & Conroy (2013). The dashed black lines indicate the universal baryon fraction and the dark grey regions and black solid lines show the best fit to the functional form of the stellar mass - halo mass (SMHM) relation from Behroozi, Wechsler & Conroy (2013). The coloured lines show the average stellar mass values for each different model.

At low redshift, the results from the models and the SMHM relation agree well at low and intermediate halo masses. However, above halo masses of $\sim 10^{13.5}\mathrm{M}_\odot$ the average stellar mass of centrals in the models is higher than suggested by the SMHM relation. This means that at low redshift, mergers or higher SFRs in high-mass haloes are more common in the models. The exceptions to this are LGALAXIES and MICE, which agree with the SMHM relation at nearly all halo masses. For most of the models, the slope of the relation at high halo masses does flatten, but not to the extent seen from the SMHM relation.

As we move to higher redshift the SMHM relation from Behroozi, Wechsler & Conroy (2013) changes little. The peak of the relation moves to slightly higher halo masses and the average stellar mass for low-mass haloes decreases by $\sim$ 0.4 dex at $10^{11.5}\mathrm{M}_\odot$. In the models the average stellar mass for low-mass haloes decreases slightly with increasing redshift, but is above the SMHM relation by $z = 1.0$ for most models. This discrepancy can be partially explained by the cut in stellar mass applied at $M_* = 10^9\mathrm{M}_\odot h^{-1}$, which may have skewed the distribution towards higher stellar masses. This might be enough to explain the difference for models such as Lgalaxies or Galform, but the discrepancy is too large for Morgana, DLB07 and ySAM. In these models, the average stellar mass for low-mass haloes at high redshift is too high. This means that star formation in these objects is very efficient, leading to an increase in the number of low-mass galaxies at $z \sim 2$. This is likely due to the way that the physics involved in the gas cycle is implemented in these models.

For intermediate- and high-mass haloes, the average stellar mass generally decreases with increasing redshift in the models and the slope of the relation decreases. This suggests that star formation was less efficient in the models at high redshift. At $z = 0.1$ the models overpredict the stellar mass in high-mass haloes, but slightly underpredict it by $z = 2.0$. For intermediate-mass haloes, the average stellar mass is too low in the models at $z = 2.0$ by up to 0.5 dex, as is the case for Galform at $10^{12.5}\mathrm{M}_\odot$. The model that changes the least with redshift is Mice; as this is an HOD model it naturally matches the SMHM relation better than the SAMs.

2.9 Discussion

Comparing several galaxy formation models allows us to distinguish areas that are challenging for the current generation of models and therefore provide direction for the future development of the field as a whole. The main issue highlighted in this chapter is the fact that most of the models produce too many low-mass, star-forming galaxies at early times, and too many low-mass passive galaxies at all times. Observationally these appear either to not exist or to be missed by the surveys. This is a difficult area observationally with the answer to this question only becoming evident when the SMF is reliably pushed to lower masses.

In the absence of a new population of low-mass, star-forming galaxies being observed at $z \sim 2$, many of the models would need improvements in order to reproduce observations. They would need to produce far fewer low-mass star-forming galaxies at essentially all but the latest times. Shifting star formation from low-mass haloes at high redshift to low-mass haloes at low redshift would also produce better agreement with observations of galaxy clustering. Reducing the number of low-mass star-forming objects would also have to be achieved without reducing the number of high-mass objects significantly.

Some of the models, such as Lgalaxies and Sag, do fit the low-mass end of both the star-forming and passive SMF at high redshift. This is likely due to their implementation of the physics involved in the treatment of gas, in particular the reincorporation timescales. MICE also matches observations at high redshift, but as this is a HOD model it matches by construction. However, there are still some observables that even these models struggle to match, such as the relation between stellar mass and sSFR and the average halo mass that galaxies occupy. Whilst this could be due to problems with the observational measurements of these quantities, this could point towards areas where the models still need to improve.

2.10 Conclusions

In this chapter we have contrasted nine different galaxy formation models and compared them to high redshift observations. In doing so we have highlighted the areas in which the models find particular difficulty in matching the observations. We can see from this chapter that some of the models still have trouble simultaneously matching the SMF at both low and high redshift. The galaxies look roughly correct at $z = 0$, but for many models there are too many low-mass galaxies at $z \sim 2$, as has also been seen previously (e.g. Fontana et al. 2006; Fontanot et al. 2009; Weinmann et al. 2012; Henriques et al. 2012; Guo et al. 2016).

To explore this further, we split galaxies into passive and star-forming populations. We find that there are too many star-forming galaxies with stellar masses below $10^{11}\mathrm{M}_{\odot}$ in many of the models at $z \sim 2$. In summary, while some of the models are remarkably successful at reproducing the evolution of the SMF, there remain significant issues. In particular:

- Whilst most of the models are able to match the observed SMF at low redshift, they tend to overproduce the number density of low-mass galaxies at high redshift.

- In most of the models the low-mass end of the star-forming SMF is already largely in place at high redshift ($z > 1$), in contrast to observations. This is because the models appear to produce too many star-forming galaxies below the knee of the SMF at early times.

- The passive SMF from the models evolves with redshift as in the observations, but does not have the same turnover or flattening in the number density at the low-mass end.

- Whilst most of the models match the passive fraction well at high masses, for some of the models the passive fraction is too high at low masses. This is despite the overproduction of low-mass star-forming galaxies.

- Most of the models are able to reproduce the relationship between sSFR and the stellar mass of the star-forming galaxies at low redshift, but underpredict the sSFR at high redshift.

- Observational measurements of halo mass, estimated from galaxy clustering, indicate clear downsizing in the average halo mass occupied by star-forming galaxies as a function of redshift. This is not clearly indicated by any of the models; both star-forming and passive galaxies in the models occupy haloes with lower masses than those inferred from observations at $z = 2$.

- The average stellar mass is higher in low-mass haloes at high redshift in the models compared to observations, meaning that star formation in low-mass haloes is more efficient in the models than in the real Universe.

Achieving consistent results at both $z = 0$ and $z = 2$ with a population of galaxies that evolves strongly with redshift is clearly difficult. The HOD model, MICE, obtains good results but the galaxies present at $z = 2$ are not evolved directly into the $z = 0$ population. Of the SAMs, the LGALAXIES and SAG models best match the growth of the observed SMF, but they share the same trends as the other models for the sSFR and average halo mass within which the objects reside. Both of these models found that they needed to modify the treatment of the gas cycle in order to match the evolution of the low-mass end of the SMF. Although is very promising for the galaxy formation modelling community, it is still not clear whether the same modifications will lead to improvements in all models.

While it is clear that current galaxy formation models can reproduce a variety of observational data, we have identified key areas of tension. Some models still overpredict the number of low-mass galaxies at high redshift, but even the models that can match the evolution of the galaxy SMF underpredict the sSFR of galaxies at early times. Future observational surveys at high redshift will help shed light on these issues and identify further areas of improvement for the models.

Chapter 3

Using LGALAXIES to generate a mock UDS catalogue

In this chapter we will describe how we constructed a mock lightcone catalogue in order to mimic observations and investigate the quenching of galaxies by tracking them through time. We firstly introduce the UKIDSS UDS survey, which we will be comparing our mock catalogue to. We then discuss the LGALAXIES semi-analytic model in more detail and summarise the baryonic physics included in the model, before detailing how we adapted it in order to produce a lightcone mock catalogue rather than a box at each output redshift. We will discuss how the mock was made to mimic the UDS and the tests that were performed. This mock is then used in Chapter 4 and 5 to investigate the mechanisms by which galaxies are quenched.

The work involved in adapting the LGALAXIES code to produce a mock catalogue in the format of a lightcone was done in collaboration with Stefan Hilbert at the Max Planck Institute for Astrophysics.

3.1 The UKIDSS Ultra Deep Survey

The mock lightcone survey that we will discuss in this chapter is designed to be a mock observation for the UKIRT Infrared Deep Sky Survey (UKIDSS) Ultra Deep Survey (UDS, Almaini et al. in preparation). The UDS covers an area of $\sim 0.77\text{deg}^2$ on the sky and in Data Release 11 (DR11) reaches 5σ depths of $J = 25.4, H = 24.8$ and $K = 25.3$ (AB magnitudes). The UDS field has also been imaged by other multi-wavelength deep photometric surveys. There is U band data from CFHT Megacam, B, V, R, i', z' optical bands from the Subaru XMM-Newton Deep Survey (SXDS, Furusawa et al. 2008), Y band from the VISTA VIDEO survey and channels 1 and 2 of IRAC (3.6 and 4.5 μm respectively) from the Spitzer UDS Legacy Program (SpUDS). After masking out the bright stars and bad regions the area with joint optical and infrared is $\sim 0.62\text{deg}^2$. The determination of the photometric redshifts is described in Simpson et al. (2013). The UDS stellar mass estimates used in this thesis are from a Principal Component Analysis (PCA) method, which is described in more detail in Chapter 4.

In the following sections we will describe how we used the LGALAXIES model to make a mock UDS survey out to $z = 3$. For simplicity, we create a mock that covers 1deg^2 with $33.9 \leq \mathrm{RA} \leq 34.9$ and $-5.5 \leq \mathrm{Dec} \leq -4.5$.

3.2 The LGALAXIES semi-analytic model

The work in Chapters 4 and 5 uses a mock catalogue made using the LGALAXIES semi-analytic model. The version of the code used was Henriques2015a, as detailed in Henriques et al. (2015). Here we shall give a brief overview of the background dark matter simulation and baryonic physics involved, as explained in Henriques et al. (2015).

The LGALAXIES model is built upon halo merger trees, drawn from a background dark-matter-only (DMO) simulation. Here the Millennium simulation (Springel 2005) is used, which is a box with a side length of $500h^{-1}$Mpc and which assumes a ΛCDM cosmology with parameters $\Omega_{\mathrm{m}} = 0.25$, $\Omega_\Lambda = 0.75$, $\Omega_{\mathrm{b}} = 0.045$, $\sigma_8 = 0.9$, $h = 0.73$ and $n_s = 1.0$. These are from a combined analysis of the 2dFGRS (Colless et al. 2001) and the first year WMAP data (Spergel et al. 2003). As part of the LGALAXIES code, the cosmology of the DMO simulation is rescaled, using the technique described in Angulo & White (2010) and Angulo & Hilbert (2015), to the more recent first year Planck cosmology (Planck Collaboration et al. 2014, $\Omega_{\mathrm{m}} = 0.315$, $\Omega_\Lambda = 0.685$, $\Omega_{\mathrm{b}} = 0.0487$, $\sigma_8 = 0.829$, $h = 0.673$, $n_s = 0.96$).

The dark matter haloes were extracted from this DMO simulation using the SUBFIND algorithm (Springel et al. 2001) to create dark matter merger trees. These merger trees are used as an input to the LGALAXIES model, where each dark matter halo is populated with baryons according to its mass and the baryon fraction. In the model, when the mass of the halo increases, further baryons are accreted onto the halo in the form of primordial gas, which is then shock heated. This gas either cools onto the galaxy disk or is added to the host atmosphere of the galaxy. Gas in this hot atmosphere will eventually accrete onto the galaxy disk later via cooling flows, whilst gas in the cool disk will fuel star formation in the galaxy. At the end of their lives, these stars will die, releasing energy and heavy metals back into the interstellar medium. Some of the gas in the cold disk will heat up and be ejected into the hot atmosphere. Gas in the hot atmosphere can also be heated and ejected to an external reservoir, which can be reincorporated at a much later time.

In the LGALAXIES model, galaxies can be affected by environmental processes. When a halo crosses the virial radius of another halo, it becomes that halo's subhalo and the galaxy in the subhalo becomes a satellite. Two different processes can act to remove material from a satellite galaxy. One is ram pressure stripping, which in the LGALAXIES model only removes the hot gas from a galaxy. The other is due to tidal forces, which can remove hot gas, cold gas and stars from the satellite. Both of the processes may act to quench a galaxy by removing sources of star formation. Mergers can also affect galaxies. Dark matter (sub)haloes can merge with each other, after which the galaxies they contain will also eventually merge. These mergers create a bulge and a burst of star formation in the resulting galaxy. Black holes in the galaxy are also affected by mergers, as they primarily grown through cold gas accretion during mergers. However, they can also grow by accreting gas from the hot atmosphere, which releases energy which can counteract the cooling flow. This can lead to even the most massive galaxies being quenched.

The LGALAXIES code also stores the star formation history of each galaxy. Stellar population synthesis (SPS) models are then used to convert these into magnitudes in various filters, using a given initial mass function (IMF). A dust model is also applied to calculate corrections due to dust extinction. The LGALAXIES model then produces a catalogue of galaxies at each output redshift value, with information on their properties including the magnitude in each band.

3.3 Changing LGALAXIES output to a lightcone format

The standard output format from LGALAXIES is a box at each output redshift, which correspond to the snapshots available in the DMO simulation. This leads to galaxies in the sample having discrete redshift values rather than a continuous distribution as you would expect from observational surveys. This leads to problems when comparing the two, as differences observed may be due to the difference in the redshift distribution of the galaxies. One way to make mock catalogues more realistic is to make a 'lightcone' to create a sample of galaxies with a continuous redshift distribution (Blaizot et al. 2005; Kitzbichler & White 2007; Overzier et al. 2013).

A lightcone is constructed by first placing a virtual observer at $z = 0$. The galaxies that are on the past light cone of this observer are then included in the lightcone. For something to be within the past light cone of an observer, light from the object must be able to reach the observer by the present time, $z = 0$. The past light cone is shown in Figure 3.1 as a surface in four dimensional space-time. Including all of the galaxies on the observer's past light cone will produce an all-sky lightcone, which can then be cut down to the redshift range and size of the field-of-view required.

In order to have a sample of galaxies with continuous redshifts from which to draw those on the observer's light cone, the galaxies in all of the snapshots must be combined. The starting position within the simulation box of the observer must first be chosen, which can be anywhere in the $(500h^{-1}\mathrm{Mpc})^3$ box. The simulation

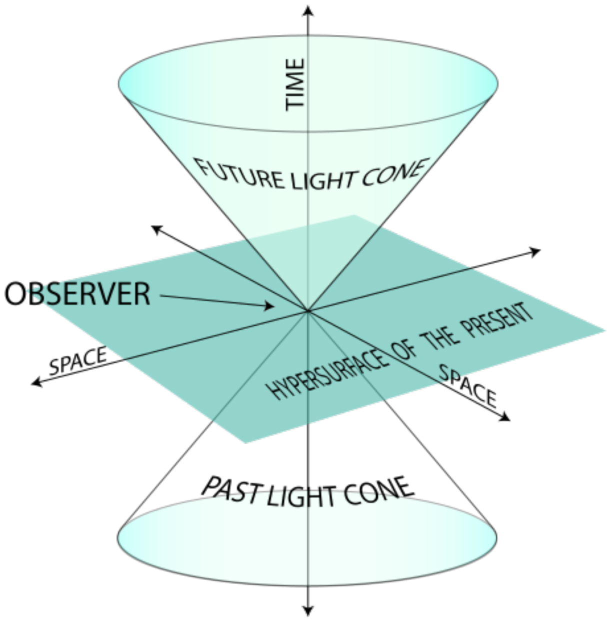

Figure 3.1. Past light cone of an observer, shown as a surface in four dimensional space-time. Image credit: K. Aainsqatsi.

volume must then be repeated in the X, Y and Z direction until a comoving distance is reached that corresponds to the maximum redshift required. For the cosmology stated in Section 3.2 and a lightcone out to $z = 3$, the maximum comoving distance a galaxy will be from the observer is $4384h^{-1}$Mpc. Taking the example of an observer being placed at (X, Y, Z) = (0, 0, 0), 9 simulation volumes must be repeated in each direction in order to reach this comoving distance.

Within each repeated volume, the galaxy (X, Y, Z) coordinates are changed to be with respect to the observer. This can be seen in a 2D example in the left panel of Figure 3.2, where the box is repeated out to $4500h^{-1}$Mpc and the X and Y axis show the new coordinates the galaxies in the boxes would be given. The RA, Dec and radial comoving distance from the observer, R, of each galaxy is then calculated using a coordinate transform from (X, Y, Z) to (RA, Dec, R).

The lightcone is then populated with galaxies, working from the observer out to the maximum comoving distance. The snapshots have a discrete set of redshift values z_i, corresponding to comoving distances from the observer R_i. The values at the observer are taken as $z_1 = 0.00$ and $\mathrm{R}_1 = 0$ h^{-1}Mpc. The volume of the lightcone with comoving distance from the observer satisfying $(\mathrm{R}_i + \mathrm{R}_{i-1})/2 < \mathrm{R} < (\mathrm{R}_i + \mathrm{R}_{i+1})/2$ forms a shell centred on the observer's position. Each shell is populated with galaxies from the snapshot with redshift z_i. The exact value of z assigned to each galaxy is then calculated using its comoving distance from the observer, R. The redshift of the galaxy is also changed slightly due to its peculiar velocity. The galaxy is only saved if its values of RA and Dec are within the field-of-view required.

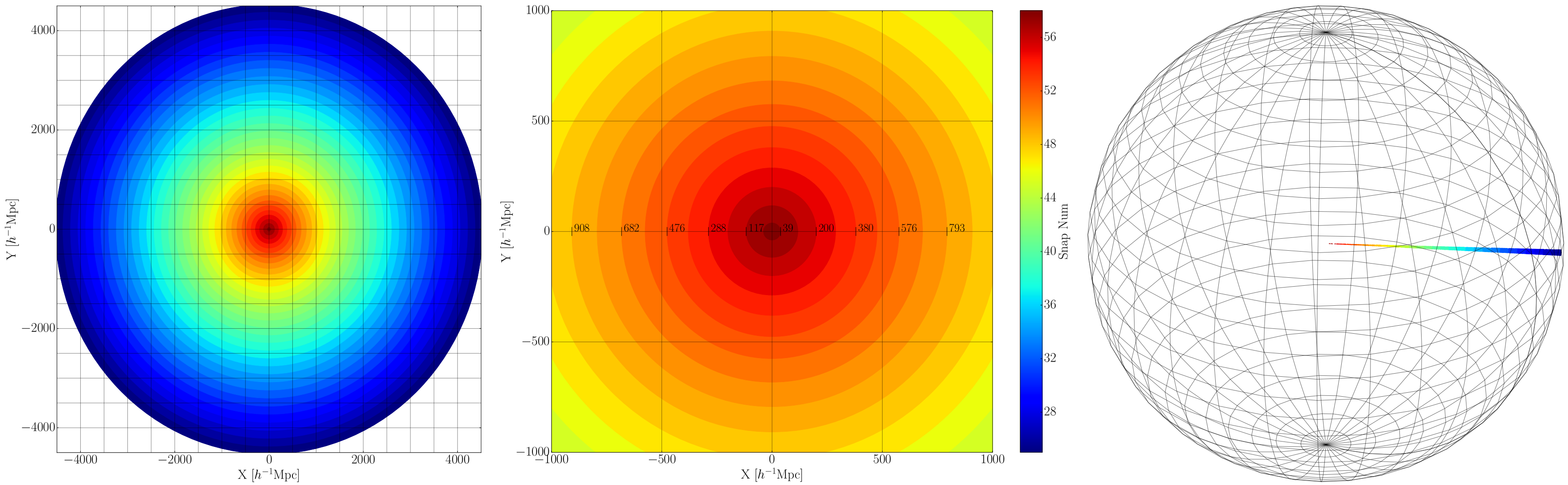

Figure 3.2. How simulation boxes are replicated to populate a mock lightcone survey. The left panel shows how many boxes are needed to produce a lightcone out to $z = 3$ in 2D. The shells are coloured to show which snapshot galaxies at any given radii are taken from, with the snapshot number given by the colourbar. The central panel shows a zoom in to the central regions and is annotated with the radius values at which the switch between snapshots occur. The right panel shows the lightcone in 3D after being cut down to the required RA and Dec ranges.

A 2D example of the shells is shown in the left panel of Figure 3.2, where each shell is coloured according to the snapshot number at redshift z_i. The central panel shows a zoom of the central region, and is annotated by the value of R at the border between each snapshot. The volume within which $0h^{-1}$Mpc $<$ R $<$ $39h^{-1}$Mpc is populated by galaxies in the 58th snapshot at $z = 0.00$, the shell within which $39h^{-1}$Mpc $<$ R $<$ $117h^{-1}$Mpc is populated by galaxies in the 57th snapshot at $z = 0.03$, etc. The right panel shows how the lightcone looks after being cut down to the required RA and Dec ranges.

The physical properties, positions and velocities of the galaxies in the lightcone are also only stored at each value of z_i, rather than at the new redshift value of the galaxy. This could be dealt with by interpolating between snapshots, but this could cause problems as changes in these properties can occur at smaller timescales than the average separation between snapshots of $\sim$ 350Myr due to processes like galaxy mergers. However, it is possible to interpolate the magnitude values of the galaxy between snapshots as an option in the LGALAXIES code is to store the magnitudes from the previous and next timestep. Therefore, the new absolute magnitude values can be linearly interpolated to find an estimate at the new redshift of the galaxy. From this, the code then calculates the apparent magnitudes, also at the new redshift.

Figure 3.3 shows two different views of galaxies in the lightcone. The left panel shows a scatter plot of the RA and Dec values of galaxies, coloured by the number of the snapshot they were taken from. The galaxies are evenly spread across this field, with none of the replication effects that can occur when making a new sightline through repeated simulation volumes (Blaizot et al. 2005). We also check for replications by ensuring that none of the galaxies have repeats of themselves at the same redshift or of their progenitors or descendants at other redshifts. The presence of repeats would indicate that the sightline goes through the same part of the simulation volume multiple times, which should be avoided if possible.

The right hand panel of Figure 3.3 then shows the distribution of R values for the galaxies in the lightcone plotted against Dec. Only a thin slice of the lightcone is shown here, with any galaxies satisfying $34.3 <$ RA < 34.5 in order to better show the structure. The galaxies are again coloured by their snapshot number. The vertical black lines show the comoving distance divisions between the snapshots and the redshift values are the values of z_i for each snapshot. Large scale structure is visible and there are no apparent discontinuities between each snapshot.

3.4 Matching the mock to the UDS

Now that we can use the LGALAXIES code to create a mock lightcone survey, we need to make the mock as similar to the UDS as possible. Therefore, we need to use the same IMF and SPS as the UDS in order to generate the magnitudes in the bands

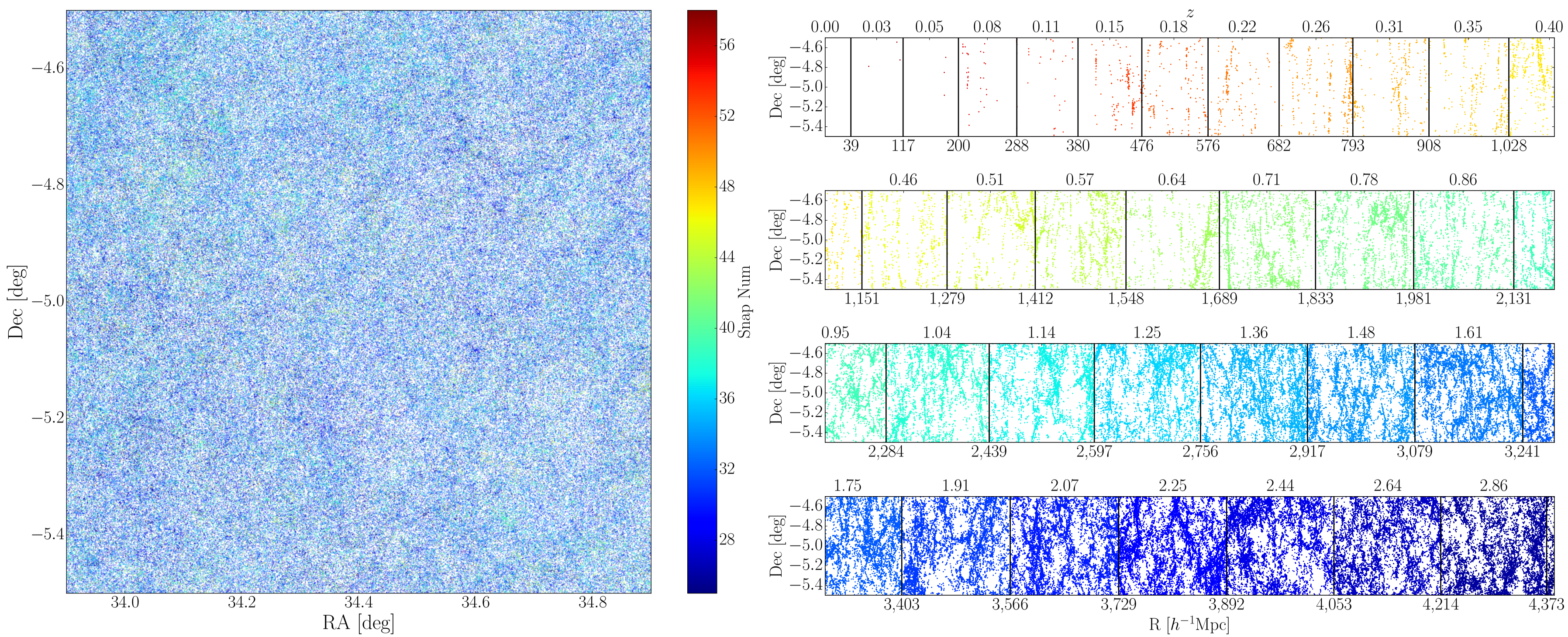

Figure 3.3. Side and end view of the mock lightcone survey. The left hand panel shows the distribution of galaxies in RA and Dec, coloured by the snapshot they were drawn from as shown by the colourbar. The right hand panel then shows the side view of the lightcone from $z = 0$ to $z = 3$. The galaxies are coloured by their snapshot number and the region of the lightcone volume populated by each snapshot is split by a black vertical line. The lower x axis shows the comoving radial distance from the observer at each of these boundaries, corresponding to the values annotated in the central panel of Figure 3.2. The upper x axis then shows the redshift (with the observer positioned at $z = 0$) of each snapshot.

that we have observational data for. Here we use the Bruzual & Charlot (2003) SPS model and the Chabrier (2003) IMF to calculate the magnitudes of galaxies in 12 bands that have been used to observe the UDS field. These are the CFHT U, Subaru B, V, R, i', z', UKIRT J, H, K, VISTA Y and Spitzer IRAC 3.6 and 4.5 μm bands.

Most of the galaxy properties output from LGALAXIES are perfect measurements, such as the stellar mass, gas content, star formation rate (SFR), etc. However, when observers measure these quantities they cannot do so perfectly, and so there is an uncertainty attached to each quantity. In order to make a more realistic mock, we need to artificially add these uncertainties into the mock catalogue by scattering the 'perfect' output values with a Gaussian.

One of the properties that we do this for is the stellar mass of the galaxy. Observers only receive information about the light emitted from a galaxy, and have to use a mass-to-light ratio in order to convert this to a stellar mass value, which introduces uncertainty. We use a Gaussian of width $0.08(1 + z)$ dex to scatter the stellar mass values. This value comes from Conroy, Gunn & White (2009), who estimate an uncertainty of ~ 0.2 dex at $z = 2$ when they fix the SPS model.

We also convolve the redshift values returned by LGALAXIES. The width of the Gaussian here is estimated by measuring the difference in the spectroscopic and photometric redshifts of sources in the UDS that have also have their spectra taken. The dispersion in the values of $\mathrm{d}z/(1 + z)$ is 0.0189, so we use a Gaussian of width $0.0189(1 + z)$ to scatter the redshift values.

The final property that we scatter with an uncertainty is the magnitude values. Observers cannot measure the magnitudes of galaxies perfectly as they receive raw images from the telescope which must be processed in order to remove background noise and isolate each source. We first estimate the uncertainty on each magnitude value. In order to do this we use the UDS DR11 catalogue and in each band fit a line to the relationship between magnitude and uncertainty. This allows us to find an estimated uncertainty for each galaxy in each band. Once we have the uncertainty on each magnitude we use this value as the width of a Gaussian to scatter the magnitude value.

Finally, we must also impose a stellar mass completeness limit on galaxies in the mock catalogue, as the DMO simulation that LGALAXIES is based on can only resolve dark matter haloes of a certain number of particles and therefore, of a certain mass. Low-mass galaxies which may reside in these haloes therefore need to be excluded. For the LGALAXIES model, we do not include any galaxies with stellar mass below $M_* = 10^{9.5}\mathrm{M}_\odot$ (Henriques et al. 2015) in our analysis. For the UDS the sample is magnitude limited in the K band so the stellar mass limit is not constant with redshift. We use the method set out by Pozzetti et al. (2010) in order to estimate what the limiting stellar mass is with respect to redshift. This method calculates the stellar mass that a galaxy would have ($M_{*,\mathrm{lim}}$) if it was at the magnitude limit

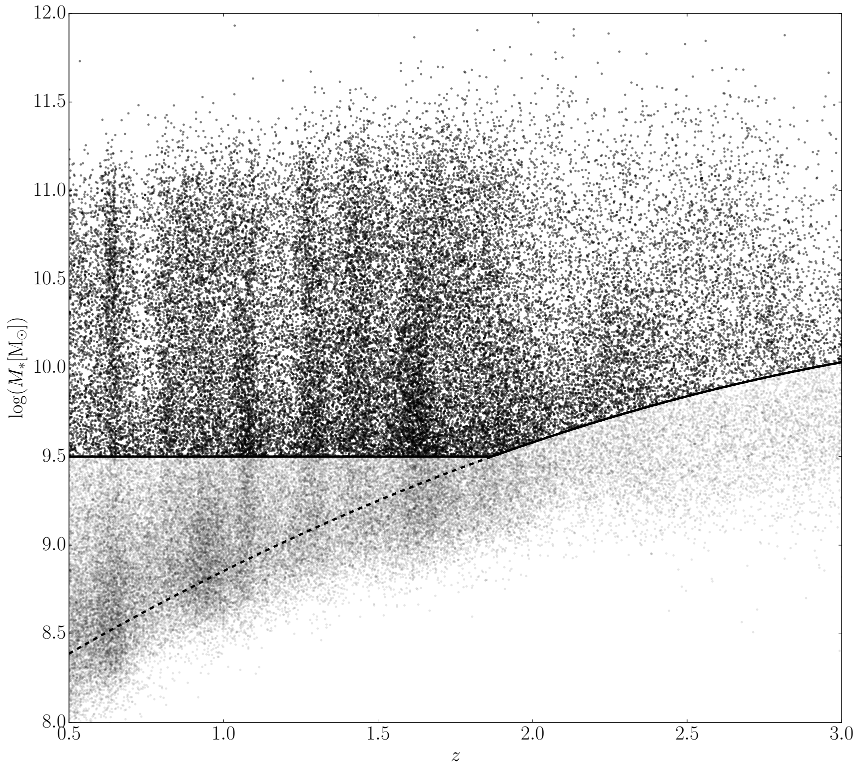

Figure 3.4. Stellar mass vs redshift distribution of all galaxies in the UDS shown as black points. The black dashed line shows the stellar mass limit of the UDS and the solid black line shows the stellar mass limit that we use, as we impose a minimum stellar mass limit of $\log(M_*/\mathrm{M}_\odot) = 9.5$ to account for the mass resolution of LGALAXIES. All galaxies below this limit are faded to show that they fall below the stellar mass limit.

of the survey ($K_{\mathrm{lim}} = 25.0$). The following equation is used:

$$\log(M_{*,\mathrm{lim}}) = \log(M_*) + 0.4(K - K_{\mathrm{lim}}), \tag{3.1}$$

where M_* and K are the stellar mass and K band apparent magnitude of the galaxy respectively.

The faintest 20% of galaxies at each redshift are used as a representative sample, in order to choose galaxies which have a typical mass-to-light ratio and are close to K_{lim}. This produces a distribution of $M_{*,\mathrm{lim}}$ values at each redshift. The 95% confidence level is then defined as the value of $M_{*,\mathrm{lim}}$ below which 95% of the distribution lies. After getting the values of $M_{*,\mathrm{lim}}$ at several different redshift values, we fit a line and find the stellar mass limit for the UDS DR11 data can be expressed as $\log(M_*/\mathrm{M}_\odot) \geq -0.14z^2 + 1.14z + 7.85$. Below $z = 1.87$ this value falls below 9.5, so $\log(M_*/\mathrm{M}_\odot) = 9.5$ is taken as the stellar mass limit for all redshift values below this. Figure 3.4 shows the redshift and stellar mass of all galaxies above the magnitude limit in the UDS DR11 catalogue as black points. The dashed black line shows the completeness limit of the UDS and the solid black line shows the completeness limit we use, adding in the minimum stellar mass value of $\log(M_*/\mathrm{M}_\odot) = 9.5$.

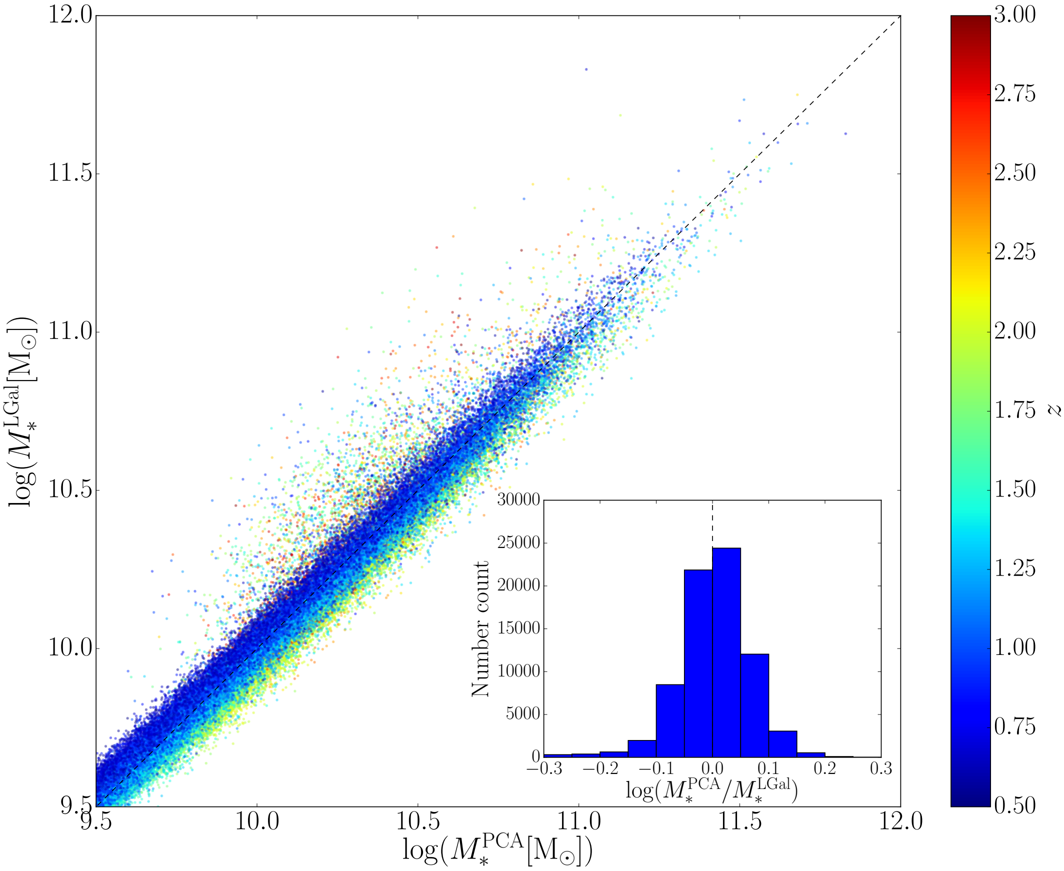

Figure 3.5. Stellar masses from the LGALAXIES mock compared with the stellar masses estimated from the PCA code. Each point is coloured by the redshift of the galaxy, shown by the colourbar. The inset shows a histogram of the log of the ratio between these two values. The black dashed line on both the main figure and the inset shows where galaxies would lie if both stellar masses were equal.

The lightcone starts off with 726,892 galaxies between $0 < z < 3$. When the limit of $K \leq 25.0$ is applied this number drops to 211,805. When the stellar mass limit is applied the number in the mock lightcone survey decreases further to 82,679.

3.5 Testing the mock catalogue

Before we can use this mock catalogue to answer any scientific questions about galaxy evolution, we need to check that the output is sensible and matches what we expect from observations. Here we check the stellar masses, number counts, colours and SFRs of galaxies in the mock catalogue.

Firstly, we can compare the stellar masses from our mock catalogue with the stellar masses derived in the same way as for the UDS, using the PCA method described in Chapter 4. Figure 3.5 shows a scatter plot of the stellar mass from the mock (scattered with a Gaussian as explained in Section 3.4) vs the stellar mass for the same galaxy from the PCA code. The inset in this figure then shows a histogram of the log of the ratio between these two stellar mass values. The general agreement between the two values is good, with the stellar mass estimates for over 99% of the galaxies being within a factor of 2 of each other. From the histogram, the stellar mass value from the PCA code appears to be slightly larger on average. There is also a tail of negative values on the histogram, which correspond to galaxies where the stellar mass from the mock is larger than from the PCA code, as can be seen on the scatter plot. When comparing the mock and the UDS we will be looking at populations of galaxies, so these small differences due to the stellar mass estimator should not affect our results.

We then look at the galaxy stellar mass function at $z = 0.1, 1.0, 2.0$ and 3.0 in Figure 3.6, comparing the mock lightcone survey to both the standard version of LGALAXIES (Henriques2015a), and the observations that were used to calibrate the LGALAXIES model. From this figure, we can see that the space density of galaxies has not been significantly altered by adapting the output of LGALAXIES to a lightcone format. This is what we would expect if the change to a lightcone format was done correctly. The small differences between the lightcone and the standard output from the code are most likely due to the small number counts in the lightcone, especially at low redshift. Because the UDS is a very deep survey, the lightcone is a pencil beam and volume of space observed at low redshift is low compared to a $(500h^{-1}\mathrm{Mpc})^3$ box at $z = 0.1$. Depending on the density of the region the lightcone passes through at low redshift, we could also get different results. One way we could investigate this effect further would be to make multiple mock lightcone surveys. By averaging the results across all of the lightcones, we would be taking cosmic variance between the cones into account. However, due to time constraints this was not possible. This should not significantly affect our findings, as in later chapters when we use this mock we focus on redshifts above $z = 0.5$, where the volume is larger and we should be less affected by cosmic variance.

Comparing the mock lightcone and standard LGALAXIES version with observations in Figure 3.6, we find that both agree well with the observations at all redshifts. The main area where the observations and models differ is at low masses above $z \sim 1$. It has been known for some time that models produce too many low-mass galaxies at high redshift (Fontanot et al. 2009; Weinmann et al. 2012). However, the level of disagreement is lower in LGALAXIES than several other galaxy formation models (Asquith et al. 2018).

We also check the colours of galaxies from our mock lightcone survey compared to observations in Figure 3.7 by plotting a $(U - V)$ vs $(V - J)$ rest-frame colour-colour diagram. The top five panels show the result from the LGALAXIES lightcone and the bottom five panels show the result for galaxies in the UDS. The black solid line on each panel shows the division used when splitting galaxies into passive and star-forming populations. The lightcone mock is able to reproduce the separate

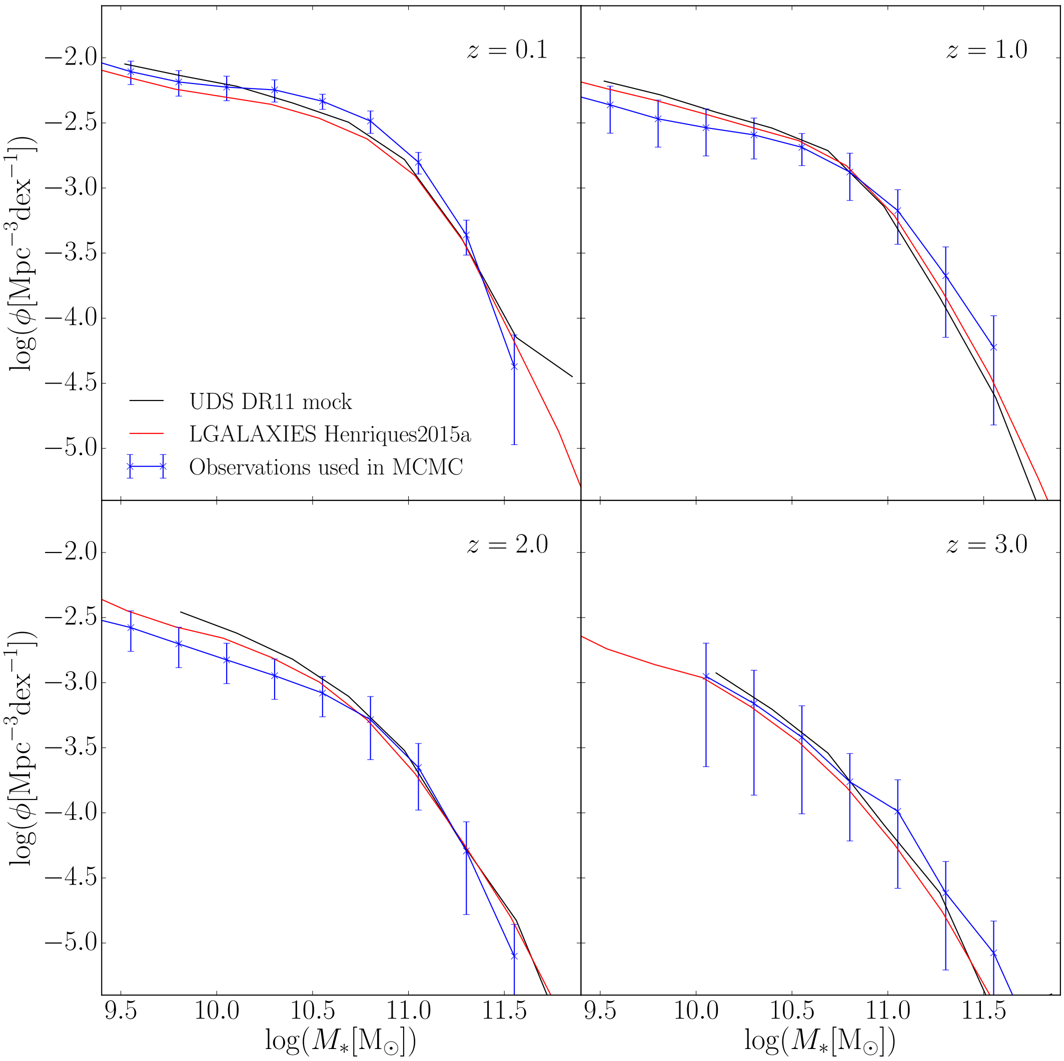

Figure 3.6. Galaxy stellar mass function of the mock lightcone survey (black line), the Henriques2015a version of LGALAXIES which is not a lightcone (red line) and the observations used to calibrate the model with MCMC (blue points). The redshift of each panel is shown in the top right. Several observations are combined at each redshift to produce one data set to calibrate the LGALAXIES model to. The surveys used are SDSS (Baldry, Glazebrook & Driver 2008; Li & White 2009) and GAMA (Baldry et al. 2012) at $z = 0.1$ and Marchesini et al. (2009), Spitzer-COSMOS (Ilbert et al. 2010), NEWFIRM (Marchesini et al. 2010), COSMOS (Domínguez Sánchez et al. 2011), UltraVISTA (Muzzin et al. 2013; Ilbert et al. 2013) and ZFOURGE (Tomczak et al. 2014) at higher redshifts. Individual observations are shown in Figure A1 of Henriques et al. (2015).

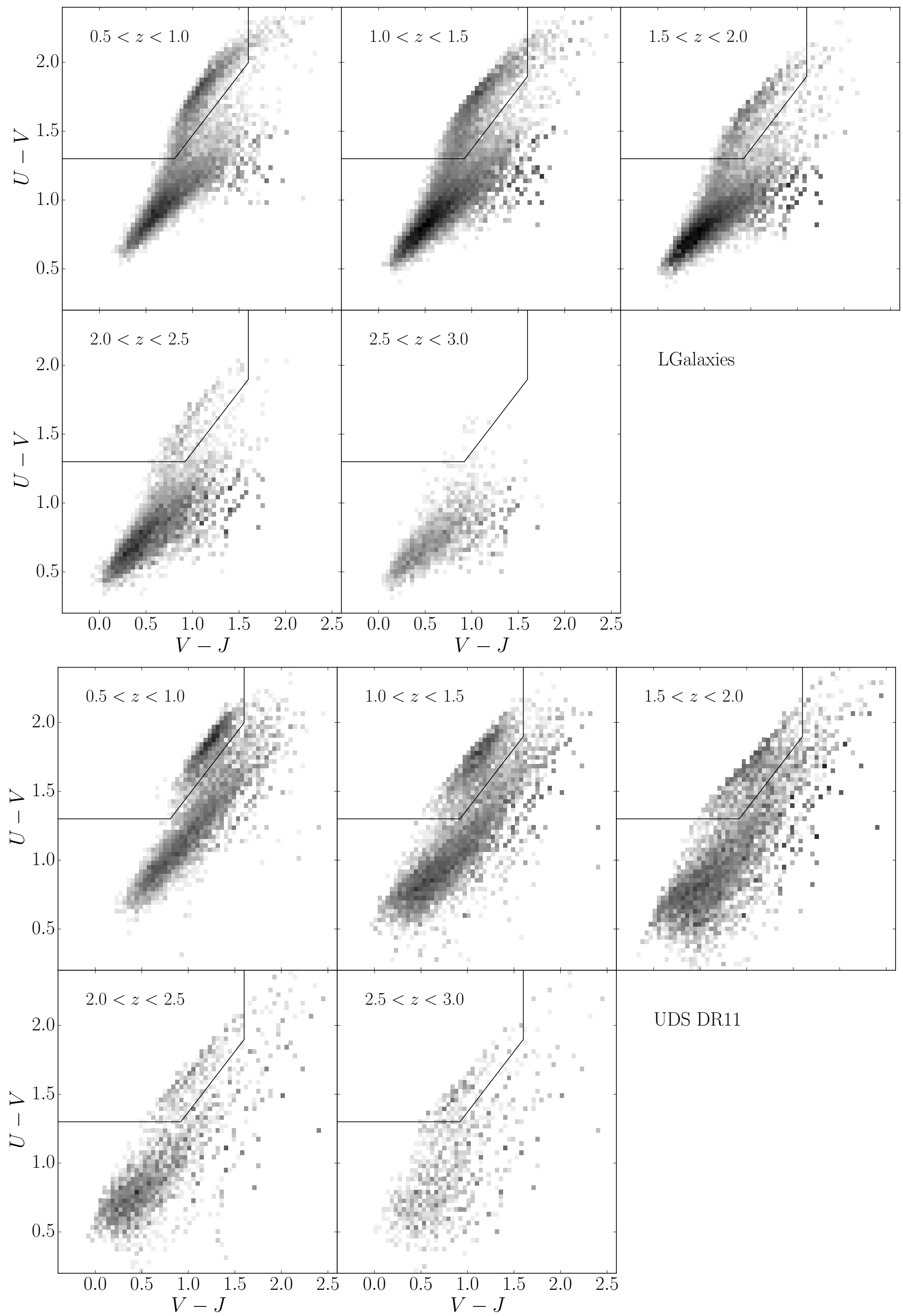

Figure 3.7. UVJ rest-frame colour-colour diagram of the mock lightcone survey (top five panels) compared to the one for the UDS (bottom five panels) in five different redshift bins, as labelled in the top left. The solid black line on each panel shows the split used to separate passive and star-forming galaxies.

population of passive and star-forming galaxies seen in observations at each redshift interval. The passive population in the mock is very similar to the passive population in the UDS, although there are fewer passive galaxies at high redshift in the mock. We can also see that there is more scatter in the UDS star-forming population than in the mock, especially for galaxies with bluer colours. The raw results from the mock will show very little scatter, as there are no uncertainties in the magnitude values output from the mock. Although here we scattered the magnitudes using a Gaussian to try and account for observational uncertainties, as explained in Section 3.4, it is very difficult to quantify and account for all the sources of uncertainty. The lack of scatter in the mock could also indicate that the processes in the models that quench a galaxy and move it into the passive population are less complex than in the real Universe, leading to less scatter on the diagram.

Finally, we investigate the difference in SFR between the mock lightcone survey and observations. In Figure 3.8 we plot the SFR vs stellar mass of galaxies at $z = 0.1, 1.0$ and 2.0 on the left to right panels respectively. Also plotted is the stellar mass - SFR correlation from Elbaz et al. (2007) at $z = 0.1$ and $z = 1.0$ and Daddi et al. (2007) at $z = 2.0$, the 'main sequence' of star formation. The evolution with redshift is very similar in both the mock survey and the observations, with the SFR decreasing from $z = 2.0$ to $z = 0.1$ and the gradient staying near constant. The agreement at low redshift is good but the SFRs predicted by the model are slightly too low at $z = 2.0$ by ~ 0.3 dex. This has been seen before (Mitchell et al. 2014; Hirschmann, De Lucia & Fontanot 2016; Asquith et al. 2018) and seems to be a common problem in galaxy formation modes. However, this discrepancy could reduce when comparing to other observations, as differences in the SFR indicator, SPS model, IMF or dust model being used can lead to up to a factor of 2 difference in the derived stellar masses and SFR (Stark et al. 2013; Speagle et al. 2014).

3.6 Conclusions

In this chapter we have shown how we have used the LGALAXIES model to construct a mock lightcone catalogue designed to mimic the UDS survey. Using a lightcone mock rather than the standard output format of a box at each snapshot redshift has two main advantages - i) the mock and the comparison survey will then have a similar physical area at any given redshift, ii) the mock will have a continuous redshift distribution, rather than discrete values. Both of these factors will mean that a comparison between the mock and observations will be easier, as any differences will not be due to the redshift distribution of galaxies or differences in survey area.

After constructing the lightcone, we then had to make the mock as similar to the UDS as possible. One part of this was to add uncertainties into the redshift, magnitude and stellar mass values for each galaxy. Observationally these can never

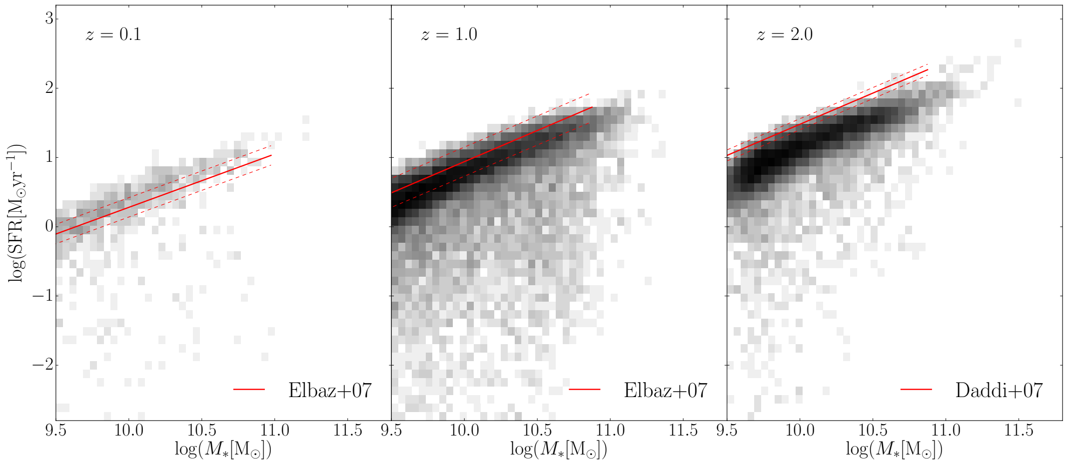

Figure 3.8. Stellar mass - SFR correlation in the mock lightcone survey at $z = 0.1$ (left panel), $z = 1.0$ (central panel) and $z = 2.0$ (right panel). The shading in each cell shows the number of galaxies at that position in the diagram, coloured by a log scale. The observations from Elbaz et al. (2007) ($z = 0.1$ and $z = 1.0$) and Daddi et al. (2007) ($z = 2.0$) are shown as red lines, with the red dashed lines showing the 1σ scatter on the correlation.

be perfectly measured, so some scatter needs to be introduced to the output values from the mock. We did this by estimating the uncertainty from observations and then convolving the mock output with a Gaussian. This then leads to a more realistic distribution for the values than straight from the LGALAXIES model. We also calculated the stellar mass limits for the UDS and applied these to the mock, adding in a minimum stellar mass of $\log(M_*/\mathrm{M}_\odot) = 9.5$ to reflect the mass resolution of LGALAXIES.

We then ran some tests on the lightcone to ensure that we still got the expected results. Firstly, we compared the stellar mass from the LGALAXIES model with added scatter to the stellar masses from the PCA method, which showed good agreement. We then compared the stellar mass function from our mock to the standard version of LGALAXIES and found that it matched with a small offset likely due to cosmic variance. We also compared to UVJ diagrams from the UDS, where the mock was similar, but had less scatter. Finally, we also checked the stellar mass - SFR correlation for galaxies at different redshifts. Although the SFR for a given stellar mass at $z = 2$ is lower in the mock this is a problem common in semi-analytic models.

We can now be confident that the mock lightcone survey we have produced can be used to investigate galaxy evolution and quenching, and can be compared with the UDS survey without any significant differences affecting our results.

Chapter 4

Identifying post-starburst galaxies in the mock UDS

In this chapter we describe the the Principal Component Analysis method that was used to classify galaxies in our mock lightcone catalogue and the UDS survey. We compare the results from our mock with the observational results from the real UDS, to highlight areas where galaxy formation models may still need to improve. We then investigate the star formation histories of galaxies classified as post-starbursts in the mock, in part to provide an independent test of the Principal Component Analysis method for selecting galaxies that have been recently and rapidly quenched. Finally, we investigate what effect changing the resolution of the star formation histories has on the properties and classification of galaxies.

The Principal Component Analysis classification of galaxies in both the real UDS and the mock UDS lightcone catalogue was done by Aaron Wilkinson at Ghent University.

4.1 The Principal Component Analysis method

In Chapter 3 we discussed how the mock lightcone survey was created using Lgalaxies to mimic the UDS survey. In order to investigate quenching processes in this mock and compare to observations, we need to be able to classify galaxies into different populations. For the observations, this would ideally be done spectroscopically, however getting spectra for every object in a survey like the UDS is too costly in terms of money and resources. Obtaining spectra for the faintest galaxies can be impossible, with spectroscopy for these objects only becoming available after the launch of the James Webb Space Telescope (JWST). For large numbers of galaxies the best way to classify them is with photometric data. Although this is less accurate than spectroscopy, the clear advantage is the ability to study the properties of large numbers of galaxies in a consistent manner. One common photometric method is spectral energy distribution (SED) fitting (e.g. da Cunha, Charlot & Elbaz 2008;

Noll et al. 2009; Acquaviva, Gawiser & Guaita 2011), but this relies on the spectral synthesis model chosen (Conroy 2013). Colour-colour diagrams are another way to commonly classify galaxies, but they also rely on spectral synthesis models to determine the rest-frame colours and can lead to degeneracies between redshift and physical properties (Lane et al. 2007).

Another option is to use a Principal Component Analysis (PCA) method. This technique is often used in statistics and is designed to reduce the number of variables used to describe a system by choosing an optimal set of parameters. For galaxy SEDs, the PCA determines which features vary most between galaxies and chooses principal components (otherwise known as eigenvectors), which when combined reproduce the variety in galaxy SEDs. It is then possible to make a 'colour-colour' diagram which combines the data from all available photometric bands and use this to classify galaxies. Although stellar population synthesis models are also used in this method to build an SED library, each galaxy is not constrained by having to match any one SED.

The application of PCA to the UDS data is described in Wild et al. (2014). In order for PCA to find the best principal components to describe the full variety of galaxy SEDs, a library of well sampled SEDs is needed. Therefore, model SEDs are used as these can be very finely sampled using all of the photometric bands from the UDS and covering the same redshift range. A library of $\sim 44,000$ stochastic burst model SEDs were used, built from Bruzual & Charlot (2003) stellar population synthesis models. These models have an exponentially decaying star formation rate (SFR) with stochastic bursts of star formation of varying ages and strengths. The formation time and metallicity were randomly sampled with a flat prior and the dust attenuation was included using the prescription from Charlot & Fall (2000). These model SEDs were then convolved with the UDS filter set and shifted in steps of $\Delta z = 0.1$ (Wild et al. 2014) between $0.5 < z < 2.0$ for DR8 (Wild et al. 2016) and $0.5 < z < 3.0$ for DR11 (Wilkinson et al. in preparation).

The rest-frame model SEDs for all redshifts are normalised at 1μm and then the mean spectrum is found (m_λ). The PCA is then applied to the difference between each model SED and the mean spectrum. Three eigenvectors ($e_{i\lambda}$) are needed in order to be able to reproduce 99.98% of the variance in the model SEDs. A normalised galaxy SED (f_λ/n) can be reproduced using a linear combination of the eigenvectors and the mean spectrum:

$$\frac{f_\lambda}{n} = m_\lambda + \sum_{i=1}^{3} a_i e_{i\lambda}, \tag{4.1}$$

where a_i are the principal component amplitudes (supercolours) associated with each eigenvector. The three eigenvectors and mean eigenvector are shown in Figure 4.1. The points on each panel show the normalised flux observed with each filter, shifted

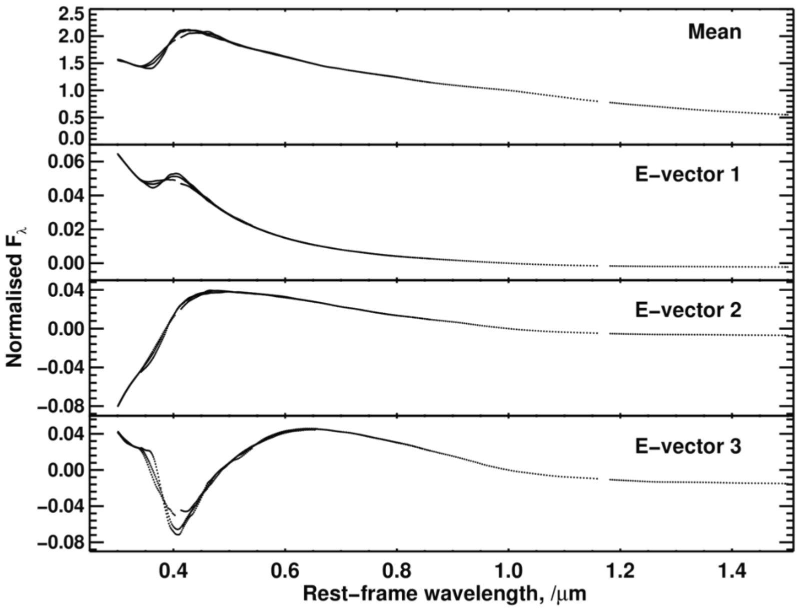

Figure 4.1. Mean and three eigenvectors used in the PCA classification of the UDS from Wild et al. (2014). Each point shows the normalised flux observed with one filter at one redshift, placed at the rest-frame wavelength of the filter. This can lead to gaps or multiple points at the same wavelength, as different filters overlap at different redshifts. Each eigenvector can be added in different amplitudes (supercolours) to the mean in order to reproduce the variance in galaxy SEDs. The first eigenvector affects the red-blue slope of the SED, whilst the second and third change the SED shape around 4000Å and the Balmer break.

to each sample redshift and placed at the rest-frame wavelength of the filter.

Therefore, starting from photometry, this method gives three supercolours (SC) for each galaxy - SC1, SC2, and SC3. SC1 changes the red-blue slope of the SED and correlates with the R band weighted mean stellar age of the galaxy or the specific star formation rate (sSFR) of the galaxy. The second supercolour, SC2, modifies the strength of the Balmer break and traces the fraction of stellar mass formed in bursts in the last Gyr. SC3 alters the shape of the SED around 4000Å and helps to break the degeneracy between the fraction of stellar mass formed in bursts in the last Gyr and metallicity. Figure 4.2 uses the SED library to show how the supercolours correlate with different physical properties - R band weighted mean stellar age, metallicity, total effective dust attenuation and fraction of stellar mass formed in bursts in the last Gyr.

Galaxies are then classified based on their position on the supercolour plane into four main categories - star-forming, passive, post-starburst (PSB), and dusty. The boundaries between the different populations are determined using both model SEDs and spectroscopy (Wild et al. 2014) and are based on the properties of the models. Young galaxies have higher SC1 values, so star-forming galaxies have high SC1 values (unless they are dusty), whilst passive galaxies have low SC1 values. PSBs have high

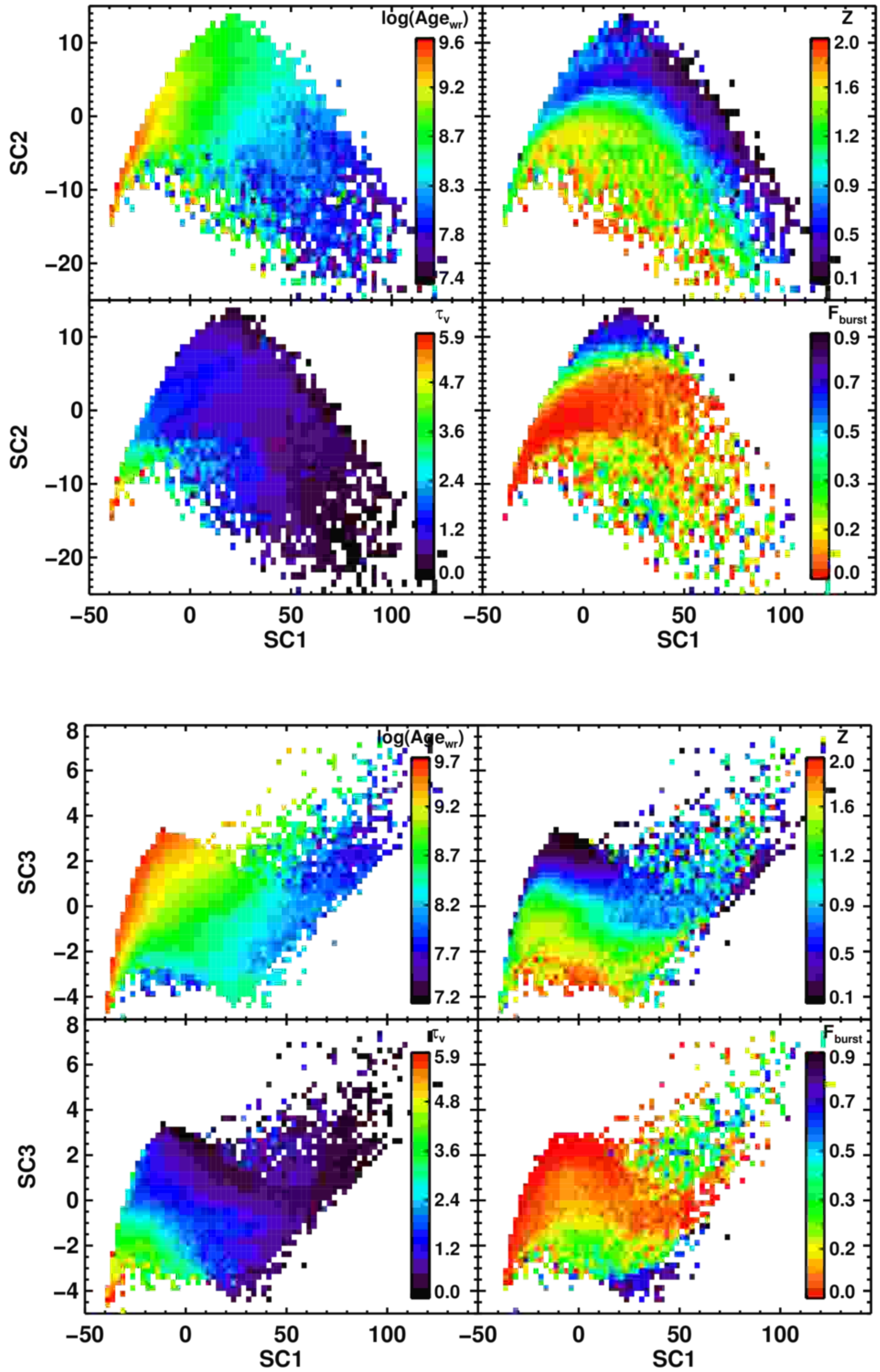

Figure 4.2. Supercolour diagrams showing SC2 vs SC1 (top panels) and SC3 vs SC1 (bottom panels) from Wild et al. (2014) for all of the model SEDs. The top left panel of each is coloured by the log of the R band light weighted mean stellar age in years, the top right by the metallicity in solar units, the bottom left by the total effective V band optical depth and the bottom right the fraction of stellar mass formed in bursts in the last Gyr.

values of SC2, but low values of SC1 and SC3, as they formed a large fraction of their stellar mass within the last Gyr but are currently passive. Dusty galaxies have low values of SC1, SC2 and SC3 as they have high values of total dust attenuation, high sSFR and metallicity.

These classifications have also been confirmed by spectra in Wild et al. (2014) and Maltby et al. (2016). Using the UDSz project (ESO Large Programme 180.A-0776, PI: Almaini), Wild et al. (2014) selected galaxies with medium resolution spectra around the 4000Å break and with photometric redshifts in the range $0.9 < z < 1.2$. The 282 galaxies in the sample were then stacked according to their class based on their supercolours. Star-forming galaxies show [OII] emission characteristic of the star- forming population. The passive galaxies showed strong 4000Å breaks, Ca H&K lines indicative of an old stellar population and low sSFR. PSB galaxies can be identified by strong Balmer absorption and Balmer breaks (Wild et al. 2009), however Wild et al. (2014) only had 5 PSB candidates with high enough signal-to-noise ratio.

Maltby et al. (2016) have since used recently acquired spectra to follow-up on this issue. Using deep optical spectroscopy from VIMOS at the VLT, combined with lower resolution spectroscopy from the UDSz, they analysed a sample of 24 PSB candidates, identified using the PCA method, in the redshift range $0.5 < z < 1.4$. They found that $\sim 80\%$ of these PSBs could be confirmed spectroscopically as they showed spectral signatures based on Hδ equivalent width and the strength of the Balmer break. Using an additional stricter requirement that they show little to no [OII] emission, the confirmation rate of PSBs drops to 60%. Above $z \sim 1.5$, spectroscopic confirmation of PSBs is made difficult due to the fact that the key spectral features move into the near-infrared.

These studies have confirmed that the majority of PSBs selected using a PCA technique show spectral signatures of having been rapidly quenched after a period of significant star formation. However, this does not necessarily mean that these galaxies have undergone a 'starburst', as similar spectral features can be produced from an abrupt termination of star formation after a more extended period (< 3 Gyr) of star formation (Wild et al. 2016). Therefore, we are using the term post-starburst to refer both to galaxies that are classic PSBs and have had a burst of star formation before being rapidly quenched, or galaxies that have had a rapid termination of their star formation. As the spectral features are not expected to last longer than ~ 1 Gyr, for both cases quenching must have been recent.

4.2 Identifying post-starburst candidates in the mock

We now have a method that can classify galaxies based on their photometry that we can apply to the mock catalogue. Using this method we can identify PSBs, which are ideal galaxies to use to investigate quenching processes. The PCA method can be used on the mock lightcone survey in the same way as for the UDS data, as we deliberately designed the mock to have the magnitudes in the same filters as the UDS so that the same eigenvector basis could be used. Only galaxies in the redshift range $0.5 < z < 3.0$ could be classified with PCA, with the low redshift cut to ensure that the V band provides a measurement bluewards of the 4000Å / Balmer break. As the mock catalogue goes from $z = 0.0$ to $z = 3.0$ we cut out any galaxies with $z < 0.5$. We also remove any galaxies with $K < 24.5$, as although the limiting magnitude of the UDS DR11 is $K_{\rm lim} = 25.0$, the PCA analysis uses a more conservative cut of $K = 24.5$ as good quality photometry is needed. Our sample then reduces from 82,679 galaxies to 76,885 galaxies in the final catalogue. After the PCA classification of the mock catalogue we have a sample of 68,437 (89.0%) star-forming galaxies, 5,695 (7.4%) passive galaxies, 1,772 (2.3%) post-starburst galaxies and 981 (1.3%) dusty galaxies. For the purpose of this thesis we include the dusty population with the star-forming galaxies.

4.2.1 Stellar mass and redshift distribution

We firstly compare the distribution of galaxies in stellar mass and redshift in LGALAXIES and the UDS in Figure 4.3. We plot the stellar mass vs redshift of galaxies in the mock survey in the left panel and those in the UDS DR11 in the right panel. The colour of each point denotes the class assigned to the galaxy, with star-forming and dusty galaxies shown as blue, passive as red, and PSBs as orange points. Also shown is the stellar mass completeness limit for each population, calculated as in Section 3.4, following the method in Pozzetti et al. (2010). The completeness limit line for each population is the same colour as the points for that population, and as in Section 3.4, takes on a minimum value of $\log(M_*/\mathrm{M}_\odot) = 9.5$ to reflect the mass limit of LGALAXIES. We apply the same limits to the UDS and LGALAXIES in order to ensure we are comparing the same population in both.

We can see that the stellar mass and redshift distribution in the LGALAXIES mock and the UDS is different. The stellar masses of the star-forming population in the two panels look similar at low redshift, but are different at high redshift, with far fewer star-forming galaxies above $10^{10.5}\mathrm{M}_\odot$ in the mock above $z = 2.0$. For the passive population the same problem is present, there are not enough high-mass passive galaxies in the mock at high redshift. However, there are also too many low-mass passive galaxies at low redshift in the mock. This issue of SAMs failing to reproduce the anti-hierarchical nature of galaxy formation was also found in Chapter 2, and is very difficult for the models to correct.

There are two main populations of PSBs in the UDS - low-mass PSBs at low redshift and high-mass PSBs at high redshift. The mock produces low-mass PSBs at low redshift, but too many of them in comparison to the UDS. There is also a

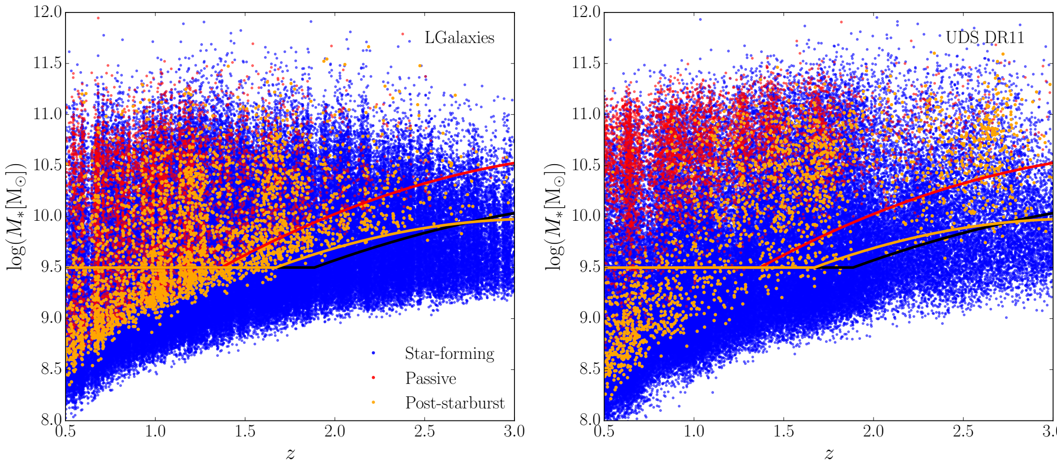

Figure 4.3. Stellar mass vs redshift distribution for both LGALAXIES (left panel) and the UDS (right panel). The blue points are star-forming galaxies, the red are passive galaxies and the orange are PSB galaxies, as classified by the PCA method. The coloured lines are the completeness curves for each population. The lines all flatten out at $10^{9.5}\mathrm{M}_\odot$ as this is the mass resolution of LGALAXIES. In the UDS there are two PSB populations - low-mass at low redshift and high-mass at high redshift. The low-mass group are present in LGALAXIES, but there are very few PSBs at high redshift.

lack of high-mass PSBs in the mock at high redshift. Some of these difference could be due to differences in area between the UDS and our mock. The area with multi-wavelength coverage and PCA analysis in the UDS is $\sim 0.62\mathrm{deg}^2$, whereas the mock survey is $1\mathrm{deg}^2$. We will now look at how the stellar mass functions of these three populations evolve with redshift, as then we are comparing the number densities in the mock and the UDS.

4.2.2 Stellar mass functions

We now investigate the number density of galaxies in each population in both the UDS and the mock by looking at the galaxy stellar mass function (SMF). Figure 4.4 shows the SMF of the three classes from $z = 0.5$ to $z = 3.0$ for all galaxies above the stellar mass limits. At low redshift, we can see that there are too many low-mass galaxies in the mock, especially in the passive population, by ~ 0.5 dex at $\log(M_*/\mathrm{M}_\odot) = 9.5$. There is also a slight excess of PSB galaxies at low redshift, although this is not so pronounced. At high masses there are too few passive galaxies, with LGALAXIES not able to recreate the shape of the passive mass function.

As we move to higher redshift, the overproduction of low-mass passive galaxies is still evident up to $z = 2.0$, where the stellar mass limit increases to $\log(M_*/\mathrm{M}_\odot) \sim 10.5$. There are also too few high-mass passive galaxies in all of the higher redshift bins. The star-forming stellar mass function matches reasonably well at low masses at high redshift, with a slight overproduction. There are too few high-mass star-forming and PSB galaxies at $z > 1.5$ and $z > 2.0$ respectively. For PSBs at all

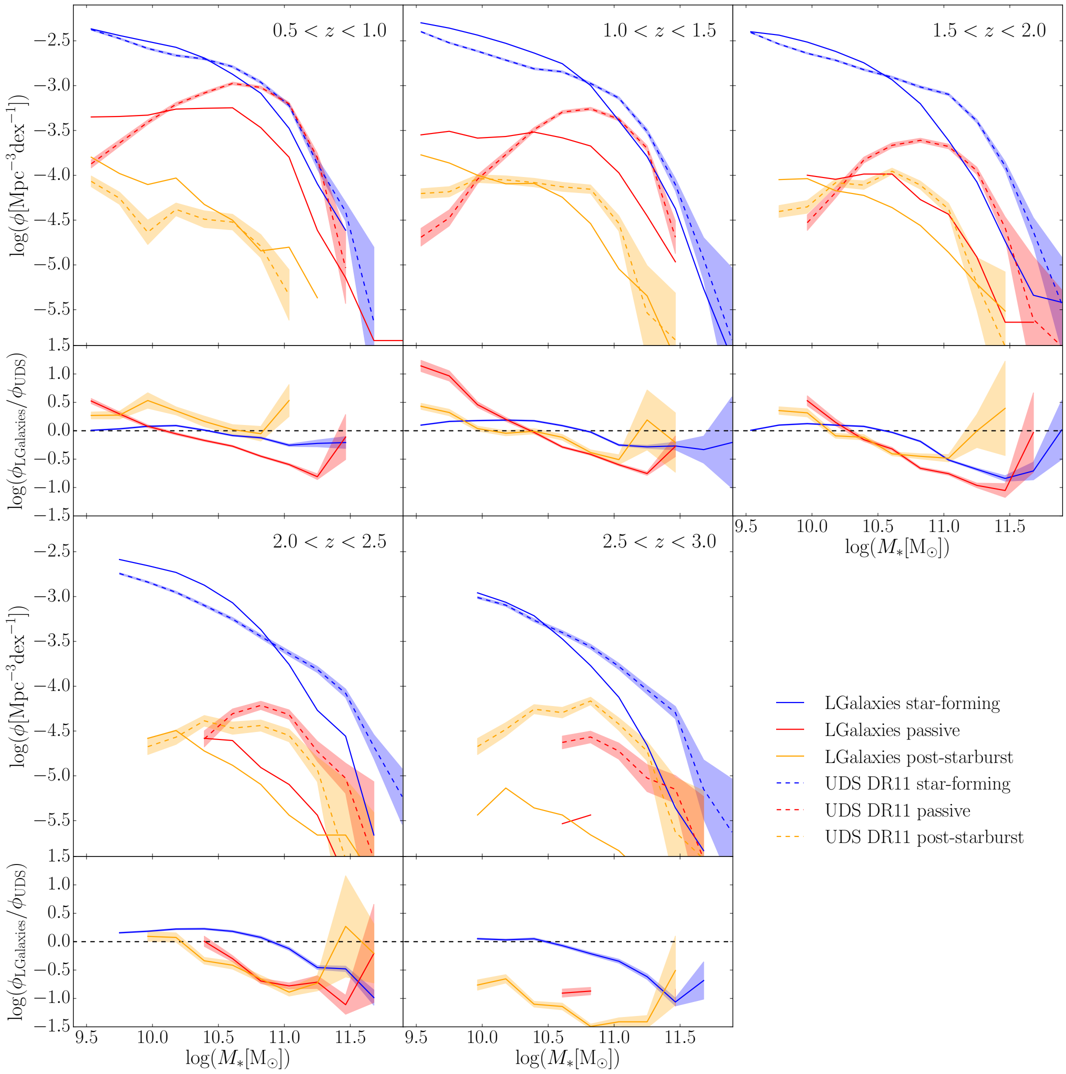

Figure 4.4. Stellar mass function for the three populations in LGALAXIES (solid lines) and the UDS (dashed lines). The redshift range increases from top left to bottom right. Blue lines are for the star-forming population, red for the passive population and orange for the PSB population. The shaded regions show the 1σ uncertainty on the UDS stellar mass functions. The smaller lower panels show the ratio of the number density in LGALAXIES to the UDS. At low redshift LGALAXIES matches the UDS well apart from a slight excess of low-mass PSB and passive galaxies, and too few passive galaxies with stellar masses of $\sim 10^{11}\mathrm{M}_{\odot}$. However, moving to high redshift there is a lack of high-mass galaxies in all the populations, especially the PSBs and passive galaxies.

redshifts the shape of the SMF in the mock is broadly similar to the UDS, but is slightly too high at low redshift and too low at high redshift.

In Chapter 2 we found that many of the galaxy formation models underproduced the number density of high-mass galaxies at high redshift. When splitting into star-forming and passive galaxies, the models overpredict the number of low-mass star-forming galaxies at high redshift, and struggled to reproduce the turnover in the passive stellar mass function. Here, LGALAXIES matches the low-mass end of the star-forming SMF to within ~ 0.2 dex at all redshifts. However, the issues with the number density of high-mass galaxies and low-mass passive galaxies still remain. Many attempts have been made to fix these problems but work is still ongoing. We need to bear the differences between the populations in the mock and the UDS in mind when doing any comparisons.

4.2.3 Supercolour diagram

Figure 4.5 shows the SC1 and SC2 distribution for the UDS and LGALAXIES for galaxies above the stellar mass limits, as shown in Figure 4.3. The galaxies in the mock have been randomly sampled so that the number of points on each panel is equal. One difference between the two diagrams is that the supercolour values have a lot less scatter in the LGALAXIES mock than in the UDS, especially in SC2. One reason for this lack of scatter could be that when making the mock, as described in Chapter 3, we didn't account for all of the observational uncertainties when measuring stellar mass, redshift and magnitudes of the galaxies. When trying to identify the redshift of a galaxy, sometimes 'catastrophic failures' are introduced, where, for example, the Balmer and 4000Å break are confused and the redshift identified for the galaxy is then very different to its actual redshift. These galaxies would be outliers when looking at the distribution of values of $\mathrm{d}z/(1+z)$, so would only very rarely, if at all, be reproduced when using a Gaussian to scatter the redshift values. Some of the extra scatter in the UDS could be due to additional data systematics that are not present in the mock, such as confusion between close galaxy pairs.

Looking at Figure 4.5, we can also see that there are fewer galaxies with high values of SC2 in the mock. This is particularly important for us as we want to use this catalogue to look at PSBs, which by definition have high values of SC2 as they have formed a large fraction of their stellar mass in the last Gyr. The fact that there are fewer galaxies with high SC2 could be for several reasons: i) the physical prescriptions in the model mean that there are not as many starbursts in the LGALAXIES model as in the real Universe, which would lead to fewer galaxies with a higher fraction of their stellar mass formed recently, ii) the galaxies that have had recent starbursts are not being identified through the PCA method, iii) the time steps separating the timesteps in the simulation are too large, so the star formation

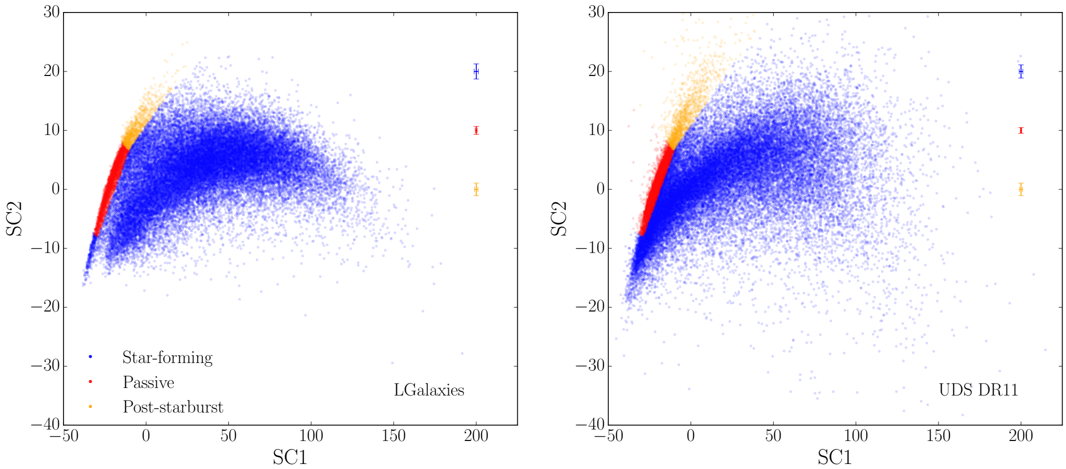

Figure 4.5. SC2 against SC1 for LGALAXIES (left panel) and the UDS (right panel). In order to ensure there was the same amount of points in each panel we have randomly sampled galaxies in the mock to match the overall number of galaxies in the UDS. The points are the same colours as in Figure 4.3 and the error bars on the right of each panel show the average uncertainty in SC1 and SC2 for each population. The PCA technique manages to identify galaxies of each class in LGALAXIES, but there are some differences between the LGALAXIES and UDS supercolour diagrams. For example, there is more scatter in the blue cloud in the UDS plot, especially at high SC1 values.

is spread across this time and it is not possible to resolve very short bursts of star formation. We explore ii) and iii) further in Section 4.3 and Section 4.4 respectively.

4.2.4 UVJ colour-colour diagram

Figure 4.6 shows the rest-frame UVJ diagram for the UDS and LGALAXIES for galaxies above our stellar mass limit, coloured by their PCA classification. As with Figure 4.5, the mock galaxies have been randomly sampled to match the total number in the UDS. The dashed lines indicate the boundaries used to separate galaxies into star-forming and passive on the UVJ colour- colour diagram from Williams et al. (2009) and Hartley et al. (2013), with an additional cut at $(V - J) < 0.9$ to separate PSBs from passive galaxies (Whitaker et al. 2012a). The UVJ diagram from LGALAXIES and the UDS agree well with each other, with fewer obvious differences than in Figure 4.5. The scatter across the diagram is similar for both the UDS and the LGALAXIES mock, although there are more galaxies at the blue end of the blue cloud in the LGALAXIES diagram.

The PCA and UVJ classifications agree well, with galaxies being in roughly the correct area of the diagram. However, there are some galaxies that would be classified differently using the two methods. This is likely due to the fact that the UVJ colour-colour diagram only uses data from three bands and ignores the rest of the galaxy SED, whereas the PCA technique takes into account the full shape of the SED, and can therefore identify higher order differences between the three populations. Some of the PSBs classified by PCA extend into the passive area of the

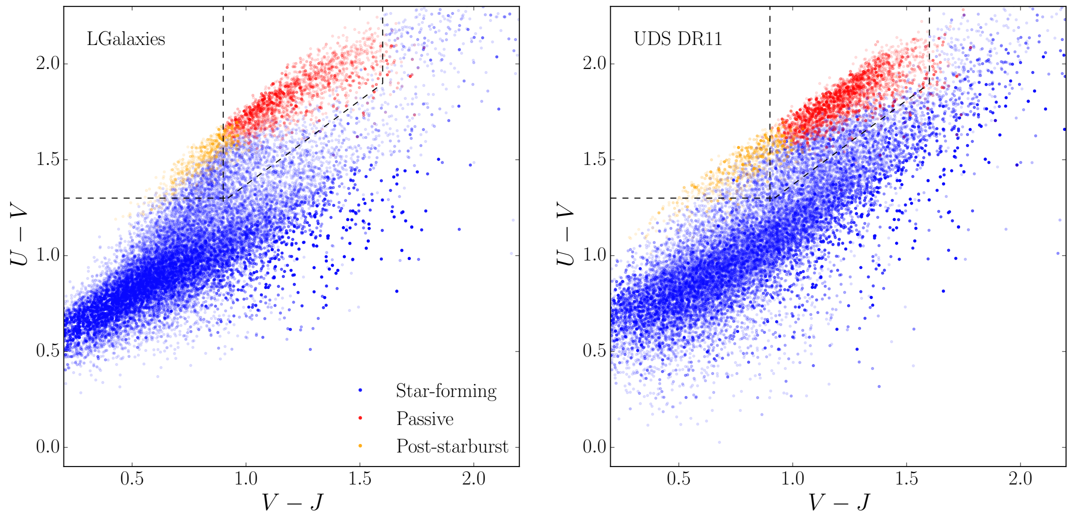

Figure 4.6. Rest-frame UVJ colour-colour diagram for LGALAXIES (left panel) and the UDS (right panel). The colour of the points is the same as in Figure 4.5 and indicates the PCA classification of each galaxy. As for Figure 4.5, we randomly sampled galaxies from the model so that the overall number of points was the same in each panel. The black dashed lines mark the separations usually used to split galaxies into star-forming, passive and post-starburst populations on the UVJ diagram. The UDS and LGALAXIES diagrams agree well, with some slight differences.

UVJ diagram. These are likely galaxies which lie near the boundary of the passive and PSB region on the PCA diagram and may not be fully quenched, but this is not distinguishable from just the U, V and J bands alone. Similarly, some galaxies classified as star-forming by the PCA method are in the PSB region of the UVJ diagram. They may be galaxies which are being currently quenched, but do not yet have PSB signatures in their SEDs.

4.3 Star formation histories of post-starburst galaxies

One advantage of semi-analytic models is that we can track individual galaxies through time and look at their evolution, whereas with observations you need to connect populations at different redshifts. For all galaxies in the LGALAXIES mock lightcone, we have a star formation history (SFH), which tracks when the galaxy formed its stellar mass over its lifetime. Using this, we can compare the SFH of galaxies of different classes, in order to check if the PCA method is picking up star-forming galaxies that were rapidly quenched and classifying them as PSBs. Figure 4.7 shows the SFH of one example PSB. The percentage of the PSB galaxy's stellar mass formed per Gyr within each bin is plotted as a function of the lookback time from when the galaxy was classified as a PSB. Each galaxy has 20 bins making up its SFH, which are more finely spaced at smaller lookback times. This is because recent star formation has a larger effect on galaxy magnitudes and SEDs than older activity. The choice of number of bins for the SFH is explained in Shamshiri et al.

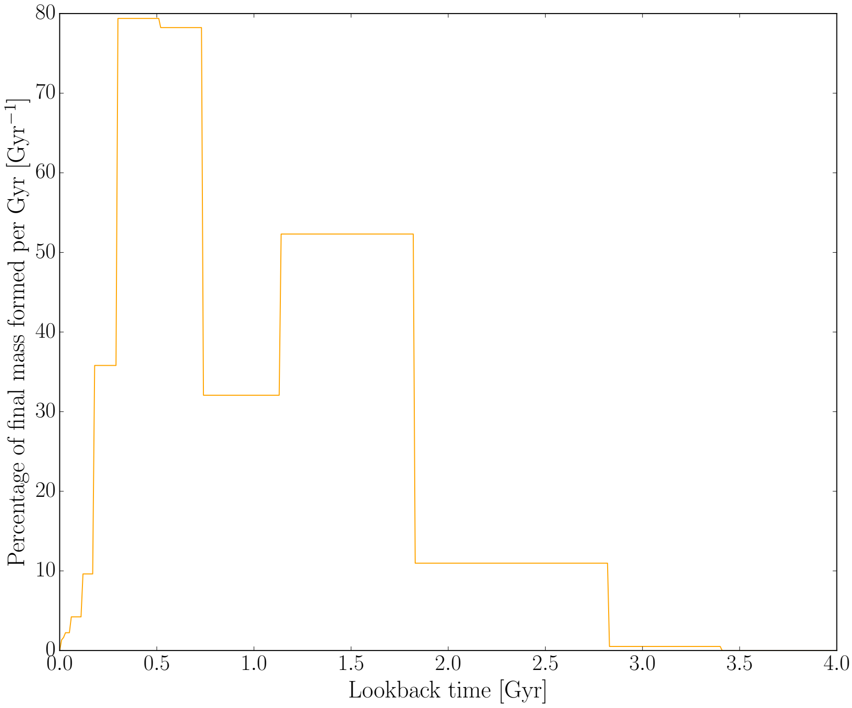

Figure 4.7. Star formation history of one example PSB at $z = 1.59$ in the mock, with the percentage of the final stellar mass of the galaxy formed within this bin, normalised to be per Gyr, vs the lookback time in Gyr from when this galaxy was classified as a PSB. This galaxy has an increase in star formation which is rapidly quenched within the last Gyr.

(2015).

From Figure 4.7 we can see that 3−4 Gyr ago there was little star formation, with the galaxy only forming a few percent of its final stellar mass within this time. The rate of star formation then increases over the next 2 Gyr, before reducing slightly at a lookback time of ~ 1 Gyr. The star formation rate then increases over the next 500 Myr, forming roughly 40% of its stellar mass during this time. The galaxy is then rapidly quenched over the next ~ 300 Myr. This rapid quenching at the end of the SFH will have imprinted the PSB signature in the galaxy SED that was identified by the PCA method. However, we cannot make conclusions about the evolution of all PSBs from looking at one galaxy alone, so in the next section we look at the SFHs of the entire PSB population.

4.3.1 Stacked star formation histories

We want to examine the SFHs of all of the PSBs, but it is not practical to examine the SFH of each PSB individually. By stacking the SFH of all the PSBs within the mock survey, we can get an idea of their general evolution. Figure 4.8 shows the stacked SFHs for all PSBs as orange lines in the background. The median SFH of PSB galaxies is then shown on top as a black dashed line. We also plot the median SFH for passive and star-forming galaxies for comparison as red and blue dashed

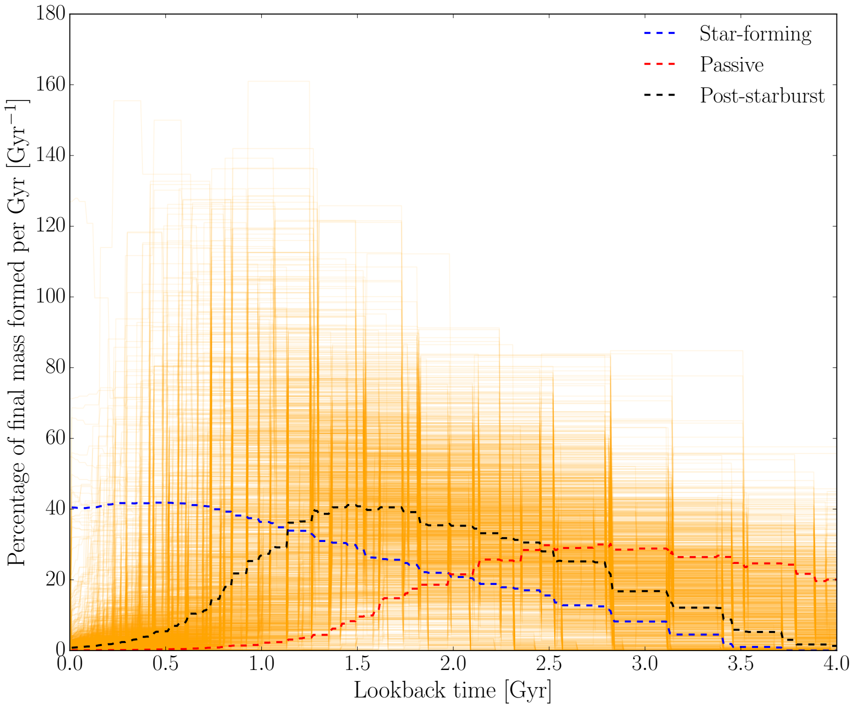

Figure 4.8. Star formation histories of all PSBs in the LGALAXIES mock. Plotted is the percentage of the final stellar mass of the galaxy formed per Gyr for that bin vs the lookback time from when the galaxy is classified as a PSB in Gyr. The black dashed line shows the median for all of the PSBs, whilst the orange lines show the SFH for individual PSB galaxies. The blue and red lines show the median for the star-forming and passive populations respectively.

lines respectively. As the area under the SFH for each galaxy sums to 100%, you cannot compare the amplitude of any of the median SFHs with each other, as this just tells you on average when within the lifetime of that type of galaxy most of their stellar mass is formed.

The passive galaxies peak in star formation earlier and are now all quenched, whereas the star-forming galaxies have increased their star formation on average. The PSB population lies between the two; the peak of their star formation is later than the passive galaxies and they have formed more of their stellar mass in the last ∼20% of their lifetime than passive galaxies. However, unlike the star-forming population they are now quenched. A few of the PSBs show a peak in star formation at late times and the average time taken for them to quench appears to be shorter than for passive galaxies, so they do appear to be different than the passive population.

4.3.2 Time taken to form last 10% of stellar mass

From the SFHs, we can also calculate the time taken to form the last 10% of the stellar mass of each galaxy, as PSBs are supposed to have formed over ∼ 10% of their stellar mass in the last Gyr (Wild et al. 2014). Figure 4.9 shows a histogram of the time taken for galaxies to form the last 10% of their stellar mass, split into

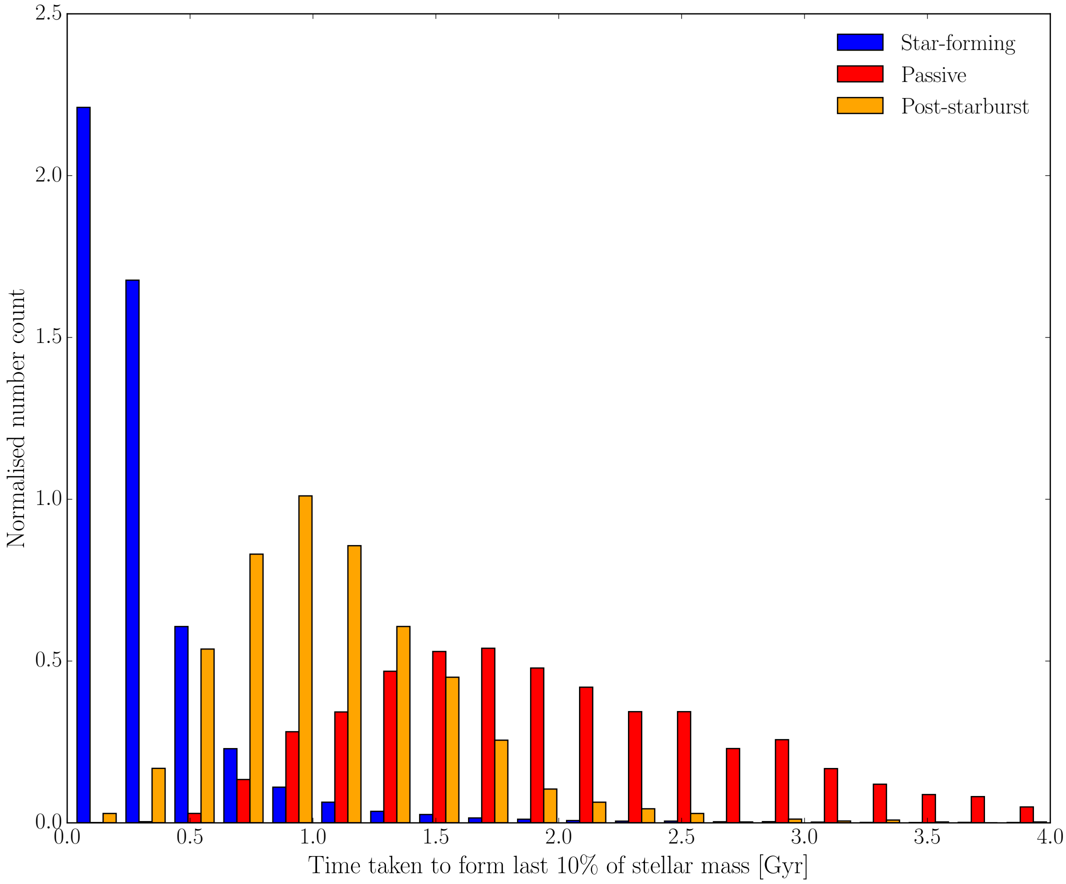

Figure 4.9. Histogram of the time taken for galaxies in each population to form the last 10% of their stellar mass. The blue, red and orange bars are for star-forming, passive and post-starburst galaxies respectively. For PSBs, the median amount of time taken is 1.0 Gyr, which shows that some of them have had recent star formation despite being currently quenched.

the three classes and coloured accordingly. For star-forming galaxies, the majority of them have formed 10% of their stellar mass within the last 500 Myr. This is what we would expect as there is still ongoing star formation in these galaxies. For the passive galaxies the range in times is much larger, going from 500 Myr to 4 Gyr, reflecting the spread in ages of these galaxies. PSBs lie in the middle of these two populations, with the median time to form the last 10% of stellar mass being 1 Gyr. This is what we expect from the definition of PSBs, as they have had recent star formation but are currently quenched. There is a tail of longer times out to 2.5 Gyr which could be an effect due to the resolution of the SFH, as the time difference between successive bins at a lookback time of 2 Gyr is $\sim$ 1 Gyr. However, it could also be contamination from the passive sample being misidentified as PSBs or the fact that the PSBs in our mock may have smaller bursts.

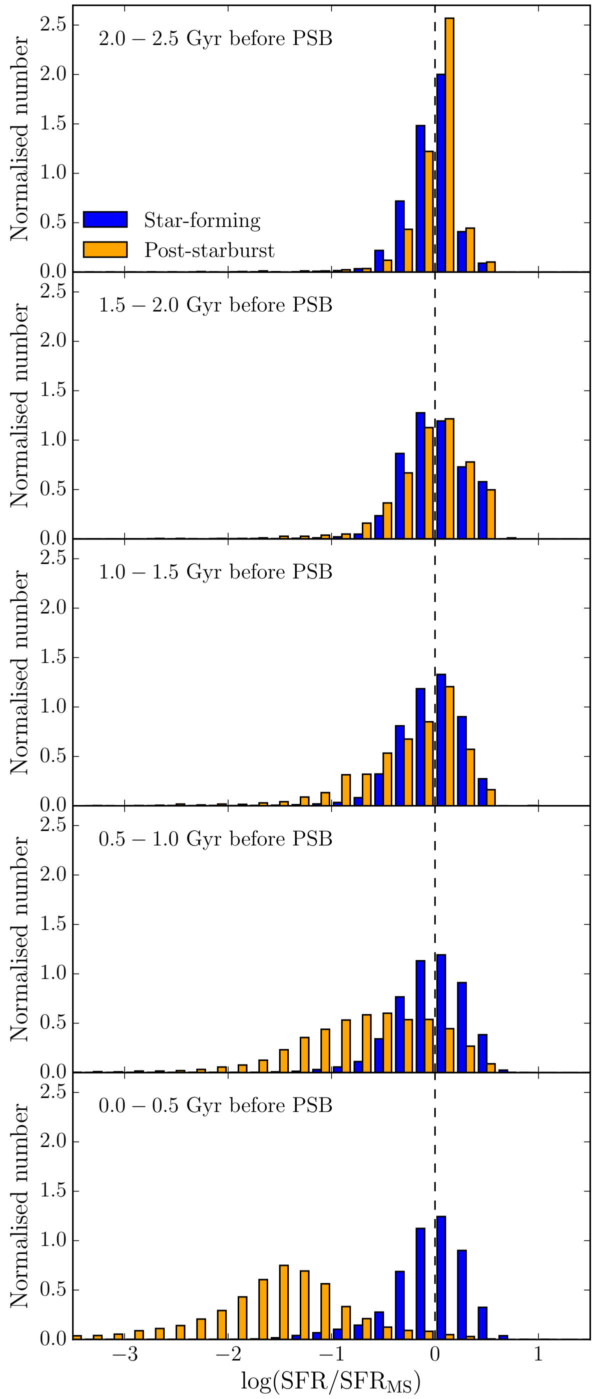

Figure 4.10. Histograms of the SFR of the progenitors of PSBs, divided by the SFR they would have if they were on the main sequence. The dashed line shows where galaxies on the main sequence would lie. The orange histograms shows PSBs, whilst the blue histograms show star-forming galaxies. The top panel shows progenitors 2.0 - 2.5 Gyr before becoming a PSB, decreasing in time to the bottom panel which is 0.0 - 0.5 Gyr before becoming a PSB. Over 1.5 Gyr before becoming a PSB, most of the progenitors lie on or just above the main sequence of star formation. Around 1 Gyr before being a PSB, the SFR starts to decrease and move off the main sequence, showing they are being quenched.

4.3.3 Evolution of post-starbursts compared to the main sequence

Another way we can also investigate whether the PSBs have had a burst of star formation is by using their SFHs to see if they were particularly star-forming for their stellar mass at any particular time in their evolution. We calculate the ratio of the SFR of each galaxy at each timestep in its SFH to the SFR it would have if it was on the main sequence. In order to do this, we have taken all of the star-forming galaxies in our sample, and fit the main sequence to the SFR and stellar mass of these galaxies in different redshift bins. We then used the fit in the corresponding redshift bin to calculate what the SFR of each galaxy would be for its stellar mass if it was on the main sequence. From this we can calculate the ratio of the SFR of each galaxy to the SFR it would have if it was on the main sequence. We then plot the log of the ratio in a histogram, split into bins of lookback time from when the galaxy is classified as a PSB.

Figure 4.10 shows how the SFR of PSB galaxies in their past compares to the SFR they would have on the main sequence in orange. Star-forming galaxies are also shown in blue, so that the typical spread of galaxies around the main sequence can be seen. The bins increase in lookback time from when they were identified as PSBs from the bottom to the top, going from a lookback time of 0.0 Gyr to 2.5 Gyr in bins of 0.5 Gyr. A value of $\log(\mathrm{SFR}/\mathrm{SFR}_{\mathrm{MS}}) = 0$ shows that the galaxy would be on the main sequence and is shown in each panel as a dashed vertical line. At a lookback time of about 2 Gyr, PSB galaxies appear to be on, or slightly above the main sequence, as they are slightly heightened compared to star-forming galaxies. The right hand tail shows galaxies with a ratio of up to $\log(\mathrm{SFR}/\mathrm{SFR}_{\mathrm{MS}}) \sim 0.6$, which would mean that galaxies had SFRs of almost 4 times that of galaxies on the main sequence. These could be galaxies that are undergoing a brief burst of star formation. However, it is not clear if all PSB galaxies go through a stage where their SFR is above that of the main sequence, as some galaxies at a lookback time of 2 Gyr are the same factor below the main sequence. At a lookback time of around 1 Gyr, the SFR of PSBs decreases and they move off the main sequence, showing that quenching is taking place. This means that the PCA method is effectively picking out galaxies that are quenched within the last Gyr. By a lookback time of 0.5 Gyr, nearly all of the PSBs are quenched and below the main sequence.

One thing that could affect the results from this plot is that if the timesteps between successive SFH steps are too large, starbursts may be smoothed over this time and therefore would not show up. We will investigate this further in Section 4.4.

4.3.4 Comparing star formation histories to the Principal Component Analysis classifications

In Section 4.2.4 we compared the UVJ and PCA classification methods for our mock. We can also compare the PCA classifications to how we would classify galaxies based on their SFH. The first step is to split galaxies based on their current sSFR, with passive and star-forming galaxies having sSFR below and above $\text{sSFR}(z) = 1/(3t_{\text{H}}(z))$ respectively, where $t_{\text{H}}(z)$ is the Hubble time at the redshift of the galaxy (Lang et al. 2014). This will separate out galaxies that are currently quenched from those with ongoing star formation. To separate passive galaxies from PSBs we use the SFHs. PSBs are defined to have had a large fraction of their stellar mass form within the last Gyr, so we sum up the percentage of stellar mass formed in the last Gyr and use this to classify PSBs. Any that have had over 10% of their stellar mass form within the last Gyr and are now quenched should show PSB signatures and be classified as PSBs with the PCA method.

Figure 4.11 shows galaxies on the supercolour diagram, coloured by the classification that they were given using their SFHs. Star-forming galaxies are blue, passive galaxies are red and PSBs are orange. 42% of the galaxies that are classified as PSBs based on their SFH are in the PSB region of the supercolour diagram. We also find galaxies in the passive region which have formed over 10% of their stellar mass and are now quenched, but are not picked up by the PCA method as being PSBs. However, we have used 10% as a cut, which is a low percentage of stellar mass to have formed within the last Gyr, so some galaxies which are actually passive rather than PSBs could meet this criteria. If we raise the percentage to 50% then 66% of galaxies that look like PSBs from their SFH are in the PSB region. However, when we do that, the contamination of passive and star-forming galaxies in the PSB region also rises from 68% to 98%, so virtually no PSBs are identified.

4.4 Resolution effects

One caveat that was mentioned in the previous section was the resolution of the SFH returned from LGALAXIES. The standard version returns the star formation in 20 bins over each galaxy's lifetime, which are finer for smaller lookback times. The process of deciding what bin widths to use and how many is explained further in Shamshiri et al. (2015). They looked at the differences in the magnitudes in each filter when using a SFH with 20 bins compared with using the full resolution SFH and found that using 20 bins was the right balance between maximising accuracy and minimising storage space required.

We can make the same checks with our catalogue, investigating the difference in the magnitudes in the filters used in the UDS. Furthermore, we can also compute

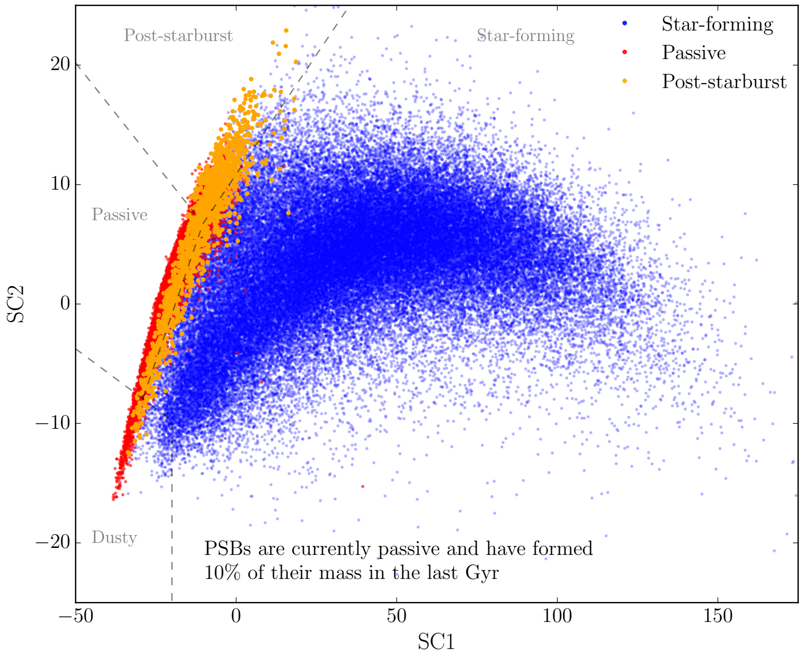

Figure 4.11. Test of the PCA method comparing to galaxy SFHs. Any galaxy with sSFR $< 1/3t_{\rm H}$ is classed as passive, whilst any galaxy with sSFR above this value is classed as star-forming. PSBs are galaxies that are classed as passive based on their sSFR, but have formed at least 10% of their stellar mass in the last Gyr. 42% of the PSBs classified using their SFH are in the correct region, but they also extend far into the passive region.

the changes in supercolours and see whether the classifications with the coarse SFH are robust. In order to perform this test, we ran LGALAXIES twice on a subset of the full simulation volume, once using 20 SFH bins and once using 300 SFH bins. For both, the PCA analysis was run on the output to calculate the supercolour values and classify each galaxy.

4.4.1 Differences in the star formation history

Figure 4.12 shows an example of the comparison between the fine and coarse SFH for the same galaxy. The coarse SFH with 20 bins is shown in blue and the fine SFH with 300 bins is shown in green. We can see how the coarse SFH follows the general shape of the finer SFH, but misses out some of the details. For example, at a lookback time of just under 1 Gyr, the galaxy seems to undergo a brief burst of star formation. However, as this is smoothed over a larger time for the coarse SFH it is missed. We want to investigate whether this smoothing means that we misidentify any PSBs as we miss these burst of star formation.

In Figure 4.10 we used the SFH of each galaxy and investigated whether it was above, on or below the main sequence for its stellar mass at that time. We noted that the coarse resolution of the SFH used could have an effect on our findings, as any starbursts could be smoothed out over a larger bin. We investigate this effect in Figure 4.13 by plotting the same histogram as in Figure 4.10, but for the two

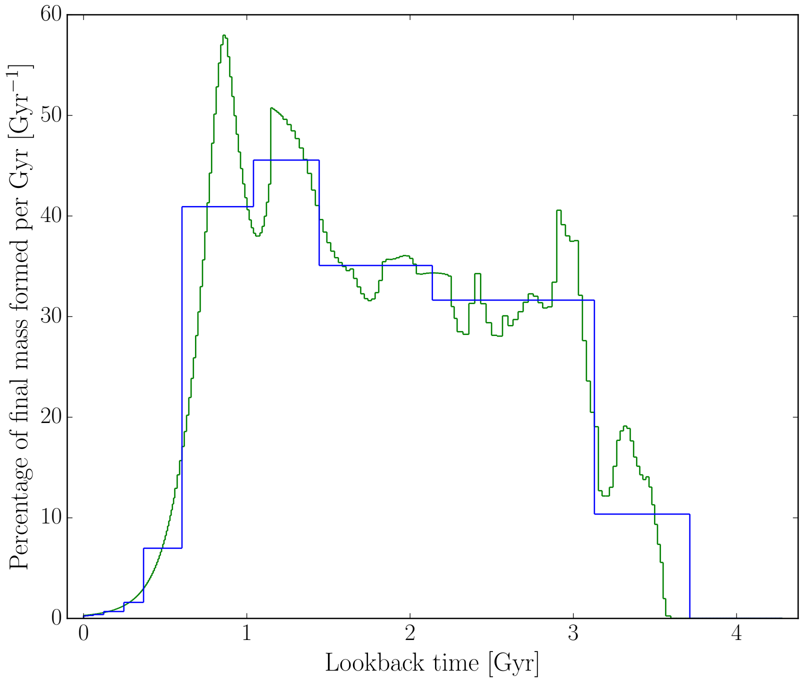

Figure 4.12. Comparison of the finely (green) and coarsely (blue) binned SFH for one example PSB at $z = 1.76$. The coarse SFH follows the general changes in the SFR of the galaxy, but cannot resolve some of the events that occur on a short timescale, e.g. a very rapid burst of star formation.

catalogues with different SFH resolution. Any differences between the two catalogues should just be down to resolution effects, as they include the same galaxies.

Figure 4.13 shows how the SFR of PSBs compares to the main sequence in bins of lookback time, for the coarse resolution SFH in blue and the fine resolution SFH in green. Both show the same general trends as in Figure 4.10, but there are some differences between the two figures which are likely due to the fact that a different sample of PSBs is used. There are also some differences between the result for the two SFH resolutions in Figure 4.13, especially at large lookback times. This is where we would expect more differences from the SFH resolution, as the bins get wider with increasing lookback time. For example, at a lookback time of 2 Gyr at $z = 1$, the width of the SFH bin is 840 Myr for the coarse SFH, but is 24 Myr for the fine SFH. Above 1.5 Gyr lookback time, when using the fine resolution SFH, the distribution of galaxy's SFR with respect to the main sequence is more spread out and appears to be more skewed to slightly above the main sequence. 13% of PSBs are more than 0.5 dex above the main sequence between $1.5 - 2.5$ Gyr lookback time when using the fine SFH, but this number is only 2% when using the coarse SFH. This suggests that when using the coarse SFH there may be bursts of star formation that we are missing. However, as these effects are only noticeable above a lookback time of 1.5 Gyr, it should not make too much difference to our classification of PSBs.

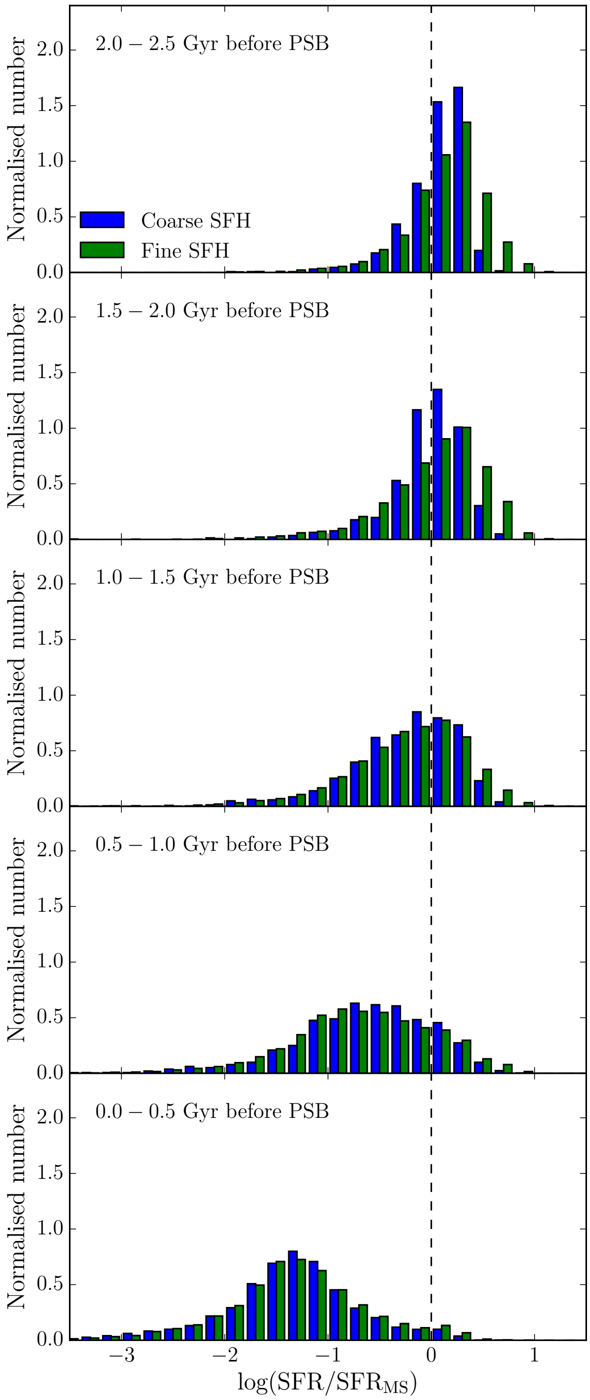

Figure 4.13. As for Figure 4.10, but for the coarse SFH and the fine SFH, shown in blue and green respectively. When using the fine SFH the results at small lookback times are very similar, but at higher values of lookback time there is more spread in the ratio of the galaxy's SFRs compared to the main sequence.

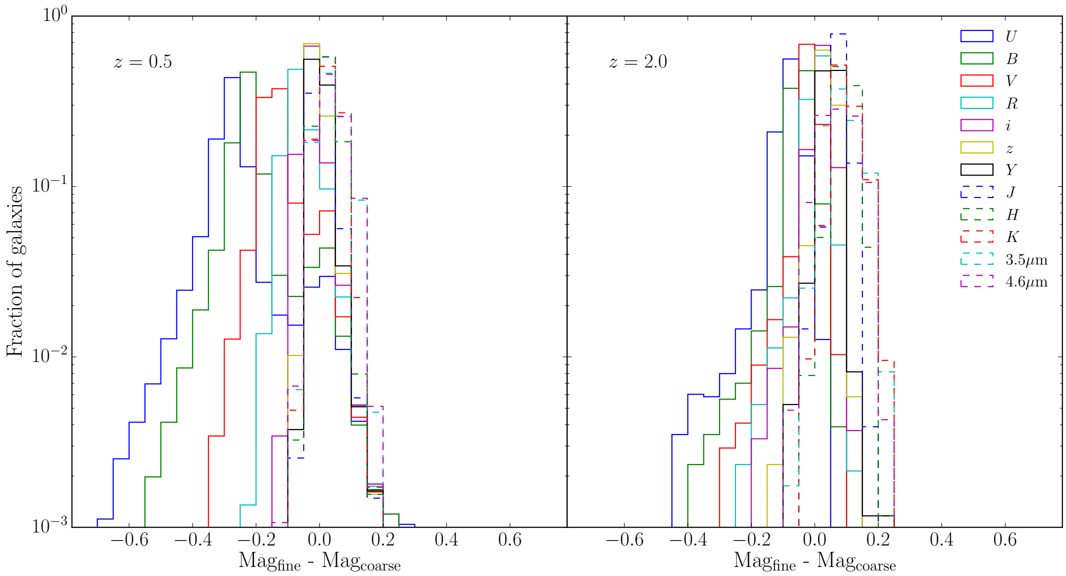

Figure 4.14. Difference in the apparent magnitude values in each band when using the fine and coarse SFHs. There is a larger difference for bands at the bluer end of the SEDs and at low redshift. Galaxies appear brighter when using the fine SFH.

4.4.2 Differences in the magnitudes

We also want to investigate how the magnitudes change when we use the fine SFH compared to the coarse SFH. Figure 4.14 shows a histogram of the difference between the apparent magnitudes for the two runs for each band. The left hand panel is at $z = 0.5$ and the right hand panel is at $z = 2.0$. We can see that the agreement between the two magnitude values is good, although for a minority of galaxies the differences are more than 0.5 mag. The agreement between magnitude values is actually slightly worse at low redshift compared to higher redshift. The reason for this is that the galaxies at $z = 2.0$ are on average younger than the galaxies at $z = 0.5$, so there is a smaller total lookback time to split into bins, resulting in smaller timesteps per bin.

The magnitude differences are noticeably higher in the bluer bands than the redder ones. This is because this part of the SED is dominated by young stellar populations, and a small change in formation time can change the flux in these bands significantly. The galaxies are also more likely to be brighter when the magnitudes are computed using the finer SFH than the coarse one. This difference is also due to young stars, where there are large changes in the luminosity when the formation time and metallicity changes.

When calculating the supercolours for each galaxy, we use dust attenuated magnitudes in order to try and mimic the effect of dust reddening. We also check the difference between the dust attenuated apparent magnitudes for the different SFH resolutions in Figure 4.15. The agreement between the magnitude values is worse than shown in Figure 4.14 and at $z = 2$ roughly 1% of the dust attenuated magni-

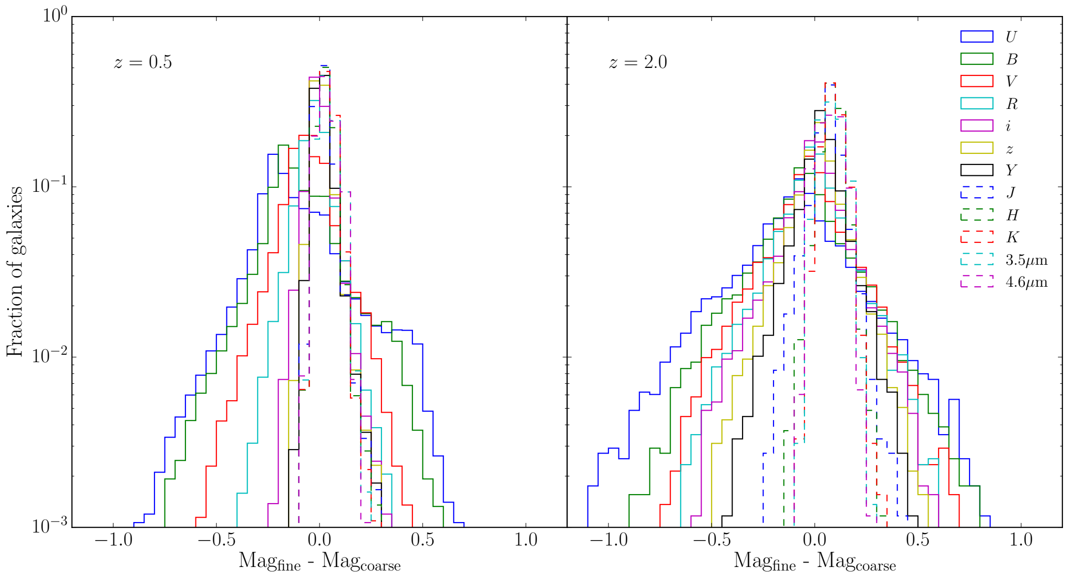

Figure 4.15. As for Figure 4.14, but for dust attenuated apparent magnitudes. The dust is added using a two component model, where the extinction from the diffuse interstellar medium and that from molecular clouds is applied separately. The component from molecular clouds includes a random Gaussian term which will differ every time the model is run. The differences here are larger due to the random nature of this dust term.

tudes change by more than 0.7 mag in the U band.

The reason that the agreement worsens in Figure 4.15 is due to the way that the dust attenuation is calculated for each galaxy. A two component dust model is used which applies extinction from the diffuse interstellar medium separately to that from molecular clouds. When calculating the component due to molecular clouds, a random Gaussian term is included. This means that for the same galaxy, even when using the same SFH resolution, the results will differ each time. Therefore, the differences in Figure 4.15 and 4.14 will be in part due to random scatter, which appears to be a larger effect than the SFH resolution, especially at high redshift. This indicates that the dust model used may actually affect our findings more than the SFH resolution.

4.4.3 Differences in the supercolour values

We have now seen the effect that the SFH resolution can have on the magnitude values of galaxies in each band. We now want to see how the corresponding supercolours change. Figure 4.16 shows a histogram of the change in each supercolour value, split into the three classes. The class of the galaxy is taken as the class it is given when classified using the fine resolution SFH, if the two are different. The left, middle and right panels show the changes in SC1, SC2 and SC3 respectively.

The three classes have different distributions, with more star-forming galaxies having a larger change in their supercolour values than either passive or PSBs. The

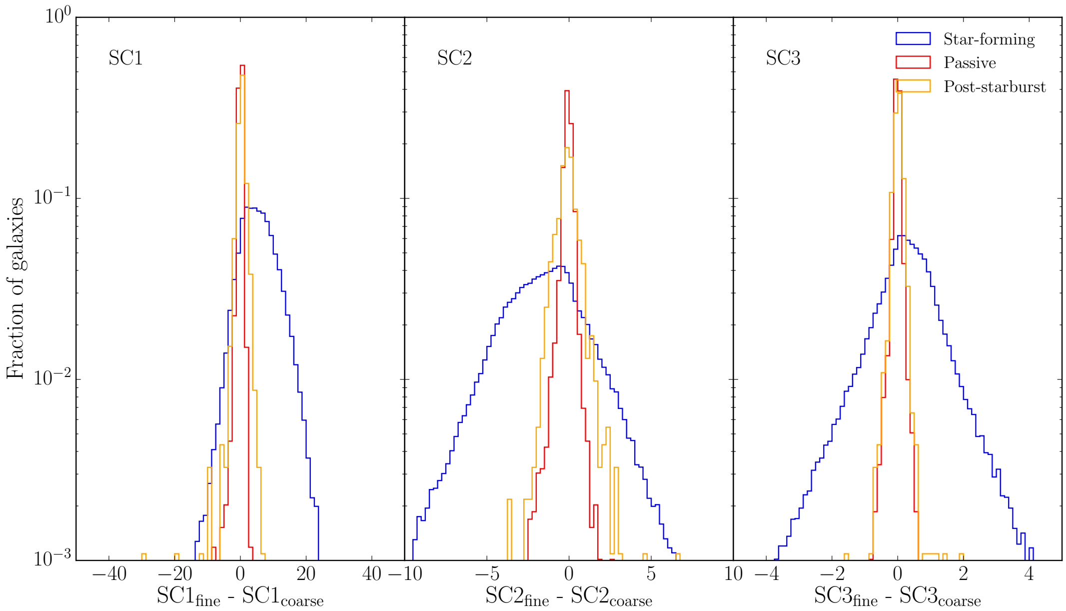

Figure 4.16. Difference in the three supercolour values for each population when using the fine and coarse SFHs. There is a larger difference for star-forming galaxies due to the blue end of the spectrum being more affected by changes in the SFH resolution. Passive and PSB galaxies change their supercolour values little.

reason for this is due to the differences in the bands we saw in Figures 4.14 and 4.15 - the bands at the bluer end of the SED are much more likely to be affected when the SFH resolution is changed. Star-forming galaxies are the bluest in colour of the three classes, so will naturally change their SED shapes, and therefore their supercolour values, much more than the other classes. As passive galaxies are typically red in colour and older, their magnitudes are less affected and therefore their supercolour values change very little.

PSB galaxies change their supercolour values slightly more than passive galaxies, as they are generally bluer. The supercolour with the largest change for PSBs compared to passive galaxies is SC2, which is interesting as this is the supercolour that correlates well with the percentage of the stellar mass formed in the last Gyr. There appears to be more spread in the values of SC2 change for PSBs than passive galaxies, which supports our idea from Section 4.4.1 that the bursts that are smoothed over in the coarse SFH will have a small effect on the magnitudes and SED.

These changes in the supercolour values should not lead to much change in the classification of these galaxies, even for star-forming galaxies. Star-forming cover the widest range in supercolour values, so galaxies can move around more on the diagram without changing class. In general, any galaxies that do end up changing class are likely to be those very near the border of another class. Galaxies on either side of these borders should have relatively similar properties so this should not significantly affect our findings.

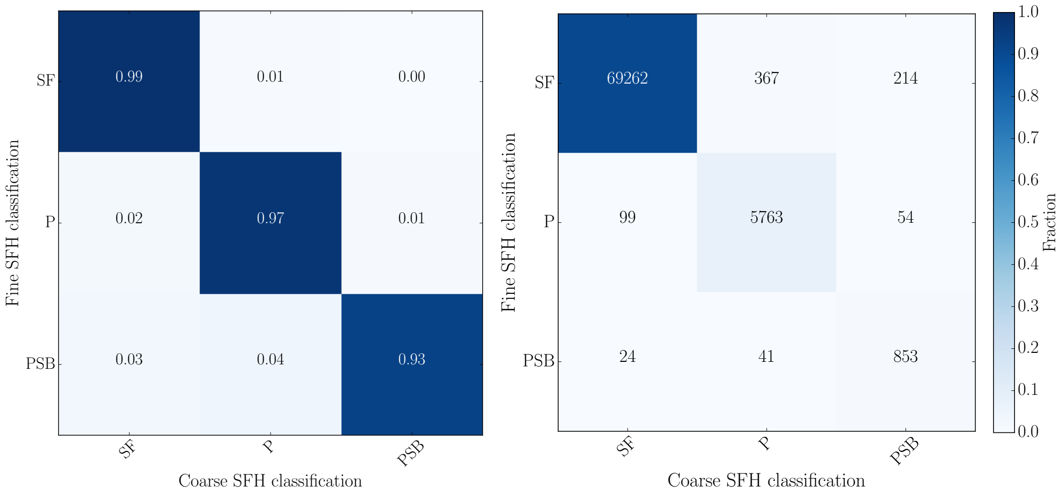

Figure 4.17. Confusion matrix to show how successful the classification is when using the coarse SFH compared to the fine SFH. The left hand panel shows and is coloured by the fraction of galaxies with a particular class from the fine SFH that are given each class when using the coarse SFH. The right hand panel shows the number of galaxies with each combination of classes. The colours of each box in this panel reflect the fraction of the total number of galaxies across all classes. Although the sample of PSBs is 93% complete when using the coarse SFH, there is contamination from the small percentage, but large number of star-forming and passive galaxies which are misclassified.

4.4.4 Differences in the Principal Component Analysis classification

Finally, we want to measure how many of the galaxies change their class when the resolution of the SFH changes. Here we take the classification made with PCA when using the fine and coarse resolution SFH as the 'actual' and 'predicted' classification of the galaxy respectively. The left hand panel of Figure 4.17 shows a confusion matrix to show how successful the classification is when using the coarse SFH compared to the fine SFH. The colour of each box reflects the fraction of galaxies of an actual class that were given each predicted class, shown by the colourbar on the far right of the plot. As an example, we can see that 97% of passive galaxies are identified correctly when the resolution of the SFH decreases, but 2% and 1% are misidentified as star-forming and PSB galaxies respectively.

The two classifications agree very well with each other, with 99% of star-forming, 97% of passive and 93% of PSB galaxies classified correctly when using the coarse SFH. As discussed in Section 4.4.3, even though the supercolour values for the star-forming population change by the most, they are still the most secure in their classification given their large range of supercolour values. Passive galaxies are the next most secure in their classification, due to their old stellar populations being less affected by the resolution of the SFH. PSB galaxies seem to be the class that changes classification the most. This is not surprising, as they are bluer than passive galaxies but occupy a small range of values on the supercolour diagram than star-forming galaxies. However, as we saw in Figure 4.16, the supercolour values of PSBs do not change by much when the resolution changes. We have checked, and of the PSBs that have changed class, 60 out of 65 lie very close to the border. The other 5 may be galaxies which changed their dust content more than average due to the randomness of the process.

This suggests that we do not need to be worried about the issue of resolution in our sample as a high fraction of galaxies of each class is given the correct classification when using the coarse SFHs. We also wanted to check the numbers of galaxies that are misidentified and have plotted this in the right hand panel of Figure 4.17. Instead of fractions, the number of galaxies with each classification combination is shown, and the colour corresponds to the fraction of the total number of galaxies (76,679). For example, there are 367 star-forming galaxies which misidentified as passive when using their class as predicted using the coarse SFH.

When not normalised by the number of galaxies with each actual classification, we can see that the resolution of the SFH may be an issue that we need to consider. Although fewer than 1% of star-forming galaxies are misidentified as PSBs, this still amounts to 214 galaxies. The total number of galaxies classified as PSBs with the coarse SFH is 1,121, so these misclassed star-forming galaxies would be accounting for 19% of our PSB sample. Therefore, although we have a high level of completeness in our sample when using the coarse SFH, we also have a relatively high contamination level due to the high numbers of galaxies in other classes scattering across. However, although we have a high level of contamination, only 6 of the 268 galaxies which are misidentified as PSBs are not near the border of the PSB region. Therefore, they should have properties similar enough to actual PSB galaxies that this issue should not affect our conclusions significantly. The contaminants also only account for 1/5 of our sample, so it should be dominated by galaxies we know actually are PSBs.

When doing this comparison, we are also including any differences due to the random dust term. However, we are only concerned about galaxies that change their intrinsic magnitudes due to the effect of the SFH resolution. One way that we could decouple these effects is to run the LGALAXIES model for once for the fine SFH and once for the coarse SFH, but ensure that we use the same random number seed for the dust term for each galaxy. This will mean that the change in the dusty magnitudes should be the same as the change in the non dust attenuated magnitudes. We would then be able to investigate how the PCA classes change only due to the SFH changing. We did not have time to perform this analysis for this thesis, but we note that the effect we find here should be an upper limit.

4.5 Conclusions

In this chapter we have shown how a PCA method has been used to classify galaxies in our mock survey from Chapter 3 into three classes of galaxies - star-forming, passive and PSB. We then compared our results with galaxies in the UDS, which have been classified using the same method. LGALAXIES does produce a population of PSBs, but their properties are different to what is observed in the UDS, where there are two main populations of PSBs - high-mass at high redshift and low-mass at low redshift. However, although the shape of the PSB SMF from the mock changes with time as in observations, there are too few PSBs at high redshift and a slight overproduction at low redshift.

When we compare the supercolour diagram for the mock survey and the UDS, we find fewer PSBs with high values of SC2 in the model. As SC2 correlates with fraction of stellar mass formed in the last Gyr, this could indicate that the PSBs in the mock do not have as large a burst of star formation as expected. To investigate this, we looked at the SFHs of PSBs in the mock and compared them to the passive and star-forming populations. In addition to checking that the mock is producing PSBs, this is a check of the PCA method, as we know if galaxies in the mock have been recently quenched from their SFHs. We find that PSBs have formed more of their stellar mass more recently than passive galaxies, are no longer forming stars and appear to have been quenched over a shorter time. We then compared the SFR of PSBs at each timestep in their evolution with the SFR they would have if they were on the main sequence, to see if there were any signs of starbursts in PSBs before they were quenched. On average, PSBs were on the main sequence or slightly above ~ 2 Gyr before being quenched.

However, our results could be affected by the resolution of the SFHs. The LGALAXIES model returns the SFH binned into 20 timesteps, which decrease in size as lookback time decreases. This can mean that any rapid bursts are smoothed over and aren't resolved in the SFH. As galaxy magnitudes are calculated in post-processing from these SFHs, we also wanted to investigate if any change in the SFH resolution results in changes to the galaxy classifications. To do this, we ran the LGALAXIES model twice for a subset of our simulation volume, once with a coarse SFH with 20 bins and once with a fine SFH with 300 bins. We found that the two SFHs agree well at small lookback times, but the coarse SFH smooths over features such as bursts at larger lookback times.

We then investigated how the apparent magnitudes, both without and with dust, change when using different resolution SFHs. For the magnitudes without dust, the agreement is worse for the bluer bands, with galaxies more likely to appear brighter when using the fine resolution SFH. We also find the agreement is worse at low redshift, where the differences can be more than 0.5 mag in the U and B bands. The agreement when using the dust attenuated magnitudes is worse, but seems to be dominated by changes in the random dust term rather than changes in the inherent magnitude value.

These changes in the magnitude values then propagate into changes in the supercolour values and classifications. The supercolour values change most for star-forming galaxies, due to their blue colours, and are more constant for passive and PSB galaxies. The galaxy classifications also agree well with each other, with 93% of PSBs classified using the fine SFHs also being classified as PSBs using the coarse SFHs. Due to the large number of star-forming galaxies compared to PSB galaxies, less than 1% of scatter from the star-forming population into the PSB population makes up 1/5 of the PSB sample. However, these star-forming galaxies were near the boundary between star-forming and PSB, so have similar properties to PSBs. This is also an upper limit on the effect, as these changes in classification are in part caused by changes in the random dust term.

Now that we have identified a population of PSBs in our mock survey, we can go on to investigate their evolution. Although the stellar mass and redshift distributions of our simulated PSBs are different to observations, it is still informative to investigate these rapidly quenched galaxies in the models. Doing so can tell us more about the mechanisms that may be quenching this rare class of galaxy, and help to inform observations about what quenching signatures to look for.

Chapter 5

The evolution of post-starburst galaxies in the mock UDS

In this chapter we investigate the evolution and quenching of post-starburst galaxies in our mock lightcone catalogue, building on the work of previous chapters. By tracking the properties of their progenitors and descendants, we can inform observations about which processes are acting to quench post-starburst galaxies. We firstly follow the specific star formation rate, hot and cold gas content, cooling rate and AGN accretion rate of the mock post-starbursts, and find that post-starbursts that fall into larger haloes appear to be quenched due to their environment. However, for post-starbursts that are centrals, the AGN may have quenched star formation by heating the gas, which prevents cooling and further star formation. In addition, by following the evolution of post-starbursts after they are quenched, we find that in some centrals the AGN feedback appears to reduce after a few Gyr, allowing the gas to cool and star formation to restart in the galaxy.

The work in this chapter, along with Chapters 3 and 4, will be presented in a forthcoming paper, currently in preparation.

5.1 Previous work on post-starburst galaxies

Locally, low-mass galaxies tend to be disky, blue and star-forming, whereas high-mass galaxies are more likely to be spheroidal, red and passive (e.g. Kennicutt 1998; Strateva et al. 2001; Kauffmann et al. 2003; Baldry et al. 2004). At high redshift ($z > 1$) we also observe this bimodality in the galaxy population (Kovač et al. 2014; Cirasuolo et al. 2007), but do not definitively know the mechanisms by which these galaxies evolve into the populations we observe locally. Various mechanisms have been suggested to move galaxies from the blue cloud to the red sequence and shut off their star formation in a process known as quenching. However, galaxies in the green valley are rare, so it is thought to be a quick transition, making this population difficult to study.

Quenching methods were investigated by Peng et al. (2010), who looked at the relationship between star formation rate (SFR), stellar mass and environment of galaxies in deep surveys out to $z \sim 1$. They found evidence of two separate quenching processes, 'mass quenching' and 'environmental quenching'. Independent of stellar mass, the fraction of passive galaxies correlated with the environment, and independent of environment, more massive galaxies were more likely to be quenched. Potential mechanisms to explain environmental quenching include ram pressure stripping of cold (Gunn & Gott 1972; Abadi, Moore & Bower 1999) and hot gas (McCarthy et al. 2008), tidal stripping (Merritt 1984; Mamon 1987), harassment (Gallagher & Ostriker 1972; Moore, Lake & Katz 1998) and mergers. The mechanisms thought to be responsible for mass quenching are feedback from active galactic nuclei (AGN) (Hopkins et al. 2005), shock heating from the hot halo (Dekel & Birnboim 2006) and outflows (Diamond-Stanic et al. 2012). However, these processes are still not fully understood. We also do not know whether the findings from Peng et al. (2010) hold at higher redshifts, where the red sequence is established.

Studies have also been done on transitional objects, such as post-starburst (PSB) galaxies, in an effort to understand quenching mechanisms. Also referred to as 'k + a' galaxies, PSBs have typically had a burst of star formation and then been rapidly quenched within the last Gyr. The shape of their spectral energy distributions (SEDs) is similar to passive galaxies, but they also have a component from A type stars that were born during the starburst phase (Dressler & Gunn 1983; Wild et al. 2009). As these stars and therefore the PSB signatures are short lived, these galaxies are rare and only account for up to 5% of the galaxy population at all redshifts (Wild et al. 2016).

Until recently, it was difficult to identify these galaxies at high redshift due to the need to have good quality spectra covering the 4000Å break region. However, PSBs can now be identified photometrically using a Principal Component Analysis (PCA) technique, as explained in Chapter 4. Using a sample of PSBs from the UKIDSS UDS survey, Wild et al. (2016) proposed different origins for PSBs depending on their redshift. At $z > 2$, PSBs most are massive galaxies which have formed their stellar mass over a short period before being quenched, whereas at $z < 1$ they are believed to be mostly the descendants of gas-rich star-forming galaxies which were rapidly quenched by environment or gas-rich mergers.

Almaini et al. (2017) looked at the structure of PSBs, finding that above $z = 1$, they are compact and centrally concentrated, with a Sérsic index distribution similar to passive galaxies. This suggests that any morphological changes in these galaxies precedes or takes place along with the quenching event. Further study by Maltby et al. (2018) supported this idea, suggesting that at $z > 1$ PSBs have been quenched by a disruptive event such as a merger or collapse that left behind a compact remnant. They also looked at PSBs at $z < 1$ and found although they are also compact, they have lower Sérsic indices, indicating that a less disruptive quenching mechanism is responsible.

PSBs in cluster environments were investigated by Socolovsky et al. (2018), who found an enhancement of low-mass PSBs in clusters compared to the field, along with a lack of star-forming galaxies. They suggest that young star-forming galaxies entering clusters are being rapidly quenched and becoming PSBs, with two quenching pathways acting on different timescales. Following this up in Socolovsky et al. (2019), they find that PSBs in clusters are compact, whereas star-forming galaxies in the cluster have on average larger effective radii than those in the field. They conclude that compact star-forming galaxies are being preferentially quenched in clusters via stellar feedback and stripping of the halo.

The properties of PSBs have also been investigated in simulations, which have the advantage of being able to examine the time evolution of individual galaxies. Davis et al. (2019) selected PSBs using their star formation histories (SFHs) from the hydrodynamical simulation EAGLE. Their criteria were that PSBs must initially be star-forming based on their specific star formation rate (sSFR $\geq 5 \times 10^{-11}\mathrm{yr}^{-1}$) and experience a drop in sSFR by at least a factor of 5 over 600 Myr. They find that the average PSB galaxy loses $\sim 90\%$ of its gas in ~ 600 Myr and that this is accompanied by a drop in the efficiency of star formation. Mergers and environmental effects are found to be primarily responsible for the gas loss in these galaxies, with feedback from AGN only being a secondary effect.

Pawlik et al. (2019) also investigated the evolution of PSBs in EAGLE. They identified PSBs at $z = 0.1$ using a spectroscopic PCA method and found that the number density was consistent with observational results. By investigating the change in colour, SFR and morphology and correlating this with the merger history of the galaxy, they found four distinct pathways that PSBs follow. Firstly, they found that some galaxies undergo a gas-rich major merger, which causes a starburst and then decline in SFR. Depending on the gas content, the galaxy then either evolved on one pathway back to the blue cloud or on another pathway to the red sequence. These mergers were also accompanied by the growth of the black hole, but they were not able to tell if this contributed to galaxy quenching. The third pathway occurred when galaxies were quenched due to environmental effects, whilst the fourth happened when a galaxy on the red sequence was rejuvenated by a merger with a gas-rich galaxy.

We build on this past work by investigating the evolution of PSBs using the mock lightcone survey that was described in Chapter 3, along with the classifications made in Chapter 4. Semi-analytic models are ideal for producing a mock catalogue for this purpose, as although the modelling of the gas is less in-depth than in a hydrodynamical simulation, they can produce catalogues over larger volumes, leading to higher numbers of galaxies. We can then also produce a lightcone catalogue, which better mimics the observations and can be put through the same pipeline to classify galaxies, as explained in Chapters 3 and 4.

5.2 Quenching processes

In order to investigate quenching processes, we can connect all of the galaxies in our lightcone survey with their main progenitors and descendants, allowing us to see how their properties change with time. All of the progenitors and descendants between $0.5 \leq z \leq 3.0$ have also been classified using a PCA method as explained in Chapter 4, so we are able to investigate how the classifications and supercolour values evolve. We can link these changes with changes in the properties of PSBs to try and disentangle the physical processes involved with quenching these galaxies.

5.2.1 Tracking galaxy properties

In Figure 4.3 we showed the stellar mass and redshift distribution of PSBs in the mock survey and in the UDS. It was clear from observations that there are two distinct populations of PSBs - low-mass PSBs at low redshift and high-mass PSBs at high redshift (Wild et al. 2016; Maltby et al. 2018). From previous observational work it seems that the low-mass PSBs may be being quenched through environmental processes whereas the high-mass PSBs may have undergone mergers (e.g. Wild et al. 2016; Maltby et al. 2016; Socolovsky et al. 2018; Almaini et al. 2017). As we can track the PSBs in the mock through time, we can investigate how they have evolved. For example, we can check whether PSBs are more likely to be in subhaloes, investigate their gas content through time, trace the accretion onto their central supermassive black holes, etc., in order to gain a deeper understanding of the processes that lead to PSBs in our mock catalogue.

Tracking galaxy type

We first investigate how the galaxy type of PSBs changes with time. In LGALAXIES a galaxy can be in one of three states - central, satellite or orphan. A central galaxy is in a halo that is not within the virial radius of another halo, so is not a subhalo. A satellite galaxy is within its own halo, but that halo is a subhalo of another halo. An orphan is a galaxy which is within a halo that is not its own because its own halo was stripped from it.

In Figure 5.1 we split the galaxies by type (at the time of being a PSB) into centrals (left panel), satellites (middle panel) and orphans (right panel). When they are classified as PSBs, 37% are centrals, 14% are satellites and 49% are orphans. We then plot the fraction of galaxies of each type with lookback time. Here the lookback time is relative to when the galaxy becomes a PSB, with positive lookback times

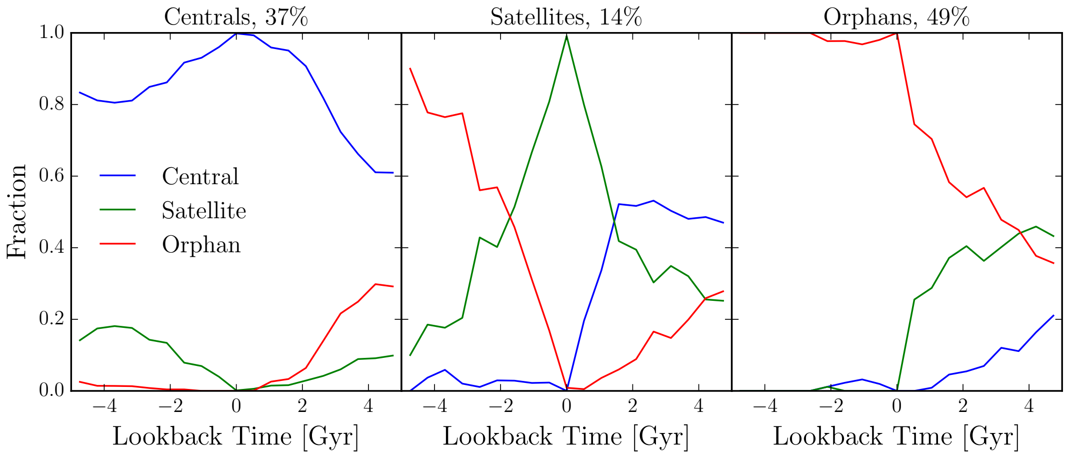

Figure 5.1. Galaxy type of PSBs as a function of lookback time, where 0 Gyr is where the galaxy is a PSB, positive values are the past and negative are the future. The galaxies are split based on their type when they are classified as a PSB into centrals (left panel, 37%), satellites (middle panel, 14%) and orphans (right panel, 49%). In each panel, the blue, green and red lines show the fraction of galaxies in that panel that are centrals, satellites and orphans at each time respectively. Galaxies tend to move from being centrals, to satellites, to orphans.

indicating the past and negative the future. The blue, green and red lines show the fraction of central, satellite and orphan galaxies respectively.

We start by looking at the left hand panel, which shows galaxies that are centrals when they are classified as PSBs. At every positive lookback time, over 60% of the galaxies which will become central PSBs are already centrals. They are therefore unlikely to have been quenched by their environment. As centrals typically have higher masses than satellites or orphans, it could be a feedback mechanism that is stopping the star formation in these galaxies. After they have been classified as PSBs the proportion of centrals decreases, when these objects fall into groups or clusters and become satellites or orphans. 5 Gyr after being PSBs, about 20% of these galaxies will no longer be centrals.

The middle panel shows galaxies that are satellites when they are classified as PSBs. At a lookback time of 5 Gyr, roughly 50% of these galaxies are centrals. This percentage stays approximately constant until about 2 Gyr before they become PSBs, where the percentage of galaxies that are satellites increases rapidly from 40% to 100% when they are classified as PSBs. These are galaxies that are falling into the halo of a larger object, such as a group or cluster. This increase in percentage suggests that these galaxies may have been quenched by environmental effects such as ram pressure stripping or tidal stripping. After these galaxies have been classified as PSBs, 90% of them will go on to become orphans.

We then look at orphans in the right hand panel of Figure 5.1. Around 35% of these galaxies have been orphans since a lookback time of 5 Gyr, with 45% and 20% classed as satellites and centrals respectively. As with the satellites, the percentage of orphans increases rapidly around 2 Gyr before these galaxies become PSBs, indicating that it would be the process which is removing the hot gas halo and turning these galaxies into orphans which quenches them. After they are PSBs, nearly all of these galaxies stay as orphans for at least 5 Gyr.

Tracking the hot and cold gas content

We now have some ideas about the quenching processes that could be affecting each type of PSB. We can investigate these further by looking at how the hot and cold gas content of these three different types of PSBs changes with lookback time. This should tell us more about the quenching method in each galaxy. For example, tidal stripping can remove the cold gas from a galaxy, so if this is occurring we should see a reduction in the amount of cold gas. Similarly, if ram pressure stripping is removing the hot gas then there should be a decrease in the hot gas content.

Figure 5.2 shows how the cold gas mass (top panels), hot gas mass (middle panels) and hot to cold gas ratio (bottom panels) changes with lookback time. In the top two rows, the cold gas mass and the hot gas mass are normalised by the stellar mass at the time. The black line shows the median value and the grey shaded region shows the 1σ scatter in each lookback time bin. Where there is no line, there is fewer than 10 galaxies with a non-zero value from which to take the median.

Starting with centrals, we can see that there is a rise in the cold gas content of roughly 1 dex about 3 Gyr before the galaxy becomes a PSB. By the time the galaxy is classified as a PSB, the cold gas content has decreased to its previous level. This increase in cold gas could be caused by several things. It could be due to a gas-rich merger taking place, where a galaxy merging onto the central brings a new supply of cold gas. An alternative is that the rate at which hot gas cools increases, although this is unlikely to be the sole reason due to the magnitude of the increase in a relatively short time. Looking at the hot gas content, there appears to be little change with time, as the amount of hot gas stays constant at roughly 30 times the stellar mass of the galaxy. The ratio of hot to cold gas decreases at the same time as the rise in cold gas content.

In the middle column of Figure 5.2 we can see how the gas content of satellite PSB galaxies changes with time. There is a similar trend with the cold gas content as with centrals, but the magnitude of the increase is smaller for satellites. However, the amount of hot gas does change in the satellites, as it starts to decrease about 1 Gyr before the galaxies are classified as PSBs. This is due to the fact that in the models, the hot gas begins to be stripped away through tidal and ram pressure stripping as soon as a galaxy becomes a subhalo. 3 Gyr after the galaxies are PSBs, virtually none of them have any hot gas left. This time corresponds to when 80% of the galaxies are now orphans, as by the time a galaxy is an orphan all of the hot gas

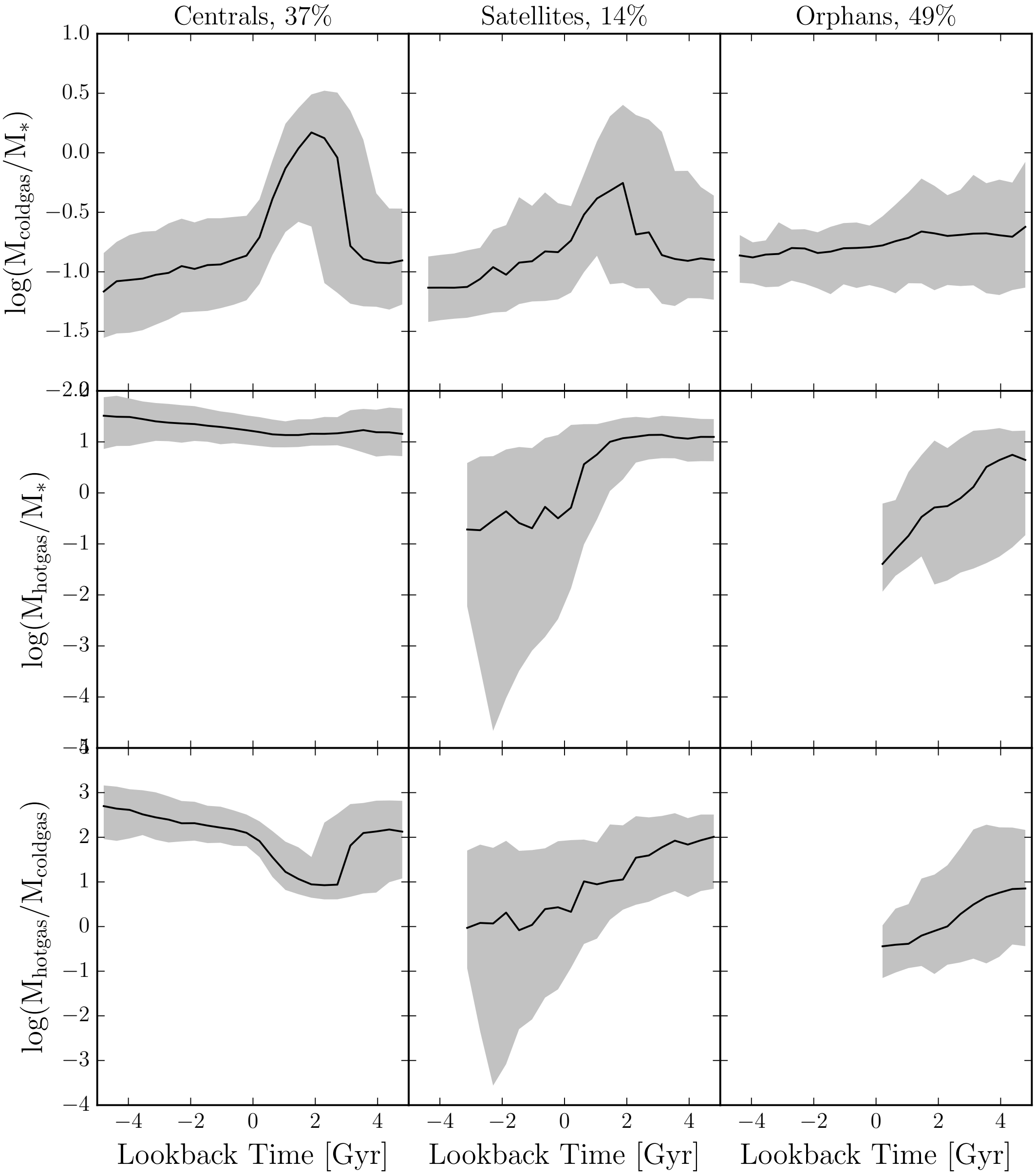

Figure 5.2. Gas content of PSBs as a function of lookback time, where 0 Gyr is where the galaxy is a PSB, positive values are the past and negative are the future. The galaxies are split based on their type when they are classified as a PSB into centrals (left panels), satellites (middle panels) and orphans (right panels). The top and middle rows show the cold and hot gas mass (normalised by the stellar mass at the time) and the bottom row shows the ratio of hot to cold gas. In each panel, the black solid line shows the median value for all galaxies of that type and the grey region shows the 1σ scatter. Where there is fewer than 10 galaxies with a non-zero value, no line or grey region is shown. The cold gas content of centrals and satellites increases about 3 Gyr before becoming PSBs, whilst the hot gas content reduces in satellites and orphans afterwards.

will be lost. The hot to cold gas ratio decreases steadily in this galaxy over time as the hot gas is stripped away.

For orphans in the right hand panels the cold gas content stays constant over the 10 Gyr shown. After the galaxies become orphans and all of their dark matter and hot gas has been stripped, tidal stripping will start to affect the cold gas in the galaxy disk and the stellar material. These will both be stripped from the galaxy, so although the normalised amount of cold gas remains constant, both the cold gas mass and the stellar mass of the galaxy actually decrease over time. As with the satellites, there is a decrease in the hot gas content until all of the galaxies are orphans at a lookback time of 0 Gyr, where they will have all lost their hot gas.

Tracking galaxy specific star formation rate

We can also track the sSFR of the galaxies with time, as there may be differences in the time when the galaxies of each type are quenched. Figure 5.3 shows how the sSFR of the galaxies of each type changes with time. The top row shows the fraction of galaxies with zero sSFR in each lookback time bin as a red line and the non-zero fraction as a blue line. The bottom row shows the median sSFR and 1σ scatter for all the galaxies with non-zero sSFR. As before, the left panels are for centrals, the middle panels for satellites and the right panels for orphans.

For the centrals in the left panels, the percentage of galaxies with non-zero sSFR 5 Gyr before they become PSBs is high, at $\sim 80\%$. From 3 to 1 Gyr before being PSBs, this percentage rises to over 95%. At the same time, the median sSFR of the galaxies with non-zero sSFR goes up by over 2 dex. This shows that nearly all of the central galaxies have some enhancement in their star formation prior to becoming PSBs. This fits with what we saw in Figure 5.2, as the increase in cold gas will fuel this star formation. After becoming PSBs, the percentage of galaxies with zero sSFR increases to around 60% and the median sSFR also decreases, showing these galaxies being quenched. However, the range covered by the 1σ scatter is wide after the PSB phase, so some galaxies might not reduce in star formation by such a large factor.

For satellite galaxies in the middle column, at all lookback times, fewer than 20% of the galaxies have zero sSFR and this percentage actually decreases with time. This could indicate that although these galaxies are being quenched, there is a very low level of residual star formation ongoing. As with the centrals, the median sSFR rises from a lookback time of 5 Gyr to 0 Gyr, showing an enhancement in star formation. From 1 Gyr before to 5 Gyr after being PSBs, the median sSFR declines over 6 dex, as the satellites are quenched. For orphan galaxies in the right panels, the sSFR reduces monotonically by ~ 4 dex in sSFR, without any enhancement at any lookback time. This means that galaxies that become PSBs when they are orphans

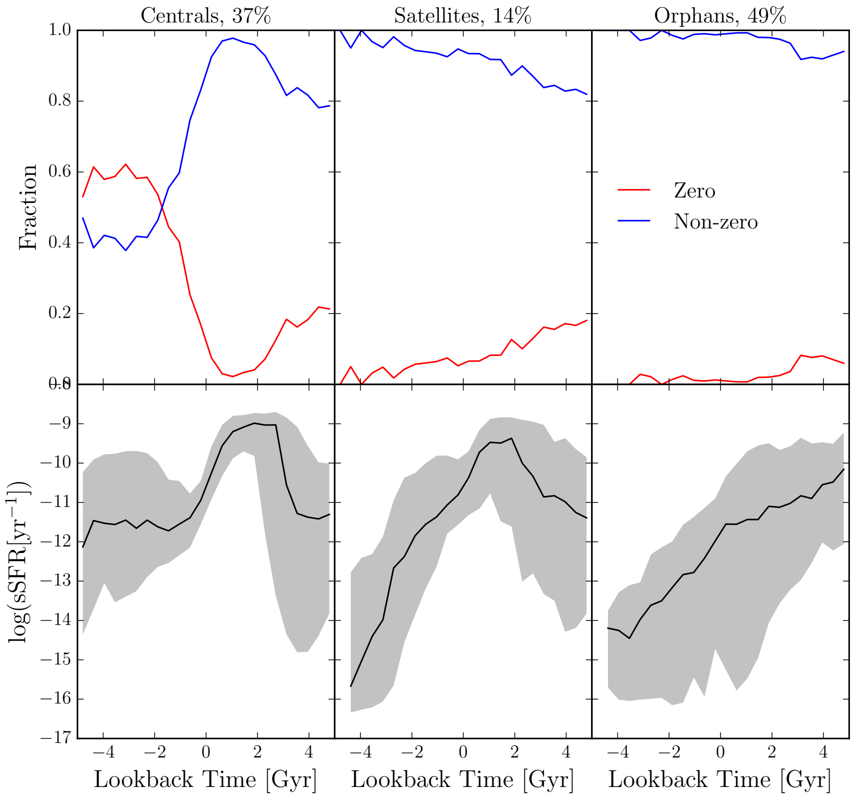

Figure 5.3. sSFR of PSBs as a function of lookback time, where 0 Gyr is where the galaxy is a PSB, positive values are the past and negative are the future. The galaxies are split based on their type when they are classified as a PSB into centrals (left panels), satellites (middle panels) and orphans (right panels). The top row shows the fraction of galaxies with zero (red line) and non-zero (blue line) sSFR, whilst the bottom row shows the median and 1σ scatter for the galaxies with non-zero sSFR. Centrals (and satellites to a lesser degree) experience an increase in star formation from about 3 Gyr before becoming PSBs that lines up with the increase in cold gas.

do not seem to have the same burst in star formation as PSBs that are centrals, which could indicate a different evolutionary pathway to become a PSB.

Tracking galaxy cooling rate

Figure 5.4 shows the same as Figure 5.3, but for the cooling rate rather than the sSFR. This is the rate that gas from the hot reservoir cools onto the cold gas disk of the galaxy. Again, the top row shows the fraction of galaxies with zero and non-zero cooling rate, whilst the bottom row shows the median for the galaxies with non-zero cooling rate.

For centrals, the median cooling rate stays constant over the entire lookback time range. However, there is a large change in the fraction of galaxies with no cooling. Initially over 80% of the galaxies have zero cooling rate, but by a lookback time of ~ 2 Gyr, this has decreased to about 25%. This increase in galaxies that are cooling coincides well with the increase in cold gas and sSFR seen in Figures 5.2 and 5.3

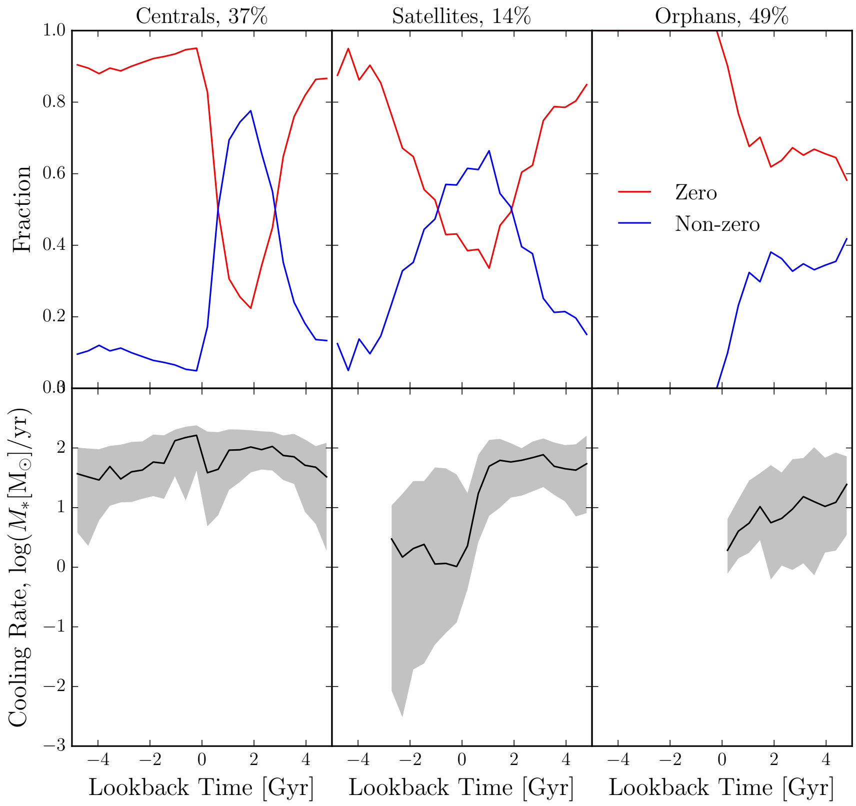

Figure 5.4. As for Figure 5.3, but for the cooling rate. Centrals experience a spike in cooling rate about 2 Gyr before becoming PSBs which coincides with the increase in cold gas.

respectively. However, if this increase in star formation was solely due to gas cooling then we would also expect the hot gas content to drop as it was turned into cold gas. One possible solution is that the galaxy undergoes a merger, which would bring a supply of both cold and hot gas. The increased amount of hot gas in the halo would mean that the cooling rate would go up, which would lead to an even larger increase in the cold gas content. This could then explain how the cold gas content of the galaxy increases by a factor of 10 whilst the hot gas content stays roughly constant. By the time that the galaxy is a PSB, the percentage of galaxies with zero cooling rate has increased back to around 90%. Some process must be reducing the amount of cooling in these galaxies, or else there would be runaway cooling within the galaxy in the form of a cooling flow. One way that a reduction in cooling rate could occur would be due to AGN feedback.

The middle column shows the cooling rates for satellite galaxies. There is a similar trend with more galaxies cooling up to 1 Gyr before they are classified as PSBs. As with the centrals, this correlates with the increase in cold gas and sSFR in these galaxies. For the centrals the fraction of galaxies being cooled decreases sharply just as they become PSBs. However, for the satellites, the fraction decreases slowly over around 6 Gyr. This could be due to the fact that as satellites, these galaxies will be having their hot gas stripped from their haloes via tidal and ram pressure stripping. When the hot gas is removed, the cooling rate of these galaxies will be zero, as there is no hot gas left in the galaxy to cool.

For the orphans, the fraction of galaxies with zero cooling rate increases over time, from 60% at a lookback time of 5 Gyr to 100% just as the galaxies are classified as PSBs. This is due to the fact that an increasing fraction of these galaxies become orphans with time, so have no hot gas left to cool. This is also why the sSFR of these galaxies only decreases with time, as the galaxy continues to form stars very slowly with the cold gas it already has, but is unable to accrete any more hot gas and has no hot gas that can cool.

Tracking radio accretion rate

Finally, we look at the radio accretion rate of the central black hole in Figure 5.5. This is the amount of hot gas that is being accreted onto the black hole per year. The top and bottom panels show the same as in Figures 5.3 and 5.4, but for the radio accretion rate instead.

The median radio accretion rate for centrals is nearly constant for all lookback times, but the fraction of galaxies with non-zero radio accretion rate changes. At a lookback time of ~ 2 Gyr, the percentage of galaxies with non-zero radio accretion rate increases from 60% to nearly 100% at the time they become PSBs. This increase in percentage lines up with the time when the fraction of galaxies with non-zero cooling rates is the highest. This suggests that these galaxies may be being affected by radio mode AGN feedback, which is built into LGalaxies to heat up the cold gas in the galaxy disk and reduce the cooling rate in order to counteract the cooling flow in a galaxy. The fraction of centrals with radio mode feedback active stays above 90% for at least 5 Gyr afterwards. This could be the process that is keeping these galaxies quenched, as they still have both hot and cold gas so otherwise should be able to cool and form stars. This would also help to explain why the hot gas content of the galaxy does not increase if there is a gas-rich merger, as the hot gas is being funnelled into the central black hole.

For both satellites and orphans, the fraction of galaxies with zero radio accretion rate increases with time. This is due to the fact that the hot gas in these galaxies is stripped, so there is nothing to accrete onto the central black hole. AGN feedback is not needed in these galaxies to keep them quenched as they have no gas to cool onto their disks, and in the case of orphans, no way to accrete any more.

Quenching methods for each galaxy type

From Figure 5.1 to 5.5, we were able to track the properties of each type of galaxy with time to try and investigate how each type of galaxy was quenched. For PSBs

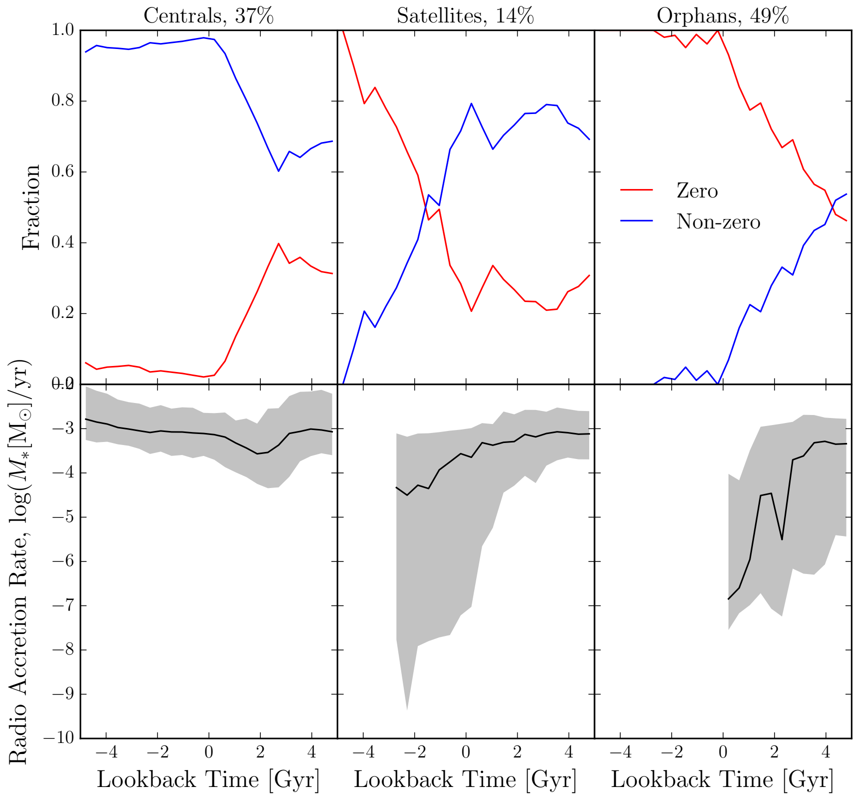

Figure 5.5. As for Figures 5.3 and 5.4, but for the radio accretion rate. Radio mode feedback seems to switch on for 40% of centrals before they become PSBs.

that are centrals, it appears that most of the them undergo a wet merger, which brings a new supply of cold and hot gas to the galaxy, some of which then also cools. This increased amount of cold gas leads to a burst of star formation. However, during the merger some of the hot gas accretes onto the central black hole, which leads to radio mode feedback heating up the cold gas in the galaxy. This effect is then stopping the galaxy from forming any more stars, effectively quenching it.

Some of the PSBs that are satellites appear to have a small burst of star formation like the centrals, perhaps due to a minor merger. However, this does not seem to trigger the AGN feedback as it does for centrals. Tidal and ram pressure stripping removes the hot gas from satellite galaxies as they fall into the haloes of other objects. As they no longer have any hot gas, once the current supply of cold gas is depleted there is no hot gas that can cool onto the disk. They also cannot accrete any more hot gas into their haloes from their surroundings. This means that these galaxies will be quenched and have no way to form any more stars.

PSBs that are orphans do not appear to have a burst of star formation prior to being quenched, unlike the centrals and satellites. As with satellites, orphans have their hot gas stripped, but they can also have some of their cold gas and stellar material removed due to tidal forces. The quenching process for these galaxies may then be even quicker than for satellites or centrals, as the cold gas that is currently

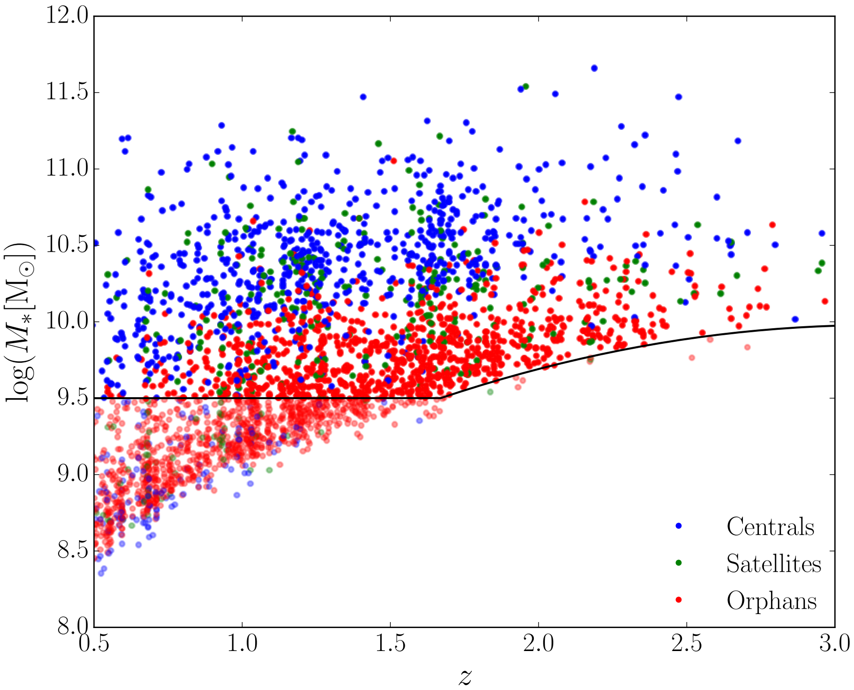

Figure 5.6. Stellar mass and redshift distribution of PSBs in the mock, coloured by their type. PSBs that are centrals, satellites and orphans are blue, green and red respectively. The black line shows the stellar mass completeness limit we use, and any points below this are faded to show they are not included in our analysis.

fuelling star formation is removed and the galaxy has no way to accrete any more hot gas to cool.

Relating our findings back to post-starburst galaxies in observations

In order to link these findings back to observations, we need to know what the properties of PSBs with the three galaxy types are. In Figure 5.6, we plot the stellar mass of all the PSBs against their redshift, coloured by galaxy type. Generally, at each redshift the high-mass PSBs are centrals and the low-mass PSBs are orphans, with satellites covering a wider range in stellar mass. Most of the high-mass PSBs in the mock at high redshift are centrals. Taking all PSBs with a stellar mass above $M_* = 10^{10.5}\mathrm{M}_\odot$ and at redshifts above $z = 1$, we find that 81% are centrals, 15% are satellites and 4% are orphans. Similarly, we can also look at the types of low-mass PSBs at low redshift in the mock. For PSBs below $M_* = 10^{10.5}\mathrm{M}_\odot$ and $z = 1$, but above our stellar mass limit, we find that 55% are centrals, 13% are satellites and 32% are orphans.

It is difficult to directly compare the findings from the models to observations due to the difference in the properties of PSBs in the mock and the UDS, as explored in Chapter 4. There are fewer high-mass PSBs at high redshift in the mock than the UDS, which may indicate that there is physics missing in the models. Additionally, although the stellar mass function of PSBs in the mock approximately matches the

UDS at low redshift, the stellar mass limit of $\log(M_*/\mathrm{M}_\odot) = 9.5$ in LGALAXIES means that we miss most of the low-mass, low redshift population in our mock. Taking PSBs with $M_* < 10^{10.5}\mathrm{M}_\odot$ and $z < 1$, above our stellar mass completeness limit shown in Figure 5.6, we have a sample of 284 PSBs. However, if we ignore the LGALAXIES limit and use just the completeness curve from the UDS, our sample increases to 995 PSBs. The majority of the galaxies that we miss are orphans, which is why the percentage of orphans at low redshift with low masses is only 32%. However, despite the differences between the mock and the UDS, it is still interesting to examine the quenching mechanisms for each of these two populations in the mock.

High-mass PSBs at high redshift in the model are most likely to be centrals. From the results discussed above, this would suggest that most of them are quenched due to radio mode AGN feedback following a merger induced starburst. This would make sense from what we know of the models, as AGN feedback is built in to stop runaway cooling in massive galaxies. However, it is still interesting to find that this is the dominant mechanism causing the rapid quenching seen in PSBs, and that it seems to occur following a merger. So far there hasn't been any evidence of AGN activity in the spectra of PSBs at high redshift (e.g. Maltby et al. submitted), but few PSBs at high redshift have been spectroscopically confirmed.

About a third of low-mass PSBs at low redshift in the models are orphans, which are likely to have been quenched due to environmental effects such as tidal and ram pressure stripping. These processes remove the hot gas from the galaxy, causing a strangulation effect, as when the cold gas is used up in star formation there is no gas left. In observations, studies have found an excess of low-mass PSBs in clusters compared to the field and suggest that this could be due to star-forming galaxies being quenched in clusters by stellar feedback and stripping of the halo (Socolovsky et al. 2018, 2019). The findings from our mock support the idea that these galaxies could be quenched due to environmental effects.

The quenching processes for low-mass centrals at low redshift are less clear. Although it is still possible that some of these galaxies were quenched by AGN feedback, this is more common in high-mass galaxies. An alternative idea is that these galaxies could have been quenched by stellar feedback. Heating and the removal of gas from the galaxy by supernovae and stellar winds could lead to similar signatures as AGN feedback. However, a more detailed follow up of these two populations in the mock will be required in order to conclusively decide what quenched them.

5.2.2 Individual galaxy tracks on the supercolour diagram

In addition to tracking the properties of the population of PSBs, we can also look at the evolution of individual galaxies. Figure 5.7 shows the evolution of one example PSB galaxy on a plot of sSFR vs stellar mass (top panel) and on the supercolour

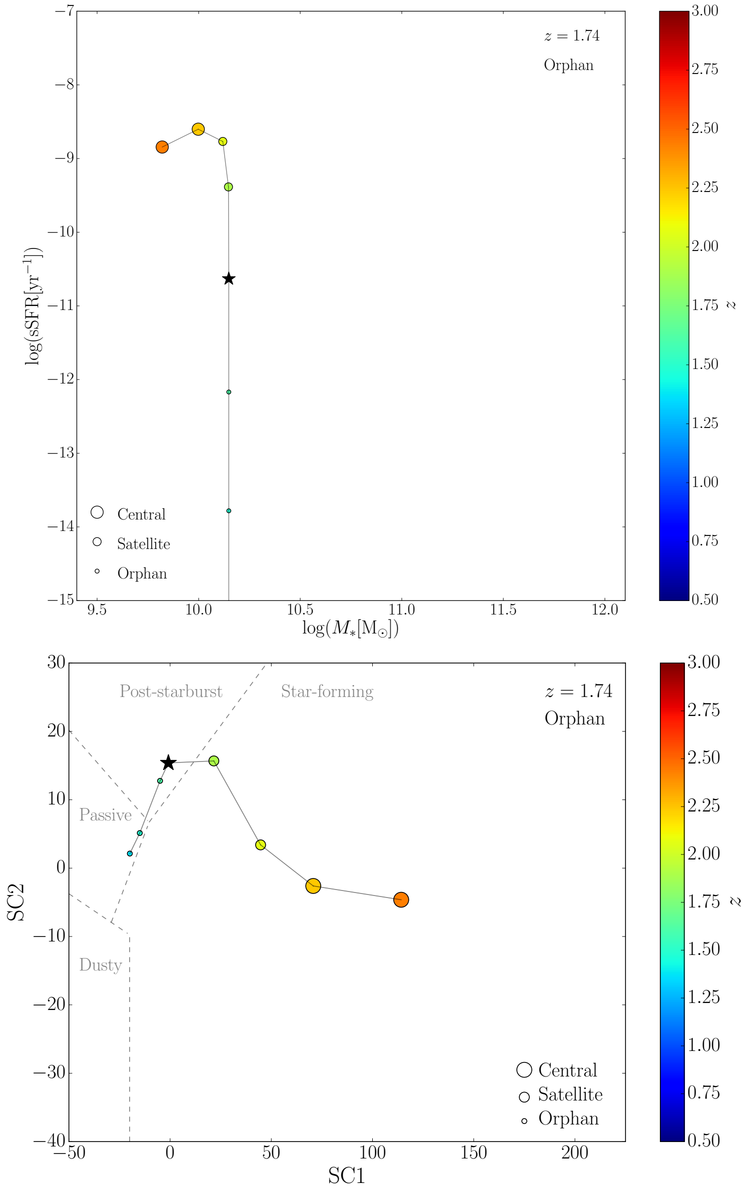

Figure 5.7. Track of a possibly environmentally quenched galaxy on a plot of sSFR against stellar mass (top panel) and on the supercolour diagram (bottom panel). The colour of the symbol is the redshift of the galaxy at that point in time, according to the colourbar on the right. The size of the symbol shows the type at that time, where the largest symbol shows it is a central, the middle symbol a satellite and the smallest symbol an orphan. The point where the galaxy is a PSB is marked by the large black star symbol and its redshift and type at this point are displayed in the top right. The sSFR of this galaxy begins to decrease rapidly when it falls into a larger halo and becomes a satellite. Its sSFR and SC1 value then decrease, when it turns into an orphan and is fully quenched.

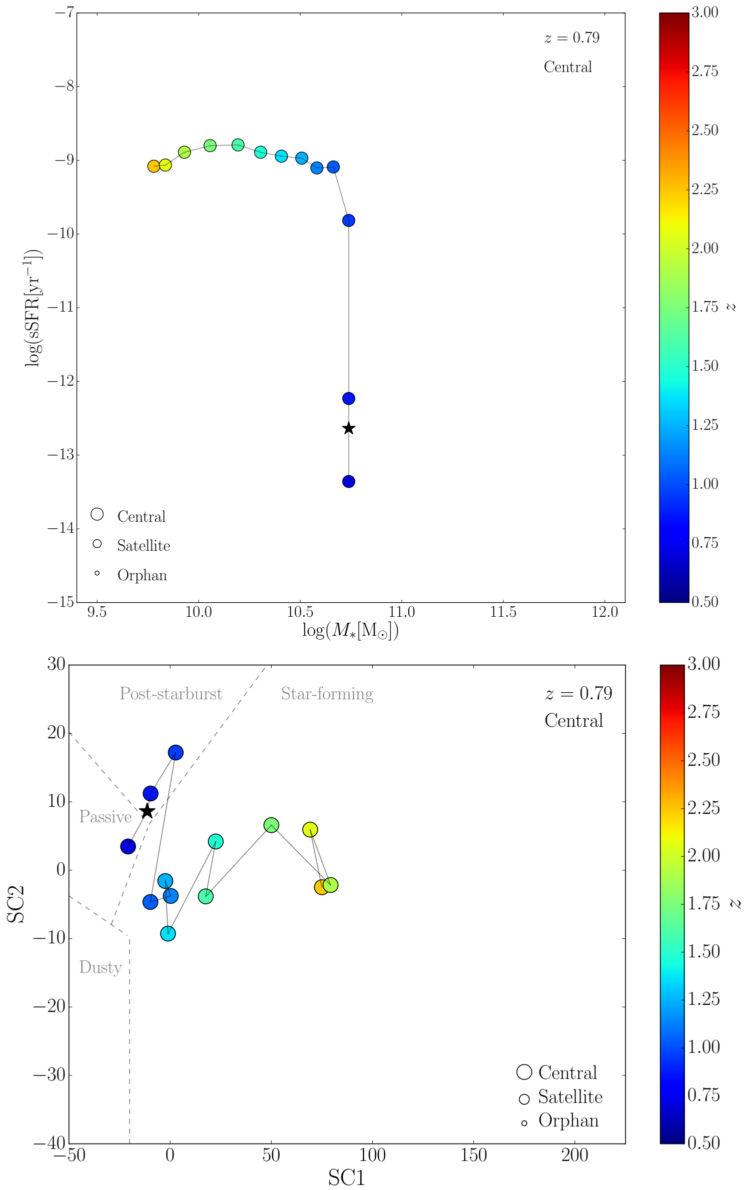

Figure 5.8. As for Figure 5.7, but for a central galaxy that may have been mass quenched. Here the galaxy is a central the entire time before it becomes a PSB, so is unlikely to have been quenched by environmental effects. This galaxy has a high SC2 value when it is first classified as a PSB, which may indicate a burst of star formation prior to quenching.

diagram (bottom panel). The black star on each diagram indicates where the galaxy in the lightcone is classified as a PSB and the other points are coloured by the redshift of the galaxy at each time, given by the colourbar on the right. The size of each symbol indicates the galaxy type at each time, as shown by the key in the bottom of each panel. The redshift and type of the galaxy when it is classified as a PSB is in the top right of each panel.

This is an example of a galaxy that may have been environmentally quenched. The sSFR of the galaxy decreases rapidly at $z \sim 2$ when the galaxy becomes a satellite. The sSFR continues to decrease and the galaxy becomes an orphan just as it is classified as a PSB. On the supercolour diagram this galaxy moves to lower values of SC1 as the sSFR of the galaxy decreases and it becomes a satellite and then an orphan. It crosses over the boundary from the star-forming to the passive region with an SC2 value of about 15, indicating that there has been some recent star formation in this galaxy. The sSFR in this galaxy decreases by ~ 1.5 dex from $z \sim 2$ to $z = 1.74$, which corresponds to around 0.6 Gyr. This recent and rapid decrease in sSFR causes the PSB signatures which will have been picked up by the PCA.

Figure 5.8 shows the same plot as Figure 5.7, but for another PSB galaxy. This example galaxy is a central, and has been since at least $z \sim 2.2$. This means that it is unlikely to have been quenched via environmental processes, as it is not within the virial radius of another halo. Instead, this galaxy has likely been mass quenched via a process such as AGN feedback. We can see that this galaxy begins by moving to lower SC1 values as it ages, as with the environmental example. However, around $z \sim 1$ the SC2 value of this galaxy increases by around 20 to SC2 ~ 18, when it is first classified as a PSB. This indicates that the galaxy has had a period of heightened star formation. Although it does not look as though it has had a very recent burst of star formation when looking at how the sSFR evolves, the level that the galaxy begins at may have been high for its stellar mass. The galaxy then continues to rapidly decrease in sSFR until it is fully quenched and is classified as passive.

5.2.3 Tracks of the population on the supercolour diagram

Although it is informative to look at the tracks of individual galaxies, it is not practical to examine each PSB individually. Therefore, we require a way to look at the average track that a PSB galaxy follows on the supercolour diagram, as this can tell us more about the quenching routes these galaxies may have followed. Galaxies are expected to take different tracks depending on when and how fast they were quenched (Wild et al. 2016), so quantifying this for our sample should provide insight into the different quenching pathways.

The top left panel of Figure 5.9 shows the combined tracks of all PSBs in the

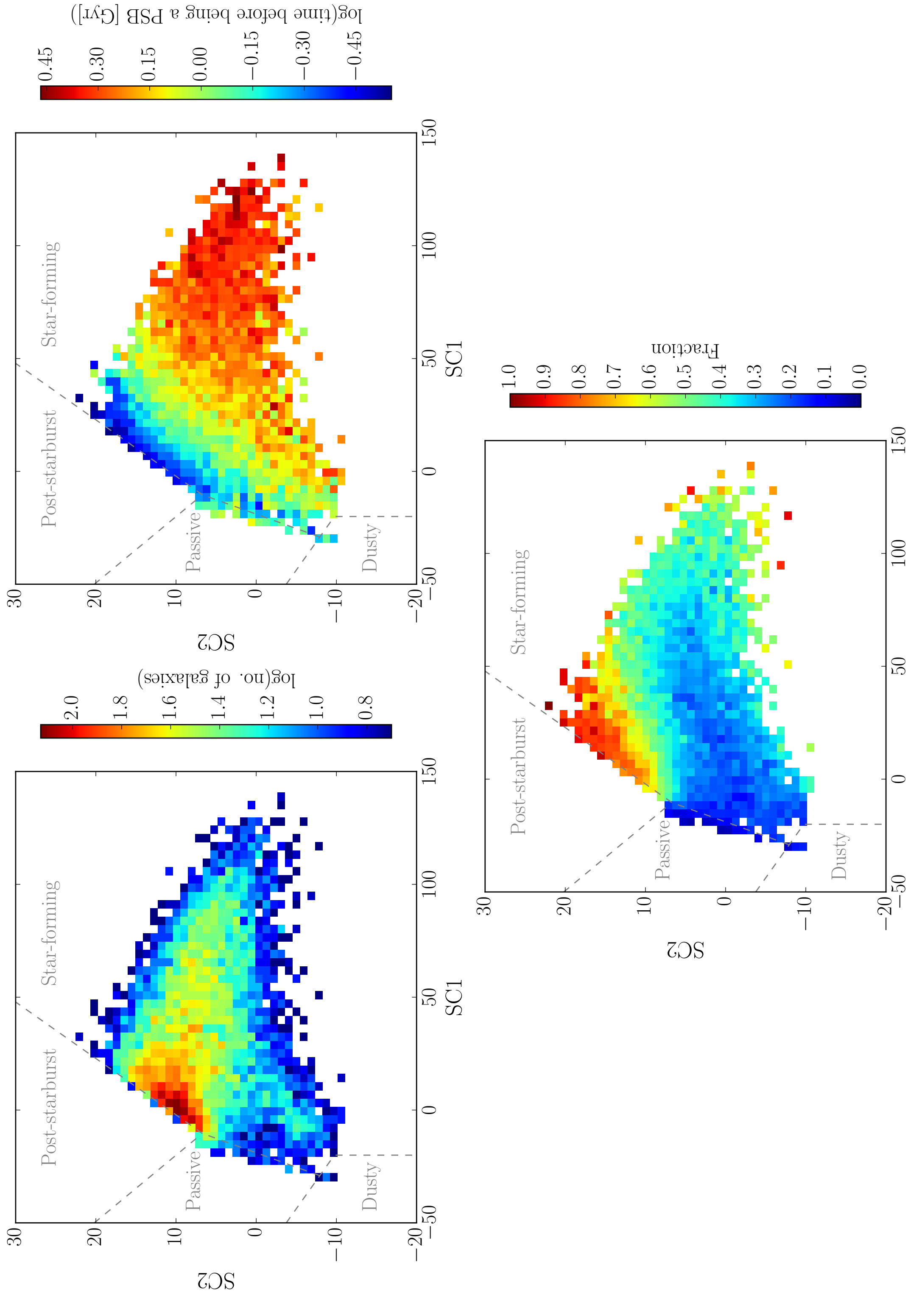

Figure 5.9. Tracks of progenitors of PSBs on the supercolour diagram. The total number of PSB progenitors that have passed through each bin on the supercolour diagram (top left panel), the median time offset between passing through each bin and being classified as a PSB (top right panel) and the fraction of galaxies in each bin on the supercolour diagram which will go on to become PSBs (bottom panel). In each panel the grey dashed lines show the separation between each population. The bins in each panel are coloured by the colourbar on the right. In the top left this is the number of galaxies to have passed through the bin, in the top right this is the median time to become a PSB and in the bottom this is the fraction of galaxies in that bin that will become PSBs. The progenitors of PSBs move diagonally up across the diagram, increasing their SC2 value whilst decreasing their SC1 values.

mock catalogue. Each PSB was tracked across this diagram until it first becomes a PSB and each of its progenitors is binned on the supercolour diagram. The log total number of galaxies in each bin is then displayed according to the colourbar on the right. From this we can see that there appears to be a general trend of moving up and left on the diagram and for PSBs to cross into the PSB region with low SC2 values. This is not surprising as any galaxies which do show signs of a starburst, and would therefore have high SC2 values, are rare. However, there do appear to be a few galaxies which have SC2 values as high as 20.

We then plot the median time before these galaxies pass into the PSB region in the top right panel of Figure 5.9. As we expected from the previous panel, the galaxies generally move up and left on this diagram. The median time separation reduces the closer to the PSB border the galaxies get. There are some galaxies which are very near the border of the star-forming and passive region and only take ~ 500 Myr to move into the PSB region. These could be galaxies which have a sudden burst just before they are completely quenched, so change classification from passive to PSB.

In the bottom panel of Figure 5.9 we then show the fraction of galaxies at any point in the diagram that can be expected to evolve into PSBs. This was calculated by taking the number counts in the top left panel and dividing by the number counts from the tracks of all galaxies. As we can see, across most of the diagram the percentage of galaxies that will become PSBs is below 50%. However, for galaxies with high values of SC2 the percentage is much higher, up to near 90% for SC2 ~ 20. This is what we expect as galaxies with high SC2 values are likely to have undergone a starburst or episode of increased star formation. The results from this panel may be able to help observers connect PSBs and their progenitors, as around 90% of the star-forming galaxies that have high SC2 values will become PSBs in the future.

5.3 Possible rejuvenation after the post-starburst phase

We can also look at what happens to PSB galaxies in the future. Figure 5.10 shows the same plots in each panel as in Figure 5.9, but showing the descendants of PSBs after they leave the PSB region rather than their progenitors. From this we can see that the majority of PSB galaxies move down into the passive region and along the red sequence as they age. This is what we would expect from PSBs, as they would be fully quenched and the value of SC2 would decrease with time as they were no longer forming any new stars. On the supercolour diagram, over 70% of the galaxies nearest the PSB-passive border were PSBs in the past, rather than crossing into this region straight from the star-forming population.

One thing that we can also see from Figure 5.10 is that several galaxies appear to go back into the star-forming region of the supercolour diagram after going through

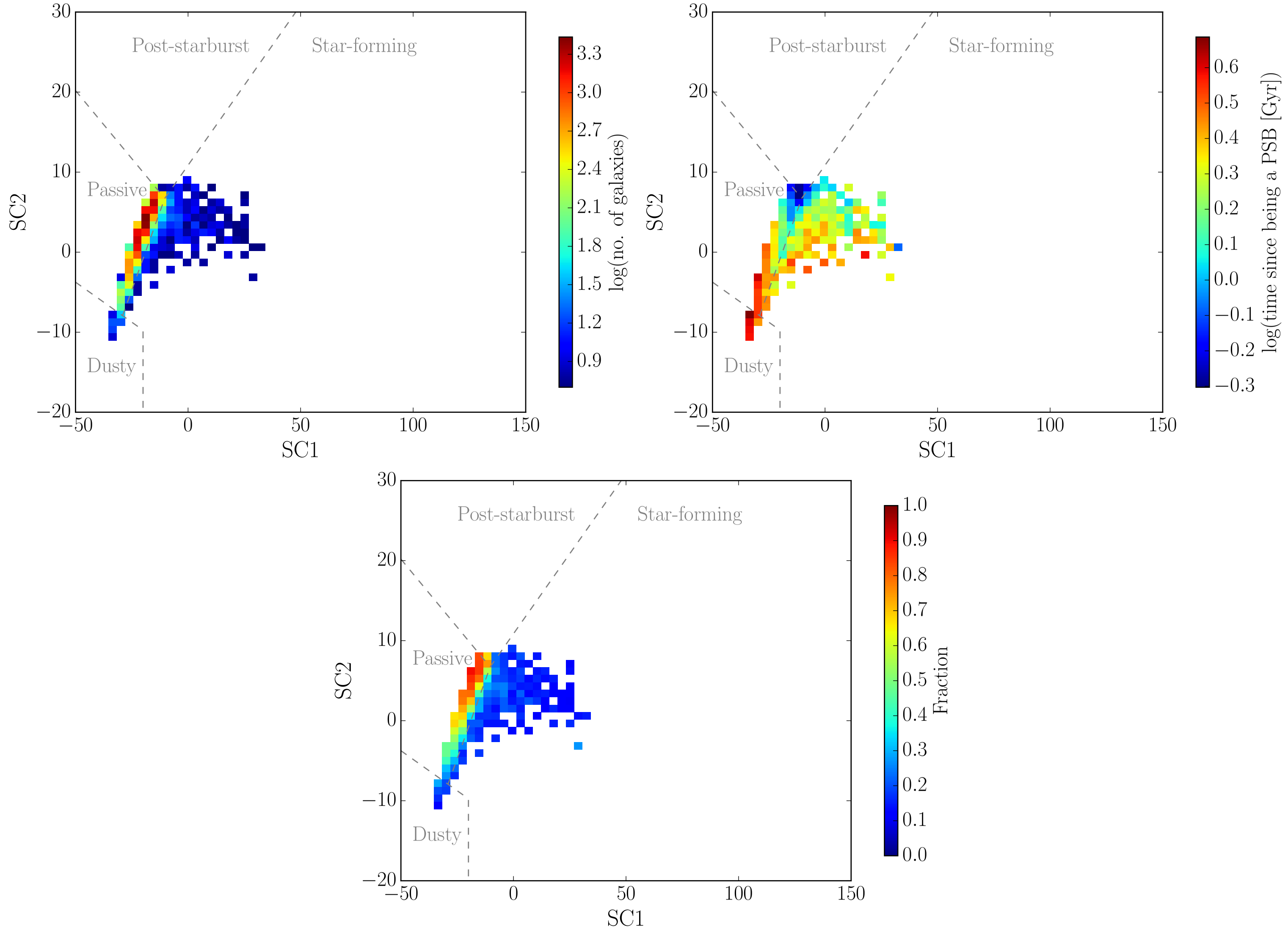

Figure 5.10. As for Figure 5.9, but for the descendants of PSBs. The majority of PSBs move down the red sequence and stay there. However, a small number move back into the star-forming region. These could be galaxies that are showing rejuvenation.

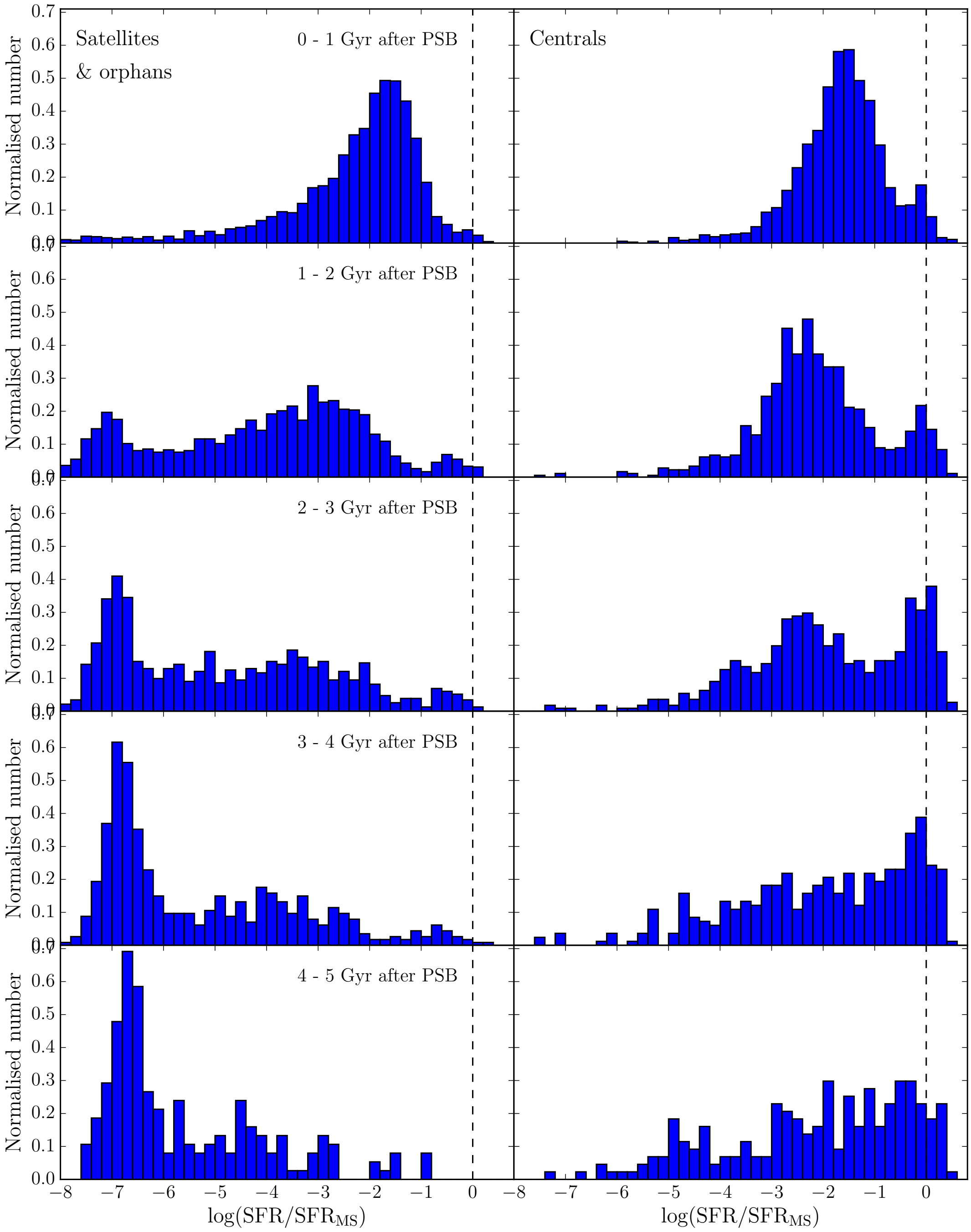

Figure 5.11. As for Figure 4.10, but for the descendants of PSBs, split into satellites and orphans (left panel) and centrals (right panel). Both start off just to the left of the main sequence (dashed line), but whilst satellite and orphan galaxies stay quenched, some of the central galaxies end up back on the main sequence around 2 to 4 Gyr after being a PSB. This could indicate that their star formation was only delayed by gas heating, and they have now been allowed to cool and form stars again. Satellites and orphans on the other hand may have had their gas removed and haven't been able to accrete more.

the PSB stage. This 'rejuvenation' is shown by $\sim 14\%$ of the galaxies in the PSB sample. There is a spread of times that galaxies appear to cross back into this region, with galaxies being classified as star-forming anywhere between 1 and 3 Gyr after being a PSB.

From Figure 5.10, we do not know which galaxies are moving back into the star-forming population after the PSB stage, just that some galaxies are. We therefore construct a histogram of the SFR of the descendants of PSBs, compared to the value they would have on the main sequence, as we did in Chapter 4. Figure 5.11 shows how the SFRs of the descendants of PSBs correspond to galaxies on the main sequence, split into centrals and satellites and orphans. Both populations start off mostly just left of the main sequence, but diverge with time. PSBs that are satellites or orphans tend to gradually reduce their SFR over a few Gyr and seem to stay quenched. However, for centrals the picture is different. They do move left with a reduction in their SFR, but from around 2 Gyr after being a PSB some of them move back onto the star-forming main sequence. The PSBs that are satellites or orphans may have all their gas stripped by environmental effects so when they have used their reserves can no longer form any stars, whereas the centrals are able to reaccrete gas from their surroundings and continue star formation. This could also support the idea that centrals are just having their gas heated, which delays star formation but doesn't stop it.

As in Section 5.2.2, we can also follow the tracks of individual galaxies, and examine the case of a central that returns to the star-forming population after it has been through a PSB phase. Figure 5.12 shows the tracks of this galaxy on a plot of sSFR against stellar mass and on the supercolour diagram. We can see that this galaxy stays as a central up until after it has been classified as a PSB and then as passive. This galaxy then becomes a satellite and temporarily moves back into the star-forming population. This onset of star formation when the galaxy becomes a satellite could indicate that the galaxy has been through a wet merger which brings a new supply of cold gas into the galaxy. The sSFR then temporarily increases by $\sim$ 3 dex between $z \sim 1.2$ to $z \sim 0.9$, which corresponds to a time difference of around 1.4 Gyr. It would be very unlikely for this galaxy to increase its sSFR this much in this timeframe just due to the cooling of its own gas, so an external source of cold gas seems more likely. It may have merged with another satellite of the central galaxy it is now a satellite of.

5.4 Conclusions

Using the methods described in Chapters 3 and 4, we have constructed a mock lightcone survey, matched to the depth of the UDS, and used a PCA method to classify galaxies based on their SEDs. Using this mock, we have investigated the

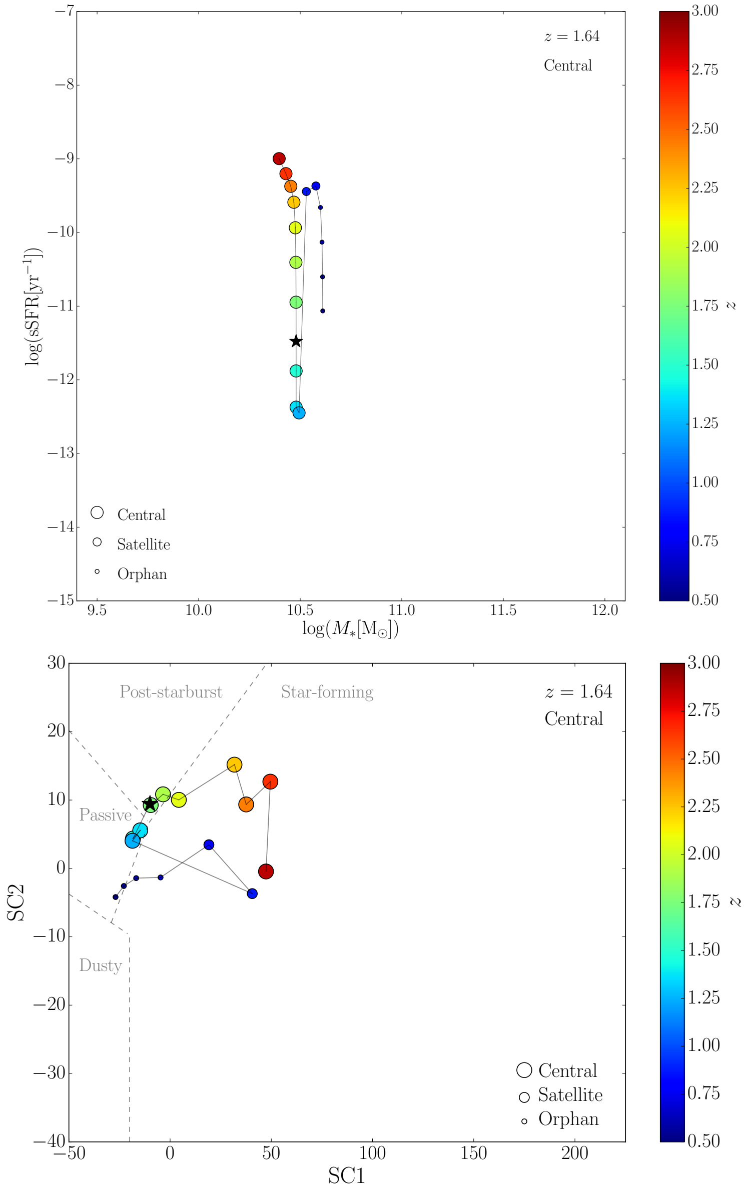

Figure 5.12. As for Figures 5.7 and 5.8, but showing a galaxy that moves back into the star-forming region after being a PSB. This galaxy follows the usual track, moving from star-forming to PSB to passive, but then moves temporarily from passive back to star-forming. This could be an example of a galaxy that has had a wet merger with another galaxy. The addition of cold gas could rejuvenate star formation in this galaxy.

evolution of PSBs, by tracking their properties through time and relating this back to changes in their classification. We also split the PSBs into centrals, satellites and orphans in order to determine if different quenching mechanisms are affecting each type. We found that satellites and orphans appear to be quenched due to environmental effects such as tidal and ram pressure stripping, whereas centrals appear to be quenched after radio mode AGN feedback kicks in after a starburst.

In summary, we find differences in the quenching mechanisms of PSBs, splitting by galaxy type:

- On average, the cold gas content in central galaxies increases about 3 Gyr before they become PSBs, but returns to its previous level by the time they are PSBs. The hot gas in satellites and orphans is stripped from the galaxies, with orphan PSBs having no hot gas at all.
- The sSFR of central PSBs rises and falls in line with the increase and decrease in cold gas content. These galaxies appear to have the starburst expected in 'post-starburst' galaxies, whereas in satellites the increase is not so large. Both satellites and orphans experience a decline in sSFR as the hot gas is stripped.
- Central PSBs have a large spike in the fraction of galaxies that are cooling at the same time as the cold gas content increases. There is also a rise in satellites as they also have a slight increase in cold gas. By 5 Gyr after becoming PSBs, over 80% of galaxies of all types are no longer cooling, as they are quenched.
- Radio mode accretion onto the central black holes is occurring for $\sim 95\%$ of PSBs that are centrals by the time they are classified as PSBs. This increase occurs as the fraction of galaxies cooling decreases after the spike.
- Most PSBs move across from the star-forming population, becoming PSBs before moving into the passive region of the supercolour diagram. However, looking at their tracks on this diagram, we can see that some galaxies move back into the star-forming population after the PSB phase. These galaxies appear to be centrals, with some of them moving back onto the main sequence after a few Gyr.

Taking all of this together, we can look at the possible quenching mechanisms affecting the different galaxy types. For centrals, the increase in the cold gas content prior to becoming PSBs may be due to a wet merger. This brings a supply of cold gas into the galaxy, as well as hot gas, which begins to rapidly cool. This increase in the cold gas content leads to a burst of star formation occurring. However, as hot gas is being accreted onto the central black hole after the merger, this leads to radio mode AGN feedback. This acts to heat up the gas in the galaxy, quenching star formation in these systems. After a few Gyr, this accretion may reduce or stop, leading to the associated gas heating stopping. The hot gas is then allowed to cool, leading to star formation being rejuvenated in some of these systems.

For satellite and orphan galaxies, the quenching mechanisms appear to be environmental. As soon as the galaxies become satellites, the hot gas begins to be stripped from them via tidal and ram pressure stripping. Some of these satellites experience a small burst of star formation, maybe due to a minor merger. Satellites become orphans after their dark matter halo and all the hot gas is stripped from them. Tidal forces can then begin to remove both cold gas and stellar material from the system. Galaxies with no hot gas will fade relatively slowly as the cold gas which is still present can be used for star formation. However, once the cold gas is stripped star formation will be terminated very abruptly. These galaxies will stay quenched as they have no way to accrete any more hot gas from their surroundings.

We can relate these findings to the two populations of PSBs seen in observations. In the UDS, PSBs seem to either be at high redshift and have high stellar masses, or they are low-mass galaxies at low redshift. Most of the PSBs that are high-mass at high redshift in the models are centrals, which appear to have been quenched due to AGN feedback following a merger induced starburst. This is not surprising as AGN feedback was originally added to the models to reduce the number of high-mass galaxies. Using our mock as a prediction, we would then expect to see AGN signatures in the spectra of high redshift PSBs. So far they have not been seen, but the number of PSBs that have been spectroscopically followed up at high redshift is low. Low-mass, low redshift PSBs in the mock are mostly either orphans or centrals. The orphans are likely to have been quenched due to environmental processes, which observations have also suggested. For low-mass centrals at low redshift, the quenching mechanisms responsible are less clear, but one possibility is stellar feedback heating up the gas in the galaxy. Short term follow up to this work could include looking at these two populations in the models in more depth, to see if we can confirm these tentative findings.

Following the PSBs through the simulation with time has allowed us to gain some valuable insight into the quenching processes affecting them. However, our conclusions may be model dependent, as if ram pressure stripping was not included as an analytical prescription then we would find no evidence of this when looking at gas content. As galaxy formation models include more physical prescriptions in order to get closer to matching observations, we will hopefully find that the PSB population is better reproduced and we can learn more about it.

Chapter 6

Conclusions and future outlook

The origin of galaxy bimodality is still a very active area of research in modern astronomy. How and why galaxies transition from the blue cloud to the red sequence is a complex question, with the answer likely depending on multiple galaxy properties such as stellar mass, redshift and environment. In this thesis we have used galaxy formation models to investigate the processes governing star formation and quenching, with the aim of both informing models about what mechanisms are missing and learning about how galaxies in the Universe may evolve. We firstly compare nine different galaxy formation models, in order to learn about the physics which is necessary to reproduce observed galaxy properties. Using one of the codes from this comparison, we then create a mock survey and use it to identify post-starburst galaxies, a population of galaxies that have been rapidly quenched, often following a starburst. From these simulated galaxies, we can learn about what processes may be shutting off star formation and quenching galaxies.

6.1 Conclusions

6.1.1 What physics do galaxy formation models need in order to produce a realistic galaxy population?

In Chapter 2, we compared the results from nine galaxy formation models with recent observational data. Doing this can help to inform us about what physical processes need to be included in the models in order to reproduce a realistic population of galaxies. By looking at the physical mechanisms included both in models that do and don't match observed galaxy properties, we can learn about how models can further improve.

We used data from the Cosmic CARNage mock galaxy comparison project (Knebe et al. 2018), which consisted of nine galaxy formation models (eight semi-analytic models (SAMs) and one halo occupation distribution model) all run on the same dark-matter-only simulation and calibrated to the same observational data. Our analysis focused on the build up of the stellar mass function from $z \sim 3$, as how the number density of galaxies changes with time is a fundamental observable for models to reproduce. We summarise our findings below:

- We find that although most models can reproduce the observed stellar mass function at $z = 0$, they struggle to simultaneously reproduce it at high redshift. Most models produce too many low-mass galaxies at early times.

- When splitting into star-forming and passive populations, we find that the number density of low-mass star-forming galaxies in the models has changed little since $z \sim 2$. The passive stellar mass function from the models does evolve with redshift, but the models are unable to reproduce the apparent turnover in the observed passive number density at low masses.

- At high redshift, galaxies in low-mass haloes have higher stellar masses in the models compared to observations. The observations also suggest a downsizing trend in halo mass, where the average halo mass of a star-forming galaxy decreases with redshift, but this is not present in the models.

Taken together, these conclusions suggest that models still struggle to reproduce the 'anti-hierarchical' assembly of galaxies, where high-mass galaxies are in place at high redshift and the number density of low-mass objects increases rapidly from $z = 2$ to $z = 0$. This is due to the fact that dark matter haloes are thought to be assembled hierarchically and it is difficult to disconnect the growth of galaxies from the growth of the halo they reside in. The gas accretion rate onto haloes, and therefore galaxies, scales with halo mass, so will increase as the halo grows. The SFR of the galaxy then scales with the amount of gas available, so it is natural to think that galaxies would grow as their haloes do. However, this does not appear to be the case in observations.

By studying the connection between stellar mass and halo mass, we found that star formation is more efficient in low-mass haloes at high redshift in the models than it appears to be in the observations. Feedback processes can act to reduce the efficiency of star formation, but the models need a process that acts to reduce star formation further in low-mass haloes at high redshift. This would then move star formation to lower redshift and help to reconcile the differences in the star-forming stellar mass function at $z = 2$. Further advances in observational astronomy will mean that the stellar mass function at high redshift will be pushed to lower stellar masses, revealing the exact level of tension between galaxy formation models and observations.

6.1.2 What can we tell about the quenching mechanisms of post-starburst galaxies from semi-analytic models?

Through the work in Chapter 2, we gained an understanding of the physics involved in modelling galaxy formation and evolution. We then decided to use one of these models to investigate an open question - why and how are galaxies quenched? We chose to investigate the evolution of a particular population of galaxies referred to as post-starburst (PSB) galaxies. These are galaxies that have usually had a heightened period of star formation before being recently and rapidly quenched. As a comparison sample, we used PSBs identified photometrically using the same method in the UDS survey.

Making the mock survey

The first step involved in answering this question was to create a mock catalogue which we could compare to observations. To make this we chose to use the LGALAXIES semi-analytic model, which we found to be one of the best models in matching the evolution of the stellar mass function in Chapter 2. The standard output format from LGALAXIES is a box of fixed comoving side length at each output redshift. However, we wanted to make our mock as similar to the UDS survey as possible, so in Chapter 3 we explain how we changed the output format to be a lightcone. After this, we ran some tests where we compared the mock lightcone survey to several observational results to check that it matched sufficiently.

Identifying post-starburst galaxies in the mock

We then needed a way to identify PSBs in the mock survey. In the UDS this is done with photometric data, using a Principal Component Analysis (PCA) method. We designed the mock so that we had the photometry in the same 12 bands that cover the UDS, so we used this same method for the galaxies in the mock catalogue we created. The PCA method is explained in Chapter 4, where comparisons to the galaxies in the UDS classified in the same way are presented. The main conclusions were:

- The stellar mass and redshift distribution of PSBs in LGALAXIES and the UDS is very different. In the observations there are two main populations - high-mass PSBs at high redshift and low-mass PSBs at low redshift. However, in the models there are very few high-mass PSBs at high redshift and far more low-mass PSBs at low redshift.

- We can see similar trends when plotting the stellar mass function. In the models, the shape of the PSB stellar mass function is broadly similar to the UDS and the overall number density increases towards low redshift. In the observations the shape of the PSB stellar mass function changes with redshift, but the overall number density of PSBs stays more constant than in the models.

- When we stacked the star formation histories (SFHs) of all galaxies in the model by class, we found that PSBs are currently passive and therefore not forming stars. However, as a population they have formed more of their stellar mass later in their lives than the passive population and appear to be quenched over a shorter time period.

- We also compare how the PSBs in the mock evolve compared to galaxies on the main sequence. PSBs are typically on the main sequence, or just above, until about 1 Gyr before becoming PSBs, when they begin to move off the main sequence. This appears to be a fast process as in under 1 Gyr these galaxies go from typical star-forming galaxies to being completely quenched.

Lgalaxies is able to produce a population of PSBs, but they have different properties to the PSBs identified in the UDS as they are generally at lower redshift. The number of PSBs in the mock seems to generally increase with decreasing redshift, whereas in the UDS there appear to be two distinct populations. This could indicate that the prescriptions included in Lgalaxies mean that galaxies at low redshift tend to be quenched more rapidly so are more likely to show PSB signatures.

From their SFHs, its appears that the PCA method is correctly selecting PSBs as galaxies that are currently passive, but have had more recent star formation than the passive population, so are more recently quenched. However, it does not look like many of the simulated PSBs are ‘classic’ PSBs, in that they have had a large burst of star formation before being quenched. Some of them show signs of being above the main sequence, but this is by no means true for the entire PSB population.

Investigating the evolution of simulated post-starburst galaxies

We investigate the evolution of our simulated PSBs in Chapter 5, tracking how their properties change with time. This allows us to gain insight into the quenching mechanisms that are affecting the PSB population and inform observations about what quenching signatures to look for. Splitting our PSB sample by galaxy type into centrals, satellites and orphans we find that:

- PSBs that are centrals experience an increase in cooling rate and sSFR about 2 Gyr before being quenched, which is fuelled by an increase in the amount of gas available for cooling and star formation. At the same time, radio mode feedback switches on for about 40% of these galaxies.

- PSBs that become orphans first fall into larger haloes, where they are classed as satellites. Once the stripping of their dark matter and hot gas is complete, they become orphans. Their sSFR then steadily decreases over the next 5 Gyr.

- Satellite PSBs appear to have a small increase in sSFR about 2 Gyr before being quenched, as with centrals. Their hot gas is then stripped as they fall into a larger halo and their sSFR declines steadily.

- When looking at how the SFR of PSBs changes after being quenched, there are differences between centrals and satellites and orphans. Some of the PSBs that are centrals move back onto the main sequence after a few Gyr in an apparent rejuvenation event, whereas satellite and orphan PSBs stay quenched.

From this, it appears that there are two main quenching pathways for PSBs in the LGALAXIES model. Orphans and satellites are being environmentally quenched, with their hot gas being stripped away by ram pressure stripping and tidal forces. This causes a strangulation effect in the galaxy, as when the existing cold gas is used up through star formation there is no gas left. For centrals the picture is different. They appear to go through a gas-rich merger, which results in a starburst in the galaxy. During the merger hot gas is funnelled into the central black hole, which switches on radio mode feedback in the galaxy. This acts to heat the cold gas, stopping star formation. However, as this gas is still present, if the AGN switches off then this gas will be allowed to cool again. This could be why several of the central PSBs have another episode of star formation a few Gyr later.

In Chapter 4 we saw that there are two main PSB populations in the observations - high-mass PSBs at high redshift and low-mass PSBs at low redshift. The PSBs found in the mock cannot be clearly split into two populations like this, as there are too few PSBs at high redshift. However, despite these differences, we can still use our mock observations to inform observations about how galaxies may be being rapidly quenched, and the models about what physics may be missing.

Most of the high-mass PSBs at high redshift in the mock are centrals, so using the predictions from this work we might expect to see AGN features in the spectra of PSBs at high redshift. Observational studies on this have so far been inconclusive, with mixed results being found (e.g. Schawinski et al. 2009; Alatalo et al. 2011; Fabello et al. 2011; Cicone et al. 2014; French et al. 2015; Rowlands et al. 2015). About a third of the low-mass, low redshift PSBs in the mock are orphans, so are likely to have been quenched due to their environment. However, just over half of the low-mass PSBs at low redshift are centrals. It is possible that these galaxies were quenched by AGN feedback, but this is more common in high-mass galaxies. One possibility could be that supernovae feedback and winds are heating up the gas in these PSBs, leading to quenching signatures similar to AGN feedback in high-mass centrals.

Short term follow up to this work could include looking at these two populations of PSBs in the models in more depth, in order to better inform observations. We would also like to investigate the quenching timescales of PSBs in the models. Observations have made predictions about how long it takes PSBs to be quenched (Wild et al. 2016), which we could compare with the SFHs in our mock. We can connect this to the tracks on the supercolour diagram, as galaxies are thought to follow different routes depending on their quenching timescale and whether they have a burst. In addition to this, we could look at how many star-forming galaxies go through a PSB phase before being quenched, as this is still not clear from observations and depends on quenching timescales. We could also learn more from the population of galaxies that start forming stars again after a PSB phase, as it is not clear if this only happens in certain situations, such as a merger after quenching.

6.2 Future outlook

6.2.1 Observational outlook

Finding out which physical processes quench galaxies and why is still a fundamental question in extragalactic astronomy. At high redshift, studies hope to observe galaxies as they are transitioning, informing us about which mechanisms are quenching galaxies, and how this depends on galaxy properties. After its launch in March 2021, the James Webb Space Telescope (JWST) will allow for unprecedented observations at high redshift. The Near Infrared Camera (NIRCam) instrument on JWST will cover the wavelength range from $0.6-5.0\mu$m with 8 broad band filters and a number of medium and narrow band filters. Using this range of filters, galaxy SEDs can be fit to $z \sim 5$, allowing for the derivation of a host of galaxy properties such as stellar mass, photometric redshift, colour, age and metallicity. This will mean that many studies will be able to extended to even higher redshifts, including the PCA technique to classify galaxies based on their SEDs. PSBs could then be identified from photometry alone up to $z \sim 5$, allowing us to study galaxy quenching even earlier in the Universe.

In addition to NIRCam, the Near Infrared Spectrograph (NIRSpec) instrument on JWST will be a valuable tool for studying galaxies at high redshift. NIRSpec covers the same wavelength range as NIRCam, so will enable studies of galaxy quenching at $z \sim 2$, where the most massive galaxies are formed and quenched. In rest-frame optical light we will be able to observe the Balmer lines, Ca H&K and the 4000Å break, allowing us to measure metallicities and look for signatures of AGN. Beyond $z = 1.5$ these spectral features move into the near-infrared, which makes spectroscopy from the ground exceptionally difficult. However, the near-infrared background is magnitudes lower in space, meaning that JWST will be able to get detailed spectra of massive passive galaxies at $z \sim 2$ for the first time.

In the meantime, more spectra at high redshift will be available from the VANDELS survey, which uses the VIMOS multi-object spectrograph to obtain deep, medium resolution spectra in the optical. The main targets for VANDELS are bright star-forming galaxies between $2.5 < z < 5.5$ in the UDS and Chandra Deep Field South (CDFS) survey fields, forming the deepest ever spectroscopic survey of the high redshift Universe. VANDELS will also target the descendants of high redshift star-forming galaxies, taking spectra of bright passive galaxies in the range $1.5 < z < 2.5$. A minimum of 20 hours will be spent on each source, providing spectra with high signal-to-noise. The spectra will complement the multi-wavelength photometry in these fields, allowing accurate measurements of galaxy SFR, stellar mass, age, metallicity, AGN activity and outflow velocity. By combining spectroscopy with photometry, the SFH of individual passive and PSB galaxies can be inferred (see Carnall et al. 2018) and correlated with these galaxy properties and time since quenching. These studies will complement rest-frame optical observations from JWST and enable us to get a more complete picture of galaxy quenching.

6.2.2 Galaxy formation modelling outlook

Observational developments will also have an impact on how galaxy formation models develop. SAMs use observational data both to calibrate and test their models, so increasing the number of galaxies observed at high redshifts will present new challenges to modellers. Spectroscopy and SFH comparisons will be particularly useful to test the analytic prescriptions in SAMs, as they will enable us to learn about the AGN or stellar driven winds, in addition to the stellar populations and metallicities of galaxies. These observations can put tighter constraints on the parameters used in SAMs and help to ensure that the physical prescriptions included are well motivated.

The tuning of analytic prescriptions also affects hydrodynamical simulations. These are simulations which model dark matter and gas coupled together with gravity, and evolve gas with hydrodynamic equations. However, prescriptions are still needed to describe the baryonic processes involved, which occur on a scale smaller than can be resolved, even by state-of-the-art models. The techniques used by hydrodynamical simulations to model 'subgrid' physics are very similar to the analytic prescriptions used in SAMs, and are in many cases based on them. Therefore, any development in one should benefit the other, as it seems most likely that the two will merge together in the future, incorporating aspects of each other.

Hydrodynamical simulations cannot yet be run on the same size boxes as SAMs, due to the computational resources required, but are advancing at a rapid pace. Simulations usually trade off between a lower mass resolution or larger box size, but even at the lowest mass resolutions they still require subgrid physics to model processes that occur on a sub-parsec scale. EAGLE and Illustris have run simulations of larger regions, with the IllustrisTNG project producing a box of $\sim 300h^{-1}$Mpc on each side. At present these boxes are too small to use to study large populations of galaxies without the effects of sample variance. However, when next generation hydrodynamical simulations can be run on cosmological volumes, they will be an invaluable tool for studying the evolution of galaxies and investigating what roles gas and galaxy environment play in galaxy quenching.

6.2.3 Bridging the gap between observations and theory

Modellers and observers must continue to work together to learn about what physical processes are important in galaxy formation and evolution. By designing observations to search for signatures of processes that are necessary in the models, both observers and modellers can benefit. New and unexpected observational results will continue to challenge galaxy formation models, but will hopefully lead to a convergence by different models on the core physical mechanisms present in the Universe. In this way, we will hopefully come to understand more about the complex processes governing the evolution of galaxies.

Bibliography

Abadi M. G., Moore B., Bower R. G., 1999. MNRAS, **308**, 947. *Ram pressure stripping of spiral galaxies in clusters.*

Abell G. O., 1965. *Annual Review of Astronomy and Astrophysics*, **3**, 1. *Clustering of Galaxies.*

Acquaviva V., Gawiser E., Guaita L., 2011. ApJ, **737**, 47. *Spectral Energy Distribution Fitting with Markov Chain Monte Carlo: Methodology and Application to $z = 3.1$ Lyα-emitting Galaxies.*

Alatalo K., Blitz L., Young L. M., Davis T. A., Bureau M., Lopez L. A., Cappellari M., Scott N., Shapiro K. L., Crocker A. F., Martín S., Bois M., Bournaud F., Davies R. L., de Zeeuw P. T., Duc P. A., Emsellem E., Falcón-Barroso J., Khochfar S., Krajnović D., Kuntschner H., Lablanche P. Y., McDermid R. M., Morganti R., Naab T., Oosterloo T., Sarzi M., Serra P., Weijmans A., 2011. ApJ, **735**, 88. *Discovery of an Active Galactic Nucleus Driven Molecular Outflow in the Local Early-type Galaxy NGC 1266.*

Almaini O., Wild V., Maltby D. T., Hartley W. G., Simpson C., Hatch N. A., McLure R. J., Dunlop J. S., Rowlands K., 2017. MNRAS, **472**, 1401. *Massive post-starburst galaxies at $z > 1$ are compact proto-spheroids.*

Angulo R. E., Hilbert S., 2015. MNRAS, **448**, 364. *Cosmological constraints from the CFHTLenS shear measurements using a new, accurate, and flexible way of predicting non-linear mass clustering.*

Angulo R. E., White S. D. M., 2010. MNRAS, **405**, 143. *One simulation to fit them all - changing the background parameters of a cosmological N-body simulation.*

Arthur J., Pearce F. R., Gray M. E., Knebe A., Cui W., Elahi P. J., Power C., Yepes G., Arth A., De Petris M., Dolag K., Garratt-Smithson L., Old L. J., Rasia E., Stevens A. R. H., 2019. MNRAS, **484**, 3968. *THETHREEHUNDRED Project: ram pressure and gas content of haloes and subhaloes in the phase-space plane.*

Asquith R., Pearce F. R., Almaini O., Knebe A., Gonzalez-Perez V., Benson A., Blaizot J., Carretero J., Castander F. J., Cattaneo A., Cora S. A., Croton D. J., Devriendt J. E., Fontanot F., Gargiulo I. D., Hartley W., Henriques B., Lee J., Mamon G. A., Onions J., Padilla N. D., Power C., Srisawat C., Stevens A. R. H., Thomas P. A., Vega-Martínez C. A., Yi S. K., 2018. MNRAS, **480**, 1197. *Cosmic CARNage II: the evolution of the galaxy stellar mass function in observations and galaxy formation models.*

Baldry I. K., Glazebrook K., Brinkmann J., Ivezić Ž., Lupton R. H., Nichol R. C., Szalay A. S., 2004. ApJ, **600**, 681. *Quantifying the Bimodal Color-Magnitude Distribution of Galaxies.*

Baldry I. K., Balogh M. L., Bower R. G., Glazebrook K., Nichol R. C., Bamford S. P., Budavari T., 2006. MNRAS, **373**, 469. *Galaxy bimodality versus stellar mass and environment.*

Baldry I. K., Driver S. P., Loveday J., Taylor E. N., Kelvin L. S., Liske J., Norberg P., Robotham A. S. G., Brough S., Hopkins A. M., Bamford S. P., Peacock J. A., Bland-Hawthorn J., Conselice C. J., Croom S. M., Jones D. H., Parkinson H. R., Popescu C. C., Prescott M., Sharp R. G., Tuffs R. J., 2012. MNRAS, **421**, 621. *Galaxy And Mass Assembly (GAMA): the galaxy stellar mass function at $z < 0.06$.*

Baldry I. K., Glazebrook K., Driver S. P., 2008. MNRAS, **388**, 945. *On the galaxy stellar mass function, the mass-metallicity relation and the implied baryonic mass function.*

Balogh M. L., McGee S. L., Mok A., Muzzin A., van der Burg R. F. J., Bower R. G., Finoguenov A., Hoekstra H., Lidman C., Mulchaey J. S., Noble A., Parker L. C., Tanaka M., Wilman D. J., Webb T., Wilson G., Yee H. K. C., 2016. MNRAS, **456**, 4364. *Evidence for a change in the dominant satellite galaxy quenching mechanism at $z = 1$.*

Bamford S. P., Nichol R. C., Baldry I. K., Land K., Lintott C. J., Schawinski K., Slosar A., Szalay A. S., Thomas D., Torki M., Andreescu D., Edmondson E. M., Miller C. J., Murray P., Raddick M. J., Vandenberg J., 2009. MNRAS, **393**, 1324. *Galaxy Zoo: the dependence of morphology and colour on environment*.*

Barnes J. E., Hernquist L. E., 1991. ApJ, **370**, L65. *Fueling Starburst Galaxies with Gas-rich Mergers.*

Barton E. J., Geller M. J., Kenyon S. J., 2000. ApJ, **530**, 660. *Tidally Triggered Star Formation in Close Pairs of Galaxies.*

Baugh C. M., Cole S., Frenk C. S., Lacey C. G., 1998. ApJ, **498**, 504. *The Epoch of Galaxy Formation.*

Baugh C. M., 2006. *Reports on Progress in Physics*, **69**, 3101. *A primer on hierarchical galaxy formation: the semi-analytical approach.*

Behroozi P. S., Wechsler R. H., Wu H.-Y., Busha M. T., Klypin A. A., Primack J. R., 2013. ApJ, **763(1)**, 18. *Gravitationally Consistent Halo Catalogs and Merger Trees for Precision Cosmology.*

Behroozi P. S., Wechsler R. H., Conroy C., 2013. ApJ, **770**, 57. *The Average Star Formation Histories of Galaxies in Dark Matter Halos from $z = 0$-8.*

Behroozi P. S., Wechsler R. H., Wu H.-Y., 2013. ApJ, **762**, 109. *The ROCKSTAR Phase-space Temporal Halo Finder and the Velocity Offsets of Cluster Cores.*

Bekki K., 1998. ApJ, **502**, L133. *Unequal-Mass Galaxy Mergers and the Creation of Cluster S0 Galaxies.*

Bell E. F., Wolf C., Meisenheimer K., Rix H.-W., Borch A., Dye S., Kleinheinrich M., Wisotzki L., McIntosh D. H., 2004. ApJ, **608**, 752. *Nearly 5000 Distant Early-Type Galaxies in COMBO-17: A Red Sequence and Its Evolution since z* $\sim$ *1.*

Bell E. F., Naab T., McIntosh D. H., Somerville R. S., Caldwell J. A. R., Barden M., Wolf C., Rix H.-W., Beckwith S. V., Borch A., Häussler B., Heymans C., Jahnke K., Jogee S., Koposov S., Meisenheimer K., Peng C. Y., Sanchez S. F., Wisotzki L., 2006. ApJ, **640**, 241. *Dry Mergers in GEMS: The Dynamical Evolution of Massive Early-Type Galaxies.*

Bennett C. L., Halpern M., Hinshaw G., Jarosik N., Kogut A., Limon M., Meyer S. S., Page L., Spergel D. N., Tucker G. S., Wollack E., Wright E. L., Barnes C., Greason M. R., Hill R. S., Komatsu E., Nolta M. R., Odegard N., Peiris H. V., Verde L., Weiland J. L., 2003. *The Astrophysical Journal Supplement Series*, **148**, 1. *First-Year Wilkinson Microwave Anisotropy Probe (WMAP) Observations: Preliminary Maps and Basic Results.*

Benson A. J., Bower R. G., Frenk C. S., Lacey C. G., Baugh C. M., Cole S., 2003. ApJ, **599**, 38. *What Shapes the Luminosity Function of Galaxies?*

Benson A. J., 2010. Phys. Rep., **495**, 33. *Galaxy formation theory.*

Berlind A. A., Weinberg D. H., 2002. ApJ, **575**, 587. *The Halo Occupation Distribution: Toward an Empirical Determination of the Relation between Galaxies and Mass.*

Berlind A. A., Weinberg D. H., Benson A. J., Baugh C. M., Cole S., Davé R., Frenk C. S., Jenkins A., Katz N., Lacey C. G., 2003. ApJ, **593**, 1. *The Halo Occupation Distribution and the Physics of Galaxy Formation.*

Birnboim Y., Dekel A., 2003. MNRAS, **345**, 349. *Virial shocks in galactic haloes?*

Blaizot J., Wadadekar Y., Guiderdoni B., Colombi S. T., Bertin E., Bouchet F. R., Devriendt J. E. G., Hatton S., 2005. MNRAS, **360**, 159. *MoMaF: the Mock Map Facility.*

Blanton M. R., Hogg D. W., Bahcall N. A., Baldry I. K., Brinkmann J., Csabai I., Eisenstein D., Fukugita M., Gunn J. E., Ivezić Ž., Lamb D. Q., Lupton R. H., Loveday J., Munn J. A., Nichol R. C., Okamura S., Schlegel D. J., Shimasaku K., Strauss M. A., Vogeley M. S., Weinberg D. H., 2003. ApJ, **594**, 186. *The Broadband Optical Properties of Galaxies with Redshifts* $0.02<z<0.22$*.*

Blanton M. R., Eisenstein D., Hogg D. W., Schlegel D. J., Brinkmann J., 2005. ApJ, **629**, 143. *Relationship between Environment and the Broadband Optical Properties of Galaxies in the Sloan Digital Sky Survey.*

Bluck A. F. L., Mendel J. T., Ellison S. L., Patton D. R., Simard L., Henriques B. M. B., Torrey P., Teimoorinia H., Moreno J., Starkenburg E., 2016. MNRAS, **462**, 2559. *The impact of galactic properties and environment on the quenching of central and satellite galaxies: a comparison between SDSS, Illustris and L-Galaxies.*

Borch A., Meisenheimer K., Bell E. F., Rix H. W., Wolf C., Dye S., Kleinheinrich M., Kovacs Z., Wisotzki L., 2006. A&A, **453(3)**, 869. *The stellar masses of 25 000 galaxies at* $0.2 \leq z \leq 1.0$ *estimated by the COMBO-17 survey.*

Boselli A., Gavazzi G., 2006. *Publications of the Astronomical Society of the Pacific*, **118**, 517. *Environmental Effects on Late-Type Galaxies in Nearby Clusters.*

Boselli A., Cortese L., Boquien M., Boissier S., Catinella B., Gavazzi G., Lagos C., Saintonge A., 2014. A&A, **564**, A67. *Cold gas properties of the Herschel Reference Survey. III. Molecular gas stripping in cluster galaxies.*

Bower R. G., Benson A. J., Malbon R., Helly J. C., Frenk C. S., Baugh C. M., Cole S., Lacey C. G., 2006. MNRAS, **370**, 645. *Breaking the hierarchy of galaxy formation.*

Brinchmann J., Charlot S., White S. D. M., Tremonti C., Kauffmann G., Heckman T., Brinkmann J., 2004. MNRAS, **351**, 1151. *The physical properties of star-forming galaxies in the low-redshift Universe.*

Bruzual G., Charlot S., 2003. MNRAS, **344**, 1000. *Stellar population synthesis at the resolution of 2003.*

Byrd G., Valtonen M., 1990. ApJ, **350**, 89. *Tidal Generation of Active Spirals and S0 Galaxies by Rich Clusters.*

Cales S. L., Brotherton M. S., 2015. MNRAS, **449**, 2374. *Post-starburst quasars: bridging the gap between post-starburst galaxies and quasars.*

Cales S. L., Brotherton M. S., Shang Z., Bennert V. N., Canalizo G., Stoll R., Ganguly R., Vanden Berk D., Paul C., Diamond-Stanic A., 2011. ApJ, **741**, 106. *Hubble Space Telescope Imaging of Post-starburst Quasars.*

Cano-Díaz M., Sánchez S. F., Zibetti S., Ascasibar Y., Bland-Hawthorn J., Ziegler B., González Delgado R. M., Walcher C. J., García-Benito R., Mast D., Mendoza-Pérez M. A., Falcón-Barroso J., Galbany L., Husemann B., Kehrig C., Marino R. A., Sánchez-Blázquez P., López-Cobá C., López-Sánchez Á. R., Vilchez J. M., 2016. ApJ, **821**, L26. *Spatially Resolved Star Formation Main Sequence of Galaxies in the CALIFA Survey.*

Carnall A. C., McLure R. J., Dunlop J. S., Davé R., 2018. MNRAS, **480**, 4379. *Inferring the star formation histories of massive quiescent galaxies with BAGPIPES: evidence for multiple quenching mechanisms.*

Carretero J., Castander F. J., Gaztañaga E., Crocce M., Fosalba P., 2015. MNRAS, **447**, 646. *An algorithm to build mock galaxy catalogues using MICE simulations.*

Cattaneo A., Blaizot J., Devriendt J. E. G., Mamon G. A., Tollet E., Dekel A., Guiderdoni B., Kucukbas M., Thob A. C. R., 2017. MNRAS, **471**, 1401. *The new semi-analytic code GalICS 2.0 - reproducing the galaxy stellar mass function and the Tully-Fisher relation simultaneously.*

Chabrier G., 2003. PASP, **115**, 763. *Galactic Stellar and Substellar Initial Mass Function.*

Charlot S., Fall S. M., 2000. ApJ, **539**, 718. *A Simple Model for the Absorption of Starlight by Dust in Galaxies.*

Chevalier R. A., Clegg A. W., 1985. Nature, **317**, 44. *Wind from a starburst galaxy nucleus.*

Cicone C., Maiolino R., Sturm E., Graciá-Carpio J., Feruglio C., Neri R., Aalto S., Davies R., Fiore F., Fischer J., García-Burillo S., González-Alfonso E., Hailey-Dunsheath S., Piconcelli E., Veilleux S., 2014. A&A, **562**, A21. *Massive molecular outflows and evidence for AGN feedback from CO observations.*

Cimatti A., Daddi E., Renzini A., 2006. A&A, **453**, L29. *Mass downsizing and "top-down" assembly of early-type galaxies.*

Cirasuolo M., McLure R. J., Dunlop J. S., Almaini O., Foucaud S., Smail I., Sekiguchi K., Simpson C., Eales S., Dye S., Watson M. G., Page M. J., Hirst P., 2007. MNRAS, **380**, 585. *The evolution of the near-infrared galaxy luminosity function and colour bimodality up to $z \sim= 2$ from the UKIDSS Ultra Deep Survey Early Data Release.*

Coil A. L., Weiner B. J., Holz D. E., Cooper M. C., Yan R., Aird J., 2011. ApJ, **743**, 46. *Outflowing Galactic Winds in Post-starburst and Active Galactic Nucleus Host Galaxies at 0.2 < z < 0.8.*

Cole S., Aragon-Salamanca A., Frenk C. S., Navarro J. F., Zepf S. E., 1994. MNRAS, **271**, 781. *A recipe for galaxy formation.*

Colless M., Dalton G., Maddox S., Sutherland W., Norberg P., Cole S., Bland-Hawthorn J., Bridges T., Cannon R., Collins C., Couch W., Cross N., Deeley K., De Propris R., Driver S. P., Efstathiou G., Ellis R. S., Frenk C. S., Glazebrook K., Jackson C., Lahav O., Lewis I., Lumsden S., Madgwick D., Peacock J. A., Peterson B. A., Price I., Seaborne M., Taylor K., 2001. MNRAS, **328**, 1039. *The 2dF Galaxy Redshift Survey: spectra and redshifts.*

Conroy C., Gunn J. E., White M., 2009. ApJ, **699**, 486. *The Propagation of Uncertainties in Stellar Population Synthesis Modeling. I. The Relevance of Uncertain Aspects of Stellar Evolution and the Initial Mass Function to the Derived Physical Properties of Galaxies.*

Conroy C., 2013. *Annual Review of Astronomy and Astrophysics*, **51**, 393. *Modeling the Panchromatic Spectral Energy Distributions of Galaxies.*

Cora S. A., Hough T., Vega-Martínez C. A., Orsi Á., 2018a. *ArXiv e-prints. Semi-Analytic Galaxies - II. Revealing the role of environmental and mass quenching in galaxy formation.*

Cora S. A., Vega-Martínez C. A., Hough T., Ruiz A. N., Orsi Á. A., Muñoz Arancibia A. M., Gargiulo I. D., Collacchioni F., Padilla N. D., Gottlöber S., Yepes G., 2018b. MNRAS, **479**, 2. *Semi-analytic galaxies - I. Synthesis of environmental and star-forming regulation mechanisms.*

Cowie L. L., Songaila A., Hu E. M., Cohen J. G., 1996. AJ, **112**, 839. *New Insight on Galaxy Formation and Evolution From Keck Spectroscopy of the Hawaii Deep Fields.*

Croton D. J., Springel V., White S. D. M., De Lucia G., Frenk C. S., Gao L., Jenkins A., Kauffmann G., Navarro J. F., Yoshida N., 2006. MNRAS, **365**, 11. *The many lives of active galactic nuclei: cooling flows, black holes and the luminosities and colours of galaxies.*

Croton D. J., Stevens A. R. H., Tonini C., Garel T., Bernyk M., Bibiano A., Hodkinson L., Mutch S. J., Poole G. B., Shattow G. M., 2016. ApJS, **222**, 22. *Semi-Analytic Galaxy Evolution (SAGE): Model Calibration and Basic Results.*

da Cunha E., Charlot S., Elbaz D., 2008. MNRAS, **388**, 1595. *A simple model to interpret the ultraviolet, optical and infrared emission from galaxies.*

Daddi E., Dickinson M., Morrison G., Chary R., Cimatti A., Elbaz D., Frayer D., Renzini A., Pope A., Alexander D. M., Bauer F. E., Giavalisco M., Huynh M., Kurk J., Mignoli M., 2007. ApJ, **670**, 156. *Multiwavelength Study of Massive Galaxies at $z \sim 2$. I. Star Formation and Galaxy Growth.*

Davidzon I., Ilbert O., Laigle C., Coupon J., McCracken H. J., Delvecchio I., Masters D., Capak P., Hsieh B. C., Le Fèvre O., Tresse L., Bethermin M., Chang Y.-Y., Faisst A. L., Le Floc'h E., Steinhardt C., Toft S., Aussel H., Dubois C., Hasinger G., Salvato M., Sanders D. B., Scoville N., Silverman J. D., 2017. A&A, **605**, A70. *The COSMOS2015 galaxy stellar mass function . Thirteen billion years of stellar mass assembly in ten snapshots.*

Davis M., Efstathiou G., Frenk C. S., White S. D. M., 1985. ApJ, **292**, 371. *The evolution of large-scale structure in a universe dominated by cold dark matter.*

Davis T. A., van de Voort F., Rowlands K., McAlpine S., Wild V., Crain R. A., 2019. MNRAS, **484**, 2447. *Evolution of the cold gas properties of simulated post-starburst galaxies.*

De Lucia G., Blaizot J., 2007. MNRAS, **375**, 2. *The hierarchical formation of the brightest cluster galaxies.*

De Lucia G., Tornatore L., Frenk C. S., Helmi A., Navarro J. F., White S. D. M., 2014. MNRAS, **445**, 970. *Elemental abundances in Milky Way-like galaxies from a hierarchical galaxy formation model.*

Dekel A., Birnboim Y., 2006. MNRAS, **368**, 2. *Galaxy bimodality due to cold flows and shock heating.*

Di Matteo T., Springel V., Hernquist L., 2005. Nature, **433**, 604. *Energy input from quasars regulates the growth and activity of black holes and their host galaxies.*

Diamond-Stanic A. M., Moustakas J., Tremonti C. A., Coil A. L., Hickox R. C., Robaina A. R., Rudnick G. H., Sell P. H., 2012. ApJ, **755**, L26. *High-velocity Outflows without AGN Feedback: Eddington-limited Star Formation in Compact Massive Galaxies.*

Domínguez Sánchez H., Pozzi F., Gruppioni C., Cimatti A., Ilbert O., Pozzetti L., McCracken H., Capak P., Le Floch E., Salvato M., Zamorani G., Carollo C. M., Contini T., Kneib J.-P., Le Fèvre O., Lilly S. J., Mainieri V., Renzini A., Scodeggio M., Bardelli S., Bolzonella M., Bongiorno A., Caputi K., Coppa G., Cucciati O., de la Torre S., de Ravel L., Franzetti P., Garilli B., Iovino A., Kampczyk P., Knobel C., Kovač K., Lamareille F., Le Borgne J.-F., Le Brun V., Maier C., Mignoli M., Pelló R., Peng Y., Perez-Montero E., Ricciardelli E., Silverman J. D., Tanaka M., Tasca L. A. M., Tresse L., Vergani D., Zucca E., 2011. MNRAS, **417**, 900. *The evolution of quiescent galaxies at high redshifts ($z > 1.4$).*

Dressler A., Gunn J. E., 1983. ApJ, **270**, 7. *Spectroscopy of galaxies in distant clusters. II. The population of the 3C 295 cluster.*

Dressler A., Thompson I. B., Shectman S. A., 1985. ApJ, **288**, 481. *Statistics of emission-line galaxies in rich clusters.*

Dressler A., 1980. ApJ, **236**, 351. *Galaxy morphology in rich clusters: implications for the formation and evolution of galaxies.*

Eggen O. J., Lynden-Bell D., Sandage A. R., 1962. ApJ, **136**, 748. *Evidence from the motions of old stars that the Galaxy collapsed.*

Eisenstein D. J., Zehavi I., Hogg D. W., Scoccimarro R., Blanton M. R., Nichol R. C., Scranton R., Seo H.-J., Tegmark M., Zheng Z., Anderson S. F., Annis J., Bahcall N., Brinkmann J., Burles S., Castand er F. J., Connolly A., Csabai I., Doi M., Fukugita M., Frieman J. A., Glazebrook K., Gunn J. E., Hendry J. S., Hennessy G., Ivezić Z., Kent S., Knapp G. R., Lin H., Loh Y.-S., Lupton R. H., Margon B., McKay T. A., Meiksin A., Munn J. A., Pope A., Richmond M. W., Schlegel D., Schneider D. P., Shimasaku K., Stoughton C., Strauss M. A., SubbaRao M., Szalay A. S., Szapudi I., Tucker D. L., Yanny B., York D. G., 2005. ApJ, **633**, 560. *Detection of the Baryon Acoustic Peak in the Large-Scale Correlation Function of SDSS Luminous Red Galaxies.*

Elbaz D., Daddi E., Le Borgne D., Dickinson M., Alexander D. M., Chary R.-R., Starck J.-L., Brandt W. N., Kitzbichler M., MacDonald E., Nonino M., Popesso P., Stern D., Vanzella E., 2007. A&A, **468**, 33. *The reversal of the star formation-density relation in the distant universe.*

Evrard A. E., Henry J. P., 1991. ApJ, **383**, 95. *Expectations for X-Ray Cluster Observations by the ROSAT Satellite.*

Fabello S., Kauffmann G., Catinella B., Giovanelli R., Haynes M. P., Heckman T. M., Schiminovich D., 2011. MNRAS, **416**, 1739. *Arecibo Legacy Fast ALFA H I data stacking - II. H I content of the host galaxies of active galactic nuclei.*

Faber S. M., Willmer C. N. A., Wolf C., Koo D. C., Weiner B. J., Newman J. A., Im M., Coil A. L., Conroy C., Cooper M. C., Davis M., Finkbeiner D. P., Gerke B. F., Gebhardt K., Groth E. J., Guhathakurta P., Harker J., Kaiser N., Kassin S., Kleinheinrich M., Konidaris N. P., Kron R. G., Lin L., Luppino G., Madgwick D. S., Meisenheimer K., Noeske K. G., Phillips A. C., Sarajedini V. L., Schiavon R. P., Simard L., Szalay A. S., Vogt N. P., Yan R., 2007. ApJ, **665**, 265. *Galaxy Luminosity Functions to $z \sim 1$ from DEEP2 and COMBO-17: Implications for Red Galaxy Formation.*

Fabian A. C., 2012. *Annual Review of Astronomy and Astrophysics*, **50**, 455. *Observational Evidence of Active Galactic Nuclei Feedback.*

Foltz R., Rettura A., Wilson G., van der Burg R. F. J., Muzzin A., Lidman C., Demarco R., Nantais J., DeGroot A., Yee H., 2015. ApJ, **812**, 138. *Evidence for the Universality of Properties of Red-sequence Galaxies in X-Ray- and Red-Sequence-Selected Clusters at $z \sim 1$.*

Font A. S., Bower R. G., McCarthy I. G., Benson A. J., Frenk C. S., Helly J. C., Lacey C. G., Baugh C. M., Cole S., 2008. MNRAS, **389**, 1619. *The colours of satellite galaxies in groups and clusters.*

Fontana A., Pozzetti L., Donnarumma I., Renzini A., Cimatti A., Zamorani G., Menci N., Daddi E., Giallongo E., Mignoli M., Perna C., Salimbeni S., Saracco P., Broadhurst T., Cristiani S., D'Odorico S., Gilmozzi R., 2004. A&A, **424**, 23. *The K20 survey. VI. The distribution of the stellar masses in galaxies up to $z \sim 2$.*

Fontana A., Salimbeni S., Grazian A., Giallongo E., Pentericci L., Nonino M., Fontanot F., Menci N., Monaco P., Cristiani S., Vanzella E., de Santis C., Gallozzi S., 2006. A&A, **459**, 745. *The Galaxy mass function up to $z = 4$ in the GOODS-MUSIC sample: into the epoch of formation of massive galaxies.*

Fontanot F., De Lucia G., Monaco P., Somerville R. S., Santini P., 2009. MNRAS, **397**, 1776. *The many manifestations of downsizing: hierarchical galaxy formation models confront observations.*

French K. D., Yang Y., Zabludoff A., Narayanan D., Shirley Y., Walter F., Smith J.-D., Tremonti C. A., 2015. ApJ, **801**, 1. *Discovery of Large Molecular Gas Reservoirs in Post-starburst Galaxies.*

Frenk C. S., White S. D. M., Davis M., 1983. ApJ, **271**, 417. *Nonlinear evolution of large-scale structure in the universe.*

Fumagalli M., Fossati M., Hau G. K. T., Gavazzi G., Bower R., Sun M., Boselli A., 2014. MNRAS, **445**, 4335. *MUSE sneaks a peek at extreme ram-pressure stripping events - I. A kinematic study of the archetypal galaxy ESO137-001.*

Furusawa H., Kosugi G., Akiyama M., Takata T., Sekiguchi K., Tanaka I., Iwata I., Kajisawa M., Yasuda N., Doi M., Ouchi M., Simpson C., Shimasaku K., Yamada T., Furusawa J., Morokuma T., Ishida C. M., Aoki K., Fuse T., Imanishi M., Iye M., Karoji H., Kobayashi N., Kodama T., Komiyama Y., Maeda Y., Miyazaki S., Mizumoto Y., Nakata F., Noumaru J., Ogasawara R., Okamura S., Saito T., Sasaki T., Ueda Y., Yoshida M., 2008. ApJS, **176**, 1. *The Subaru/XMM-Newton Deep Survey (SXDS). II. Optical Imaging and Photometric Catalogs.*

Gallagher, John S. I., Ostriker J. P., 1972. AJ, **77**, 288. *A Note on Mass Loss during Collisions between Galaxies and the Formation of Giant Systems.*

Gan J., Kang X., van den Bosch F. C., Hou J., 2010. MNRAS, **408**, 2201. *An improved model for the dynamical evolution of dark matter subhaloes.*

Gao L., Springel V., White S. D. M., 2005. MNRAS, **363**, L66. *The age dependence of halo clustering.*

Gómez P. L., Nichol R. C., Miller C. J., Balogh M. L., Goto T., Zabludoff A. I., Romer A. K., Bernardi M., Sheth R., Hopkins A. M., Castander F. J., Connolly A. J., Schneider D. P., Brinkmann J., Lamb D. Q., SubbaRao M., York D. G., 2003. ApJ, **584**, 210. *Galaxy Star Formation as a Function of Environment in the Early Data Release of the Sloan Digital Sky Survey.*

Gonçalves T. S., Martin D. C., Menéndez-Delmestre K., Wyder T. K., Koekemoer A., 2012. ApJ, **759**, 67. *Quenching Star Formation at Intermediate Redshifts: Downsizing of the Mass Flux Density in the Green Valley.*

Gonzalez-Perez V., Lacey C. G., Baugh C. M., Lagos C. D. P., Helly J., Campbell D. J. R., Mitchell P. D., 2014. MNRAS, **439**, 264. *How sensitive are predicted galaxy luminosities to the choice of stellar population synthesis model?*

Gonzalez-Perez V., Comparat J., Norberg P., Baugh C. M., Contreras S., Lacey C., McCullagh N., Orsi A., Helly J., Humphries J., 2018. MNRAS, **474**, 4024. *The host dark matter haloes of [O II] emitters at 0.5 $<z<$ 1.5.*

Goto T., Nichol R. C., Okamura S., Sekiguchi M., Miller C. J., Bernardi M., Hopkins A., Tremonti C., Connolly A., Castander F. J., Brinkmann J., Fukugita M., Harvanek M., Ivezic Z., Kleinman S. J., Krzesinski J., Long D., Loveday J., Neilsen E. H., Newman P. R., Nitta A., Snedden S. A., Subbarao M., 2003. *Publications of the Astronomical Society of Japan*, **55**, 771. *Hδ-Strong Galaxies in the Sloan Digital Sky Survey: I. The Catalog.*

Goto T., 2004. A&A, **427**, 125. *Are E+A galaxies dusty-starbursts?: VLA 20 cm radio continuum observation.*

Gruppioni C., Calura F., Pozzi F., Delvecchio I., Berta S., De Lucia G., Fontanot F., Franceschini A., Marchetti L., Menci N., Monaco P., Vaccari M., 2015. MNRAS, **451(4)**, 3419. *Star formation in Herschel's Monsters versus semi-analytic models.*

Gunn J. E., Gott J. R. I., 1972. ApJ, **176**, 1. *On the Infall of Matter Into Clusters of Galaxies and Some Effects on Their Evolution.*

Guo Q., White S., Boylan-Kolchin M., De Lucia G., Kauffmann G., Lemson G., Li C., Springel V., Weinmann S., 2011. MNRAS, **413**, 101. *From dwarf spheroidals to cD galaxies: simulating the galaxy population in a ΛCDM cosmology.*

Guo Q., Gonzalez-Perez V., Guo Q., Schaller M., Furlong M., Bower R. G., Cole S., Crain R. A., Frenk C. S., Helly J. C., Lacey C. G., Lagos C. d. P., Mitchell P., Schaye J., Theuns T., 2016. MNRAS, **461**, 3457. *Galaxies in the EAGLE hydrodynamical simulation and in the Durham and Munich semi-analytical models.*

Hartley W. G., Almaini O., Mortlock A., Conselice C. J., Grützbauch R., Simpson C., Bradshaw E. J., Chuter R. W., Foucaud S., Cirasuolo M., Dunlop J. S., McLure R. J., Pearce H. J., 2013. MNRAS, **431**, 3045. *Studying the emergence of the red sequence through galaxy clustering: host halo masses at $z>2$.*

Henriques B. M. B., White S. D. M., Lemson G., Thomas P. A., Guo Q., Marleau G.-D., Overzier R. A., 2012. MNRAS, **421**, 2904. *Confronting theoretical models with the observed evolution of the galaxy population out to $z=4$.*

Henriques B. M. B., White S. D. M., Thomas P. A., Angulo R. E., Guo Q., Lemson G., Springel V., 2013. MNRAS, **431**, 3373. *Simulations of the galaxy population constrained by observations from $z=3$ to the present day: implications for galactic winds and the fate of their ejecta.*

Henriques B. M. B., White S. D. M., Thomas P. A., Angulo R., Guo Q., Lemson G., Springel V., Overzier R., 2015. MNRAS, **451**, 2663. *Galaxy formation in the Planck cosmology - I. Matching the observed evolution of star formation rates, colours and stellar masses.*

Hernquist L., 1989. Nature, **340**, 687. *Tidal triggering of starbursts and nuclear activity in galaxies.*

Hirschmann M., De Lucia G., Fontanot F., 2016. MNRAS, **461**, 1760. *Galaxy assembly, stellar feedback and metal enrichment: the view from the GAEA model.*

Hogg D. W., Blanton M., Strateva I., Bahcall N. A., Brinkmann J., Csabai I., Doi M., Fukugita M., Hennessy G., Ivezić Ž., Knapp G. R., Lamb D. Q., Lupton R., Munn J. A., Nichol R., Schlegel D. J., Schneider D. P., York D. G., 2002. AJ, **124**, 646. *The Luminosity Density of Red Galaxies.*

Hopkins P. F., Hernquist L., Cox T. J., Di Matteo T., Martini P., Robertson B., Springel V., 2005. ApJ, **630**, 705. *Black Holes in Galaxy Mergers: Evolution of Quasars.*

Hopkins P. F., Hernquist L., Cox T. J., Di Matteo T., Robertson B., Springel V., 2006. *The Astrophysical Journal Supplement Series*, **163**, 1. *A Unified, Merger-driven Model of the Origin of Starbursts, Quasars, the Cosmic X-Ray Background, Supermassive Black Holes, and Galaxy Spheroids.*

Hubble E., Humason M. L., 1931. ApJ, **74**, 43. *The Velocity-Distance Relation among Extra-Galactic Nebulae.*

Hubble E. P., 1936. *Realm of the Nebulae.*

Ilbert O., Salvato M., Le Floc'h E., Aussel H., Capak P., McCracken H. J., Mobasher B., Kartaltepe J., Scoville N., Sanders D. B., Arnouts S., Bundy K., Cassata P., Kneib J.-P., Koekemoer A., Le Fèvre O., Lilly S., Surace J., Taniguchi Y., Tasca L., Thompson D., Tresse L., Zamojski M., Zamorani G., Zucca E., 2010. ApJ, **709**, 644. *Galaxy Stellar Mass Assembly Between 0.2 $< z <$ 2 from the S-COSMOS Survey.*

Ilbert O., McCracken H. J., Le Fèvre O., Capak P., Dunlop J., Karim A., Renzini M. A., Caputi K., Boissier S., Arnouts S., Aussel H., Comparat J., Guo Q., Hudelot P., Kartaltepe J., Kneib J. P., Krogager J. K., Le Floc'h E., Lilly S., Mellier Y., Milvang-Jensen B., Moutard T., Onodera M., Richard J., Salvato M., Sanders D. B., Scoville N., Silverman J. D., Taniguchi Y., Tasca L., Thomas R., Toft S., Tresse L., Vergani D., Wolk M., Zirm A., 2013. A&A, **556**, A55. *Mass assembly in quiescent and star-forming galaxies since $z \sim 4$ from UltraVISTA.*

Jenkins A., Frenk C. S., White S. D. M., Colberg J. M., Cole S., Evrard A. E., Couchman H. M. P., Yoshida N., 2001. MNRAS, **321**, 372. *The mass function of dark matter haloes.*

Jiang L., Helly J. C., Cole S., Frenk C. S., 2014. MNRAS, **440**, 2115. *N-body dark matter haloes with simple hierarchical histories.*

Kauffmann G., Heckman T. M., White S. D. M., Charlot S., Tremonti C., Brinchmann J., Bruzual G., Peng E. W., Seibert M., Bernardi M., Blanton M., Brinkmann J., Castander F., Csábai I., Fukugita M., Ivezic Z., Munn J. A., Nichol R. C., Padmanabhan N., Thakar A. R., Weinberg D. H., York D., 2003. MNRAS, **341**, 33. *Stellar masses and star formation histories for 10^5 galaxies from the Sloan Digital Sky Survey.*

Kauffmann G., White S. D. M., Heckman T. M., Ménard B., Brinchmann J., Charlot S., Tremonti C., Brinkmann J., 2004. MNRAS, **353**, 713. *The environmental dependence of the relations between stellar mass, structure, star formation and nuclear activity in galaxies.*

Kauffmann G., White S. D. M., Guiderdoni B., 1993. MNRAS, **264**, 201. *The formation and evolution of galaxies within merging dark matter haloes.*

Kaviani A., Haehnelt M. G., Kauffmann G., 2003. MNRAS, **340**, 739. *Modelling SCUBA sources in a ΛCDM cosmology: hot starbursts or cold extended galactic dust?*

Kaviraj S., Kirkby L. A., Silk J., Sarzi M., 2007. MNRAS, **382**, 960. *The UV properties of E+A galaxies: constraints on feedback-driven quenching of star formation.*

Kawata D., Cen R., Ho L. C., 2007. ApJ, **669**, 232. *Gravitational Stability of Circumnuclear Disks in Elliptical Galaxies.*

Kennicutt, Jr. R. C., 1992. ApJS, **79**, 255. *A spectrophotometric atlas of galaxies.*

Kennicutt, Jr. R. C., 1998. ARA&A, **36**, 189. *Star Formation in Galaxies Along the Hubble Sequence.*

Kereš D., Katz N., Weinberg D. H., Davé R., 2005. MNRAS, **363**, 2. *How do galaxies get their gas?*

Kimm T., Yi S. K., Khochfar S., 2011. ApJ, **729**, 11. *The Impact of Gas Stripping and Stellar Mass Loss on Satellite Galaxy Evolution.*

Kitzbichler M. G., White S. D. M., 2007. MNRAS, **376**, 2. *The high-redshift galaxy population in hierarchical galaxy formation models.*

Knebe A., Knollmann S. R., Muldrew S. I., Pearce F. R., Aragon-Calvo M. A., Ascasibar Y., Behroozi P. S., Ceverino D., Colombi S., Diemand J., Dolag K., Falck B. L., Fasel P., Gardner J., Gottlöber S., Hsu C.-H., Iannuzzi F., Klypin A., Lukić Z., Maciejewski M., McBride C., Neyrinck M. C., Planelles S., Potter D., Quilis V., Rasera Y., Read J. I., Ricker P. M., Roy F., Springel V., Stadel J., Stinson G., Sutter P. M., Turchaninov V., Tweed D., Yepes G., Zemp M., 2011. MNRAS, **415**, 2293. *Haloes gone MAD: The Halo-Finder Comparison Project.*

Knebe A., Pearce F. R., Lux H., Ascasibar Y., Behroozi P., Casado J., Moran C. C., Diemand J., Dolag K., Dominguez-Tenreiro R., Elahi P., Falck B., Gottlöber S., Han J., Klypin A., Lukić Z., Maciejewski M., McBride C. K., Merchán M. E., Muldrew S. I., Neyrinck M., Onions J., Planelles S., Potter D., Quilis V., Rasera Y., Ricker P. M., Roy F., Ruiz A. N., Sgró M. A., Springel V., Stadel J., Sutter P. M., Tweed D., Zemp M., 2013. MNRAS, **435**, 1618. *Structure finding in cosmological simulations: the state of affairs.*

Knebe A., Pearce F. R., Thomas P. A., Benson A., Blaizot J., Bower R., Carretero J., Castander F. J., Cattaneo A., Cora S. A., Croton D. J., Cui W., Cunnama D., De Lucia G., Devriendt J. E., Elahi P. J., Font A., Fontanot F., Garcia-Bellido J., Gargiulo I. D., Gonzalez-Perez V., Helly J., Henriques B., Hirschmann M., Lee J., Mamon G. A., Monaco P., Onions J., Padilla N. D., Power C., Pujol A., Skibba R. A., Somerville R. S., Srisawat C., Vega-Martínez C. A., Yi S. K., 2015. MNRAS, **451**, 4029. *nIFTy cosmology: comparison of galaxy formation models.*

Knebe A., Pearce F. R., Gonzalez-Perez V., Thomas P. A., Benson A., Asquith R., Blaizot J., Bower R., Carretero J., Castander F. J., Cattaneo A., Cora S. A., Croton D. J., Cui W., Cunnama D., Devriendt J. E., Elahi P. J., Font A., Fontanot F., Gargiulo I. D., Helly J., Henriques B., Lee J., Mamon G. A., Onions J., Padilla N. D., Power C., Pujol A., Ruiz A. N., Srisawat C., Stevens A. R. H., Tollet E., Vega-Martínez C. A., Yi S. K., 2018. MNRAS, **475**, 2936. *Cosmic CARNage I: on the calibration of galaxy formation models.*

Knollmann S. R., Knebe A., 2009. *The Astrophysical Journal Supplement Series*, **182**, 608. *AHF: Amiga's Halo Finder.*

Kormendy J., Ho L. C., 2013. ARA&A, **51(1)**, 511. *Coevolution (Or Not) of Supermassive Black Holes and Host Galaxies.*

Kovač K., Lilly S. J., Knobel C., Bschorr T. J., Peng Y., Carollo C. M., Contini T., Kneib J.-P., Le Févre O., Mainieri V., Renzini A., Scodeggio M., Zamorani G., Bardelli S., Bolzonella M., Bongiorno A., Caputi K., Cucciati O., de la Torre S., de Ravel L., Franzetti P., Garilli B., Iovino A., Kampczyk P., Lamareille F., Le Borgne J.-F., Le Brun V., Maier C., Mignoli M., Oesch P., Pello R., Montero E. P., Presotto V., Silverman J., Tanaka M., Tasca L., Tresse L., Vergani D., Zucca E., Aussel H., Koekemoer A. M., Le Floc'h E., Moresco M., Pozzetti L., 2014. MNRAS, **438**, 717. *zCOSMOS 20k: satellite galaxies are the main drivers of environmental effects in the galaxy population at least to $z \sim 0.7$.*

Krumholz M. R., McKee C. F., Klein R. I., 2005. Nature, **438**, 332. *The formation of stars by gravitational collapse rather than competitive accretion.*

Lacey C., Cole S., 1993. MNRAS, **262**, 627. *Merger rates in hierarchical models of galaxy formation.*

Lagos C. D. P., Baugh C. M., Zwaan M. A., Lacey C. G., Gonzalez-Perez V., Power C., Swinbank A. M., van Kampen E., 2014. MNRAS, **440**, 920. *Which galaxies dominate the neutral gas content of the Universe?*

Lane K. P., Almaini O., Foucaud S., Simpson C., Smail I., McLure R. J., Conselice C. J., Cirasuolo M., Page M. J., Dunlop J. S., Hirst P., Watson M. G., Sekiguchi K., 2007. MNRAS, **379**, L25. *The colour selection of distant galaxies in the UKIDSS Ultra Deep Survey Early Data Release.*

Lang P., Wuyts S., Somerville R. S., Förster Schreiber N. M., Genzel R., Bell E. F., Brammer G., Dekel A., Faber S. r. M., Ferguson H. C., Grogin N. A., Kocevski D. D., Koekemoer A. M., Lutz D., McGrath E. J., Momcheva I., Nelson E. J., Primack J. R., Rosario D. J., Skelton R. E., Tacconi L. J., van Dokkum P. G., Whitaker K. E., 2014. ApJ, **788**, 11. *Bulge Growth and Quenching since $z = 2.5$ in CANDELS/3D-HST.*

Larson R. B., Tinsley B. M., Caldwell C. N., 1980. ApJ, **237**, 692. *The evolution of disk galaxies and the origin of S0 galaxies.*

Larson R. B., 1974. MNRAS, **169**, 229. *Effects of supernovae on the early evolution of galaxies.*

Lawrence A., Warren S. J., Almaini O., Edge A. C., Hambly N. C., Jameson R. F., Lucas P., Casali M., Adamson A., Dye S., Emerson J. P., Foucaud S., Hewett P., Hirst P., Hodgkin S. T., Irwin M. J., Lodieu N., McMahon R. G., Simpson C., Smail I., Mortlock D., Folger M., 2007. MNRAS, **379**, 1599. *The UKIRT Infrared Deep Sky Survey (UKIDSS).*

Lee J., Yi S. K., 2013. ApJ, **766**, 38. *On the Assembly History of Stellar Components in Massive Galaxies.*

Leitherer C., Robert C., Drissen L., 1992. ApJ, **401**, 596. *Deposition of Mass, Momentum, and Energy by Massive Stars into the Interstellar Medium.*

Lewis I., Balogh M., De Propris R., Couch W., Bower R., Offer A., Bland -Hawthorn J., Baldry I. K., Baugh C., Bridges T., Cannon R., Cole S., Colless M., Collins C., Cross N., Dalton G., Driver S. P., Efstathiou G., Ellis R. S., Frenk C. S., Glazebrook K., Hawkins E., Jackson C., Lahav O., Lumsden S., Maddox S., Madgwick D., Norberg P., Peacock J. A., Percival W., Peterson B. A., Sutherland W., Taylor K., 2002. MNRAS, **334**, 673. *The 2dF Galaxy Redshift Survey: the environmental dependence of galaxy star formation rates near clusters.*

Li C., White S. D. M., 2009. MNRAS, **398**, 2177. *The distribution of stellar mass in the low-redshift Universe.*

Lintott C. J., Schawinski K., Slosar A., Land K., Bamford S., Thomas D., Raddick M. J., Nichol R. C., Szalay A., Andreescu D., Murray P., Vandenberg J., 2008. MNRAS, **389**, 1179. *Galaxy Zoo: morphologies derived from visual inspection of galaxies from the Sloan Digital Sky Survey.*

Maltby D. T., Almaini O., Wild V., Hatch N. A., Hartley W. G., Simpson C., McLure R. J., Dunlop J., Rowlands K., Cirasuolo M., 2016. MNRAS, **459**, L114. *The identification of post-starburst galaxies at $z \sim 1$ using multiwavelength photometry: a spectroscopic verification.*

Maltby D. T., Almaini O., Wild V., Hatch N. A., Hartley W. G., Simpson C., Rowlands K., Socolovsky M., 2018. MNRAS, **480**, 381. *The structure of post-starburst galaxies at $0.5 < z < 2$: evidence for two distinct quenching routes at different epochs.*

Mamon G. A., 1987. ApJ, **321**, 622. *The Dynamics of Small Groups of Galaxies. I. Virialized Groups.*

Marchesini D., van Dokkum P. G., Förster Schreiber N. M., Franx M., Labbé I., Wuyts S., 2009. ApJ, **701**, 1765. *The Evolution of the Stellar Mass Function of Galaxies from $z = 4.0$ and the First Comprehensive Analysis of its Uncertainties: Evidence for Mass-Dependent Evolution.*

Marchesini D., Whitaker K. E., Brammer G., van Dokkum P. G., Labbé I., Muzzin A., Quadri R. F., Kriek M., Lee K.-S., Rudnick G., Franx M., Illingworth G. D., Wake D., 2010. ApJ, **725**, 1277. *The Most Massive Galaxies at $3.0 <= z < 4.0$ in the Newfirm Medium-band Survey: Properties and Improved Constraints on the Stellar Mass Function.*

Martig M., Bournaud F., Teyssier R., Dekel A., 2009. ApJ, **707**, 250. *Morphological Quenching of Star Formation: Making Early-Type Galaxies Red.*

McCarthy I. G., Frenk C. S., Font A. S., Lacey C. G., Bower R. G., Mitchell N. L., Balogh M. L., Theuns T., 2008. MNRAS, **383**, 593. *Ram pressure stripping the hot gaseous haloes of galaxies in groups and clusters.*

McConnell N. J., Ma C.-P., 2013. ApJ, **764(2)**, 184. *Revisiting the Scaling Relations of Black Hole Masses and Host Galaxy Properties.*

McCracken H. J., Milvang-Jensen B., Dunlop J., Franx M., Fynbo J. P. U., Le Fèvre O., Holt J., Caputi K. I., Goranova Y., Buitrago F., Emerson J. P., Freudling W., Hudelot P., López-Sanjuan C., Magnard F., Mellier Y., Møller P., Nilsson K. K., Sutherland W., Tasca L., Zabl J., 2012. A&A, **544**, A156. *UltraVISTA: a new ultra-deep near-infrared survey in COSMOS.*

Mendez A. J., Coil A. L., Lotz J., Salim S., Moustakas J., Simard L., 2011. ApJ, **736**, 110. *AEGIS: The Morphologies of Green Galaxies at $0.4 < z < 1.2$.*

Merritt D., 1983. ApJ, **264**, 24. *Relaxation and tidal stripping in rich clusters of galaxies. I. Evolution of the mass distribution.*

Merritt D., 1984. ApJ, **276**, 26. *Relaxation and tidal stripping in rich clusters of galaxies. II. Evolution of the luminosity distribution.*

Mihos J. C., Hernquist L., 1996. ApJ, **464**, 641. *Gasdynamics and Starbursts in Major Mergers.*

Mitchell P. D., Lacey C. G., Cole S., Baugh C. M., 2014. MNRAS, **444**, 2637. *The evolution of the star-forming sequence in hierarchical galaxy formation models.*

Mo H. J., White S. D. M., 2002. MNRAS, **336**, 112. *The abundance and clustering of dark haloes in the standard ΛCDM cosmogony.*

Monaco P., Fontanot F., Taffoni G., 2007. MNRAS, **375**, 1189. *The MORGANA model for the rise of galaxies and active nuclei.*

Moore B., Katz N., Lake G., Dressler A., Oemler A., 1996. Nature, **379**, 613. *Galaxy harassment and the evolution of clusters of galaxies.*

Moore B., Lake G., Katz N., 1998. ApJ, **495**, 139. *Morphological Transformation from Galaxy Harassment.*

Mortlock A., Conselice C. J., Hartley W. G., Ownsworth J. R., Lani C., Bluck A. F. L., Almaini O., Duncan K., van der Wel A., Koekemoer A. M., Dekel A., Davé R., Ferguson H. C., de Mello D. F., Newman J. A., Faber S. M., Grogin N. A., Kocevski D. D., Lai K., 2013. MNRAS, **433**, 1185. *The redshift and mass dependence on the formation of the Hubble sequence at $z > 1$ from CANDELS/UDS.*

Moster B. P., Somerville R. S., Maulbetsch C., van den Bosch F. C., Macciò A. V., Naab T., Oser L., 2010. ApJ, **710**, 903. *Constraints on the Relationship between Stellar Mass and Halo Mass at Low and High Redshift.*

Mundy C. J., Conselice C. J., Ownsworth J. R., 2015. MNRAS, **450**, 3696. *Tracing galaxy populations through cosmic time: a critical test of methods for connecting the same galaxies between different redshifts at $z < 3$.*

Muratov A. L., Kereš D., Faucher-Giguère C.-A., Hopkins P. F., Quataert E., Murray N., 2015. MNRAS, **454**, 2691. *Gusty, gaseous flows of FIRE: galactic winds in cosmological simulations with explicit stellar feedback.*

Muzzin A., Wilson G., Yee H. K. C., Gilbank D., Hoekstra H., Demarco R., Balogh M., van Dokkum P., Franx M., Ellingson E., Hicks A., Nantais J., Noble A., Lacy M., Lidman C., Rettura A., Surace J., Webb T., 2012. ApJ, **746**, 188. *The Gemini Cluster Astrophysics Spectroscopic Survey (GCLASS): The Role of Environment and Self-regulation in Galaxy Evolution at $z \sim 1$.*

Muzzin A., Marchesini D., Stefanon M., Franx M., McCracken H. J., Milvang-Jensen B., Dunlop J. S., Fynbo J. P. U., Brammer G., Labbé I., van Dokkum P. G., 2013. ApJ, **777**, 18. *The Evolution of the Stellar Mass Functions of Star-forming and Quiescent Galaxies to $z = 4$ from the COSMOS/UltraVISTA Survey.*

Nair P. B., Abraham R. G., 2010. *The Astrophysical Journal Supplement Series*, **186**, 427. *A Catalog of Detailed Visual Morphological Classifications for 14,034 Galaxies in the Sloan Digital Sky Survey.*

Navarro J. F., Frenk C. S., White S. D. M., 1996. ApJ, **462**, 563. *The Structure of Cold Dark Matter Halos.*

Noll S., Burgarella D., Giovannoli E., Buat V., Marcillac D., Muñoz-Mateos J. C., 2009. A&A, **507**, 1793. *Analysis of galaxy spectral energy distributions from far-UV to far-IR with CIGALE: studying a SINGS test sample.*

Norton S. A., Gebhardt K., Zabludoff A. I., Zaritsky D., 2001. ApJ, **557**, 150. *The Spatial Distribution and Kinematics of Stellar Populations in E+A Galaxies.*

Onions J., Knebe A., Pearce F. R., Muldrew S. I., Lux H., Knollmann S. R., Ascasibar Y., Behroozi P., Elahi P., Han J., Maciejewski M., Merchán M. E., Neyrinck M., Ruiz A. N., Sgró M. A., Springel V., Tweed D., 2012. MNRAS, **423**, 1200. *Subhaloes going Notts: the subhalo-finder comparison project.*

Overzier R., Lemson G., Angulo R. E., Bertin E., Blaizot J., Henriques B. M. B., Marleau G. D., White S. D. M., 2013. MNRAS, **428**, 778. *The Millennium Run Observatory: first light.*

Pawlik M. M., McAlpine S., Trayford J. W., Wild V., Bower R., Crain R. A., Schaller M., Schaye J., 2019. *Nature Astronomy. The diverse evolutionary pathways of post-starburst galaxies.*

Peng Y.-j., Lilly S. J., Kovač K., Bolzonella M., Pozzetti L., Renzini A., Zamorani G., Ilbert O., Knobel C., Iovino A., Maier C., Cucciati O., Tasca L., Carollo C. M., Silverman J., Kampczyk P., de Ravel L., Sanders D., Scoville N., Contini T., Mainieri V., Scodeggio M., Kneib J.-P., Le Fèvre O., Bardelli S., Bongiorno A., Caputi K., Coppa G., de la Torre S., Franzetti P., Garilli B., Lamareille F., Le Borgne J.-F., Le Brun V., Mignoli M., Perez Montero E., Pello R., Ricciardelli E., Tanaka M., Tresse L., Vergani D., Welikala N., Zucca E., Oesch P., Abbas U., Barnes L., Bordoloi R., Bottini D., Cappi A., Cassata P., Cimatti A., Fumana M., Hasinger G., Koekemoer A., Leauthaud A., Maccagni D., Marinoni C., McCracken H., Memeo P., Meneux B., Nair P., Porciani C., Presotto V., Scaramella R., 2010. ApJ, **721**, 193. *Mass and Environment as Drivers of Galaxy Evolution in SDSS and zCOSMOS and the Origin of the Schechter Function.*

Penzias A. A., Wilson R. W., 1965. ApJ, **142**, 419. *A Measurement of Excess Antenna Temperature at 4080 Mc/s.*

Perlmutter S., Aldering G., Goldhaber G., Knop R. A., Nugent P., Castro P. G., Deustua S., Fabbro S., Goobar A., Groom D. E., Hook I. M., Kim A. G., Kim M. Y., Lee J. C., Nunes N. J., Pain R., Pennypacker C. R., Quimby R., Lidman C., Ellis R. S., Irwin M., McMahon R. G., Ruiz-Lapuente P., Walton N., Schaefer B., Boyle B. J., Filippenko A. V., Matheson T., Fruchter A. S., Panagia N., Newberg H. J. M., Couch W. J., Project T. S. C., 1999. ApJ, **517**, 565. *Measurements of Ω and Λ from 42 High-Redshift Supernovae.*

Planck Collaboration, Ade P. A. R., Aghanim N., Arnaud M., Ashdown M., Aumont J., Baccigalupi C., Baker M., Balbi A., Banday A. J., Barreiro R. B., et al., 2011. A&A, **536**, A1. *Planck early results. I. The Planck mission.*

Planck Collaboration, Ade P. A. R., Aghanim N., Armitage-Caplan C., Arnaud M., Ashdown M., Atrio-Barandela F., Aumont J., Baccigalupi C., Banday A. J., Barreiro R. B., et al., 2014. A&A, **571**, A16. *Planck 2013 results. XVI. Cosmological parameters.*

Planck Collaboration, Aghanim N., Akrami Y., Ashdown M., Aumont J., Baccigalupi C., Ballardini M., Banday A. J., Barreiro R. B., Bartolo N., Basak S., et al., 2018. *arXiv e-prints. Planck 2018 results. VI. Cosmological parameters.*

Porter L. A., Somerville R. S., Primack J. R., Johansson P. H., 2014. MNRAS, **444**, 942. *Understanding the structural scaling relations of early-type galaxies.*

Pozzetti L., Bolzonella M., Lamareille F., Zamorani G., Franzetti P., Le Fèvre O., Iovino A., Temporin S., Ilbert O., Arnouts S., Charlot S., Brinchmann J., Zucca E., Tresse L., Scodeggio M., Guzzo L., Bottini D., Garilli B., Le Brun V., Maccagni D., Picat J. P., Scaramella R., Vettolani G., Zanichelli A., Adami C., Bardelli S., Cappi A., Ciliegi P., Contini T., Foucaud S., Gavignaud I., McCracken H. J., Marano B., Marinoni C., Mazure A., Meneux B., Merighi R., Paltani S., Pellò R., Pollo A., Radovich M., Bondi M., Bongiorno A., Cucciati O., de la Torre S., Gregorini L., Mellier Y., Merluzzi P., Vergani D., Walcher C. J., 2007. A&A, **474**, 443. *The VIMOS VLT Deep Survey. The assembly history of the stellar mass in galaxies: from the young to the old universe.*

Pozzetti L., Bolzonella M., Zucca E., Zamorani G., Lilly S., Renzini A., Moresco M., Mignoli M., Cassata P., Tasca L., Lamareille F., Maier C., Meneux B., Halliday C., Oesch P., Vergani D., Caputi K., Kovač K., Cimatti A., Cucciati O., Iovino A., Peng Y., Carollo M., Contini T., Kneib J.-P., Le Févre O., Mainieri V., Scodeggio M., Bardelli S., Bongiorno A., Coppa G., de la Torre S., de Ravel L., Franzetti P., Garilli B., Kampczyk P., Knobel C., Le Borgne J.-F., Le Brun V., Pellò R., Perez Montero E., Ricciardelli E., Silverman J. D., Tanaka M., Tresse L., Abbas U., Bottini D., Cappi A., Guzzo L., Koekemoer A. M., Leauthaud A., Maccagni D., Marinoni C., McCracken H. J., Memeo P., Porciani C., Scaramella R., Scarlata C., Scoville N., 2010. A&A, **523**, A13. *zCOSMOS - 10k-bright spectroscopic sample. The bimodality in the galaxy stellar mass function: exploring its evolution with redshift.*

Prada F., Klypin A. A., Cuesta A. J., Betancort-Rijo J. E., Primack J., 2012. MNRAS, **423**, 3018. *Halo concentrations in the standard Λ cold dark matter cosmology.*

Press W. H., Schechter P., 1974. ApJ, **187**, 425. *Formation of Galaxies and Clusters of Galaxies by Self-Similar Gravitational Condensation.*

Quintero A. D., Hogg D. W., Blanton M. R., Schlegel D. J., Eisenstein D. J., Gunn J. E., Brinkmann J., Fukugita M., Glazebrook K., Goto T., 2004. ApJ, **602**, 190. *Selection and Photometric Properties of K+A Galaxies.*

Refregier A., 2003. *Annual Review of Astronomy and Astrophysics*, **41**, 645. *Weak Gravitational Lensing by Large-Scale Structure.*

Riess A. G., Filippenko A. V., Challis P., Clocchiatti A., Diercks A., Garnavich P. M., Gilliland R. L., Hogan C. J., Jha S., Kirshner R. P., Leibundgut B., Phillips M. M., Reiss D., Schmidt B. P., Schommer R. A., Smith R. C., Spyromilio J., Stubbs C., Suntzeff N. B., Tonry J., 1998. AJ, **116**, 1009. *Observational Evidence from Supernovae for an Accelerating Universe and a Cosmological Constant.*

Roberts M. S., Haynes M. P., 1994. *Annual Review of Astronomy and Astrophysics*, **32**, 115. *Physical Parameters along the Hubble Sequence.*

Rodrigues L. F. S., Vernon I., Bower R. G., 2017. MNRAS, **466**, 2418. *Constraints on galaxy formation models from the galaxy stellar mass function and its evolution.*

Rowlands K., Wild V., Nesvadba N., Sibthorpe B., Mortier A., Lehnert M., da Cunha E., 2015. MNRAS, **448**, 258. *The evolution of the cold interstellar medium in galaxies following a starburst.*

Rubin V. C., Ford, W. K. J., Thonnard N., 1978. ApJ, **225**, L107. *Extended rotation curves of high-luminosity spiral galaxies. IV. Systematic dynamical properties, Sa -> Sc.*

Salim S., Rich R. M., Charlot S., Brinchmann J., Johnson B. D., Schiminovich D., Seibert M., Mallery R., Heckman T. M., Forster K., Friedman P. G., Martin D. C., Morrissey P., Neff S. G., Small T., Wyder T. K., Bianchi L., Donas J., Lee Y.-W., Madore B. F., Milliard B., Szalay A. S., Welsh B. Y., Yi S. K., 2007. *The Astrophysical Journal Supplement Series*, **173**, 267. *UV Star Formation Rates in the Local Universe.*

Schawinski K., Lintott C., Thomas D., Sarzi M., Andreescu D., Bamford S. P., Kaviraj S., Khochfar S., Land K., Murray P., Nichol R. C., Raddick M. J., Slosar A., Szalay A., VandenBerg J., Yi S. K., 2009. MNRAS, **396**, 818. *Galaxy Zoo: a sample of blue early-type galaxies at low redshift*.*

Schawinski K., Urry C. M., Simmons B. D., Fortson L., Kaviraj S., Keel W. C., Lintott C. J., Masters K. L., Nichol R. C., Sarzi M., Skibba R., Treister E., Willett K. W., Wong O. I., Yi S. K., 2014. MNRAS, **440**, 889. *The green valley is a red herring: Galaxy Zoo reveals two evolutionary pathways towards quenching of star formation in early- and late-type galaxies.*

Sérsic J. L., 1968. *Atlas de Galaxias Australes.*

Shamshiri S., Thomas P. A., Henriques B. M., Tojeiro R., Lemson G., Oliver S. J., Wilkins S., 2015. MNRAS, **451**, 2681. *Galaxy formation in the Planck cosmology - II. Star-formation histories and post-processing magnitude reconstruction.*

Shankar F., Buchan S., Rettura A., Bouillot V. R., Moreno J., Licitra R., Bernardi M., Huertas-Company M., Mei S., Ascaso B., Sheth R., Delaye L., Raichoor A., 2015. ApJ, **802**, 73. *Avoiding Progenitor Bias: The Structural and Mass Evolution of Brightest Group and Cluster Galaxies in Hierarchical Models since $z \sim< 1$.*

Simpson C., Westoby P., Arumugam V., Ivison R., Hartley W., Almaini O., 2013. MNRAS, **433**, 2647. *The prevalence of AGN feedback in massive galaxies at $z \sim 1$.*

Skibba R. A., Bamford S. P., Nichol R. C., Lintott C. J., Andreescu D., Edmondson E. M., Murray P., Raddick M. J., Schawinski K., Slosar A., Szalay A. S., Thomas D., Vandenberg J., 2009. MNRAS, **399**, 966. *Galaxy Zoo: disentangling the environmental dependence of morphology and colour.*

Smoot G., Bennett C., Weber R., Maruschak J., Ratliff R., Janssen M., Chitwood J., Hilliard L., Lecha M., Mills R., Patschke R., Richards C., Backus C., Mather J., Hauser M., Weiss R., Wilkinson D., Gulkis S., Boggess N., Cheng E., Kelsall T., Lubin P., Meyer S., Moseley H., Murdock T., Shafer R., Silverberg R., Wright E., 1990. ApJ, **360**, 685. *COBE Differential Microwave Radiometers: Instrument Design and Implementation.*

Socolovsky M., Almaini O., Hatch N. A., Wild V., Maltby D. T., Hartley W. G., Simpson C., 2018. MNRAS, **476**, 1242. *The enhancement of rapidly quenched galaxies in distant clusters at $0.5 < z < 1.0$.*

Socolovsky M., Maltby D. T., Hatch N. A., Almaini O., Wild V., Hartley W. G., Simpson C., Rowlands K., 2019. MNRAS, **482**, 1640. *Compact star-forming galaxies preferentially quenched to become PSBs in $z < 1$ clusters.*

Somerville R. S., Davé R., 2015. ARA&A, **53**, 51. *Physical Models of Galaxy Formation in a Cosmological Framework.*

Somerville R. S., Hopkins P. F., Cox T. J., Robertson B. E., Hernquist L., 2008. MNRAS, **391**, 481. *A semi-analytic model for the co-evolution of galaxies, black holes and active galactic nuclei.*

Somerville R. S., Primack J. R., Faber S. M., 2001. MNRAS, **320**, 504. *The nature of high-redshift galaxies.*

Speagle J. S., Steinhardt C. L., Capak P. L., Silverman J. D., 2014. ApJS, **214**, 15. *A Highly Consistent Framework for the Evolution of the Star-Forming "Main Sequence" from $z \sim 0$-6.*

Spergel D. N., Verde L., Peiris H. V., Komatsu E., Nolta M. R., Bennett C. L., Halpern M., Hinshaw G., Jarosik N., Kogut A., Limon M., Meyer S. S., Page L., Tucker G. S., Weiland J. L., Wollack E., Wright E. L., 2003. *The Astrophysical Journal Supplement Series*, **148**, 175. *First-Year Wilkinson Microwave Anisotropy Probe (WMAP) Observations: Determination of Cosmological Parameters.*

Springel V., White S. D. M., Tormen G., Kauffmann G., 2001. MNRAS, **328**, 726. *Populating a cluster of galaxies - I. Results at z=0.*

Springel V., White S. D. M., Jenkins A., Frenk C. S., Yoshida N., Gao L., Navarro J., Thacker R., Croton D., Helly J., Peacock J. A., Cole S., Thomas P., Couchman H., Evrard A., Colberg J., Pearce F., 2005. Nature, **435**, 629. *Simulations of the formation, evolution and clustering of galaxies and quasars.*

Springel V., Frenk C. S., White S. D. M., 2006. Nature, **440**, 1137. *The large-scale structure of the Universe.*

Springel V., 2005. MNRAS, **364**, 1105. *The cosmological simulation code GADGET-2.*

Srisawat C., Knebe A., Pearce F. R., Schneider A., Thomas P. A., Behroozi P., Dolag K., Elahi P. J., Han J., Helly J., Jing Y., Jung I., Lee J., Mao Y.-Y., Onions J., Rodriguez-Gomez V., Tweed D., Yi S. K., 2013. MNRAS, **436**, 150. *Sussing Merger Trees: The Merger Trees Comparison Project.*

Stark D. P., Schenker M. A., Ellis R., Robertson B., McLure R., Dunlop J., 2013. ApJ, **763**, 129. *Keck Spectroscopy of $3 < z < 7$ Faint Lyman Break Galaxies: The Importance of Nebular Emission in Understanding the Specific Star Formation Rate and Stellar Mass Density.*

Starobinskii A. A., 1979. *ZhETF Pisma Redaktsiiu*, **30**, 719. *Spectrum of relict gravitational radiation and the early state of the universe.*

Steinhauser D., Schindler S., Springel V., 2016. A&A, **591**, A51. *Simulations of ram-pressure stripping in galaxy-cluster interactions.*

Stevens A. R. H., Brown T., 2017. MNRAS, **471**, 447. *Physical drivers of galaxies' cold-gas content: exploring environmental and evolutionary effects with Dark Sage.*

Stevens A. R. H., Croton D. J., Mutch S. J., 2016. MNRAS, **461**, 859. *Building disc structure and galaxy properties through angular momentum: the DARK SAGE semi-analytic model.*

Strateva I., Ivezić Ž., Knapp G. R., Narayanan V. K., Strauss M. A., Gunn J. E., Lupton R. H., Schlegel D., Bahcall N. A., Brinkmann J., Brunner R. J., Budavári T., Csabai I., Castander F. J., Doi M., Fukugita M., Győry Z., Hamabe M., Hennessy G., Ichikawa T., Kunszt P. Z., Lamb D. Q., McKay T. A., Okamura S., Racusin J., Sekiguchi M., Schneider D. P., Shimasaku K., York D., 2001. AJ, **122**, 1861. *Color Separation of Galaxy Types in the Sloan Digital Sky Survey Imaging Data.*

Tanaka M., Goto T., Okamura S., Shimasaku K., Brinkmann J., 2004. AJ, **128**, 2677. *The Environmental Dependence of Galaxy Properties in the Local Universe: Dependences on Luminosity, Local Density, and System Richness.*

Tecce T. E., Cora S. A., Tissera P. B., Abadi M. G., Lagos C. D. P., 2010. MNRAS, **408**, 2008. *Ram pressure stripping in a galaxy formation model - I. A novel numerical approach.*

Tomczak A. R., Quadri R. F., Tran K.-V. H., Labbé I., Straatman C. M. S., Papovich C., Glazebrook K., Allen R., Brammer G. B., Kacprzak G. G., Kawinwanichakij L., Kelson D. D., McCarthy P. J., Mehrtens N., Monson A. J., Persson S. E., Spitler L. R., Tilvi V., van Dokkum P., 2014. ApJ, **783**, 85. *Galaxy Stellar Mass*

Functions from ZFOURGE/CANDELS: An Excess of Low-mass Galaxies since z = 2 and the Rapid Buildup of Quiescent Galaxies.

Tormen G., Bouchet F. R., White S. D. M., 1997. MNRAS, **286**, 865. *The structure and dynamical evolution of dark matter haloes.*

Trayford J. W., Theuns T., Bower R. G., Crain R. A., Lagos C. d. P., Schaller M., Schaye J., 2016. MNRAS, **460**, 3925. *It is not easy being green: the evolution of galaxy colour in the EAGLE simulation.*

Tremonti C. A., Moustakas J., Diamond-Stanic A. a. M., 2007. ApJ, **663**, L77. *The Discovery of 1000 km s^{-1} Outflows in Massive Poststarburst Galaxies at z=0.6.*

van den Bosch F. C., Aquino D., Yang X., Mo H. J., Pasquali A., McIntosh D. H., Weinmann S. M., Kang X., 2008. MNRAS, **387**, 79. *The importance of satellite quenching for the build-up of the red sequence of present-day galaxies.*

van Dokkum P. G., 2005. AJ, **130**, 2647. *The Recent and Continuing Assembly of Field Elliptical Galaxies by Red Mergers.*

Vergani D., Zamorani G., Lilly S., Lamareille F., Halliday C., Scodeggio M., Vignali C., Ciliegi P., Bolzonella M., Bondi M., Kovač K., Knobel C., Zucca E., Caputi K., Pozzetti L., Bardelli S., Mignoli M., Iovino A., Carollo C. M., Contini T., Kneib J. P., Le Fèvre O., Mainieri V., Renzini A., Bongiorno A., Coppa G., Cucciati O., de la Torre S., de Ravel L., Franzetti P., Garilli B., Kampczyk P., Le Borgne J. F., Le Brun V., Maier C., Pello R., Peng Y., Perez Montero E., Ricciardelli E., Silverman J. D., Tanaka M., Tasca L., Tresse L., Abbas U., Bottini D., Cappi A., Cassata P., Cimatti A., Guzzo L., Koekemoer A. M., Leauthaud A., Maccagni D., Marinoni C., McCracken H. J., Memeo P., Meneux B., Oesch P., Porciani C., Scaramella R., Capak P., Sanders D., Scoville N., Taniguchi Y., 2010. A&A, **509**, A42. *K+a galaxies in the zCOSMOS survey . Physical properties of systems in their post-starburst phase.*

Weinmann S. M., Kauffmann G., von der Linden A., De Lucia G., 2010. MNRAS, **406**, 2249. *Cluster galaxies die hard.*

Weinmann S. M., Pasquali A., Oppenheimer B. D., Finlator K., Mendel J. T., Crain R. A., Macciò A. V., 2012. MNRAS, **426**, 2797. *A fundamental problem in our understanding of low-mass galaxy evolution.*

Whitaker K. E., Kriek M., van Dokkum P. G., Bezanson R., Brammer G., Franx M., Labbé I., 2012a. ApJ, **745(2)**, 179. *A Large Population of Massive Compact Post-starburst Galaxies at $z > 1$: Implications for the Size Evolution and Quenching Mechanism of Quiescent Galaxies.*

Whitaker K. E., van Dokkum P. G., Brammer G., Franx M., 2012b. ApJ, **754**, L29. *The Star Formation Mass Sequence Out to z = 2.5.*

White S. D. M., Frenk C. S., 1991. ApJ, **379**, 52. *Galaxy Formation through Hierarchical Clustering.*

White S. D. M., Rees M. J., 1978. MNRAS, **183**, 341. *Core condensation in heavy halos: a two-stage theory for galaxy formation and clustering.*

White S. D. M., Frenk C. S., Davis M., 1983. ApJ, **274**, L1. *Clustering in a neutrino-dominated universe.*

White C. E., Somerville R. S., Ferguson H. C., 2015. ApJ, **799**, 201. *A Parametric Study of Possible Solutions to the High-redshift Overproduction of Stars in Modeled Dwarf Galaxies.*

Wild V., Walcher C. J., Johansson P. H., Tresse L., Charlot S., Pollo A., Le Fèvre O., de Ravel L., 2009. MNRAS, **395**, 144. *Post-starburst galaxies: more than just an interesting curiosity.*

Wild V., Almaini O., Cirasuolo M., Dunlop J., McLure R., Bowler R., Ferreira J., Bradshaw E., Chuter R., Hartley W., 2014. MNRAS, **440**, 1880. *A new method for classifying galaxy SEDs from multiwavelength photometry.*

Wild V., Almaini O., Dunlop J., Simpson C., Rowlands K., Bowler R., Maltby D., McLure R., 2016. MNRAS, **463**, 832. *The evolution of post-starburst galaxies from z=2 to 0.5.*

Williams R. J., Quadri R. F., Franx M., van Dokkum P., Labbé I., 2009. ApJ, **691**, 1879. *Detection of Quiescent Galaxies in a Bicolor Sequence from Z = 0-2.*

Yang Y., Zabludoff A. I., Zaritsky D., Lauer T. R., Mihos J. C., 2004. ApJ, **607**, 258. *E+A Galaxies and the Formation of Early-Type Galaxies at z* $\sim$ *0.*

Yun K., Pillepich A., Zinger E., Nelson D., Donnari M., Joshi G., Rodriguez-Gomez V., Genel S., Weinberger R., Vogelsberger M., Hernquist L., 2019. MNRAS, **483**, 1042. *Jellyfish galaxies with the IllustrisTNG simulations - I. Gas-stripping phenomena in the full cosmological context.*

Zabludoff A. I., Zaritsky D., Lin H., Tucker D., Hashimoto Y., Shectman S. A., Oemler A., Kirshner R. P., 1996. ApJ, **466**, 104. *The Environment of "E+A" Galaxies.*

Zehavi I., Zheng Z., Weinberg D. H., Blanton M. R., Bahcall N. A., Berlind A. A., Brinkmann J., Frieman J. A., Gunn J. E., Lupton R. H., Nichol R. C., Percival W. J., Schneider D. P., Skibba R. A., Strauss M. A., Tegmark M., York D. G., 2011. ApJ, **736**, 59. *Galaxy Clustering in the Completed SDSS Redshift Survey: The Dependence on Color and Luminosity.*

Zheng Z., Berlind A. A., Weinberg D. H., Benson A. J., Baugh C. M., Cole S., Davé R., Frenk C. S., Katz N., Lacey C. G., 2005. ApJ, **633**, 791. *Theoretical Models of the Halo Occupation Distribution: Separating Central and Satellite Galaxies.*

Zwicky F., 1933. *Helvetica Physica Acta*, **6**, 110. *Die Rotverschiebung von extragalaktischen Nebeln.*